2005

# Evaluation of Numerical, Analytical, and Experimental Particle Deposition in Simple and Lung Geometries

Pamela M. Snyder

# EVALUATION OF NUMERICAL, ANALYTICAL, AND EXPERIMENTAL PARTICLE DEPOSITION IN SIMPLE AND LUNG GEOMETRIES

By

Pamela M. Snyder

A Thesis Submitted
In Partial Fulfillment
Of the Requirement for the

**MASTER OF SCIENCE**
**IN**
**MECHANICAL ENGINEERING**

Approved by:

**Dr. Risa J. Robinson**
Department of Mechanical Engineering

**Dr. Steven W. Day**
Department of Mechanical Engineering

**Dr. Amitabha Ghosh**
Department of Mechanical Engineering

**Dr. Edward C. Hensel**
Department Head of Mechanical Engineering

**DEPARTMENT OF MECHANICAL ENGINEERING**
**ROCHESTER INSTITUTE OF TECHNOLOGY**

**OCTOBER 2005**

# Permission to Duplicate

***Permission Granted***

**Title:**

## EVALUATION OF NUMERICAL, ANALYTICAL, AND EXPERIMENTAL PARTICLE DEPOSITION IN SIMPLE AND LUNG GEOMETRIES

I, Pamela Snyder, hereby grant permission to the Wallace Library of the Rochester Institute of Technology to reproduce my thesis in whole or in part. Any reproduction will not be for commercial use or profit.

Date: _____ Signature: Pamela Snyder

# Acknowledgements

I would like to take a moment to recognize the people and organization that have made this research possible.

I would like to start by thanking my parents, Daniel and Gail Snyder, brother, Keith, and the rest of my family for their constant love and support throughout this process. I know you haven't always understood what I've been doing, but you were always there. You support has been one of the few things I could always count on the past five years. And yes the "paper" is finally done!

My advisor, Dr. Risa Robinson, thank you for pushing me to excel in my research. I know we have had our bumps along the way. None the less I am truly grateful for your support and guidance through this progress. I appreciate the sacrifices you have made for my research, particularly the many late nights reviewing Chapters. You have taught me a lot about the research process.

To the members of my committee, Dr. Day and Dr. Ghosh, I appreciate the time and energy you have put into reviewing my thesis.

Dr. Carrano, in the Industrial Engineering department, for graciously allowing me to utilize the Brinkman Lab. Thank you for the time you spent assisting me with developing a molding process for the bifurcations and teaching me to use the various pieces of equipment necessary to characterize the molds.

To the faculty and staff of the Mechanical Engineering Department at Rochester Institute of Technology, I have learned so much from my time here at RIT.

This research was supported by the American Cancer Society Grant #RSG-05-021-01.

# Abstract


## EVALUATION OF NUMERICAL, ANALYTICAL, AND EXPERIMENTAL PARTICLE DEPOSITION IN SIMPLE AND LUNG GEOMETRIES

Pamela M. Snyder

Advisor: Dr. Risa J. Robinson

Particle deposition is utilized to determine exposure limits, design inhaled medications, and study pulmonary disorders that are a result of airborne pathogens. This information can be obtained from analytical equations, experimental studies, empirical relationships, and numerical analysis.

This research utilizes analytical equations, empirical relationships, and experimental data to investigate the accuracy of three Computational Fluid Dynamics (CFD) software packages; Fluent Discrete Phase Model (DPM), Fluent Fine Particle Model (FPM) and CFX. The sedimentation, molecular diffusion and impaction deposition mechanisms are investigated in a straight tube, bifurcating tube, and three generation lung geometry.

Sedimentation is evaluated in the straight tube for $\varepsilon$ values between 1E-5 and 1. CFD predictions for parabolic flow are compared to Pich (1972), Wang (1975) and Yeh and Schum (1980), while predictions for uniform flow are compared to Yu, et al. (1977) and Yeh and Schum (1980). Diffusion is evaluated in the straight tube for $\Delta$ values between 1E-6 and 1E-1. CFD predictions for parabolic and uniform flow conditions are compared to Ingham's (1975) analytical equation for parabolic and uniform flow conditions, respectively. Impaction is evaluated in the bifurcating tube for Stokes number between 0.017 and 0.27. CFD predictions in a bifurcating tube are compared to Kim and Iglesias' (1989) experimental data for nearly the same geometry and theoretical predictions from Zhang, et al. (1997), Cai and Yu (1988), and Yeh and Schum (1980) for parabolic and uniform flow conditions. Finally, CFD predictions in the three generation lung geometry are compared to experimental data gather by Dr. Oldham at the University of California, Irvine for 3 μm, and 10 μm

particles at 1.5 lpm (12lpm tracheal flow rate) and 1 μm, 3 μm, and 10 μm at 7.5 lpm (60 lpm tracheal flow rate).

Fluent FPM aligns almost exactly with predictions from Pich (1972) and Wang (1975) for sedimentation from parabolic flow at all ε values in the straight tube. Fluent DPM and CFX agree well with predictions from Yu, et al. (1977) for sedimentation from uniform flow at all ε values investigated in the straight tube. Fluent FPM is the only software package able to accurately predict deposition by diffusion in the straight tube at the Δ value investigated when compared to predictions from Ingham (1975). There is substantial variation in the analytical equations and CFD predictions for deposition by impaction in the bifurcating tube geometry.

In the three generation lung geometry, CFD predictions from CFX are able to accurately predict experimental data at the 7.5 lpm flow rate for the 10 μm particle size with combined impaction and sedimentation and the parabolic velocity profile. Fair to poor correlation was obtained at all other particle sizes at both the 1.5 and 7.5 lpm flow rates. Discrepancies between CFD and theoretical predictions in straight tube and three generation lung geometry are consistent for the sedimentation and diffusion deposition mechanism; therefore, simple straight tube geometry predictions can be used to ascertain the uncertainty in CFD predictions for more complicated geometries.

# Preface

The goal of this research is to explore the accuracy of three CFD software package (Fluent DPM, Fluent FPM, and CFX) in predicting deposition by the sedimentation, molecular diffusion, and impaction mechanisms. Three geometries (straight tube, bifurcating tube, and three generation lung) are utilized to determine if accuracy is effected by geometry. CFD predictions are compared to analytical and empirical equations from three well known Models for deposition in the lung; NCRP Model (United States National Council on Radiation Protection and Measurements, 1997), Trumpet Model (Yu, 1978; Robinson and Yu, 2001), and MPPD Model (Anjilvel and Asgharian, 1995). When possible, deposition efficiencies are compared to experimental data for the same or nearly same geometry.

Chapter 1 provides a brief overview of particle deposition and why this research is necessary. The various deposition mechanisms are introduced and briefly explained. Finally, the work plan and methodology for this research are provided.

Chapter 2 provides a brief introduction to each of the CFD software packages being utilized in this research. The particle tracking algorithms are introduced to show the differences in the various software packages. Limitations and issues encountered with each software package during the research are also provided to assist future graduate students.

Chapter 3 contains background on the lung structure and the development of Weibel's ideal lung model. The dimensions and flow conditions in the ideal Weibel lung geometry are provided. The non-dimensional parameter governing each deposition mechanism studied in this research is presented. The relative influence of each deposition mechanism in terms of the governing non-dimensional parameter is provided for three common breathing conditions; 10 lpm (resting), 20 lpm (light exertion), and 60 lpm (moderate exertion).

Chapter 4 provides background on the three geometries utilized in this research. The physical dimensions, mesh characteristics, and meshing techniques are supplied for of the each geometries.

Chapter 5 presents the sedimentation deposition mechanism. The analytical equations developed by Pich (1972), Wang (1975), Yu, et al. (1977), and Yeh and Schum (1980) to predict deposition by sedimentation are provided. The flow conditions and particle

properties utilized in the straight tube to evaluate sedimentation are provided. CFD predictions for deposition efficiency are compared to the analytical equations for parabolic and uniform velocity profiles.

Chapter 6 presents the diffusion deposition mechanism. Ingham (1975) and Yeh and Schum's (1980) analytical equations for deposition by diffusion are provided. The flow conditions and particle properties utilized in the straight tube to evaluate diffusion are provided. CFD predictions for deposition efficiency are compared to the analytical equations for parabolic and uniform velocity profiles.

Chapter 7 presents the impaction deposition mechanism and compares CFD predictions in the bifurcating tube geometry to Kim and Iglesias' (1989) experimental data for the same flow conditions. Theoretical equations developed by Yeh and Schum (1980), Cai and Yu (1988), and Zhang, et al. (1997) for deposition by impaction are provided. Kim and Iglesias' (1988) experimental data is presented and analysis of the dominate deposition mechanism for each flow rate is conducted. Deposition efficiencies predicted by CFD are compared to the theoretical equations and experimental data for each particle size and flow rate, in which impaction is the most prevalent mechanism, examined by Kim and Iglesias (1989) for the 30° symmetric bifurcation.

Chapter 8 compares experimental data gathered by Dr. Oldham at the University of California, Irvine for the three generation lung geometry to CFD predictions. The experimental data, flow conditions and particle properties are provided. The dominate deposition mechanisms are determine based on predictions from the various theoretical equations utilized in Chapters 5, 6, and 7 for each flow rate and particle size. Total and local deposition predictions from CFD are compared to theoretical and experimental data.

Finally, Chapter 9 presents the conclusions that could be drawn from this research. It also provides several areas for future work.

# Table of Contents

# List of Figures

# List of Tables

# Nomenclature

| | |
|---|---|
| A | Constant in parabolic profile equation |
| B | Constant in parabolic profile equation |
| C | Constant in parabolic profile equation |
| $C_c$ | Cunningham correction factor |
| $C_D$ | Coefficient of drag |
| CFD | Computational Fluid Dynamics |
| D | Diffusion coefficient |
| $D_p$ | Diameter of airway entering the bifurcation |
| DPM | Discrete Phase Model |
| EPA | Environmental Protection Agency |
| F | Sub-equation in Cai and Yu's (1988) impaction equation for uniform flow |
| $F_b$ | Buoyancy force |
| $F_D$ | Force of drag |
| FPM | Fine Particle Model |
| $F_x$ | Other forces acting on a particle in Fluent DPM's particle trajectory equation |
| G | Sub-equation in Cai and Yu's (1988) impaction equation for parabolic flow |
| ICRP | International Commission on Radiological Protection |
| L | Length of a generation of the lung |
| $L_c$ | Critical length at which all particles deposit by sedimentation |
| Ls | Length scale for k-epsilon turbulence solver |
| M | Moments associated with particle motion in Fluent FPM |
| MDE | Moment Dynamics Equation |
| MPPD | Multiple-Path Particle Dosimetry |
| NAAQS | National Ambient Air Quality Standards |
| NCRP | National Council on Radiation Protection and Measurements |
| PIV | Particle Image Velocimetry |
| PRB | Physiologically Realist Bifurcations |
| R | Radius of a generation of the lung |
| R | Radius of a generation of the lung |
| Re | Reynolds number of the flow, $(\rho V D_p / \mu)$ |
| $R_d$ | Radius of the daughter, or generation following the bifurcation |
| $R_p$ | Radius of the parent, or generation entering the bifurcation |
| Stk | Stokes number, ratio of stopping distance to characteristic length, $(\rho_p d_p V C_c / 18 \mu D_p)$ |
| T | Absolute temperature |
| V | Average velocity of fluid (air) |
| $V_f$ | Velocity of the fluid at a particular location |
| $V_p$ | Velocity of the particle |
| $V_{ts}$ | Settling velocity |
| *conv* | Convective transport in Fluent FPM's "Moment Dynamics Equation" |
| $dep_{bif3}$ | Deposition in the bifurcation between generations 3 and 4 |

| | |
|---|---|
| $dep_{bif4}$ | Deposition in the bifurcation between generations 4 and 5 |
| $dep_d$ | Deposition in the daughter |
| $dep_{gen3}$ | Deposition in generation 3 |
| $dep_{gen4}$ | Deposition in generation 4 |
| $dep_{gen5}$ | Deposition in generation 5 |
| $dep_p$ | Deposition in the parent |
| $dep_{tot}$ | Total deposition |
| *diff* | Diffusive transport in Fluent FPM's "Moment Dynamics Equation" |
| $d_p$ | Particle diameter |
| *ext* | External forces in Fluent FPM's "Moment Dynamics Equation" |
| $f_0$ | Sub-equation in Cai and Yu's (1988) impaction equation for parabolic flow |
| $f_1$ | Sub-equation in Cai and Yu's (1988) impaction equation for parabolic flow |
| g | Gravity (9.81 m/s) |
| lpm | Liter/min |
| k | Boltzmann's constant (1.38E-23) |
| $m_p$ | Particle mass |
| t | Time |
| $\alpha_n$ | $N^{th}$ root of the Bessel function |
| $\Delta$ | Diffusion parameter, ratio of residence time to diffusion time, $(LD/R^2V)$ |
| $\delta$ | Stopping distance |
| $\varepsilon$ | Sedimentation parameter, ratio of residence time to settling time, $(3V_{ts}L/8RV)$ |
| $\phi$ | Angle of inclination with respect to the horizontal |
| $\gamma$ | Variable in Wang's sedimentation equations for uphill parabolic flow |
| $\eta_d$ | Diffusion deposition efficiency |
| $\eta_i$ | Impaction deposition efficiency |
| $\eta_s$ | Sedimentation deposition efficiency |
| $\lambda$ | Mean free path (0.066 μm for air) |
| $\mu$ | Dynamic viscosity of air |
| $\theta$ | Bifurcation angle, half the total bifurcation angle for symmetric bifurcations |
| $\rho$ | Density of fluid (air) |
| $\rho_p$ | Density of the particle |
| $\sigma$ | Variable in Wang's sedimentation equations for uphill parabolic flow |
| $\tau$ | Relaxation time |
| $\omega$ | Twice the characteristic length |
| $\zeta$ | Variable in Wang's sedimentation equation for downhill parabolic flow |
| $\varsigma$ | Variable in Wang's sedimentation equations for uphill parabolic flow |

# Chapter 1
# Introduction

## 1.1 Overview of Particle Deposition in the Lung

Particle deposition in the lung is studied numerous ways; analytically, experimentally, empirically, and numerically. Analytic equations are derived from first principles to explain the flow and particle physics in human airways. Experimental methods are utilized to analyze particle deposition and flow physics in human subjects and hollow cast of various lung geometries, which are described below. Particle Image Velocimetry (PIV) is used to analyze velocity profiles for experimental models and better understand the flow physics within the lung. Empirical equations are developed from trends in experimental data to characterize particle deposition and flow physics within the lung. Particle deposition is studied numerically using Computational Fluid Dynamics (CFD) software with particle tracking algorithms.

There are currently several lung geometries that have been used to analyze particle deposition in the lung including: ideal, ideal with physiologically realistic bifurcations (PRB), and replica casts. The most widely used ideal lung geometry was developed by Weibel in 1963. The Weibel geometry was developed based on measurements gathered from actual human lungs. It represents the lung with a series of branching straight tubes, where each tube, or generation as they are referred to, branches into two identical daughter generations. The Weibel ideal lung geometry has 23 generations beginning at the trachea and extending to the alveoli (Weibel, 1963). The model is accepted as the standard for ideal lung geometries and is described in more detail in Section 3.1. There are also PRB ideal lung geometries that utilize realistic geometries at the bifurcations. Additionally, replica casts can be made of actual human lungs.

When studying particle deposition in the lung it is best to integrate analytical, experimental, and numerical data to gain a better understanding of where particles are

depositing and by which mechanisms. Currently, there are few research groups within the United States that are able to produce analytical, experimental, and numerical data for the exact same geometries.

## 1.2 Reasons to Study Particle Deposition

Detailed information concerning how and where particulate matter deposits in the lung is used when examining exposure limits, designing inhaled medication, and studying pulmonary disorders that are a result of airborne pathogens. Such airborne pathogens include, cigarette smoke, diesel particles, allergens like mold spores or dust mites, infectious diseases, and biological weapons. Understanding where and how particles deposit within the lung can help physicians and pharmaceutical companies target medication, improve the accuracy of exposure risk assessments, and provide greater insight into how some respiratory diseases develop and affect the lung.

The Environmental Protection Agency (EPA) established the National Ambient Air Quality Standards (NAAQS) in 1971, due to the associated health risk with particulate matter in the air. The standards are reviewed as needed by scientist at the EPA and adjusted when necessary. On July 1$^{st}$, 2005, the EPA staff scientist released their report on the third review of the NAAQS. The report recommends the regulations be tightened on both fine (less than 2.5 μm) and coarse (less than 10 μm) particles in the air, based on new knowledge of particle behavior and deposition in the lung and associated health risk with certain levels of exposure (United States Environmental Protection Agency, 2005).

The American Lung Association currently estimated that as many as 35 million Americans suffer from one or more chronic lung diseases such as asthma, emphysema, and chronic bronchitis. In 2002, surveys show that approximately 7.5% of adults in the United States report having asthma. It is estimated that 6.1 million Americans with asthma are under 18 years old. The American Lung Association estimates 9.1 million Americans have been diagnosed with chronic bronchitis and another 3.1 million with emphysema (American Lung Association, 2004[a]; American Lung Association, 2004[b]). These lung diseases can flare up or be made worse by exposure to particulate material. These lung diseases can also alter the geometry of the lung. Both of these issues provide several opportunities for research

into accurate deposition and exposure risk assessments for diseases lungs, in addition to on going research for healthy lungs.

## 1.3 Deposition Mechanisms

There are five distinct ways that particles can deposit; sedimentation, diffusion, impaction, interception, and electro-static. Electro-static deposition occurs when electrical charges pull the particles near the walls causing the particles to deposit. Electro-static deposition typically only occurs when there are greater than 30 charges/particle. This is not a condition that is commonly found in the environment (Bailey and Robinson, 2005) and is therefore ignored. Interception occurs when particles hit the walls due to size, rather than inertia, as in impaction. Interception only occurs in large particles (larger than 10 μm) and fibrous particles, both of which are excluded from this research. The other three deposition mechanisms are studied in this research and are explained in greater detail in the following sections.

### 1.3.1 Sedimentation

Sedimentation occurs when gravity acts on a particle and causes it to gradually settle out of the free stream flow. Figure 1.1 shows a graphic of particle deposition due to sedimentation. This gradual settling occurs due to the particle's buoyancy. If the weight of the particle is greater than the buoyant force exerted by the fluid on the particle, it will settle. As the particle settles, it experiences drag from the fluid causing it to quickly reach its terminal or settling velocity, as it is more commonly referred to in particle physics. Sedimentation in the lung primarily occurs with particles larger than 1 μm in diameter. The deposition efficiency is affected by both the geometry and flow conditions utilized (See Sections 3.2.1 and 5.1).

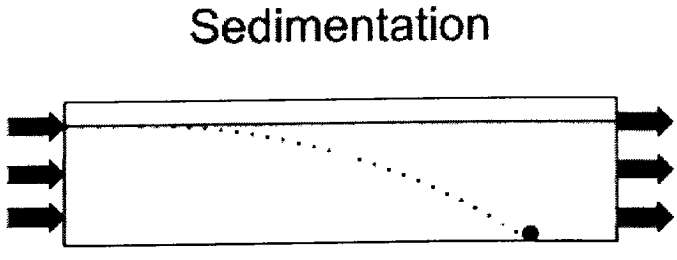


**Figure 1.1. Particle deposition due to the sedimentation mechanism, where gravity is acting downward. Note: The solid line is the streamline and the dotted line is the particle path.**

There are three well known models used to predict total and regional deposition in the lung; the Trumpet Model (Yu, 1978; Chen and Yu, 1993; Robinson and Yu, 2001), the National Council on Radiation Protection and Measurements (NCRP) Model (United States National Council on Radiation Protection and Measurements, 1997), and the Multiple-Path Particle Dosimetry (MPPD) Model (Anjilvel and Asgharian, 1995). The sedimentation equations used in these models are taken from studies listed in Table 1.1. The equations from these models have been selected to evaluate the accuracy of the CFD software packages in predicting deposition by the sedimentation mechanism based on their wide recognition and extensive peer review. These equations are presented in Section 5.1. Other sedimentation equations not compared to in this research are presented in Section 1.4 for completeness.

**Table 1.1. Sedimentation studies used in the Trumpet, NCRP, and MPPD Models.**

| Study | Model(s) Used In | What Equation(s) Predict |
|---|---|---|
| Pich, J. (1972) | Trumpet | Sedimentation from parabolic flow |
| Wang, C.S (1975) | MPPD | Sedimentation for uphill and downhill parabolic flow. |
| Yu, C.P, et al. (1977) | Trumpet | Sedimentation from uniform flow |
| Yeh, H. C. and G. M. Schum (1980) | NCRP | Sedimentation independent of flow conditions |

### 1.3.2 Diffusion

The second deposition mechanism is molecular diffusion, which is due to random motion of the particles within the free stream due to molecular bombardment; this is illustrated in Figure 1.2. There is also turbulent diffusion, which is caused by turbulent eddies in the free stream flow acting on the particles. This mechanism is not studied due to the Reynolds numbers present in the lung at normal breathing conditions (see Section 3.1) for flow conditions in the lung. Diffusion in the lung typically occurs for particles less than 0.1 μm in diameter, due to their small mass relative to that of the molecules and higher mobility compared to larger particles (Hinds, 1999). Particles larger than 1.0 μm usually have negligible deposition by diffusion in the lung.

The diffusion equations used in the Trumpet Model, NCRP Model, and MPPD Model programs are taken from studies listed in Table 1.2. The equations from these models have been selected to evaluate the accuracy of the CFD software packages in predicting deposition by diffusion based on their wide recognition and extensive peer review. These equations are

presented in Section 6.1. Other diffusion equations not compared to in this research are presented in Section 1.4 for completeness.

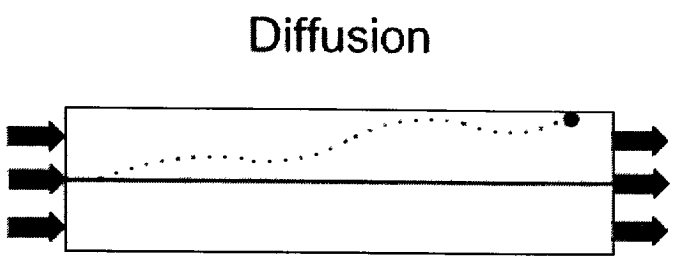


**Figure 1.2. Particle deposition due to the molecular diffusion mechanism. Note: The solid line is the streamline and the dotted line is the particle path.**

**Table 1.2. Diffusion studies used in the Trumpet, NCRP, and MPPD Models.**

| Study | Model(s) Used In | What Equation(s) Predict |
|---|---|---|
| Ingham, D. B. (1975) | Trumpet & MPPD | Diffusion from uniform and parabolic flow |
| Yeh, H. C. and G. M. Schum (1980) | NCRP | Diffusion for laminar and turbulent flow conditions |

### 1.3.3 Impaction

The final deposition mechanism studied in this research is impaction. Impaction is due to the inertial effects of the particle. Impaction occurs when a streamline changes direction due to a bifurcation or obstruction. When the streamline curves the particle's inertia can cause the particle to deviate from the streamline and intercept a wall, resulting in impaction. This is illustrated in Figure 1.3. Impaction is more common with larger particles, which lack the mobility of smaller ones, but depending on the angle of the bifurcation and flow conditions, can occur at almost all particle sizes.

The impaction equations used in the Trumpet Model, NCRP Model, and MPPD Model are taken from studies listed in Table 1.3. These equations used in these models have been selected to evaluate the accuracy of the CFD software packages in predicting deposition by impaction based on their wide recognition and extensive peer review. These equations are presented in detail in Section 7.1. Other impaction equations not compared to in this research are presented in Section 1.4 for completeness.

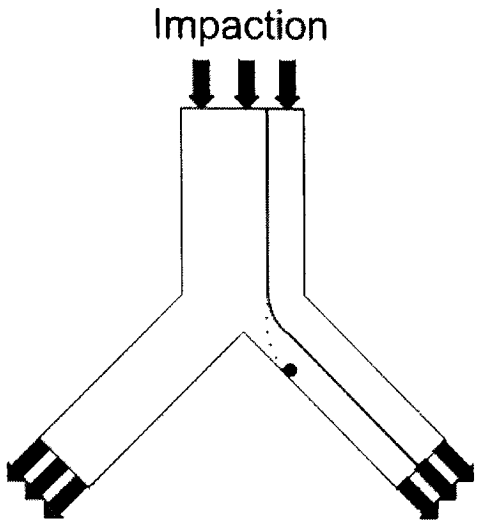


**Figure 1.3. Particle deposition due to the impaction mechanism. Note: The solid line is the streamline and the dotted line is the particle path.**

**Table 1.3. Impaction studies used in the Trumpet, NCRP, and MPPD Models.**

| Study | Model(s) Used In | What Equation(s) Predict |
|---|---|---|
| Yeh, H. C. (1974) | NCRP | Impaction in a bend for uniform flow conditions* |
| Cai, F. S. and C. P. Yu (1988) | MPPD | Impaction in a bifurcation from uniform** and parabolic flow |
| Zhang, et al. (1997) | Trumpet | Impaction in a bifurcation from uniform and parabolic flow inlet velocity profiles |

* Utilized for both parabolic and uniform flow conditions in the NCRP Model.
**Only parabolic flow equation is utilized in the MPPD model (Anjilvel and Asgharian, 1995; Asgharian, et al., 2001); both equations are utilized in this research.

## 1.4 Literature Review

Particle deposition in the lung has been actively studied since the 1960s and 1970s. There was earlier research and development of analytical equations in the 1930s, 1940s, and 1950s; however many of these studies have been proven to be invalid in more recent research. As mentioned in Section 1.1, there are several different ways to study particle deposition. The primary focus of this research is CFD research, and therefore the literature review will focus on other CFD research that has been done. The literature review includes discussion of some of the key experimental studies that have been conducted, as well as analytical equations and deposition programs not being utilized in this research. An overview of the research groups discussed in the literature review is provided in Table 1.4

The CFD research is presented in Section 1.4.1. The experimental research is presented in Section 1.4.2. Finally, the deposition programs and analytical equations not utilized in this research are presented in Section 1.4.2. An overview of the research groups being discussed in the following sections and the type of research each is involved is provided in Table 1.4.

**Table 1.4 Overview of key research groups involved in particle deposition. Groups are arranged alphabetically by research group.**

| Research Group / Location | Key Members or Publishing Authors | Time of Publications | Type of Research |
|---|---|---|---|
| Aerosol Research Laboratory (later U.S. EPA) | Kim, C. S., A. J. Iglesias, and D. M. Fisher | 1980s - Present | Experimental |
| Chemical Industry Institute of Toxicology and Duke University | Asgharian, B. and S. Anjilvel | 1990s - Present | CFD and Deposition Programs/Analytical Equations |
| Hahn-Meitner – Institut fur Kernforschung | Martin D. and W. Jacobi | 1970s | Experimental |
| Institute of Environmental Medicine | Cohen, B. S., M. Lippmann, T. L. Chan, and R. G. Sussman | 1980s - Present | Experimental and Deposition Programs/Analytical Equations |
| Institute of Occupational Medicine | Johnston, J. R., K. D. Isles, and D. C. F. Muir | 1970s | Experimental |
| Interuniversitair Reactor Instituut | Ferron, G. A. | 1970s | Experimental |
| KFKI Atomic Energy Research Institute and University of Salzburg | Balashazy, I., W. Hofmann, and Y. Heistracher | 1990s - Present | CFD and Deposition Programs/Analytical Equations |
| Lovelace Biomedical and Environmental Research Institute | Cheng, Y. S. and H. C. Yeh | 1980s | CFD and Experimental |
| Pohang Institute of Science and Technology | Lee, J. W. and J. H. Goo | 1990s | CFD |
| State University of Buffalo | Yu, C. P, Y. K. Chen, R. J. Robinson, and Y. Shaw | 1970s - Present | Deposition Program/Analytical Equations and CFD |
| University of California, Irvine | Phalen, R. F., M. J. Oldham, R. C. Mannix | 1990s - Present | Experimental |
| University of North Carolina , North Carolina State University, and U.S EPA | Zhang, Z., C. Kleinstreuer, and C. S. Kim | 2000 - Present | CFD |
| University of Rhode Island | Zhang, G. Y. and R. Lessman | 1990s | CFD |

### 1.4.1 CFD Research

CFD has been utilized to examine particle deposition in the lung since the 1990s. There are several groups which have focused their research on improving CFD predictions in various lung geometries, while others have merely explored the technique to gain insight on flow conditions and deposition patterns. This literature review will focus on articles related to CFD predictions in bifurcating tubes and lung geometries within the human tracheobroncial region. Articles related to flow conditions, oral and nasal airways, and other mammals airways structures are not relevant to this research and are therefore not included here. A more detailed analysis of relevant articles is provided in Appendix A.

One of the biggest issues with CFD research currently is that very few groups are able to compare results to experimental data for the exact same geometry. It is common to alter the geometry for ease of computer modeling, limitations of computer systems, or lack of knowledge of the experimental geometry. However, as many groups have concluded geometry plays a key role in deposition efficiency, especially if impaction is the key deposition mechanism (Balashazy, et al., 2002; Balashazy, et al., 1996; Comer, et al., 2000; Lee, J. W., et al., 1996; Shi, et al., 2004). With much of the CFD research being focused on multi-generation systems where impaction is a contributing deposition mechanism, changes in geometry can greatly effect the deposition efficiencies measured.

Zhang, et al. (1997), Asgharian and Anjilvel (1994), Balashazy and Hofmann (1993) [a], Balashazy and Hofmann (1993) [b], and Lee and Goo (1992) have all compared Kim and Iglesias' (1989) experimental data for a bifurcating tube to bifurcating tube geometries that have been modified from Kim and Iglesias' (1989) original geometry. Asgharian and Anjilvel (1994) and Lee and Goo (1992) both utilized square cross sections with different dimensions then those provided by Kim and Iglesias (1989) to show that square bifurcating tubes were provide similar results to circular tubes with similar flow conditions. Both Balashazy and Hofmann (1993) [a, b] articles utilize a bifurcation very similar to Kim and Iglesias (1989), but with a sharp carina region and shorter parent and daughter tubes then those utilized to obtain the experimental data. In these articles the data for this geometry is also compared to a second bifurcation with a wide bifurcation region. Zhang, et al. (1997) utilizes a bifurcation geometry similar to Balashazy and Hofmann's (1993) wide bifurcation. None of these studies were able to predict Kim and Iglesias' (1989) deposition efficiencies at

all flow rates or particle sizes investigated by Kim and Iglesias (1989). Several of these studies did not even utilize the flow conditions or particle sizes investigated by Kim and Iglesias (1989).

There are several variations of Weibel's ideal lung geometry that have been studied in CFD over the years. Shi, et al. (2004) and Comer, et al. (2000) have investigated non-planar or asymmetric lung geometries. Both articles concluded that the asymmetric geometry had little effect on the deposition efficiencies observed at more than one flow rate and particle size. In both of these studies it was found that variations in inlet conditions had a more significant impact on the total deposition than variations in geometry. The research teams at KFKI Atomic Energy Research Institute and University of Salzburg has been working with a model of generations three through five of the ideal Weibel lung geometry that utilizes physiologically realistic bifurcations (PRB) (Hoffman, et al., 2003; Balashazy, et al., 2002; Balashazy, et al., 1996). This lung geometry is utilized in this research.

The majority of the CFD studies conducted have focus on inpiratory flow; however there are a handful of studies that investigate expiratory flow (Balashazy, et al., 2002; Balashazy and Hofmann, 1993). Nearly all CFD studies investigate both parabolic and uniform flow conditions. However uniform flow in some studies actually describes developing flow conditions because the walls are defined as no slip boundaries, which allows the velocity profile to develop as it passes through the geometry.

It should be noted that several research groups are using external programs or user refined functions to track particle deposition in order to obtain reasonable accuracy compared to theoretical predictions and experimental data (Asgharian and Anjilvel, 1994; Hoffman, et al., 2003; Balashazy, et al., 2002; Balashazy, et al. 1996; Balashazy and Hofmann, 1993 [a, b]; Shi, et al., 2004; Comer, et al., 2000). The programs and user defined function typically utilized established analytical and empirical equations for various deposition mechanisms. They also commonly utilize higher order numerical techniques than those employed in commercial CFD software packages. The documented external programs utilized to determine particle deposition are described briefly Section 1.4.3.

### 1.4.2 Experimental Research

The purpose of this section is to provide brief introduction to some of the types of experimental data that has been gathered for human lung geometries and bifurcations. These articles and research groups are well known and frequently referenced in CFD, analytical, and empirical analysis.

Ferron (1977) measured deposition in a glass model of the ideal human airway geometry from the mouth to generation six of the lung. This experimental data has been referenced by several of the regional and total deposition models and was one of the earliest large lung geometries studied experimentally.

Diffusion in hollow cast has been studied by Smith, et al. (2001), Cohen, et al. (1990, 1987), and Martin and Jacobi (1972). Cohen's (1990; 1987) research on deposition by diffusion in the first six generations of the lung is some of the best known. This research has been utilized by Ingham (1991; 1984) to improve Ingham's (1975) diffusion equations for entrance regions and Cohen and Asgharian (1990) to develop empirical equations for Ultrafine particle deposition.

Johnston, et al. (1977) researched deposition in a bend. These results have been compared to some impaction studies in bifurcation geometries due to the shortage of impaction studies in simple bifurcations. Empirical relations developed from this study were also originally utilized in the Trumpet model before Zhang, et al. (1997) was added.

Kim and Iglesias (1989) [a, b] are the most commonly utilized bifurcation experiment when evaluating CFD predictions for a bifurcation geometry. The studies researched deposition during inhalation and expiration in several bifurcations geometries with different angles, orientations, and allowable flow area. Kim and Fisher (1999) investigated deposition in a glass model of generations three through five of the ideal lung. This study is commonly utilized to compare regional and total deposition in ideal three generation lung models. More research has been conducted by Kim in recent years with the focus on Ultrafine and nanoparticles.

Schlesinger and Lippmann's research group has investigated particle deposition in hollow casts (1977; 1976; 1972) and conducted in vivo research with human subjects (1980; 1976). These hollow cast studies are utilized for comparison in some CFD studies.

The research group at the University of California, Irvine has focused their research on particle deposition in hollow cast of the adult and child tracheobroncial generations (2000; 1997). They have also conducted several studies investigating the effects of side stream smoke in the tracheobroncial region (1998; 1994).

### 1.4.3 Additional Deposition Programs and Analytical Equations

The Trumpet Model, NCRP Model, and MPPD Model are currently three of the best known models for evaluating particle deposition in the whole lung; there are still other models currently being utilized. The best known of these models is the International Commission on Radiological Protection (ICRP) (1993) Human Respiratory Tract Model. The ICRP Model utilizes analytical equations and experimental data to predict particle deposition. The ICRP Model was adopted in 1993 and is more commonly referenced in publications outside the United States. The oldest model still referenced was developed by Landahl (1950). Some of the assumptions used to develop this model have been disproved, but the ideas within this model contributed to the modern Trumpet Model.

There are two documented external particle tracking codes that have been utilized in several CFD studies to improve the accuracy of total and regional deposition efficiencies. Both programs utilize the velocity vectors from a solved flow field to calculate particle trajectories. Koblinger and Hofmann (1990) details the program utilized by the KFKI Atomic Energy Research Institute and University of Salzburg. This program utilizes Monte Carlo techniques to generate particles and evaluate particle deposition. Asgharian and Anjilvel (1994) details the program utilized by the Chemical Industry Institute of Toxicology and Duke University. The program utilizes the fourth order Runge-Kutta method to evaluate the equations of motion.

Finally, there have been analytical and empirical equations developed for diffusion and sedimentation. The countless empirical equations for impaction are not presented, since most of these equations have either been improved in recent years or are not used for comparison to CFD studies. Yeh (1974), Cohen and Asgharian (1990), and Broday (2004) developed analytical and empirical equations for the diffusion mechanism. Some of the assumptions utilized by Yeh (1974) to derive his equation from heat transfer principles have been proven invalid. Cohen and Asgharian (1990) and Broday (2004) are newer models and

have not yet been integrated into any of the major programs. Ingham (1991; 1984) contain slight improvements to Ingham's (1975) diffusion equations. Most of these changes are rather complex and have little effect on deposition at most flow rates and particle sizes. Yeh (1974) also derived a sedimentation equation from heat transfer principles; this model too had some invalid assumptions and was never utilized by the larger scientific community (Yeh and Schum, 1980).

## 1.5 Statement of Work

### 1.5.1 Purpose

There was a time when it took someone with a Ph.D in CFD to use commercial CFD software packages. In recent years, commercial CFD software packages have become increasingly easier to use, allowing individuals from various backgrounds and a few hours or days of training to utilize the software. As the knowledge base of people utilizing CFD software packages widens it becomes increasingly important that the software provide accurate results for the actual flow conditions. This new breed of user does not always have the technical expertise to adjust the settings which control the numerical solvers. Additionally, as problems become more complicated there is not always experimental data to calibrate a model with, therefore it is even more important that CFD software packages accurately predict particle deposition for realistic flow conditions. Otherwise, these models lose their validity.

The purpose of this research is to determine which of three commercially available CFD software packages provides the most accurate prediction of particle deposition for the sedimentation, diffusion, and impaction deposition mechanisms. As discussed in Section 1.4, there are still issues with accurately predicting total and local deposition in commercial CFD software packages for all particle sizes and breathing conditions when compared to experimental data for identical geometries and flow conditions.

There are three objectives of this research. The first objective is to determine the influence of each deposition mechanisms in all 23 generations of the ideal Weibel lung geometry for resting (10 lpm tracheal flow rate), light exertion (20 lpm tracheal flow rate), and moderate exertion (60 lpm tracheal flow rate) breathing conditions. The second objective is to identify which deposition mechanisms each software package advertises being

capable of predicting and evaluate each using a straight tube and single bifurcation geometry. The third objective is to utilize the most accurate software package for each mechanism to evaluate the deposition in the three generation lung geometry for resting (1.5 lpm at generation 3 or 12 lpm tracheal flow rate) and active (7.5 lpm at generation 3 or 60 lpm tracheal flow rate) breathing conditions. The third objective is completed for both total and local deposition in each software package, when feasible.

The results of this research will be used to improve CFD deposition predictions in replica lung geometries at Rochester Institute of Technology.

### 1.5.2 Approach to Research

The accuracy of three CFD software packages' particle tracking algorithms is investigated; Fluent Discrete Phase Model (DPM) version 6.1.22, Fluent Fine Particle Model (FPM) version 1.0.4, and CFX by ANSYS version 5.7.1. Three geometries are explored; a straight tube, a bifurcating tube, and a PRB ideal lung geometry of generations three through five, which will be referred to as the three generation lung geometry. A more detailed explanation of each of these geometries and mesh utilized is provided in Chapter 4.

To evaluate the accuracy of each software package, each deposition mechanism is isolated and evaluated independently by using either the straight tube or bifurcating tube geometry. The accuracy of each software package is evaluated by comparing predicted values to analytical and/or experimental data.

The straight tube is utilized to isolate the sedimentation and diffusion deposition mechanisms over the full range of analytical deposition efficiencies. Sedimentation is isolated by turning off Brownian motion and enabling gravity (-9.81 m/s in the z-direction or buoyant conditions). Diffusion is isolated by turning on Brownian motion and setting gravity to zero (running non-buoyant conditions). The flow conditions selected allow for the full range of deposition efficiencies to be explored for particles between 2 nm and 10 μm, which are inhalable sizes, while providing Reynolds numbers for the free stream flow comparable to those found in the lung at physically realistic breathing conditions. These conditions are discussed in more detail in Chapters 3, 5, and 6. The bifurcating tube is utilized to isolate the impaction deposition mechanism, by setting gravity to zero (running non-buoyant conditions) and turning off Brownian motion. The flow conditions selected are based on existing

experimental data for the geometry published by Kim and Iglesias (1989). These conditions are discussed in more detail in Chapter 7. Finally, the three generation lung geometry is utilized to verify the accuracy of the deposition efficiencies predicted by the CFD software packages in a multi-bifurcation system, based on the results of objective two. The predicted deposition efficiencies from the various software packages are compared to experimental data for the identical geometry and flow conditions obtained by Dr. Oldham at the University of California, Irvine. These conditions are discussed in more detail in Chapters 3 and 8. The details of the work plan and scope of the research are provided in Section 1.5.3.

### 1.5.3 Scope of Research

The scope of the research is limited by the capabilities of each of the CFD software packages and the geometries being examined. Table 1.5 provides the deposition mechanisms each software package advertises having capabilities to track. These capabilities are discussed in more depth in Chapter 2, where the numerical methods employed by each software package are presented. As can be seen in Table 1.5, only Fluent DPM advertises having the capability to track all three deposition mechanisms being investigated in this research.

**Table 1.5. Particle tracking capabilities advertised by each CFD software package.**

| | Fluent DPM | Fluent FPM | CFX |
|---|---|---|---|
| Sedimentation | Yes | Yes | Yes |
| Molecular Diffusion | Yes | Yes | No |
| Impaction | Yes | No | Yes |

Table 1.6 provides the flow conditions and particle sizes utilized in each of the software packages for the straight tube geometry to investigate the sedimentation and diffusion deposition mechanisms. For each case, both parabolic and uniform velocity profiles are tested. In addition for the FPM diffusion runs, a developing velocity profile is also tested. The conditions selected and results related to the sedimentation deposition mechanism are presented in Chapter 5. The conditions selected and results related to the diffusion deposition mechanism are presented in Chapter 6.

Table 1.7 provides the flow conditions and particle sizes investigated in each of the software packages to investigate the impaction deposition mechanism. The values selected are based on existing experimental data for a glass bifurcating tube published by Kim and

Iglesias (1989). This study was chosen because the flow conditions indicated that impaction is the dominant mechanism and is isolated from the diffusion and sedimentation mechanisms, for most flow conditions and particle sizes (see Section 6.2). Combined impaction and sedimentation is investigated at the 4 lpm flow condition, where sedimentation is also a contributing deposition mechanism (theoretically >2% of the total experimental deposition). Diffusion is not investigated in the bifurcation, since all particles investigated are 3 μm and larger, and outside the diffusion range. In each case, uniform, parabolic and developing inlet velocity profiles are tested. The deposition efficiencies in the bifurcating tube geometry are presented in Chapter 7 for all flow conditions and particle sizes.

**Table 1.6 Conditions run in the straight tube geometry in each of the CFD software packages.**

| Geometry | Deposition Mechanism Investigated | Fluent DPM | | Fluent FPM | | CFX | |
|---|---|---|---|---|---|---|---|
| | | Flow Conditions | Particle sizes (μm) | Flow Conditions | Particle sizes (μm) | Flow Conditions | Particle sizes (μm) |
| Straight Tube | Sedimentation | 0.03 lpm Uniform & Parabolic | 0.03, 0.3, 1, 2, 3, 4, 5, 6, 7, 7.5, 8, 8.5, 9 | 0.03 lpm Uniform & Parabolic | 0.003, 0.03, 0.3, 1, 2, 3, 4, 5, 6, 7, 7.5, 8, 8.5, 9 | 0.03 lpm Uniform & Parabolic | 0.03, 0.3, 1, 2, 3, 4, 5, 6, 7, 7.5, 8, 8.5, 9 |
| | Diffusion | 0.03 lpm Uniform & Parabolic | 0.02, 0.03, 0.08, 0.3, 0.8 | 0.03 lpm Uniform & Parabolic | 0.003, 0.004, 0.006, 0.008, 0.01, 0.02, 0.03, 0.08, 0.3, 0.8 | | |
| | | | | 0.03 lpm Developing | 0.003, 0.008, 0.03, 0.08, 0.3 | | |

Table 1.8 contains the deposition mechanisms, flow conditions, and particle sizes investigated in each of the software packages for the three generation lung geometry. The flow conditions and particle sizes selected are based on existing experimental data for the identical model of generations three through five of the ideal PRB lung geometry, provided by Dr. Oldham at the University of California, Irvine. The deposition mechanisms selected are based on the experimental flow conditions and the relative influence of each mechanism. The relative influence of each deposition mechanism is presented in Section 8.3. The CFD software packages used are based on the results of objective two, which are presented in

**Table 1.7. Conditions run in the bifurcating tube geometry in each of the CFD software packages.**

| Geometry | Deposition Mechanism Investigated | Fluent DPM | | Fluent FPM | | CFX | |
|---|---|---|---|---|---|---|---|
| | | Flow Conditions | Particle sizes (μm) | Flow Conditions | Particle sizes (μm) | Flow Conditions | Particle sizes (μm) |
| Bifurcating Tube | Impaction | 4 lpm Uniform, Parabolic, & Developing | 3, 5, 7 | | | 4 lpm Uniform, Parabolic, & Developing | 3, 5, 7 |
| | | 8 lpm* Uniform, Parabolic, & Developing | 3, 5, 7 | | | 8 lpm* Uniform, Parabolic, & Developing | 3, 5, 7 |
| | | 12 lpm* Uniform, Parabolic, & Developing | 3, 5, 7 | | | 12 lpm* Uniform, Parabolic, & Developing | 3, 5, 7 |
| | Impaction & Sedimentation | 4 lpm Uniform, Parabolic, & Developing | 3, 5, 7 | | | 4 lpm Uniform, Parabolic, & Developing | 3, 5, 7 |

*Both the laminar and k-epsilon solvers are investigated. K-epsilon solver is investigated for 1%, 5%, and 10% turbulence intensities for all inlet conditions.

**Table 1.8. Conditions run in three generation lung geometry in each of the CFD software packages.**

| Geometry | Deposition Mechanism Investigated | Fluent DPM | | Fluent FPM | | CFX | |
|---|---|---|---|---|---|---|---|
| | | Flow Conditions | Particle sizes (μm) | Flow Conditions | Particle sizes (μm) | Flow Conditions | Particle sizes (μm) |
| Three Generation Lung Geometry | Impaction | 1.5 lpm Uniform & Parabolic | 0.44, 1, 3, 10 | | | 1.5 lpm Uniform & Parabolic | 0.44, 1, 3, 10 |
| | | 7.5 lpm Uniform & Parabolic | 0.44, 1, 3, 10 | | | 7.5 lpm Uniform & Parabolic | 0.44, 1, 3, 10 |
| | Impaction & Sedimentation | 1.5 lpm Uniform & Parabolic | 0.44, 1, 3, 10 | | | 1.5 lpm Uniform & Parabolic | 0.44, 1, 3, 10 |
| | | 7.5 lpm Uniform & Parabolic | 0.44, 1, 3, 10 | | | 7.5 lpm Uniform & Parabolic | 0.44, 1, 3, 10 |
| | Diffusion | | | 1.5 lpm Developing | 0.44, 1, 3, 10 | | |
| | | | | 7.5 lpm Developing | 0.44, 1, 3, 10 | | |

Chapters 5, 6 and 7. The experimental data and the results of these simulations are presented in Chapter 8.

# Chapter 2

# Introduction to CFD Software Packages Utilized

There are three commercially available CFD software packages investigated in this research; Fluent DPM (Discrete Phase Model) version 6.1.22, Fluent FPM (Fine Particle Model) version 1.0.4, and CFX 5.7.1. Each software package is capable of tracking particle deposition for several mechanisms. A brief introduction to each software package, their particle tracking algorithms, and some limitations encountered in this research are provided in the following sections. Fluent DPM is discussed in Section 2.1, Fluent FPM is discussed in Section 2.2, and CFX is discussed in Section 2.3.

## 2.1 Fluent – Discrete Phase Model (DPM)

Fluent DPM is a common CFD software package developed by Fluent Inc. It uses the Lagrangian solution technique to predict the trajectory of discrete phase particles. The particle trajectories are calculated by integrating the force balance equation defined as,

$$\frac{dV_p}{dt} = F_D + \frac{g}{\rho_p} + F_x \text{ (Fluent Inc., 2003),} \qquad \textbf{Equation (2.1)}$$

where $V_p$ is the velocity of the particle, t is time, $F_D$ is the force of drag ($F_D$ is defined as a negative value), g is gravity, $\rho_p$ is the density of the particle, and $F_x$ is other forces, including but not limited to Brownian diffusion and "virtual mass." In Fluent DPM, Brownian motion is handled as random external forces applied to particles. The force balance equation can either be solved with the momentum and energy equation for the continuum flow (by turning on Interactions with the Continuous Phase) or after the momentum and energy equations have converged. Selecting Interactions with the Continuous Phase allows the particles to interact with the fluid flow and affect the flow solution. For this research, Interactions with the Continuous Phase is not utilized. In preliminary research, there was little variation in the

deposition efficiency for the significantly longer computation time required to obtain particle deposition by utilizing the Interactions with the Continuous Phase option.

For this research, the 3D-double precision, segregated implicit solver is utilized for steady flow conditions. The inlet boundary is defined as a velocity inlet and the outlet boundaries are defined as either pressure outlets or outflows. The pressure outlet boundary cannot be utilized for mutli-outlet geometries, so the outflow boundary is utilized.

In Fluent DPM, particles can be defined several different ways; single particles, as a group, by file, or one of seven other methods. For this research, particles are defined by file, since 50,000 particles are being injected at a time. The files are created by a Java script utilized previously with a 7-generation lung model (Robinson, et al., 2005) and compiled in J-Builder SE 7, a software package developed by Borland Software Corporation. The Java script randomly locates the particles in a circle of defined radius and y-position. The files contain the particles position, initial velocity (0 m/s), size, temperature and other necessary information for Fluent DPM to calculate the trajectory of each particle. From correspondence with Fluent Inc.'s technical support it has been determined that particles should not be injected in the first element within the flow field. There are occasionally issues with the grid resolution in the first element that can interfere with particle injection, by the second element all issues should be resolved and particles can be injected. Additionally, it is recommended that particle not be injected any closer than one element from walls to avoid immediate deposition.

Fluent DPM is only capable of tracking and creating spherical particles. The Fluent 6.1 User's Guide (Fluent Inc, 2003) states the software is capable of tracking submicron particles, but does not specify the smallest particle size that can be tracked. In this research, particles smaller than 20 nm are not able to be tracked by Fluent DPM. Particles smaller than 20 nm result in a particle fate of "evaporated", this is explained in the next paragraph.

In Fluent DPM, there are five possible particle fates; "escaped", "incomplete", "trapped", "evaporated", or "aborted". The "escaped" fate is a result of particles leaving through an escape boundary, the inlet and outlets in this research. The "incomplete" fate is a result of the maximum number of time steps being exceeded by the particle. The maximum number of time steps is defined in Fluent DPM by the Max. Number of Steps input and cannot exceed 10E9, this was sufficient for all runs conducted in this research. The

"trapped" fate is a result of particle tracking terminating at a trap boundary, the walls in this research. Particles are considered trapped when they get within one particle diameter of a trap boundary, which is part of why it is suggested to inject particles at least one element from the wall boundary. The "evaporated" fate is a result of particles evaporating or being too small to track. The "aborted" fate is a result of an error in calculating the particle trajectory. The error is typically a result of round off issues and can be resolved by modifying the length scale. (Fluent Inc., 2003)

Fluent DPM has a few different ways to handle local deposition. If a small number of particles are being tracked, the particle tracks can be displayed in Fluent DPM using the Particle Tracks feature. This feature provides a visual representation of the particles traveling through the flow field and where each terminates. The particle tracks method of observing local deposition typically becomes too cumbersome when more than 20 to 100 particles are tracked depending on the size of the flow field. Fluent DPM can also write the particles position at the various boundaries and defined planes to a text file, using the Report feature. This is useful for large numbers of particles or when the exact location of the particle termination is critical. The Report feature is utilized to obtain the local deposition data presented in Section 8.5. More information on how Fluent DPM tracks particles or analyzes the flow field can be found in the Fluent 6.1 User's Guide (Fluent Inc., 2003).

## 2.2 Fluent – Fine Particle Model (FPM)

Fluent FPM is a relatively new CFD software package, at the time this research was started there were only five users in the United States including Rochester Institute of Technology. The software is an add-on to the basic Fluent DPM package developed by Chimera Technologies Inc. Fluent FPM claims to be able to more accurately track particles less than 10 μm in diameter than Fluent DPM.

Fluent FPM utilizes an Eulerian solution technique to predict the particle trajectories. Particle trajectories are calculated by integrating the "Moment Dynamics Equation (MDE)" (Whitby, et al. 2003). The MDE is defined as,

$$\frac{\partial M_{j.k}}{\partial t} = conv_{j.k} + ext_{j.k} + diff_{j.k} \text{ (Whitby, et al., 2003),} \qquad \textbf{Equation (2.2)}$$

for the deposition mechanisms investigated in this research. In Equation (2.2), M is the moments associated with particle motion due to external and internal forces, t is time, *conv* is convective transport, *ext* is transport by "external" forces, and *diff* is diffusive transport. The convection term is the same basic transport equation utilized in Fluent DPM. Sedimentation is one of the external forces included in Fluent FPM. Impaction currently cannot be calculated in Fluent FPM, since momentum forces are not included for this mechanism. In Fluent FPM, Brownian diffusion is handled as an additional random particle velocity. In Fluent FPM, the MDE equation can only be solved with the momentum and energy equation, because of the Eulerian solution technique being utilized. There is no option of solving the particle trajectory equation after the flow solution has converged like in Fluent DPM.

For this research, the 3D-double precision, segregated implicit solver is utilized for steady flow conditions. Chimera Technologies Inc. recommends only the double precision solver be utilized with Fluent FPM (Whitby, et al., 2003). The inlet boundary is defined as a velocity inlet and the outlet boundaries are defined as either pressure outlets or outflows. The pressure outlet boundary cannot be utilized for mutli-outlet geometries, so the outflow boundary is utilized.

Fluent FPM is designed to handle large groups of particles; it is not possible to track single particles. Fluent FPM is only capable of tracking spherical particles. Fluent FPM will allow for particles as small as 1 nm to be tracked. Particles are defined in Fluent FPM in the boundary conditions panel for the inlet by a particle diameter, lognormal distribution of particle size, and the number of particles in a cubic meter. For this research a lognormal distribution of 1.1 is utilized, this is as close to a uniform particle size distribution Fluent FPM will allow. The number of particles is defined as 50,000 particles per cubic meter, through personal correspondence with Evan Whitby at Chimera Technologies Inc. it was determined this value is comparable to the 50,000 particles utilized in Fluent DPM and CFX.

Particle deposition in Fluent FPM is determined by dividing mass flux values at various boundaries. Additionally, because Fluent FPM tracks a group of particles rather then individual particles there is limited local deposition data that can be obtained. Fluent FPM will plot the change in concentration in the flow field or at a boundary. More information on how Fluent FPM tracks particles or analyzes the flow field can be found in Fine Particle Model (FPM) for Fluent (Whitby, et al., 2003).

## 2.3 CFX

CFX is a common CFD software package developed by ANSYS Inc. The Lagrangian tracking method is utilized to calculate the particle trajectories within the flow field. The particle tracking algorithm utilized by CFX for the deposition mechanisms explored in this research is defined as,

$$m_p \frac{dV_p}{dt} = \frac{1}{8}\pi\rho d_p^2 C_D \left|V_f - V_p\right|\left(V_f - V_p\right) + F_b \text{ (ANSYS Inc., 2003),} \qquad \textbf{Equation (2.3)}$$

where $m_p$ is the particle mass, $V_p$ is the particle velocity, t is time, $\rho$ is the density of the fluid, $d_p$ is the particle diameter, $C_D$ is the coefficient of drag, $V_f$ is the fluid velocity at the particle's position, and $F_b$ is the buoyancy force. CFX is not capable of calculating diffusion by Brownian motion; only turbulent diffusion has been built into the complete particle trajectory equation. The particle trajectory equation can either be solved with the momentum and energy equation for the continuum flow (by utilizing the Fully Coupled option) or after the momentum and energy equations have converged (by utilizing the One Way Coupled option). The Fully Coupled option allows the particles to interact with the flow fluid and affect the flow solution. CFX does not recommend using this option when a large number of particles are being tracked (ANSYS Inc., 2003). For this research, the One Way Coupled option is utilized.

To track particles in CFX, it must be a steady state flow solution; tracking particles in transient flow is currently not built into the commercial CFX software package. The inlet boundaries are defined by a velocity profile. The outlet boundaries are all defined as a constant pressure.

CFX utilizes discrete particles that are created within the software. The number of particles, particle diameter, whether there is a size distribution, and position scheme are defined. There are several different position schemes, which can be utilized to control the particle location at the boundary where they are injected. For this research, 50,000 particles are injected at the inlet boundary, with a specified diameter, no size distribution, and the uniform, which means random, scheme to position the particles.

CFX is capable of accounting for particle shapes other than spherical in its calculations. A shape correction factor and equivalent aerodynamic diameter can be defined in order to obtain particle behavior for fibers and other shapes. CFX does not specify the

smallest particles that can successful be tracked. In this research particles as small as 30 nm have been tracked without any issues. However, since smaller particle sizes are in the diffusion range, and diffusion is not included in the commercial tracking algorithm; smaller particles are currently not required in CFX.

CFX reports the number of particles that enter the flow field, leave at an outlet, are trapped at a boundary, encounter integration errors, and exceed the time or integration limit. Issues with particles exceeding the time and integration limit can typically be resolved by adjusting the maximum number of integration steps or tracking time in the solver controls.

In CFX, local deposition can be plotted with particle tracks similar to Fluent DPM. This is again effective for small numbers of particles, but too cumbersome for the 50,000 particles being investigated in this research. Efforts are being made to work with CFX's technical support to develop a script that will export the particles ending position from CFX. At this point in time the computational resources are not available to report particle positions for 50,000 particles without exceeding memory or time limitations on the available computers used for this research. More information on how CFX tracks particles or analyzes the flow field can be found in the CFX 5.7.1 User's Manual (ANSYS Inc., 2003).

# Chapter 3

# Flow Conditions and Dominate Deposition Mechanisms in the Lung for Various Breathing Conditions

The ideal Weibel lung geometry was developed in 1963 by Ewald R Weibel. The geometry utilizes statistical data from actual autopsies to divide the lung into 23 generations starting at the trachea. Weibel assumed dichotomous branching, where every parent generation has two symmetrical daughter branches. It has been known since the late 1800s that this is not actually the case at all generations; however Weibel is still the most widely accepted standardized lung geometry. Figure 3.1 shows a cast of a human lung. Figure 3.2 shows a graphic explaining the Weibel lung geometry and the various regions of the lung.

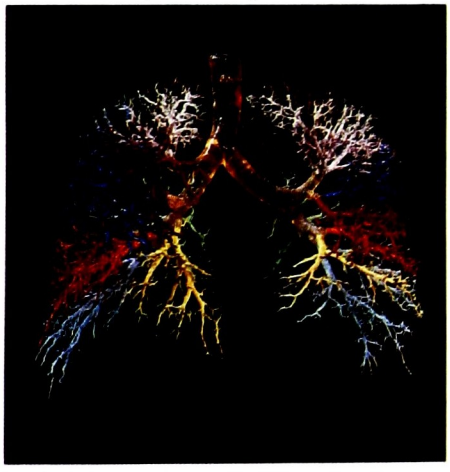

**Figure 3.1 Lung cast of an actual human lung, Sebel, et al. (1985).**

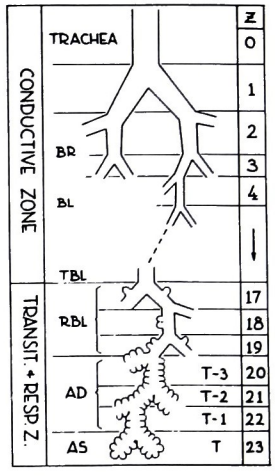


**Figure 3.2. Weibel lung geometry, Crystal, et al. (1997).**

## 3.1 Geometry & Flow Conditions

Weibel provided the diameter, length, cross sectional area, volume, and number of each per generation for the Ideal lung geometry. Figure 3.3 shows generation length and diameter for all generations (0-23) of the Ideal Weibel lung geometry. Based on the dimensions of the Ideal Weibel lung geometry flow rates and Reynolds number are determined in each generation for 10 lpm (resting), 20 lpm (light exertion), and 60 lpm (moderate exertion) breathing conditions. The three flow rates chosen are well documented breathing rates, which correspond with conditions typically investigated in particle deposition research for the lung. Figure 3.4 contains the flow rate in each generation based on 10 lpm, 20 lpm, and 60 lpm breathing conditions at the trachea, generation 0. Figure 3.5 contains the Reynolds number in each generation based on 10 lpm, 20 lpm, and 60 lpm breathing rates at the trachea, generation 0. The Reynolds number drops down below 1.0 near the end of the conducting airways which are considered to end at generation 16. The drop in flow rate and Reynolds number is expected here, since this is where respiration actually takes place and oxygen molecules diffuse into the blood stream.

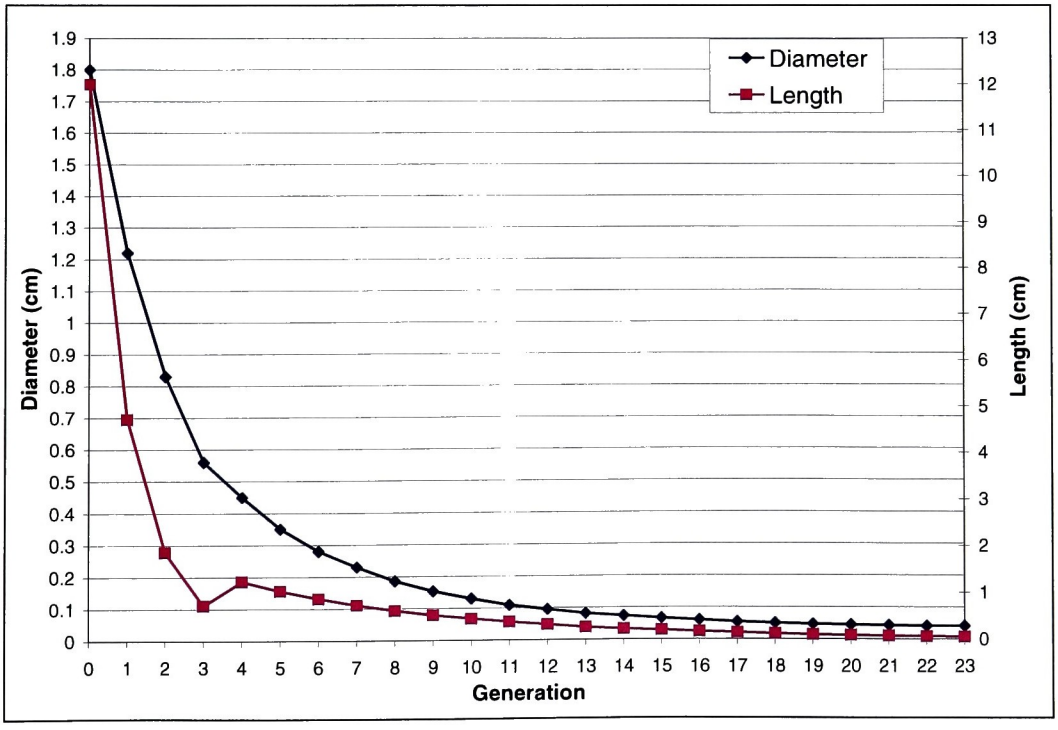


**Figure 3.3. Diameter and length of each generation, 0-23, of the Ideal Weibel geometry, where generation 0 is the trachea.**

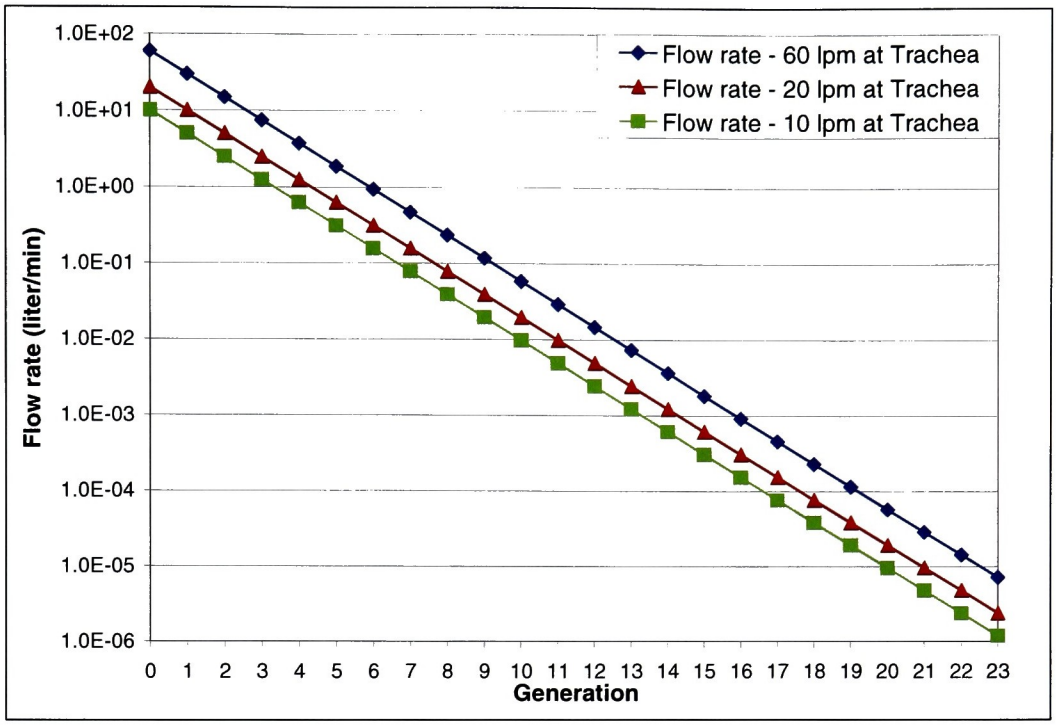


**Figure 3.4. Flow rate for each generation of the Ideal Weibel lung geometry for various breathing conditions, where generation 0 is the trachea.**

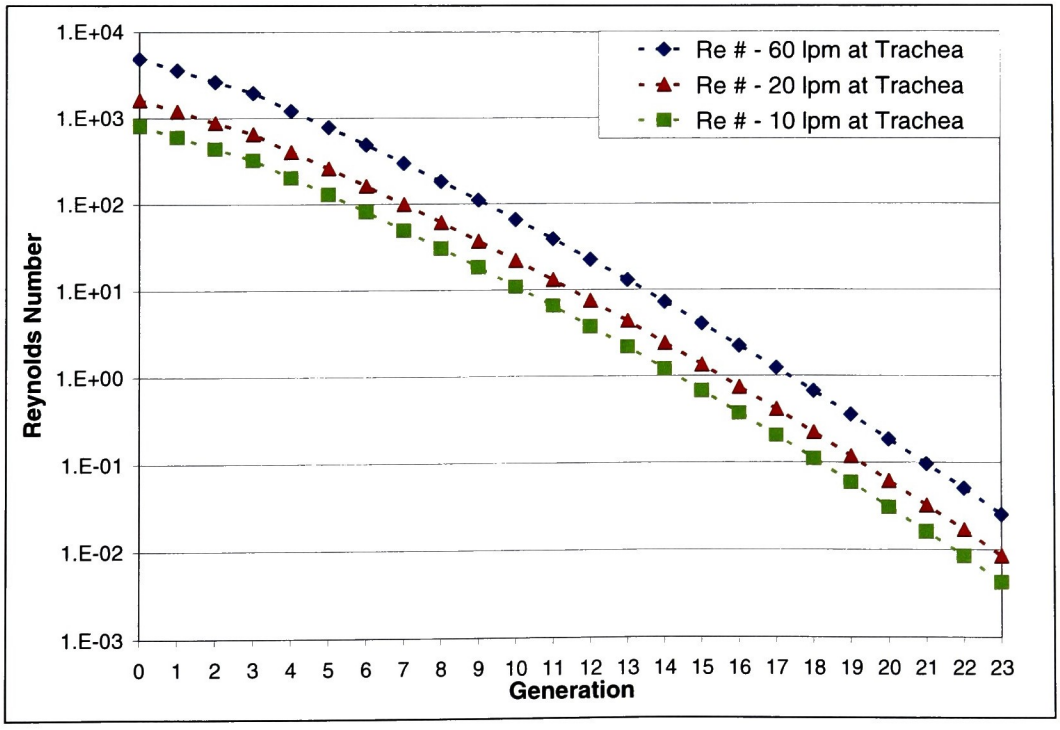


**Figure 3.5. Reynolds number in each generation of the Ideal Weibel lung geometry for various breathing conditions, where generation 0 is the trachea.**

## 3.2 Deposition Mechanisms in the Ideal Weibel Lung Model

### 3.2.1 Sedimentation

The sedimentation deposition mechanism is governed by a non-dimensional parameter ε. ε is the ratio of residence time to settling time and is defined in its most general form by,

$$\varepsilon = \frac{\text{residence time}}{\text{settling time}} = \frac{L/V}{R/V_{ts}} = \frac{LV_{ts}}{RV}, \qquad \textbf{Equation (3.1)}$$

where L is the length of a generation of the lung, $V_{ts}$ is the settling velocity, R is the radius of a generation of the lung, and V is the average velocity of air in a generation of the lung.

In 1972, Pich added a scaling factor to Equation (3.1), making ε defined as,

$$\varepsilon = \frac{3V_{ts}L}{8RV}. \qquad \textbf{Equation (3.2)}$$

Equation (3.2) is currently the most commonly utilized definition for ε. Figure 3.6, Figure 3.7, and Figure 3.8 show ε values, as defined by Equation (3.2), for generations 0 to 23 of the Weibel lung geometry for 10 lpm, 20 lpm, and 60 lpm breathing conditions, respectively.

Based on Pich's (1972) deposition efficiency equation for sedimentation from parabolic flow, measurable sedimentation will only occur for ε values greater than 1.0E-2. For ε values less than 1.0E-3 sedimentation will result in less than 0.2% of the injected particles depositing. When ε values are greater than 1 all injected particles should deposit by the sedimentation mechanism. Yu, et al. (1977), Wang (1975), and Yeh and Schum's (1980) deposition efficiency equations for sedimentation have limits on the same orders of magnitude. Pich (1972) and Yu, et al. (1977) are used for evaluation, since they each provide the most information regarding the nature of their equations and the sedimentation mechanism, see Section 5.1. Sedimentation is a dominate deposition mechanism for slower breathing conditions, larger particles and in the later generations of the lung where air is moving slower.

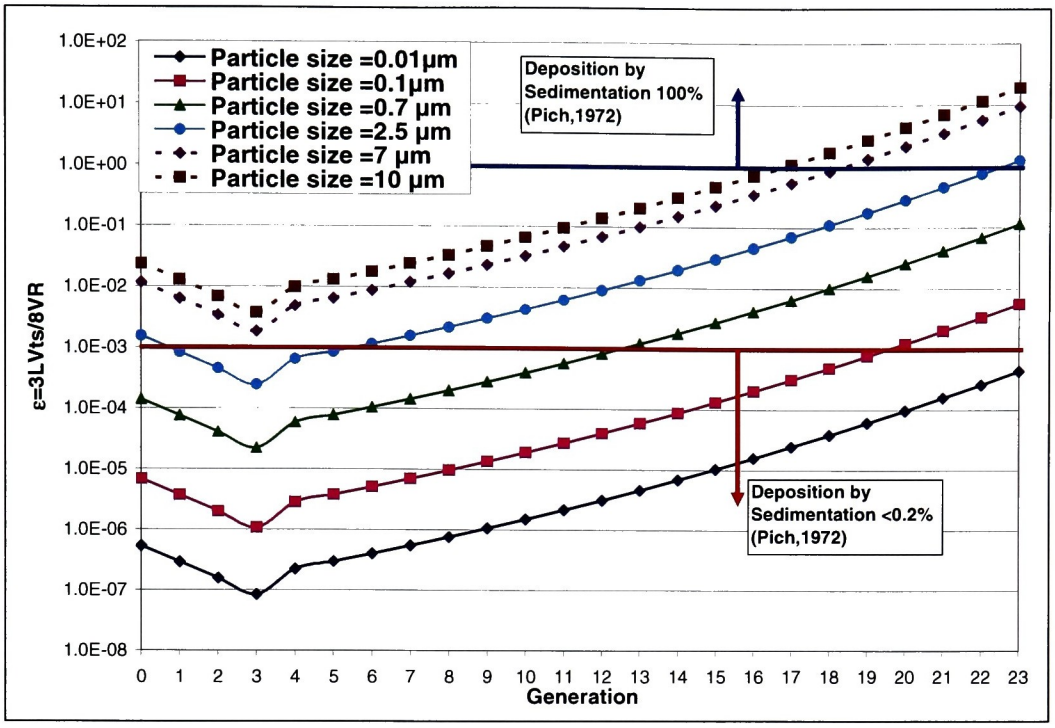


**Figure 3.6. ε values for generations 0-23 of the Weibel lung geometry for 10 lpm breathing conditions at the trachea, where generation 0 is the trachea.**

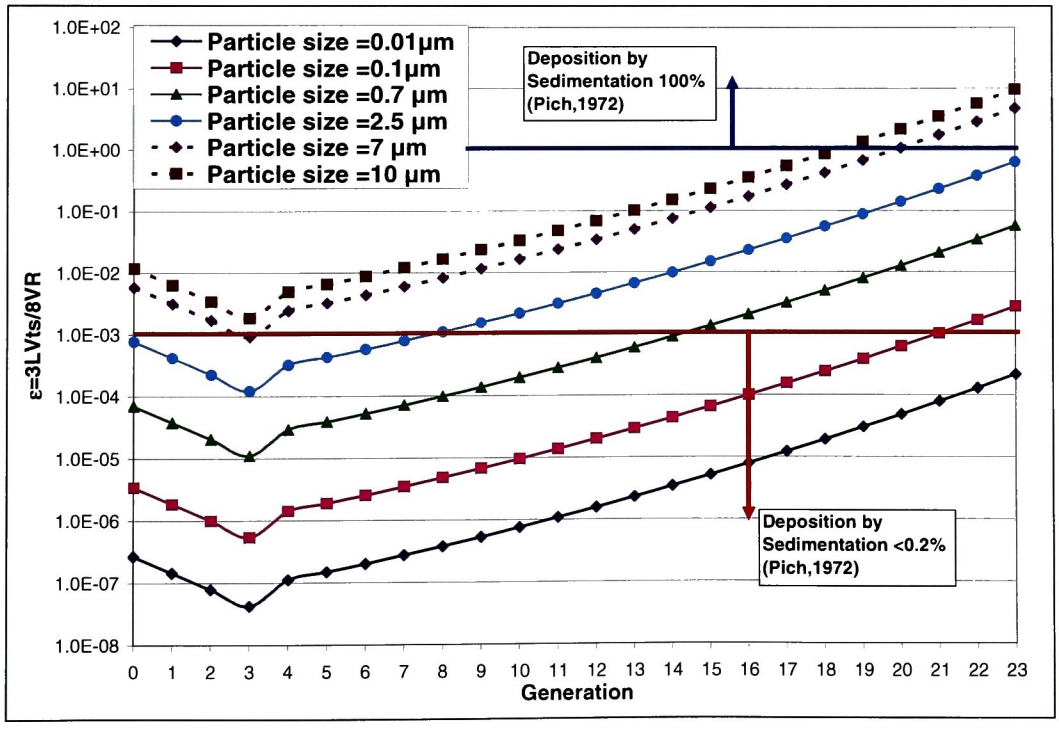


**Figure 3.7. ε values for generations 0-23 of the Weibel lung geometry for 20 lpm breathing conditions at the trachea, where generation 0 is the trachea.**

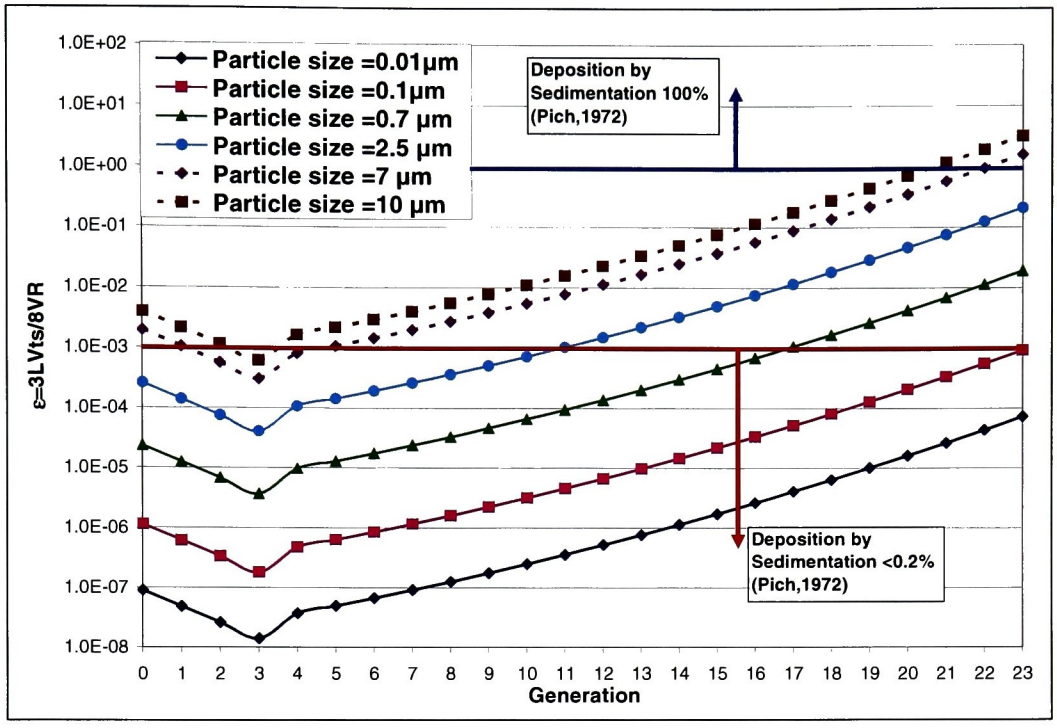


**Figure 3.8. ε values for generations 0-23 of the Weibel lung geometry for 60 lpm breathing conditions at the trachea, where generation 0 is the trachea.**

### 3.2.2 Diffusion

The diffusion deposition mechanism is governed by the non-dimensional parameter Δ. Δ is the ratio of residence time to diffusion time and is defined in its most general form as,

$$\Delta = \frac{\text{residence time}}{\text{diffusion time}} = \frac{L/V}{R^2/D} = \frac{LD}{R^2 V}, \qquad \textbf{Equation (3.3)}$$

where L is the length of a generation of the lung, D is the diffusion coefficient, R is the radius of a generation of the lung, and V is the velocity in a generation of the lung. Figure 3.9, Figure 3.10, and Figure 3.11 show Δ values for generations 0 to 23 of the Weibel lung geometry for 10 lpm, 20 lpm, and 60 lpm breathing conditions, respectively.

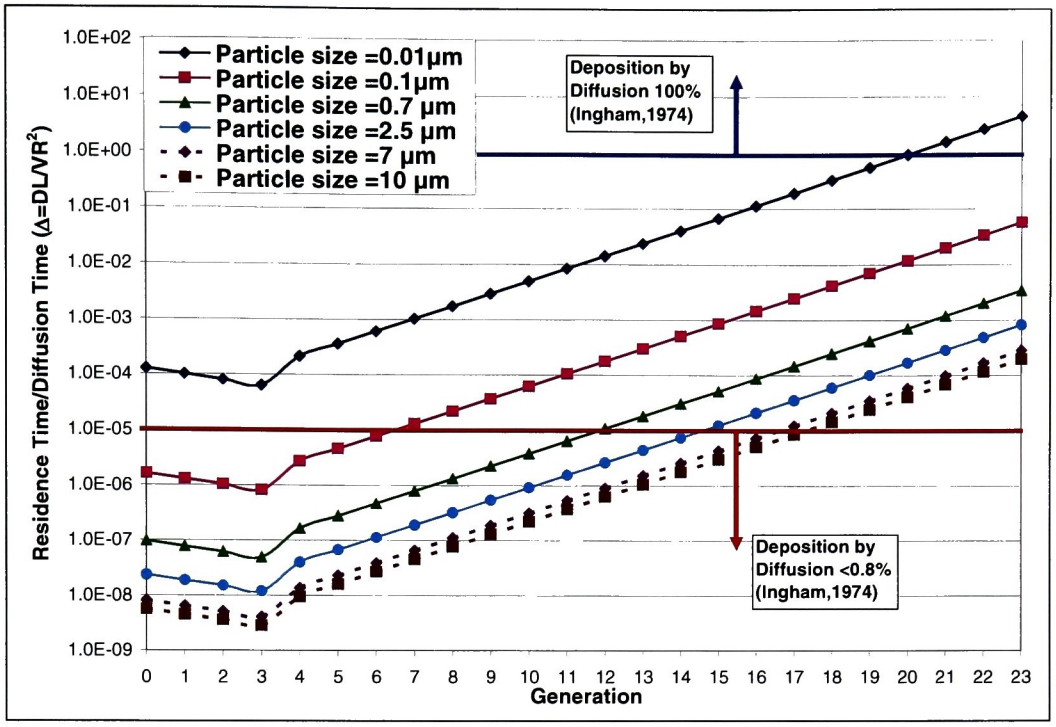


**Figure 3.9. Δ values for generations 0-23 of the Weibel lung geometry for 10 lpm breathing conditions at the trachea, where generation 0 is the trachea.**

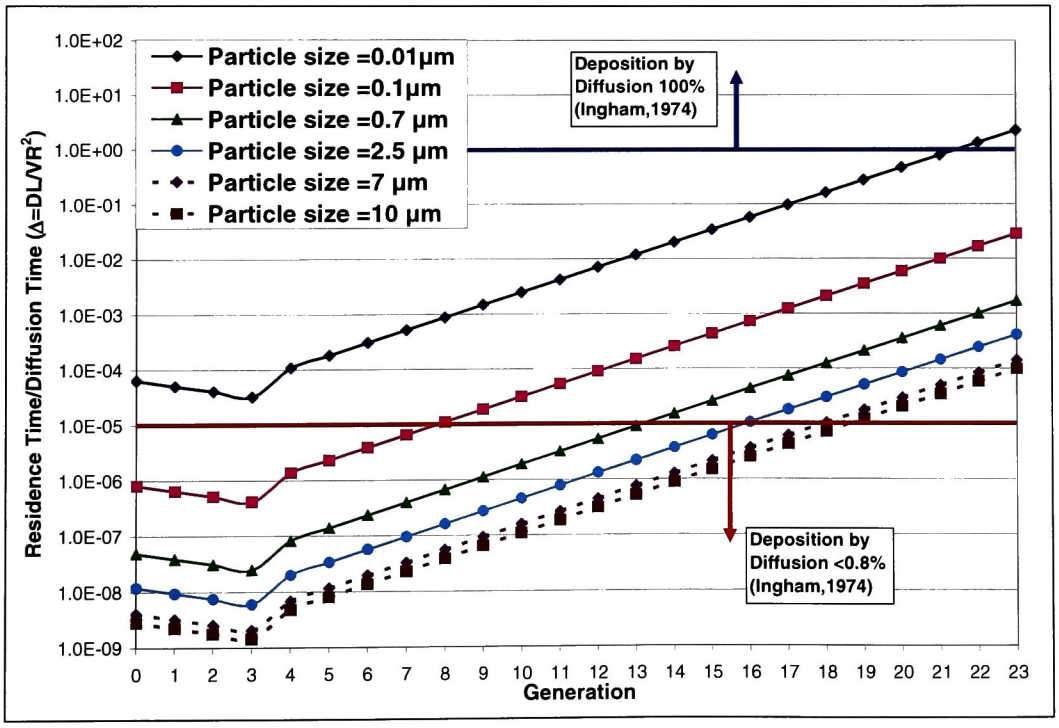


**Figure 3.10. Δ values for generations 0-23 of the Weibel lung geometry for 20 lpm breathing conditions at the trachea, where generation 0 is the trachea.**

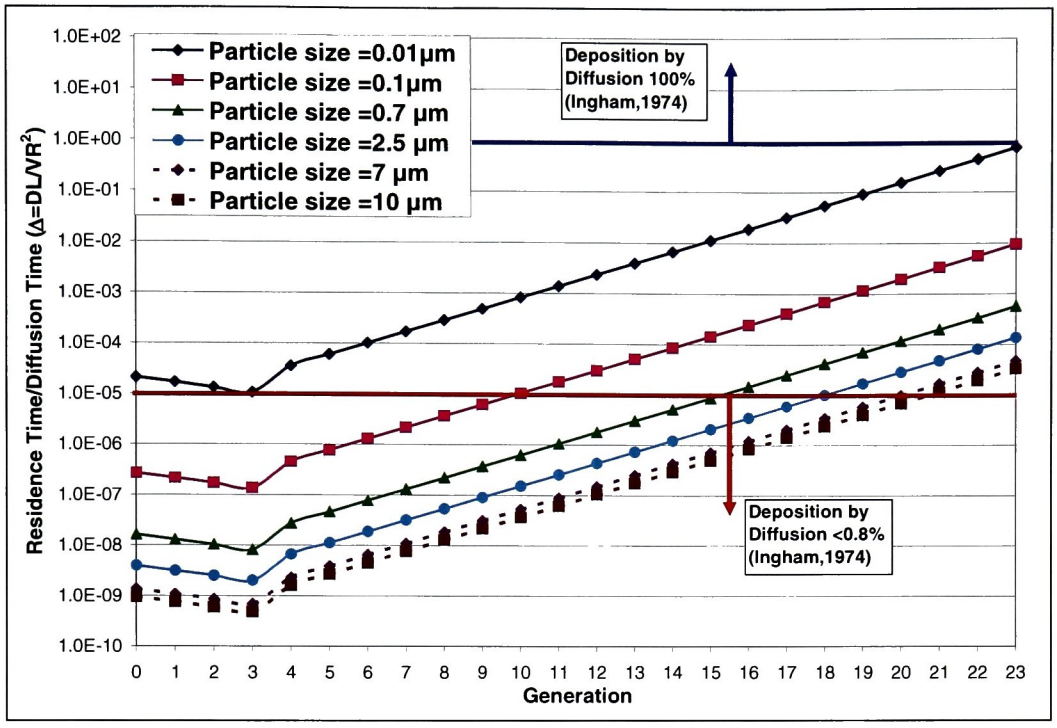


**Figure 3.11. Δ values for generations 0-23 of the Weibel lung geometry for 60 lpm breathing conditions at the trachea, where generation 0 is the trachea.**

Based on a deposition equations created by Ingham (1972), measurable deposition by diffusion will only occur for Δ values greater than 1E-5. For Δ values less than 1E-5, less than 0.32% of the injected particles will deposit by the diffusion mechanism from parabolic flow. In the case of uniform flow less than 0.71% of the injected particles will deposit when Δ values are less than 1E-5. When Δ values are greater than 1, all injected particles theoretically deposited by the diffusion mechanism. Diffusion has a larger impact in the later generations of the lung and for smaller particles at lower breathing rates.

For the generations of the lung in the conduction zone (Generations 0-16) diffusion has minimal measurable effect on deposition for all particle sizes.

### 3.2.3 Impaction

Impaction is governed by the Stokes number. The Stokes number is the ratio of stopping distance to the characteristic length and is defined in its most general form as,

$$Stk = \frac{\text{stopping distance}}{\text{characteristic length}} = \frac{\delta}{\omega/2}, \qquad \textbf{Equation (3.4)}$$

where the characteristic length is determined by the generation entering the bifurcation, or parent. For the geometries utilized in this research, ω is the diameter of the parent generation or $D_p$ and the characteristic length is the radius of the parent generation or $R_p$. The characteristic length is dependant on the cross section of the generation entering the bifurcation. If a non-circular cross section is utilized the definition of ω will change. The stopping distance is defined as,

$$\delta = \int_0^{\theta} V\tau \sin\theta d\theta, \qquad \textbf{Equation (3.5)}$$

where V is the particle velocity, τ is relaxation time, and θ is the angle the particle travels. The Stokes number is generally solved for flow into a flat plate, where θ is 90°, resulting in the Stokes number being defined as,

$$Stk = \frac{\rho d_p V C_c}{18\mu D_p}, \qquad \textbf{Equation (3.6)}$$

where ρ is the density, $d_p$ is the particle diameter, V is the average velocity of the particle, Cc is the Cunningham slip correction factor, μ is the dynamic viscosity, and $D_p$ is the diameter of the airway entering the bifurcation. This form of the Stokes number is typically used in theoretical equations for deposition in the lung, with angle corrections being included in the equations.

Figure 3.12, Figure 3.13, and Figure 3.14 show the Stokes numbers for the bifurcations into generations 1 to 23 of the Weibel lung geometry for 10 lpm, 20 lpm, and 60 lpm breathing conditions, respectively. Equations developed by Zhang, et al. (1997), Cia and Yu (1988), and Yeh's Bend Model (1974) all predict less than 0.1% deposition by impaction when the Stokes number is less than 1E-3 and 100% deposition by impaction when the Stokes number is greater than 1. For all breathing conditions examined impaction is highest at the bifurcation from generation three to four. Additionally, the Stokes number never reaches 1 for the breathing conditions examined.

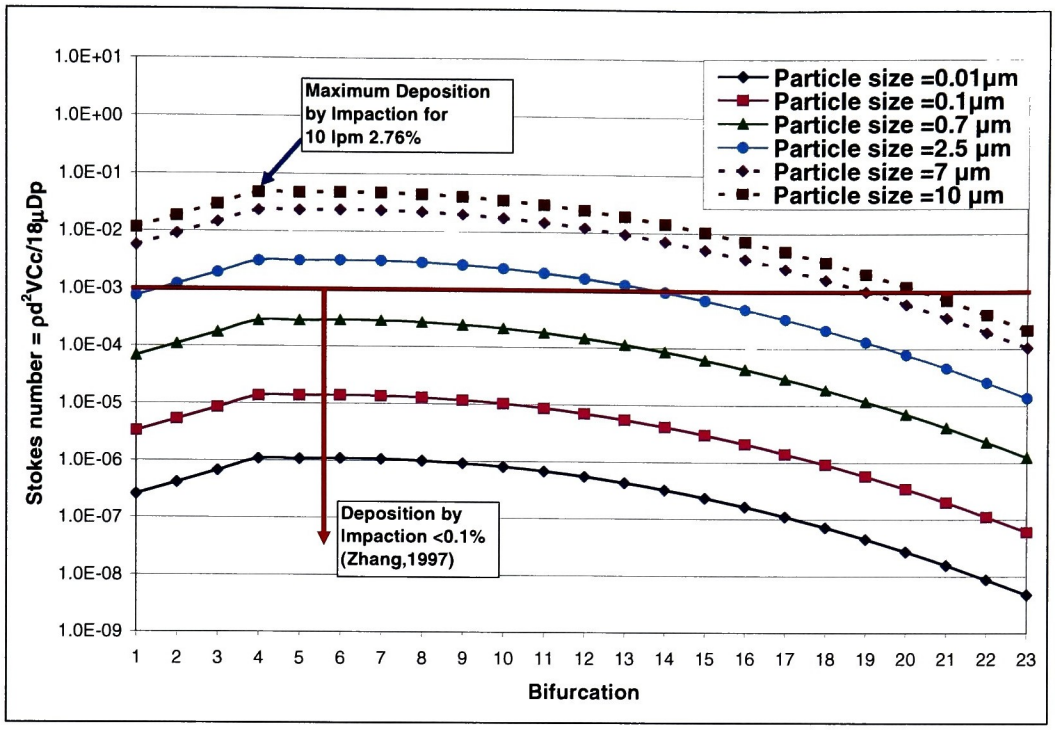


**Figure 3.12. Stokes number values for generations 0-23 of the Weibel lung geometry for 10 lpm tracheal flow rate, where bifurcation 1 is the bifurcation from the trachea to generation 1.**

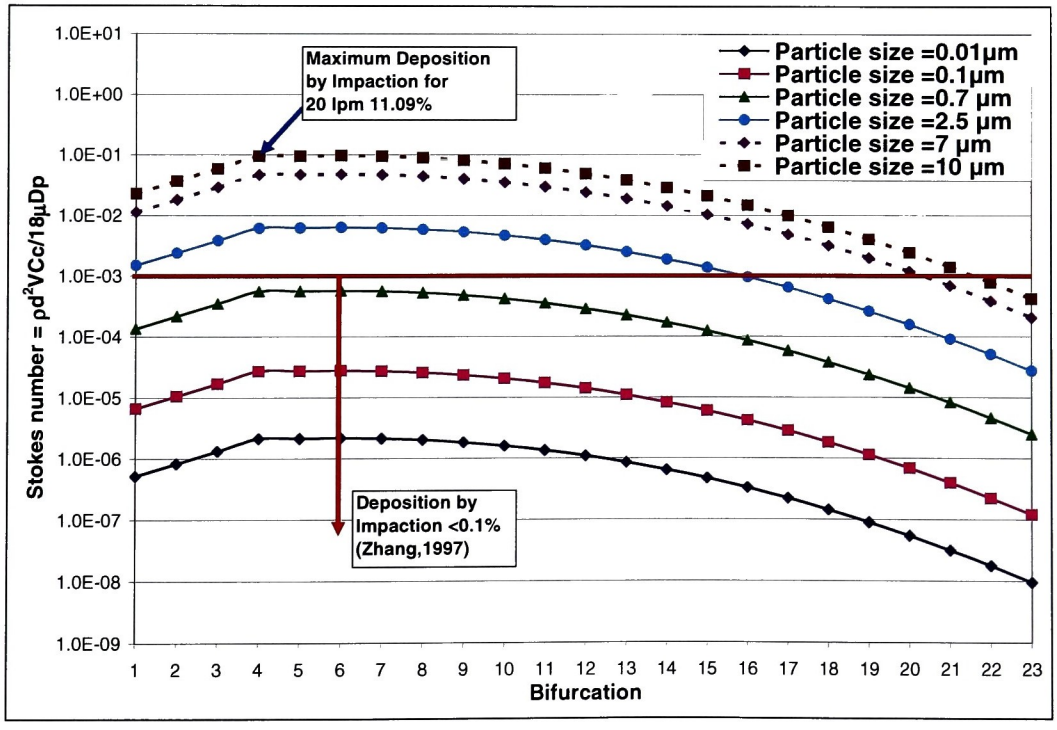


**Figure 3.13. Stokes number values for generations 0-23 of the Weibel lung geometry for 20 lpm tracheal flow rate, where bifurcation 1 is the bifurcation from the trachea to generation 1.**

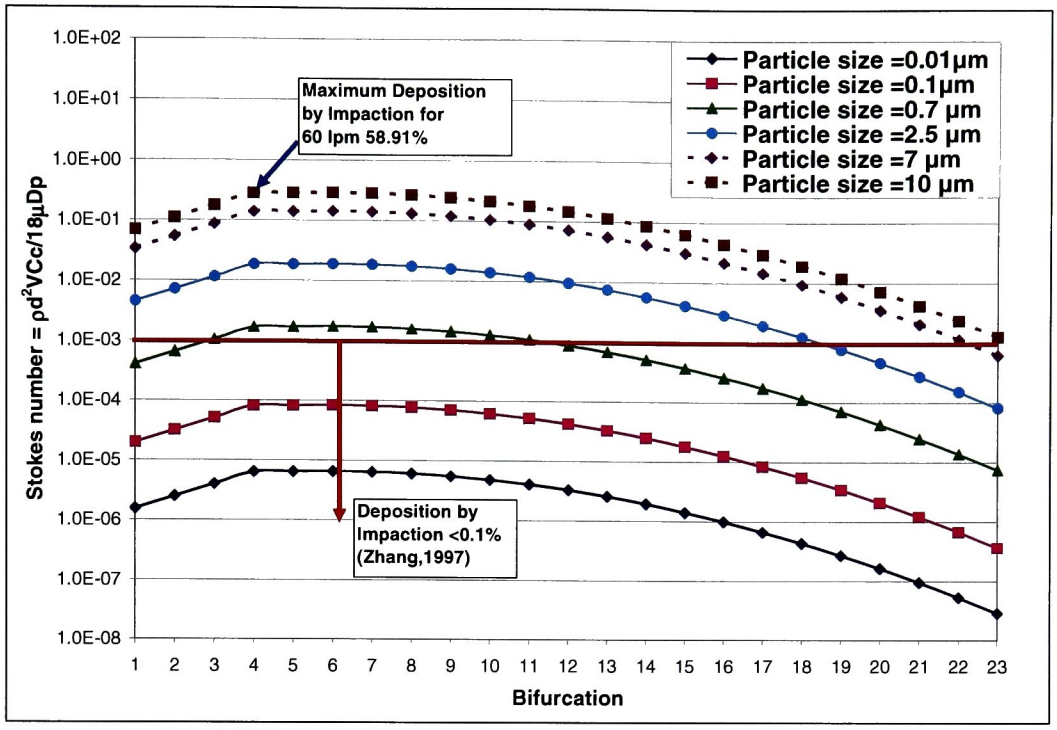


**Figure 3.14. Stokes number values for generations 0-23 of the Weibel lung geometry for 60 lpm tracheal flow rate, where bifurcation 1 is the bifurcation from the trachea to generation 1.**

# Chapter 4

# Model Geometries

There are three geometries which are being explored in this research; a straight tube, a bifurcating tube, and the three generation lung geometry of generations three through five of an ideal lung (Weibel Model A) with physiologically realistic bifurcations (PRB). The straight tube and bifurcating tube were created as part of this research; the three generation model was obtained from previous research originally conducted at the University of Salzburg, Austria and continued at the University of California Irvine and Rochester Institute Technology. The physical dimensions, how each of the geometries was created, and mesh utilized are presented in the following sections. The straight tube geometry is presented in Section 4.1, the bifurcating tube is presented in Section 4.2, and the three generation geometry is presented in Section 4.3. The straight tube and bifurcating tube meshes have been optimized for skew and checked for grid independence as part of this research.

## 4.1 Straight Tube Model

The straight tube geometry utilized in this research was designed to allow for deposition efficiencies between 0% and 100% to be obtained for the sedimentation and diffusion deposition mechanism for inhalable particles at the lower limit of Reynolds numbers seen in generations three through five of the lung, see Sections 5.2.1 and 6.2.1.

The straight tube geometry was created and meshed in Gambit. The geometry was drawn in meters and oriented with flow in the positive y-direction. A schematic of the geometry with dimensions is contained in Figure 4.1. The volume was created using a cylindrical primitive with radius 0.01 m and length 1.0 m.

The final mesh applied to the straight tube geometry is shown in Figure 4.2. The face mesh on each end of the straight tube is shown in Figure 4.3. The geometry was meshed first with an edge mesh on the circular faces of 30 intervals at a ratio of 1. An edge mesh of 100 intervals at a ratio of 1 was applied to the length of the straight tube volume. A boundary

mesh was applied to the edge of one of the circular faces extending into the flow with characteristics described in Table 4.1. A hex cooper volume mesh of size 0.01 m was applied to the straight tube creating 239,956 elements, see Figure 4.2.

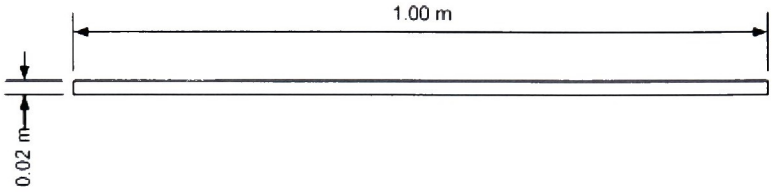


**Figure 4.1 Schematic of straight tube geometry with dimensions.**

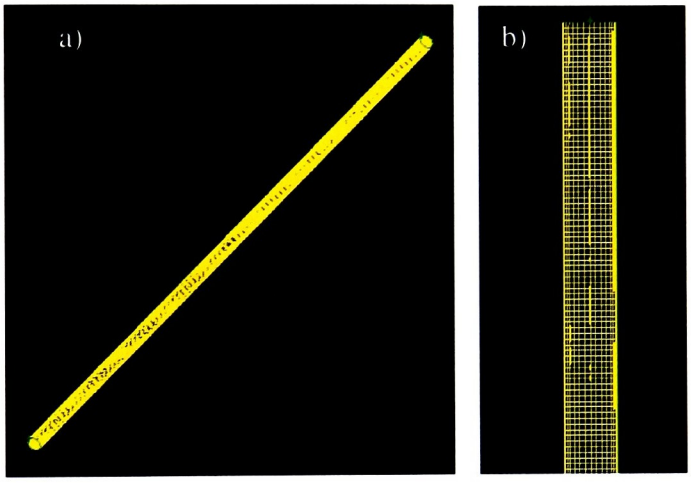


**Figure 4.2 Straight tube mesh a) whole geometry b) zoomed in on end (239,956 elements).**

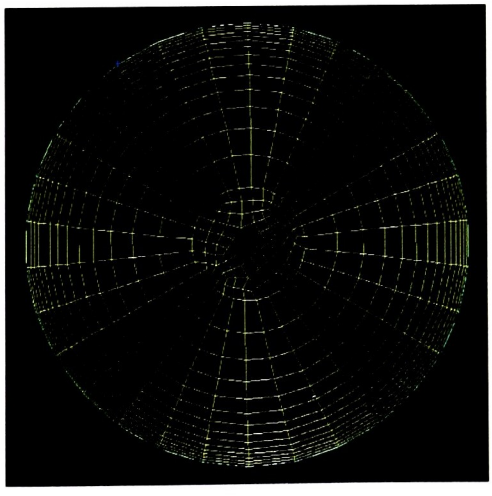

**Figure 4.3 Face mesh at ends of straight tube.**

**Table 4.1 Characteristics of the boundary layer mesh utilized in the straight tube geometry.**

| | |
|---|---|
| 1st Row Height | 0.0001 m |
| Growth Factor | 1.23 |
| Number of Rows | 14 |
| Depth | 0.0075 m |

The maximum skew in the straight tube geometry is 0.56 in 43 elements (0.02% of the elements), see Figure 4.4. The elements with maximum skew in the straight tube mesh are located near the center of the geometry. The placement of the highest skewed elements is optimal, since they are away from the wall were the deposition algorithms determine if the particles intercept the walls. The level of skew in these elements will not affect the flow solution. The final mesh passed grid checks in all three CFD software packages investigated without smoothing or swapping the grid.

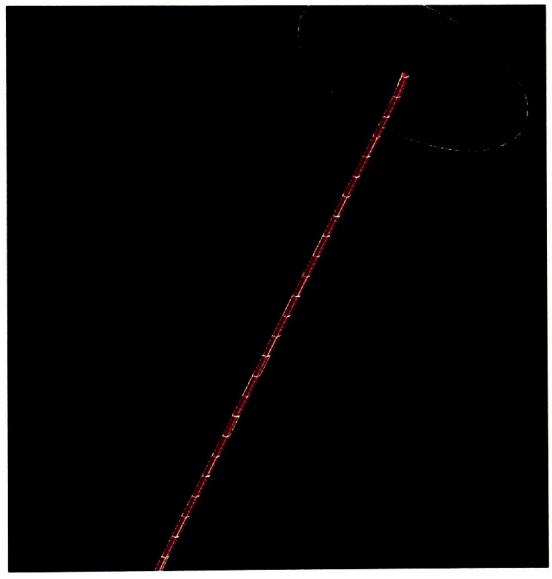

**Figure 4.4 Elements with 0.56 skew in the straight tube geometry.**

## 4.2 Bifurcating Tube Geometry

The bifurcating tube geometry utilized in this research is designed to match the glass bifurcating tube utilized by Kim and Igelsias (1989) to obtain impaction data for a bifurcating tube. Experimental data for a second bifurcation geometry obtained by Dr. Oldham is contained in Appendix B. There is also data which characterizes the bifurcation geometry utilized to obtain this data, which was gathered as part of this research contained in Appendix

B. The data obtained by Dr. Oldham was not utilized in this research because the flow conditions isolated the sedimentation mechanism rather than the impaction mechanism; see Appendix B for more information.

The CAD model of Kim and Igelsias' (1989) geometry was created in I-DEAS and meshed in GAMBIT. A schematic and dimensions of the geometry is provided in Figure 4.5. In addition to these dimensions, there is a fillet of radius 0.75 mm at the bifurcation. This fillet radius is the midpoint of fillet radii (0.5 mm – 1.0 mm) measured by Kim and Fisher (1999) on a multiple generation lung geometry fabricated by the same process as the bifurcation utilized in Kim and Iglesias (1989).

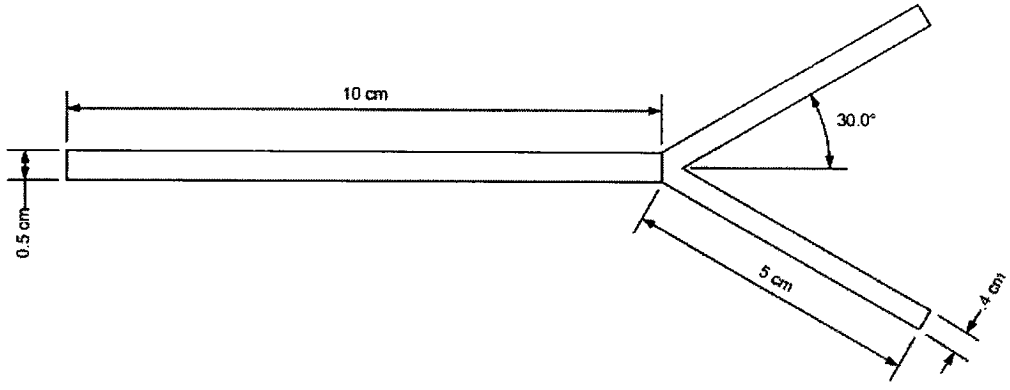


**Figure 4.5 Schematic of the bifurcation geometry with dimensions.**

The geometry was created in I-DEAS, drawn in centimeters, and oriented with flow in the positive y-direction. A solid model was created of the entire flow region, so it could be meshed for CFD analysis. The parent generation was created by revolving a 0.25 cm x 10 cm rectangle to create a cylindrical volume. To create the daughter generations, a four sided polygon of width 0.2 cm and length 5 cm, 30° off the central axis of the parent generation, with one width edge along the diameter of the top of the parent generation, was revolved around the length edge closest to the central axis of the parent generation to create a solid volume. The daughter generation was split along the central axis of the parent generation and the section over the central axis is deleted. In order to fill the gap between the daughter generation and parent generation in the bifurcation region, a quarter circle of radius 0.25 cm was revolved 180° on top of the parent generation. The daughter generation and quarter sphere were joined and reflected about the central axis of the parent bifurcation to create the

bifurcation region and daughter tubes. To create the bifurcation geometry as a single volume the two bifurcation volumes and parent volume were joined. The final step in creating the bifurcation geometry was adding the fillet at the bifurcation. Figure 4.6 shows the bifurcation region in the final I-DEAS model and Figure 4.7 shows the complete model of the bifurcating tube geometry. The bifurcating tube geometry was exported as an IGES file so it could be imported into GAMBIT for meshing. The transition between the parent tube and daughter tubes is not rounded; there is a sharp bent at the outside edges of the bifurcation. This was done for ease of meshing. It is unknown whether the model utilized by Kim and Iglesias (1989) had a sharp or rounded transition from the parent to daughter tubes, but it is possible with the fabrication process. This is a very small area and should not impact the final flow solution.

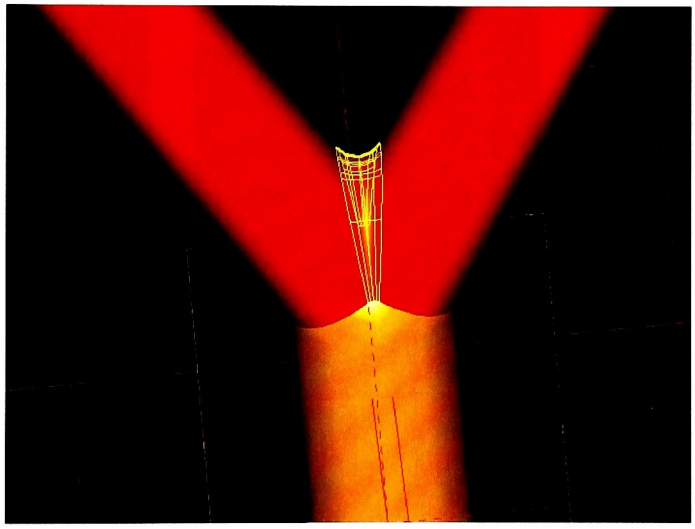

**Figure 4.6 Bifurcation region in the bifurcating model created in I-DEAS.**

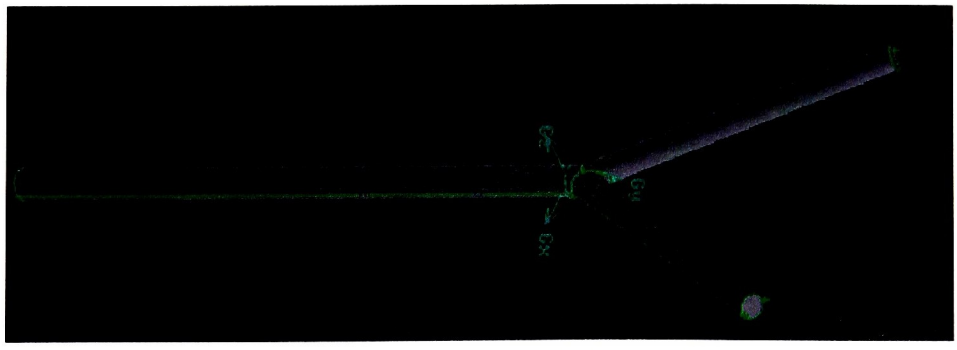

**Figure 4.7 Complete bifurcation geometry.**

To mesh the bifurcating tube geometry with a quad pave mesh with acceptable skew the geometry first had to be broken into five smaller geometries; bifurcation, daughter 1, daughter 2, transition zone, and parent. Each of the smaller geometries is shown in Figure 4.8. The volumes were created by adding edges to create faces and utilizing these faces to split the geometry into smaller volumes. These faces include the faces on both sides of the fillet, the bottom of the bifurcation, the faces connecting the daughters to the transition zone, and a face 1 cm into the parent generation.

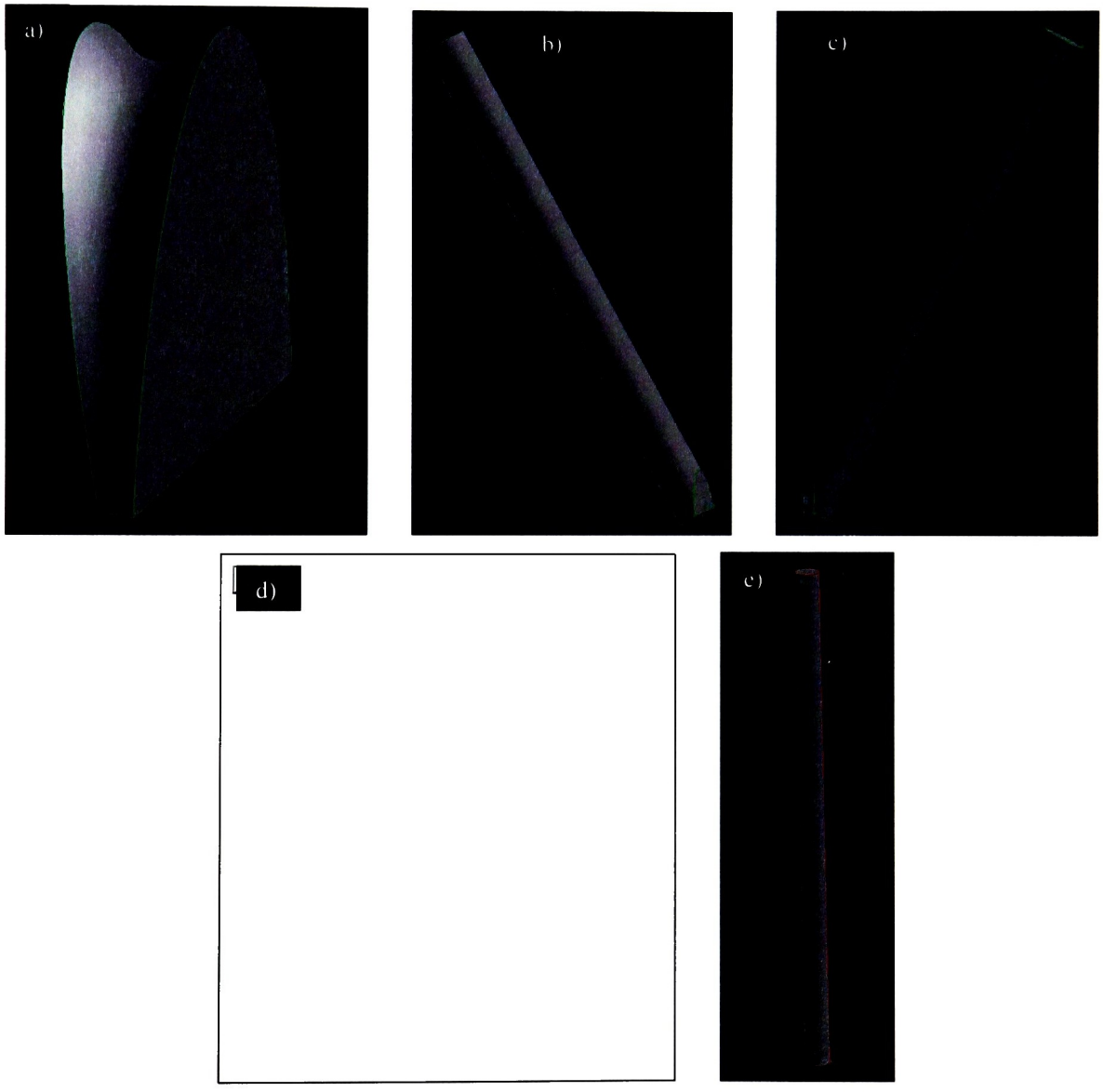


**Figure 4.8 Volumes the bifurcating tube geometry was split into in order to mesh the geometry; a) bifurcation, b) daughter 1, c) daughter 2, d) transition zone, and e) parent.**

To obtain a hex mesh for the bifurcating tube geometry the bifurcation volume had to be the first volume meshed. The final mesh applied to the bifurcation volume is shown in Figure 4.9. The bifurcation volume was meshed with an edge mesh of 40 intervals with a ratio of 1 on the edges which connect to the daughters and an edge mesh of 6 with a ratio of 1 on the edges which span the width of the bifurcation and join to the transition zone. A boundary layer mesh was added to all these edges except the edge connecting to daughter 1. The characteristics of the boundary layer mesh are contained in Table 4.2. A quad pave face mesh of size 0.025 cm was placed on the face connecting the bifurcation and daughter 2. Finally, the bifurcation volume was meshed with a hex cooper volume mesh of size 0.025 cm creating 3,774 elements, see Figure 4.9.

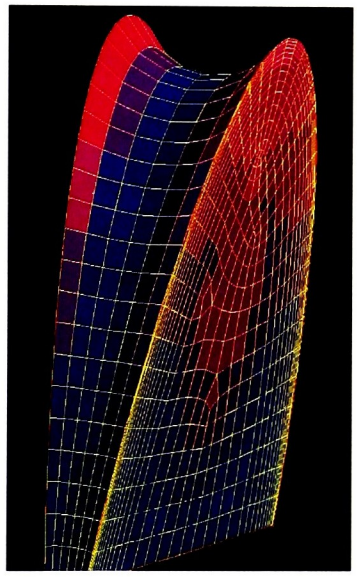

**Figure 4.9 Mesh for the bifurcation volume of the bifurcating tube geometry (3,774 elements).**

**Table 4.2 Characteristics of the boundary layer mesh utilized in the bifurcating tube geometry.**

| | |
|---|---|
| 1st Row Height | 0.002 cm |
| Growth Factor | 1.2 |
| Number of Rows | 12 |
| Depth | 0.0792 cm |

The max skew in the bifurcation volume is 0.61 in 12 elements (0.32% of the elements), see Figure 4.10. The elements with maximum skew are located at the wall, but occupy the least area and have the lowest skew of any of the meshes applied to the

bifurcation volume. Additionally, this is not an excessively high skew for the nature of the geometry.

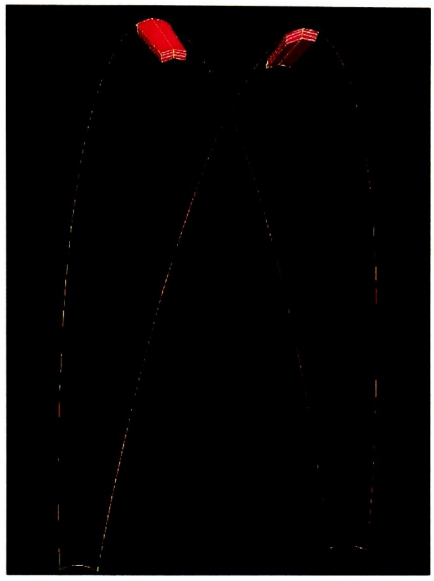

**Figure 4.10 Elements with 0.61 skew in the bifurcation volume of the bifurcating tube geometry.**

The next volumes meshed were the daughter volumes. The same mesh was utilized on both daughter volumes and will only be described once. The final mesh applied to the daughter 2 volume is shown in Figure 4.11. An edge mesh of 100 intervals at a ratio of 1 was placed along the length of each daughter volume. An edge mesh of 15 intervals at a ratio of 1 was placed on each of the two edges joining the daughter volumes to the transition zone. The boundary mesh described in Table 4.2 was applied to the two edges joining the daughter volumes to the transition zone. Finally, a hex cooper volume mesh of size 0.025 cm was applied creating 10,900 elements in each of the daughter volumes, see Figure 4.11.

The maximum skew was 0.73 in 235 elements (0.22% of the elements), see Figure 4.12. The maximum skew is located on the internal walls of the bifurcation which is not optimal, but also was found to be unavoidable. The maximum skew in these elements was reduced from 0.91 and has been reduced as far as possible, while maintaining hex elements.

The next volume to be meshed was the transitional zone. The final mesh applied to the transition zone is shown in Figure 4.13. The first step to meshing this volume was to merge the faces on the side of the transition zone volume to create a virtual face and a virtual volume. The initial faces are not shown, but the side of the volume was split at the top of the

parent generation. This adds a curve which intercepts the edges connecting the transition zone to the daughter volumes. The faces had to be merged because the initial transition zone had seven faces and four to six faces are required to utilize the hex volume mesh. The curved faces of the transition zone and the cylindrical face created by the cut into the parent generation were merged, creating a 5 faced volume. Three of the faces of the volume were already meshed and only a volume mesh was necessary. A hex cooper volume mesh of size 0.01 cm was applied creating 11,260 elements, see Figure 4.13.

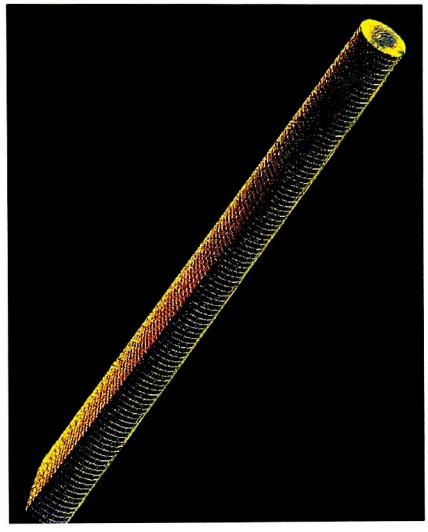

**Figure 4.11 Mesh on the daughter 2 volume of the bifurcating tube geometry (10,900 elements).**

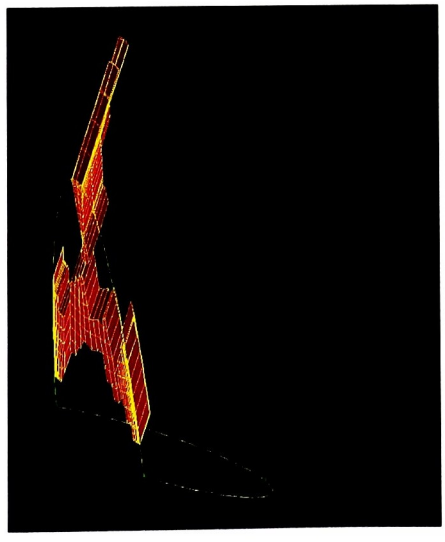

**Figure 4.12 Elements with 0.73 skew in the daughter 2 volume of the bifurcating tube geometry.**

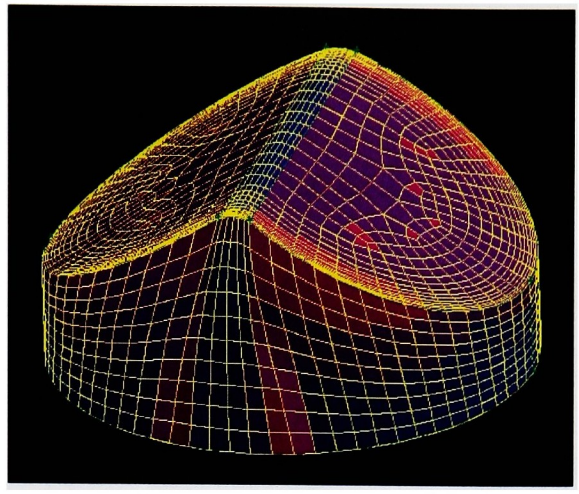

**Figure 4.13 Mesh on the transition zone volume of the bifurcating tube geometry (11,260 elements).**

The maximum skew in the transition volume is 0.84 in 4 elements (0.04% of the elements), see Figure 4.14. This skew is slightly higher than typically desired, however, due to the curvature in the transition zone volume and three face meshes being collapsed and projected onto a single face this is the best volume mesh that could be obtain with GAMBIT for this geometry. The elements with the largest skew are located in the parent tube section of the transition zone volume, where there should not be too much deposition. It would be better for the elements to be away from the wall were the deposition algorithms determine if particles are depositing, but this could not be avoided.

**Figure 4.14 Elements with 0.84 skew in the transition zone volume of the bifurcating tube geometry.**

The final volume to be meshed was the parent. The final mesh applied to the parent volumes is shown in Figure 4.15. An edge mesh of 100 intervals with a ratio of 1 was applied to the length of the parent generation. A hex cooper volume mesh of size 0.025 cm was applied to the parent volume creating 47,200 elements, see Figure 4.15.

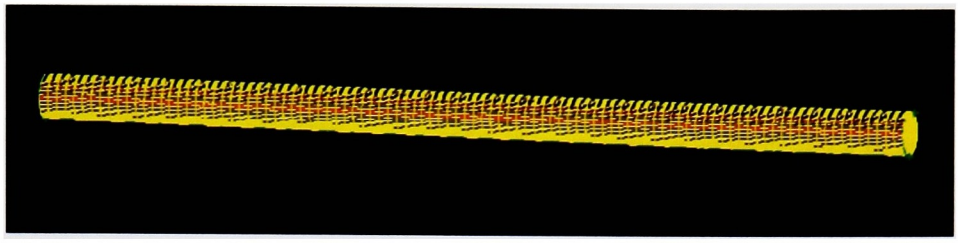

**Figure 4.15 Mesh on the parent volume of the bifurcating tube geometry (47,200 elements).**

The maximum skew is 0.84 in 400 elements (0.36% of the elements), see Figure 4.16. The elements with the highest skew in the parent volume line up with the 4 elements with high skew in the transition zone and run the length of the parent volume. The elements are located at the wall, which is not optimal; however the bifurcation geometry is being utilized to examine the impaction deposition mechanism where deposition primarily occurs at the bifurcation. Additionally, the area occupied by these highly skewed is extremely small compared to the total flow area.

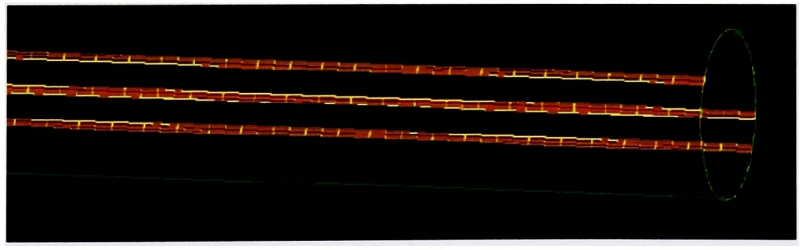

**Figure 4.16 Elements with 0.84 skew in the parent volume of the bifurcating tube geometry.**

The final bifurcation mesh has 345,634 elements and a maximum skew of 0.84. The grid passed checks in both Fluent DPM and CFX, with no smoothing or swapping required.

## 4.3 Three Generation Lung Model

The three generation lung geometry was originally created by Heistracher (1995) and further used for research conducted by Oldham, et al. (2000). The geometry has also been utilized for research at Rochester Institute of Technology in recent years (Rai, 2004; Pruyne, 2004). The geometry and mesh were not changed for this research to allow for comparison with existing data for the same geometry and mesh from other software packages and earlier experiments.

"Heistracher and Hofmann (1995) utilized the morphometric work of Horsfield, et al. (1971) and Hammersley and Olson (1992) to construct a more realistic bifurcation that completely defines the airway bifurcation mathematically. These anatomical models were labeled PRB (physiologically realistic bifurcation) models. Subsequently their work was extended to a double bifurcation model with three airway generations (Heistracher and Hofmann, 1997)." (Oldham, 2000) This PRB double bifurcation model was chosen by Dr. Oldham "for experimental particle deposition work, since it was completely defined mathematically, enabling construction of a hollow model, and because it appears to be the most realistic CFD bifurcation model that has yet been described." (Oldham, 2000)

A schematic of the volume is shown in Figure 4.17. The dimensions of each generation and bifurcation angles for the three generation lung geometry are provided in Table 4.3. Heistracher and Hofmann (1997) obtained CFD predictions for the 10 μm particle size at a flow rate of 7.5 lpm utilizing the k-epsilon turbulence with fair results compared to Oldham (2000), using FIRE, a commercial CFD package not utilized in this research.

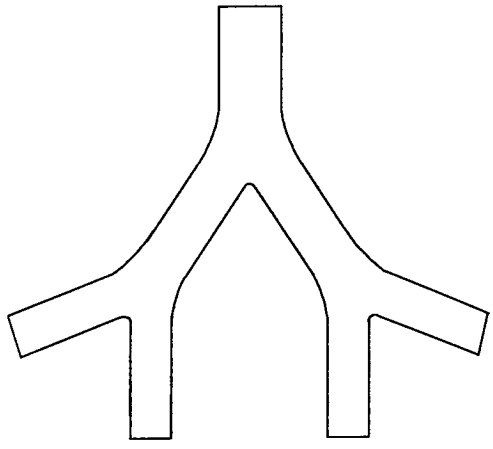

**Figure 4.17 Schematic of the three generation lung geometry, generations three through five of the ideal PRB lung model.**

**Table 4.3 Dimensions for the three generation lung geometry, generations three through five of the ideal lung model.**

| Generation (Global) | Generation (Local) | Generation Diameter (mm) | Generation Length (mm) | Branch Angle (degrees) |
|---|---|---|---|---|
| 3 | 1 | 5.6 | 11.0 | 0 |
| 4 | 2 | 4.5 | 9.2 | 35 |
| 5 | 3 | 3.6 | 7.7 | 35 |

The geometry is meshed with a tetrahedral volume mesh containing 834,288 elements. Part of the final mesh utilized for the three generation lung geometry can be seen in Figure 4.17. The geometry is oriented with flow in the positive y-direction.

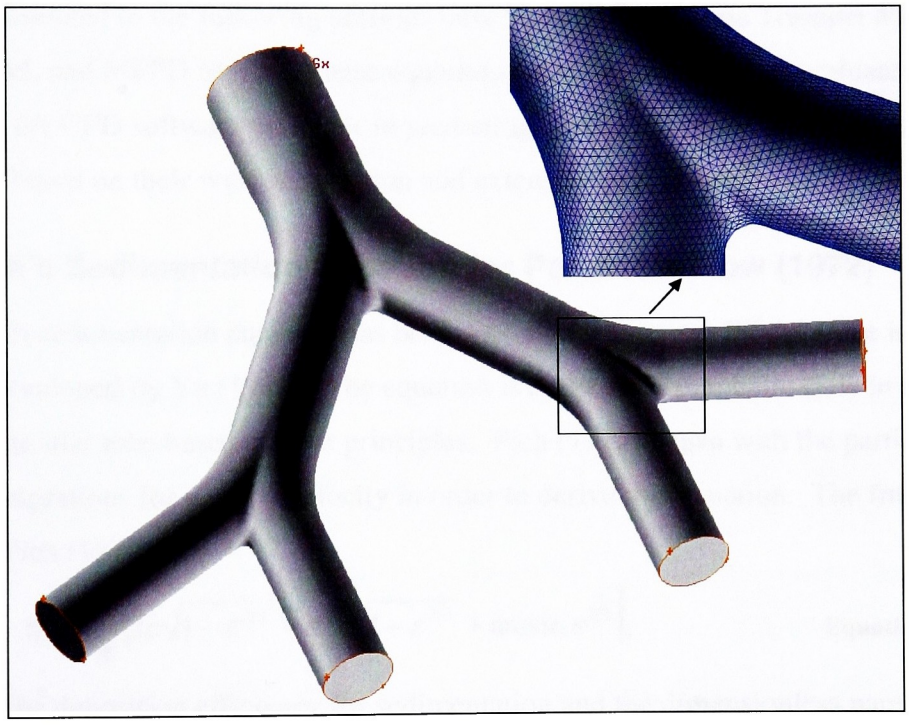

**Figure 4.18 Three generation lung geometry and mesh at the bifurcation between generation 3 and 4, Pruyne, 2004.**

# Chapter 5

# Sedimentation Deposition Mechanism

## 5.1 Sedimentation Analytical Equations

There are several analytical equations that have been developed for deposition by the sedimentation mechanism in the lung and straight tubes, as discussed in Section 1.3.1. The equations presented in the following sections have been utilized in the Trumpet Model, NCRP Model, and MPPD Model. These equations have been selected to evaluate the accuracy of the CFD software packages in predicting deposition by the sedimentation mechanism based on their wide recognition and extensive peer review.

### 5.1.1 Pich's Sedimentation Equation for Parabolic Flow (1972)

Pich's (1972) sedimentation equation has been used in the Trumpet Model since it was originally developed by Yu (1978). The equation is derived for parabolic flow in a horizontal circular tube based on first principles. Pich (1972) began with the partial differential equations for particle velocity in order to derive this equation. The final equation derived by Pich (1972) is,

$$\eta_s = \frac{2}{\pi}\left[2\varepsilon\sqrt{1-\varepsilon^{2/3}} - \varepsilon^{1/3}\sqrt{1-\varepsilon^{2/3}} + \arcsin\varepsilon^{1/3}\right], \qquad \textbf{Equation (5.1)}$$

where $\eta_s$ is the deposition efficiency for sedimentation and the dimensionless parameter $\varepsilon$ is defined as,

$$\varepsilon = \frac{3V_{ts}L}{8RV}. \qquad \textbf{Equation (5.2)}$$

In Equation (5.2), L is the length of the generation, R is the radius of the generation, V is the average velocity of air in the generation, and $V_{ts}$ is the particle settling velocity defined as,

$$V_{ts} = \frac{\rho_p d_p^2 g C_c}{18\mu} \text{ (Hinds, 1999).} \qquad \textbf{Equation (5.3)}$$

In Equation (5.3), $\rho_p$ is the density of the particle, $d_p$ is the particle diameter, g is gravity, $\mu$ is the dynamic viscosity of air, and $C_c$ is the Cunningham slip correction factor defined as,

$$C_c = 1 + \frac{\lambda}{d_p}\left[2.34 + 1.05\exp\left(-0.39\frac{d_p}{\lambda}\right)\right] \text{ (Hinds, 1999),} \qquad \textbf{Equation (5.4)}$$

where $\lambda$ is the mean free path. For air the mean free path is 0.066 $\mu$m.

Equation (5.1) is valid for $\varepsilon$ values between 0 and 1. When $\varepsilon$ is 0, 0% of the injected particles deposit by sedimentation. When $\varepsilon$ is 1, 100% of the injected particles deposit by sedimentation. It is possible to obtain values of $\varepsilon$ greater than 1, which will result in deposition efficiencies greater than 100%. This is of course not possible. Therefore, if $\varepsilon$ is greater than 1 it is safe to assume that all the particles have deposited in the generation, or a deposition efficiency of 100%.

Pich (1972) also developed an equation for the critical length at which all particles of a given size will deposit. The critical length equation is,

$$L_c = \frac{8RV}{3V_{ts}}, \qquad \textbf{Equation (5.5)}$$

where $L_c$ is the critical length.

### 5.1.2 Wang's Sedimentation Equation for Parabolic Flow (1975)

Wang's (1975) sedimentation equations are used in the MPPD Model (Anjilvel and Asgharian, 1995). Wang developed a series of equations to predict deposition by sedimentation in the lung from fully developed parabolic flow in circular tubes derived from the partial differential equations for particle motion. There are three equations for uphill flow depending on the angle with respect to the horizontal and one equation for downhill flow. All the equations are presented below for completeness, but only the downhill equation is being compared to CFD data in this research. The uphill equations cannot be utilized for a horizontal tube and the straight tube is only evaluated in the horizontal position, where deposition by sedimentation is at its maximum.

Wang's (1975) equation for sedimentation from a parabolic downhill flow is given by,

$$\eta_s = 1 - \frac{2}{\pi}\sin^{-1}\sqrt{1-\zeta^2} - \left[\frac{\sqrt{1-\zeta^2}\left(\frac{3V_{ts}L}{2VR}\cos\phi - \left(2+\frac{V_{ts}}{V}\sin\phi\right)\zeta\right)}{\pi\left(1+\left(V_{ts}/V\right)\sin\phi\right)}\right], \qquad \textbf{Equation (5.6)}$$

where $\eta_s$ is the deposition efficiency for sedimentation, L is the length of the generation, V is the average velocity of air in the generation, R is the radius of the generation, $\phi$ is the angle of inclination with respect to the horizontal, $V_{ts}$ is given by Equation (5.3), and $\zeta$ is defined as,

$$\zeta = \left(\frac{\frac{3V_{ts}L}{8VR}\cos\phi}{1+\frac{3V_{ts}}{4V}\sin\phi}\right)^{1/3}. \qquad \textbf{Equation (5.7)}$$

For a horizontal tube Equation (5.7) simplifies to,

$$\zeta = \left(\frac{3V_{ts}L}{8VR}\right)^{1/3} = \varepsilon^{1/3}, \qquad \textbf{Equation (5.8)}$$

and Equation (5.6) simplifies to,

$$\eta_s = 1 - \frac{2}{\pi}\sin^{-1}\sqrt{1-\varepsilon^{2/3}} - \left[\frac{\sqrt{1-\varepsilon^{2/3}}\left(\frac{3V_{ts}L}{2VR} - 2\varepsilon^{1/3}\right)}{\pi}\right]. \qquad \textbf{Equation (5.9)}$$

Equation (5.9) is compared to the CFD data gathered for sedimentation from a parabolic flow in the straight tube.

Wang's (1975) sedimentation equations for deposition from parabolic uphill flow are provided below. For,

$$0 < \phi < \frac{\pi}{2} - \frac{2R}{9L}\left(\frac{2V_{ts}}{3V}\right)^{1/2}$$

$$\eta_s = \frac{1}{\pi}\left(3\sqrt{\sigma(1-\sigma)} + \sin^{-1}\sqrt{1-\sigma} + (1-9\sigma^2)\sin^{-1}\sqrt{\frac{1-\sigma}{1+3\sigma}}\right), \qquad \textbf{Equation (5.10)}$$
$$-\frac{2}{\pi}\left(\sqrt{\gamma(1-\gamma)}(1-2\gamma) + \sin^{-1}\sqrt{1-\gamma}\right)$$

where,

$$\sigma = \frac{\frac{V_{ts}}{6V}\sin\phi}{\left(1-\frac{V_{ts}}{2V}\sin\phi\right)}, \qquad \textbf{Equation (5.11)}$$

and

$$\gamma = \frac{\left(\frac{3V_{ts}L}{8VR}\cos\phi\right)^{2/3}}{\left(1-\frac{V_{ts}}{2V}\sin\phi\right)}. \qquad \textbf{Equation (5.12)}$$

Equation (5.10) is not valid for horizontal tubes and will provide a deposition efficiency 10% less than Equation (5.9) if employed for a horizontal tube. Appendix C contains a check of Wang's (1975) derivation for horizontal flow from Equation (5.10), which proves that Equation (5.10) does not equal Equation (5.9) or Wang's (1975) simplification of Equation (5.10) for a horizontal tube when $\phi$ is 0.

Wang's (1975) second equation for sedimentation from an uphill parabolic flow is for,

$$\frac{\pi}{2}-\frac{2R}{9L}\left(\frac{2V_{ts}}{3V}\right)^{1/2} < \phi < \frac{\pi}{2}-\frac{RV_{ts}}{8VL},$$

where,

$$\eta_s = \frac{1+3\sigma}{\pi}\sqrt{1-\varsigma^2}\left(\varsigma+\frac{4\gamma^{3/2}}{\sqrt{1+3\sigma}}-\sqrt{\varsigma^2-\frac{3\sigma}{1+3\sigma}}\right) + \frac{1-9\sigma^2}{\pi}\sin^{-1}\sqrt{1-\varsigma^2}-\frac{1}{\pi}\sin^{-1}\sqrt{(1+3\sigma)(1-\varsigma^2)}, \qquad \textbf{Equation (5.13)}$$

and,

$$\varsigma = \frac{RV_{ts}\sin^2\phi}{8VL\cos\phi}-\frac{1}{16}\sqrt{\frac{V_{ts}}{6V}\sin\phi}+\frac{7L}{8R}\cot\phi. \qquad \textbf{Equation (5.14)}$$

Wang's (1975) final equation for sedimentation from an uphill parabolic flow is for,

$$\phi > \frac{\pi}{2}-\frac{RV_{ts}}{8VL},$$

where,

$$\eta_s = 0. \qquad \textbf{Equation (5.15)}$$

Equation (5.10), Equation (5.13), and Equation (5.15) are again not utilized in this research, since the straight tube model is run in the horizontal position.

### 5.1.3 Yu, Lui, and Taulbee's Sedimentation Equation for Uniform Flow (1977)

The earliest appearance of Yu, et al.'s (1977) sedimentation equation in the Trumpet Model that could be located was 1993 (Chen and Yu, 1993). The exact origin of the form of Yu, et al.'s (1977) sedimentation equation for uniform flow used in the Trumpet Model could not be located. The first appearance of a similar equation is contained in Yu, et al. (1977). The equation from Yu, et al. (1977) was derived from the partial derivative of concentration. Yu, et al.'s (1977) sedimentation for uniform flow used in the Trumpet model is,

$$\eta_s = \frac{2}{\pi}\left[\sin^{-1}\left(\frac{4}{3}\varepsilon\right) + \frac{4}{3}\varepsilon\sqrt{1-\left(\frac{4}{3}\varepsilon\right)^2}\right], \qquad \textbf{Equation (5.16)}$$

where $\eta_s$ is the deposition efficiency for sedimentation and the dimensionless parameter $\varepsilon$ is defined by Equation (5.2).

There are not specific values of $\varepsilon$ that Equation (5.16) is valid for provided in the Trumpet Model or any of the papers related to the Trumpet Model (Yu, 1978; Chen and Yu, 1993; Robinson and Yu, 2001); however after using the equation it has been determined that Equation (5.16) is valid for $\varepsilon$ values between 0 and 0.75. When $\varepsilon$ is 0, the deposition efficiency is 0%. When $\varepsilon$ is 0.75, the deposition efficiency is 100%. For $\varepsilon$ greater than 0.75, the square root term becomes negative and it is not possible to obtain a real number solution to Equation (5.16). However, when $\varepsilon$ is greater than 0.75 it is safe to assume 100% of the particles have deposited.

### 5.1.4 Yeh and Schum's Sedimentation Equation (1980)

Yeh and Schum's (1980) sedimentation equation is used in the NCRP Model (United States National Council on Radiation Protection and Measurements, 1997). The equation's original derivation has not been able to be tracked down; its introduction is commonly credited to Yeh and Schum (1980). The equation is a general sedimentation equation with no specific

flow conditions requirements. Yeh and Schum's (1980) sedimentation equation is defined as,

$$\eta_s = 1 - \exp\left[\frac{-4gC_c\rho_p\left(d_p/2\right)^2 L\cos\phi}{9\pi\mu RV}\right], \qquad \textbf{Equation (5.17)}$$

where $\eta_s$ is the deposition efficiency for sedimentation, g is gravity, $C_c$ is the Cunningham slip correction factor, given by Equation (5.4), $\rho_p$ is the particle density, $d_p$ is the particle diameter, L is the length of the generation, $\phi$ is the angle of inclination relative to the horizontal, $\mu$ is the dynamic viscosity of air, R is the radius of the generation and V is the average velocity of air. Equation (5.17) is bounded by the exponential term, which must be between 0 and -∞. When the exponential term is 0, 0% of the particles injected deposit by sedimentation. As the exponential term approaches -∞, there is 100% particle deposition. For a horizontal tube Equation (5.17) simplifies to,

$$\eta_s = 1 - \exp\left[\frac{-4gC_c\rho_p\left(d_p/2\right)^2 L}{9\pi\mu RV}\right]. \qquad \textbf{Equation (5.18)}$$

Equation (5.18) is the form of Yeh and Schum's (1980) sedimentation equation that is compared to CFD data in Sections 5.2.2.1 and 5.2.2.2.

## 5.2 Results for Sedimentation in a Straight Tube from Various CFD Software Packages

### 5.2.1 Flow Conditions and Particle Properties

The flow conditions utilized in the straight tube geometry to investigate the sedimentation deposition mechanism have been selected to provide ε values between 0 and 1, the bounds in which all the sedimentation equations fall within. These flow conditions are located in Table 5.1. In addition to allowing for the full range of valid ε values to be investigated, the flow conditions provide a Reynolds Number comparable to lowest Reynolds Numbers seen in generations three through five of the ideal Weibel lung geometry for 60 lpm and 10 lpm

tracheal flow rates, see Section 3.1. To isolate the sedimentation deposition mechanism, Brownian diffusion is turned off and gravity is turned on in the negative z direction, perpendicular to the flow.

**Table 5.1 Flow condition run in the straight tube to investigate the sedimentation deposition mechanism.**

| | |
|---|---|
| Average Velocity | 0.1 m/s |
| Flow Rate | 3.142E-5 $m^3/s$ (3.142E-2 lpm) |
| Reynolds Number | 137 |
| Viscosity (air STP) | 1.789E-5 $Ns/m^2$ |
| Air Density | 1.225 $kg/m^3$ |
| Mean Free Path | 0.066 μm |

Two velocity profiles are utilized in the straight tube geometry to investigate the sedimentation deposition mechanism; parabolic and uniform velocity profiles. Plots of the parabolic and uniform velocity profiles at the inlet and 0.99 m down the straight tube for each of the software packages are contained in Appendix D. The parabolic velocity profile is defined by

$$y = Ax^2 + Bz^2 + C, \qquad \textbf{Equation (5.19)}$$

where flow is in the positive y-direction and the values for A, B, and C are provided in Table 5.2.

**Table 5.2 Constants for the parabolic velocity profile equation for investigating sedimentation and diffusion in the straight tube geometry.**

| Constants | Values |
|---|---|
| A | -2000 $m^{-1}s^{-1}$ |
| B | -2000 $m^{-1}s^{-1}$ |
| C | 0.2 m/s |

For the parabolic flow runs the walls are defined as no slip boundaries and the velocity profile is defined at the inlet using a user defined function in Fluent DPM and FPM and an expression in CFX. A sample of the user defined function used in Fluent DPM and FPM to define the parabolic velocity profile can be found in Appendix E. The uniform velocity profile is defined by a constant velocity of 0.1 m/s at the inlet. For the uniform flow runs the walls are defined as free slip or 0 shear stress boundary conditions.

The particles run in the straight tube geometry to investigate the sedimentation deposition mechanism are 1000 $kg/m^3$, or unit density. The particles utilized are between 3 nm and 9 μm, all within the inhalable range. Additionally, these particle sizes when

combined with the flow conditions provide ε values between 0 and 1. Figure 5.1 shows the ε values obtained for the particle diameters and flow conditions run in the straight tube geometry to evaluate the sedimentation deposition mechanism.

As mentioned in Chapter 2, each software package generates particles differently. Fluent FPM and CFX automatically generate particles and inject them near the inlet. In Fluent, the particles are defined by an injection file created in J Builder from a Java script. In all the software packages the particles are randomly distributed. Fluent FPM is only capable of generating random particle distributions. In CFX, the random distribution is created by using the uniform scheme for the particle placement. The J Builder code used to generate the particles for Fluent DPM is written to obtain a random particle distribution. For the straight tube geometry in Fluent DPM the particles were injected at 0.1 mm from the inlet and no less than 0.5 mm from the walls, occupying 95% of the available radius.

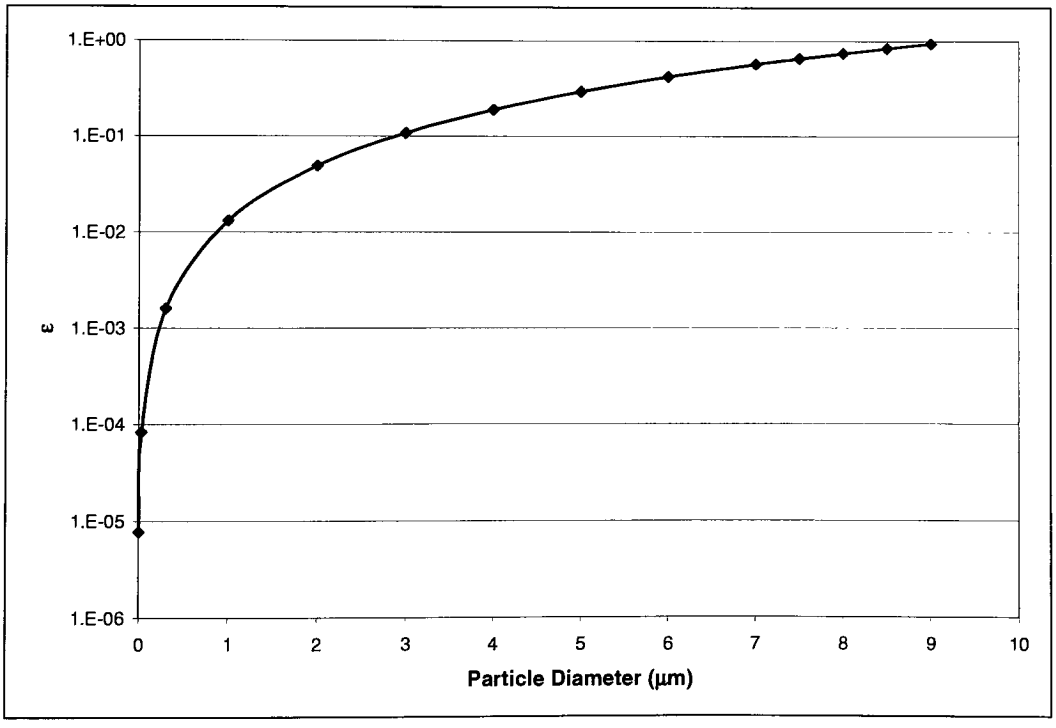


**Figure 5.1 ε values for particle diameters and flow conditions run to evaluate the sedimentation deposition mechanism in the straight tube geometry.**

### 5.2.2 Comparison of CFD Results and Analytical Equations

The CFD data obtained from Fluent DPM, Fluent FPM, and CFX for sedimentation in the straight tube geometry is compared to the analytical equations introduced in Section 5.1. The data is split into parabolic and uniform flow conditions. Pich (1972), Wang (1975), and Yeh and Schum (1980) are compared to the parabolic flow data in Section 5.2.2.1. Yu, et al. (1977) and Yeh and Schum (1980) are compared to the uniform flow data in Section 5.2.2.2. The straight tube utilized for both flow conditions is 1 m in length, has a radius of 0.01 m (10 mm), and flow is in the positive y-direction, see Section 4.1 for more detail.

#### 5.2.2.1 Parabolic Flow Conditions

The data obtained from Fluent DPM, Fluent FPM, and CFX for sedimentation from parabolic flow in a straight tube is compared to Equation (5.1), Pich (1972), Equation (5.9), Wang (1975), and Equation (5.18), Yeh and Schum (1980). The deposition efficiencies are compared in terms of ε, Figure 5.2, and particle diameter, Figure 5.3.

Figure 5.2 provides deposition efficiency verses ε for the three software packages and three analytical equations. It should be noted that for ε values below 0.1, all the analytical equations predict the same deposition efficiency. Above a ε value of 0.1 Yeh and Schum (1980) predicts a lower deposition efficiency for the same ε values compared to Pich (1972) and Wang (1975), which predict the same deposition efficiency within a few thousandths of a percent. For a ε value of 1, Yeh and Schum (1980) is nearly 20% below Pich (1972) and Wang's (1975) prediction. When comparing the deposition efficiencies obtained from the various CFD packages to the analytical equations' predictions, the CFD predictions are always closer to Pich (1972) and Wang's (1975) predictions for ε values above 0.1. All the software packages predict deposition efficiencies higher than the analytical equations for ε values between 0.015 and 0.57. Fluent FPM predictions have great agreement with the analytical equations for ε values below 0.015, while CFX and Fluent DPM over predict by as much as 8% in this region. For ε values between 0.015 and 0.19, Fluent FPM over predicts the analytical equations by several percent less than CFX and Fluent DPM. For ε values between 0.19 and 1, CFX and Fluent DPM predictions are closer to the analytical equations' predictions, and for ε greater than 0.57 they are within 1% of Pich (1972) and Wang's (1975) predictions.

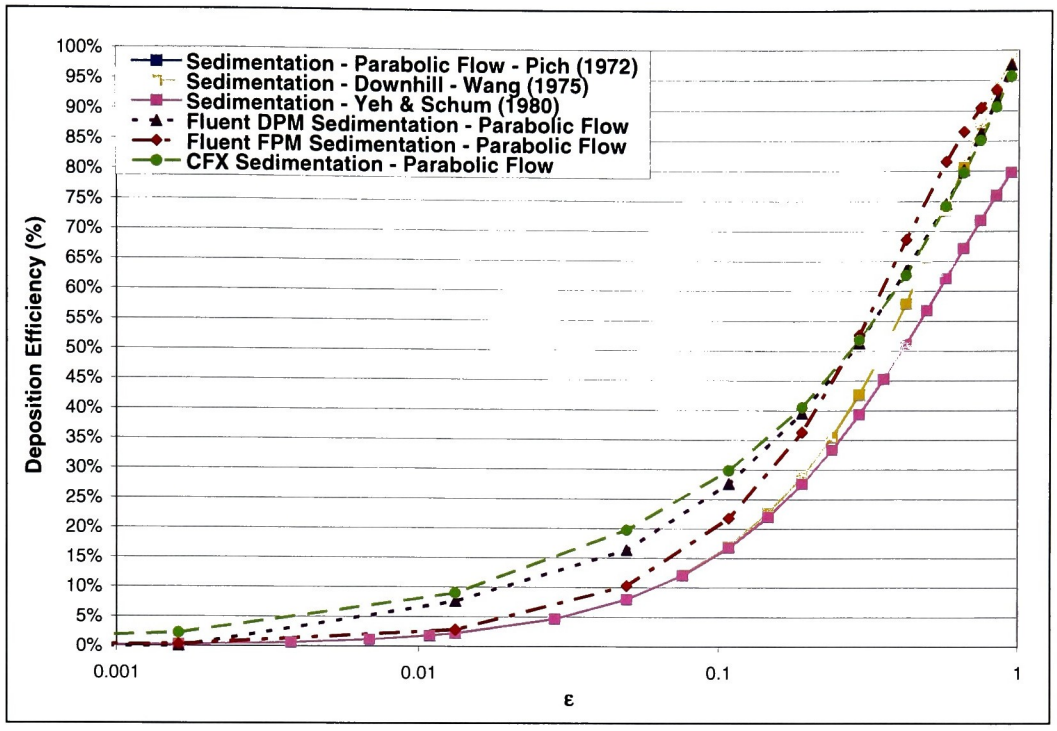


**Figure 5.2 Comparison of CFD data and analytical equations for sedimentation from parabolic flow in a straight tube in terms of ε.**

Figure 5.3 provides deposition efficiency for the particle sizes that correspond to the ε values in Figure 5.2, for the three software packages and three analytical equations. For the flow conditions run in the straight tube geometry at particle sizes below 3.5 μm, the three analytical equations predict the same deposition efficiency within a few hundredths of a percent. Above 3.5 μm, Pich (1972) and Wang (1975) continue to predict the same deposition efficiency, while Yeh and Schum (1980) predict deposition efficiencies several percent lower, as much as 20% by 9 μm. As seen in Figure 5.2, the CFD software packages vary widely in their predictions of deposition efficiencies compared to those predicted by the analytical equations, but always align closer with predictions from Pich (1972) and Wang (1975). Below 5 μm and above 8.5 μm, Fluent FPM more accurately predicts Pich (1972) and Wang's (1975) deposition efficiencies. In this same region, CFX over predicts Fluent DPM by between 0.5% and 3.0%. Between 5 μm and 8 μm, Fluent DPM and CFX predict the same deposition efficiencies and more accurately predict Pich (1972) and Wang's (1975) deposition efficiencies. It should be noted that all three analytical equations and the Fluent

FPM predictions' provide an S-shaped curve, while CFX and Fluent DPM predictions' provide a linear curve.

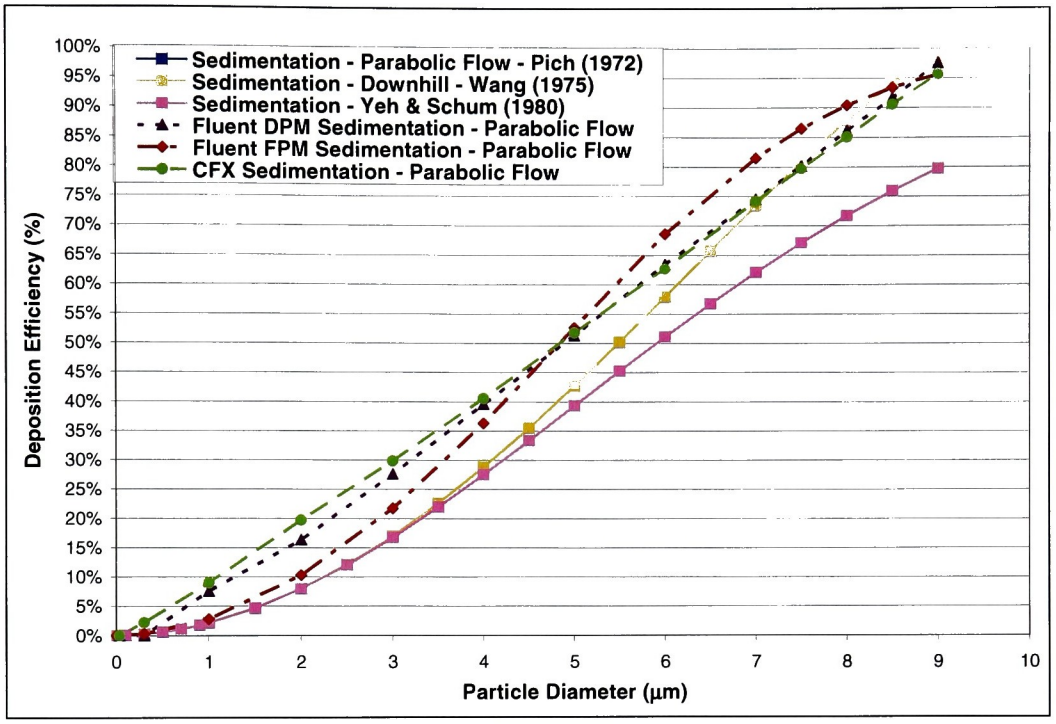


**Figure 5.3 Comparison of CFD data and analytical equations for sedimentation from parabolic flow in a straight tube in terms of particle size.**

### 5.2.2.2 Uniform Flow Conditions

The data obtained from Fluent DPM, Fluent FPM, and CFX for sedimentation from uniform flow in a straight tube is compared to Equation (5.16), Yu, et al. (1977) and Equation (5.18), Yeh and Schum (1980). The deposition efficiencies are compared in terms of ε, Figure 5.4, and particle diameter, Figure 5.5.

Figure 5.4 provides the deposition efficiency verses ε for the three CFD software packages and two analytical equations. The two analytical equations predict the same deposition efficiency below ε values of 0.05. Above ε values of 0.05 Yeh and Schum's (1980) equation predicts noticeably lower deposition efficiency than Yu, et al.'s (1977) equation. Additionally, Yu, et al.'s (1977) prediction takes on a true S-shape curve, where Yeh and Schum (1980) has not yet flattened back out to form a complete S-shaped curve.

When examining the CFD software packages' deposition efficiency predictions they all most closely align with Yu, et al.'s (1977) equation. CFX's predictions are almost exactly the same as Yu, et al.'s (1977) equation, never more than 1% under, for all values of ε. Fluent DPM also matches Yu, et al.'s (1977) predictions almost exactly for ε values great than 0.18, never more than 3.0% over. However, below a ε value of 0.18 Fluent DPM is as much as 4.5% under all the analytical equations' predictions. Of the CFD software packages, Fluent FPM is the most inaccurate compared to the analytical equations' predictions for uniform conditions in the straight tube geometry. For ε values between 0.01 and 0.57 Fluent FPM over predicts Yu, et al.'s (1977) equation by as much as 12%. For ε values greater than 0.65 Fluent FPM under predicts Yu, et al. (1977) by as much as 5%, while still over predicting Yeh and Schum (1980) by as much as 21%.

Figure 5.5 provides the deposition efficiency for the particle sizes that correspond to the ε values in Figure 5.4, for the three CFD software packages and two analytical equations. For the flow conditions run in the straight tube geometry at particle sizes below 2.5 μm both of the analytical equations predict the same deposition efficiency. Above 2.5 μm, Yu, et al. (1977) always predicts a higher deposition efficiency than Yeh and Schum (1980). As observed about Figure 5.4, Yu, et al.'s (1977) equation creates a true S-shaped curve. In Figure 5.5, Yeh and Schum (1980) also provide an S-shaped curve that has not yet reached the maximum possible deposition efficiency of 100%. As far as the CFD software packages' predictions are concerned, they all agree relatively well with Yu, et al.'s (1977) equation predictions. CFX is within 1% of Yu, et al.'s (1977) predictions for all particle sizes run in the straight tube model. Fluent DPM is always within 4.5% of Yu, et al.'s (1977) predictions. For particle sizes less than 3.5 μm, in these flow conditions, Fluent DPM under predicts all the analytical equations. For particle sizes greater than 5 μm, in these flow conditions, Fluent DPM over predicts all the analytical equations. Of the CFD software packages Fluent FPM is the least accurate in predicting the analytical equations deposition efficiencies. Between 1 μm and 7.5 μm, Fluent FPM over predicts Yu, et al.'s (1977) equation by as much as 12%, for these flow conditions. As far as the shape of the CFD prediction curves, all have the S-shape seen in the analytical equations' predictions. CFX aligns closest with Yu, et al.'s (1977) equation and Fluent DPM is very similar to Yu, et al.'s (1977) equation. Fluent FPM has a similar shape but is shifted to the left of the analytical

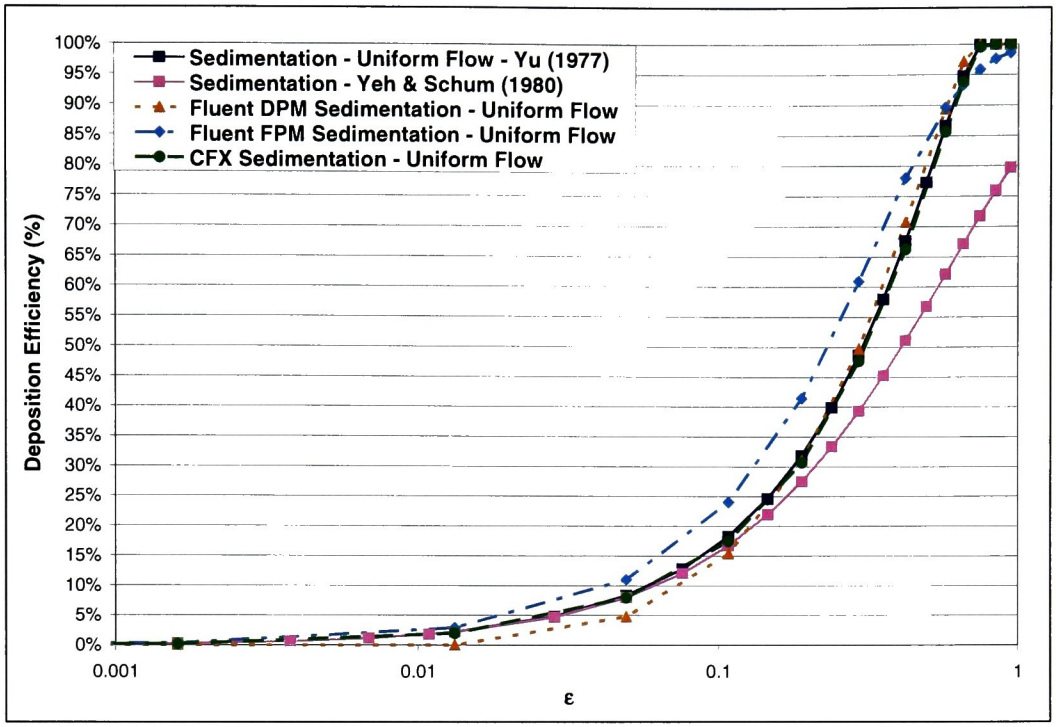


**Figure 5.4 Comparison of CFD data and analytical equations for sedimentation from uniform flow in a straight tube in terms of ε.**

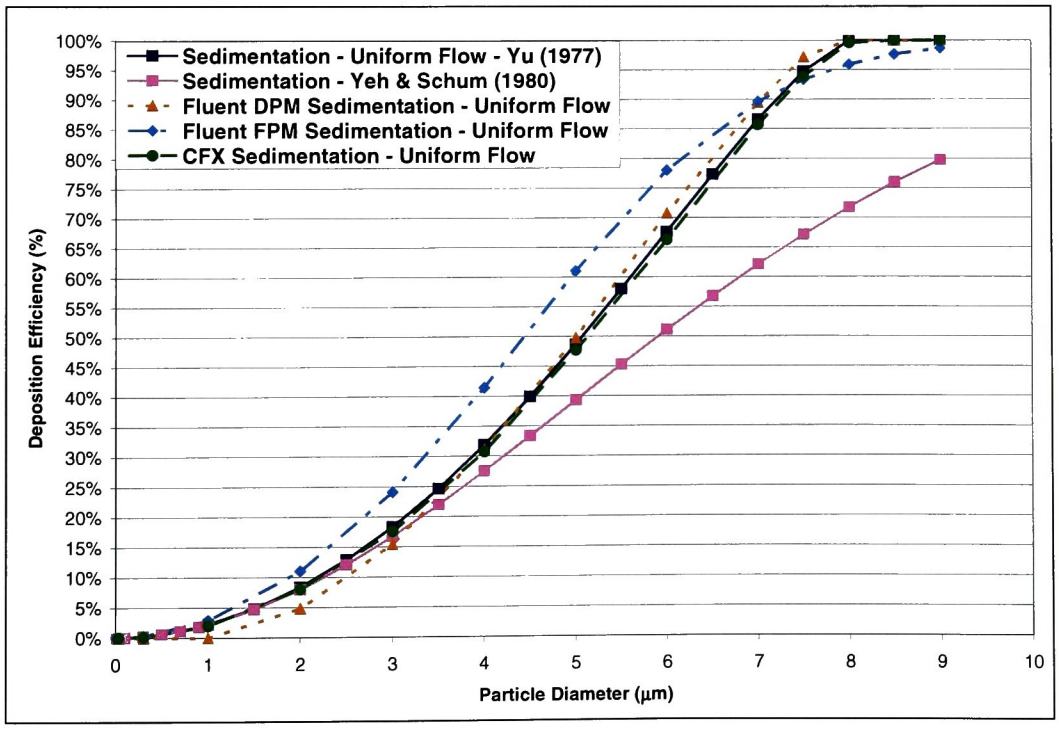


**Figure 5.5 Comparison of CFD data and analytical equations for sedimentation from uniform flow in a straight tube in terms of particle size.**

equations' predictions.

### 5.2.3 Summary

The deposition efficiency predicted by each CFD software package and analytical equation for sedimentation is provided in Table 5.3. As can be seen in Table 5.3, there is currently no published experimental data for isolated sedimentation in a straight tube. This data could assist with improving understanding of both analytical and numerical predictions for the sedimentation deposition mechanism.

For parabolic flow conditions Pich (1972) and Wang (1975)'s equations provide the same deposition efficiencies, while Yeh & Schum's (1980) equation is lower at values of $\varepsilon$ greater than 0.1. The three CFD software packages over predict the three analytical equations for nearly all particle sizes and values of $\varepsilon$. The predictions from the CFD software packages are closer to Pich (1972) and Wang's (1975) equations. Fluent FPM does a better job of predicting the analytical S-shaped curve for deposition efficiency verses particle diameter, despite over predicting deposition by as much as 11%, compared to the Fluent DPM and CFX that predict a linear behavior.

For the uniform flow conditions the analytical equations provide different deposition efficiencies above $\varepsilon$ of 0.05 or a particle size of 2.5 $\mu$m. The Yu, et al. (1977) equation provides higher deposition efficiencies than Yeh and Schum (1980), by as much as 20% when $\varepsilon$ is 1 or a particle diameter of 9 $\mu$m for these flow conditions. All three CFD software packages over predict Yeh and Schum (1980) for larger particle sizes or values of $\varepsilon$ and agree closer with Yu, et al. (1977). CFX's predictions are within 1% of Yu, et al. (1977) for all particles sizes. Fluent DPM is never more than 3% above or below Yu, et al. (1977)'s predictions. An S-shaped behavior is found for all CFD and analytical equations.

In general, the CFD software packages do a better job aligning with the analytical equations for the uniform flow conditions. For uniform flow, all the software packages predict the same curve shape as the analytical equations. Additionally, the CFD software packages' predictions do not over and under predict the analytical equations as often or by as much as they do for the parabolic flow conditions.

**Table 5.3 Summary of deposition efficiencies observed in the straight tube geometry for sedimentation for each flow condition and particle size.**

| Flow Rate (lpm) | Velocity Profile | Particle Size (μm) | ε Value | Fluent DPM | Fluent FPM | CFX | Pich (1972) | Wang (1975) | Yeh & Schum (1980) | Yu, et al. (1977) | Experimental Data |
|---|---|---|---|---|---|---|---|---|---|---|---|
| 0.03 | Parabolic | 0.03 | 7.73E-06 | 0.00% | 0.013% | 0.002% | 0.014% | 0.014% | 0.014% | N/A | N/A |
| 0.03 | Parabolic | 0.3 | 8.31E-05 | 0.00% | 0.32% | 2.22% | 0.27% | 0.27% | 0.27% | N/A | N/A |
| 0.03 | Parabolic | 1 | 1.60E-03 | 7.62% | 2.81% | 9.00% | 2.20% | 2.20% | 2.21% | N/A | N/A |
| 0.03 | Parabolic | 2 | 1.32E-02 | 16.36% | 10.30% | 19.71% | 8.01% | 8.01% | 8.02% | N/A | N/A |
| 0.03 | Parabolic | 3 | 4.92E-02 | 27.61% | 21.77% | 29.86% | 17.04% | 17.04% | 16.76% | N/A | N/A |
| 0.03 | Parabolic | 4 | 0.11 | 39.56% | 36.31% | 40.54% | 28.81% | 28.81% | 27.55% | N/A | N/A |
| 0.03 | Parabolic | 5 | 0.19 | 51.31% | 52.65% | 51.82% | 42.70% | 42.70% | 39.33% | N/A | N/A |
| 0.03 | Parabolic | 6 | 0.29 | 63.46% | 68.61% | 62.68% | 57.92% | 57.92% | 51.13% | N/A | N/A |
| 0.03 | Parabolic | 7 | 0.42 | 74.56% | 81.54% | 74.19% | 73.49% | 73.49% | 62.13% | N/A | N/A |
| 0.03 | Parabolic | 7.5 | 0.57 | 80.17% | 86.50% | 79.74% | 80.97% | 80.97% | 67.15% | N/A | N/A |
| 0.03 | Parabolic | 8 | 0.66 | 86.17% | 90.45% | 85.07% | 87.94% | 87.94% | 71.77% | N/A | N/A |
| 0.03 | Parabolic | 8.5 | 0.75 | 91.63% | 93.40% | 90.60% | 94.05% | 94.05% | 75.98% | N/A | N/A |
| 0.03 | Parabolic | 9 | 0.84 | 97.57% | 95.63% | 95.70% | 98.67% | 98.67% | 79.76% | N/A | N/A |
| 0.03 | Uniform | 0.03 | 7.73E-06 | 0.00% | 0.014% | 0.05% | N/A | N/A | 0.014% | 0.014% | N/A |
| 0.03 | Uniform | 0.3 | 8.31E-05 | 0.00% | 0.33% | 0.15% | N/A | N/A | 0.27% | 0.27% | N/A |
| 0.03 | Uniform | 1 | 1.60E-03 | 0.00% | 2.92% | 1.98% | N/A | N/A | 2.21% | 2.24% | N/A |
| 0.03 | Uniform | 2 | 1.32E-02 | 4.79% | 11.03% | 8.00% | N/A | N/A | 8.02% | 8.35% | N/A |
| 0.03 | Uniform | 3 | 4.92E-02 | 15.39% | 24.09% | 17.49% | N/A | N/A | 16.76% | 18.29% | N/A |
| 0.03 | Uniform | 4 | 0.11 | 31.09% | 41.46% | 30.72% | N/A | N/A | 27.55% | 31.87% | N/A |
| 0.03 | Uniform | 5 | 0.19 | 49.73% | 60.99% | 47.68% | N/A | N/A | 39.33% | 48.66% | N/A |
| 0.03 | Uniform | 6 | 0.29 | 70.76% | 78.04% | 66.29% | N/A | N/A | 51.13% | 67.62% | N/A |
| 0.03 | Uniform | 7 | 0.42 | 89.43% | 89.63% | 85.70% | N/A | N/A | 62.13% | 86.63% | N/A |
| 0.03 | Uniform | 7.5 | 0.57 | 97.18% | 93.34% | 93.85% | N/A | N/A | 67.15% | 94.75% | N/A |
| 0.03 | Uniform | 8 | 0.66 | 100.00% | 95.93% | 99.56% | N/A | N/A | 71.77% | 100.00% | N/A |
| 0.03 | Uniform | 8.5 | 0.75 | 100.00% | 97.66% | 100.00% | N/A | N/A | 75.98% | 100.00% | N/A |
| 0.03 | Uniform | 9 | 0.84 | 100.00% | 98.66% | 100.00% | N/A | N/A | 79.76% | 100.00% | N/A |

# Chapter 6

# Diffusion Deposition Mechanism

## 6.1 Diffusion Analytical Equations

There are several analytical equations that have been developed for deposition by diffusion in the lung and straight tubes, as discussed in Section 1.3.2. The equations presented in the following sections have been utilized in the Trumpet Model, NCRP Model, and MPPD Model. These equations have been selected to evaluate the accuracy of the CFD software packages in predicting deposition by the diffusion mechanism based on their wide recognition and extensive peer review.

### 6.1.1 Ingham's Diffusion Equation for Parabolic Flow (1975)

Ingham's (1975) diffusion equation for parabolic flow in a cylindrical tube is utilized in both the Trumpet Model (Yu, 1978; Chen and Yu, 1993; Robinson and Yu, 2001) and MPPD Model (Anjilvel and Asgharian, 1995). The equation is derived from the steady state mass diffusion equation for concentration using a parabolic velocity profile in the derivation. The diffusion equation for parabolic flow developed by Ingham (1975) is,

$$\eta_d = 1 - 0.819\exp(-3.66\Delta) - 0.0976\exp(-22.31\Delta) - 0.0325\exp(-57\Delta) - 0.0509\exp\left(-51.55\Delta^{2/3}\right), \qquad \textbf{Equation (6.1)}$$

where $\eta_d$ is the deposition efficiency for diffusion and the dimensionless parameter, $\Delta$, is defined by,

$$\Delta = \frac{DL}{VR^2}. \qquad \textbf{Equation (6.2)}$$

In Equation (6.2), L is the length of the generation, V is the average velocity of air in the generation, R is the radius of the generation, and D is the diffusion coefficient defined by,

$$D = \frac{kTC_c}{3\pi\mu d_p}. \qquad \textbf{Equation (6.3)}$$

In Equation (6.3), k is the Boltzmann's constant, 1.38E-23, T is the absolute temperature in degrees Kelvin, $C_c$ is Cunningham's correction factor given by Equation (5.4), $\mu$ is the dynamic viscosity, and $d_p$ is the particle diameter. Some of the constants in Equation (6.1) have been altered from Ingham's (1975) original equation to allow for $\Delta$ to be expressed in the general form, given by Equation 6.2, which can be applied to all diffusion equations.

Ingham (1975) provides values for Equation (6.1) for $\Delta$ between 0 and 0.4. At a $\Delta$ value of 0, the deposition efficiency for Equation (6.1) is 100%, according to Ingham (1975). At a $\Delta$ value of 0.4, the deposition efficiency for Equation (6.1) is 81.04%, according to Ingham (1975). After utilizing the equation it has been determined that Equation (6.1) is valid for all positive real numbers, however for $\Delta$ values above 2.7, the deposition efficiency is maximized at 100% and no longer increases. Equation (6.1) is utilized to analyze the accuracy of the CFD software packages for parabolic flow conditions, in Section 6.2.2.1.

### 6.1.2 Ingham's Diffusion Equation for Uniform Flow (1975)

Ingham's (1975) diffusion equation for uniform flow in a cylindrical tube is utilized in the Trumpet Model (Yu, 1978; Chen and Yu, 1993; Robinson and Yu, 2001). The equation is derived from the steady state mass diffusion equation for concentration using a uniform flow velocity profile in the derivation. Ingham's (1975) diffusion equation for uniform flow is defined by,

$$\eta_d = 1 - \frac{4}{\alpha_1^2}\exp\left(-\alpha_1^2\Delta\right) + \frac{4}{\alpha_2^2}\exp\left(-\alpha_2^2\Delta\right) + \frac{4}{\alpha_3^2}\exp\left(-\alpha_3^2\Delta\right) + \left\{1 - 4\left(\frac{1}{\alpha_1^2} + \frac{1}{\alpha_2^2} + \frac{1}{\alpha_3^2}\right)\exp\left[-\frac{4\Delta^{1/2}}{\sqrt{\pi}\left[1 - 4\left(\frac{1}{\alpha_1^2} + \frac{1}{\alpha_2^2} + \frac{1}{\alpha_3^2}\right)\right]}\right]\right\}, \qquad \textbf{Equation (6.4)}$$

where $\eta_d$ is the deposition efficiency for diffusion, $\alpha_1$, $\alpha_2$, and $\alpha_3$ are the first three roots of the Bessel function ($\alpha_1 = 2.4048$, $\alpha_2 = 5.5201$, $\alpha_3 = 8.6537$ (Arde and Westergren, 1992)), and the dimensionless parameter $\Delta$ is defined by Equation (6.2).

Ingham (1975) provides deposition efficiencies for values of Δ between 0 and 0.1. For a Δ value of 0 Equation (6.4) returns a deposition efficiency of 0%. For a Δ value of 0.1 Equation (6.4) provides a deposition efficiency of 60.5%. For values of Δ greater than 1.65, Equation (6.4) will always return a deposition efficiency of 100%. Equation (6.4) is utilized to evaluate the accuracy of the various CFD software packages in predicting deposition by diffusion for uniform flow conditions in Section 6.2.2.2.

### 6.1.3 Yeh and Schum's Diffusion Equation for Laminar Flow (1980)

Yeh and Schum's diffusion equation for laminar flow is utilized in the NCRP Model (United States National Council on Radiation Protection and Measurements, 1997). The original derivation of the equation was unable to be tracked down. The equation is commonly credited to Yeh and Schum (1980), as it will be in this work. Yeh and Schum's diffusion equation for laminar flow is defined by,

$$\eta_d = 1 - 0.819\exp(-3.66\Delta) - 0.0976\exp(-22.31\Delta) - 0.0325\exp(-57\Delta) - 0.0509\exp\left(-51.55\Delta^{2/3}\right), \quad \textbf{Equation (6.5)}$$

where $\eta_d$ is the deposition efficiency for diffusion and the dimensionless parameter Δ is defined by Equation (6.2). Some of the constants in Equation (6.5) have been altered from Yeh and Schum's (1980) original equation to allow for Δ to be expressed in a general form that could be applied to all diffusion equations.

Equation (6.5) and Equation (6.1) are the same equation, despite being reported with slightly different constants by the respective authors, they simplify to the same equation when Δ is defined in its most basic form. Since the equations are the exact same it is only necessary to compare one of the equations to the CFD software packages' predictions. The equation will be referred to as Ingham's (1975) in the comparison, since the equation's derivation could be tracked down and the source of Yeh and Schum's (1980) equation is still unknown. Additionally, Ingham's (1975) equation is derived in an older publication and despite not being cited by Yeh and Schum (1980) could still be the source of the equation found in their publication.

### 6.1.4 Yeh and Schum's Diffusion Equation for Turbulent Flow (1980)

Yeh and Schum's (1980) diffusion equation for turbulent flow is utilized in the NCRP Model (United States National Council on Radiation Protection and Measurements, 1997). The original derivation of this equation could not be tracked down, but is commonly credited to Yeh and Schum (1980). Yeh and Schum's (1980) equation for turbulent diffusion is defined by,

$$\eta_{dt} = 1.999\sqrt{\Delta}\left(1 - 0.222\sqrt{\Delta} + ...\right), \qquad \textbf{Equation (6.6)}$$

where $\eta_{dt}$ is the deposition by turbulent diffusion and the dimensionless parameter $\Delta$ is defined by Equation (6.2). Some of the constants in Equation (6.6) have been altered from Yeh and Schum's (1980) original equation to allow for $\Delta$ to be expressed in a general form that could be applied to all diffusion equations.

Equation (6.6) is not being utilized in this research to evaluate the accuracy of the various CFD software packages in predicting deposition by diffusion in the straight tube, since the flow remains within the laminar region. Additionally, Equation (6.6) predicts deposition by turbulent diffusion, described in Section 1.3.2, rather than molecular diffusion, which is being explored in this research.

## 6.2 Results for Diffusion in a Straight Tube from Various CFD Software Packages

The diffusion deposition mechanism is evaluated in Fluent DPM and FPM. CFX is not evaluated due to the software only being capable of predicting turbulent diffusion, which is not being studied in this research; see Sections 1.3.2, 1.5.3 and 2.3. Turbulent impaction is studied in Chapter 7 to evaluate the transitional flow region investigated by Kim and Igelesias (1989). Fully turbulent conditions are not present in any generation of the ideal Weibel lung geometry, even at the 60 lpm flow rate (see Figure 3.5).

### 6.2.1 Flow Conditions and Particle Properties

The flow conditions utilized in the straight tube geometry to investigate the diffusion deposition mechanism have been selected to provide $\Delta$ values between 1E-5 and 0.06, which correspond to deposition efficiencies between 0% and 50% for the equations being investigated. The flow conditions are provided in Table 6.1. These flow conditions provide

the maximum range of Δ values, while providing a Reynolds number comparable to the lowest Reynolds Number found in the three generation geometry for the 60 lpm and 10 lpm tracheal flow rates, see Section 3.1. The diffusion deposition mechanism is isolated by turning on Brownian diffusion and turning off gravity or buoyancy.

**Table 6.1 Flow conditions run in the straight tube to investigate the diffusion deposition mechanism.**

| | |
|---|---|
| Average Velocity | 0.1 m/s |
| Flow Rate | 3.142E-5 $m^3/s$ (3.142E-2 lpm) |
| Reynolds Number | 137 |
| Viscosity (air STP) | 1.789E-5 $Ns/m^2$ |
| Air Density | 1.225 $kg/m^3$ |
| Temperature | 300 K |
| Mean Free Path | 0.066 μm |

Three velocity profiles are utilized in the straight tube geometry to investigate the diffusion deposition mechanism; parabolic, developing (FPM only), and uniform velocity profile. Plots of the velocity profiles for each of the three flow conditions investigated at the inlet and 0.99 m down the straight tube are contained in Appendix D for Fluent DPM and Fluent FPM. The parabolic velocity profile is defined previously by Equation (5.19), for flow in the positive y-direction. The constants A, B, and C in Equation (5.19) are the same as those utilized to investigate sedimentation deposition mechanism in Chapter 5 and are provided in Table 5.2. For the parabolic flow runs the walls are defined as no slip boundaries and the velocity profile is defined at the inlet using a user defined function in Fluent DPM and FPM.

The developing flow velocity profile is defined by a constant velocity of 0.1 m/s at the inlet. The walls are defined as no slip boundaries for the developing flow allowing the velocity profile to develop. The developing flow conditions are compared with the parabolic flow data in Section 6.2.2.1, since the entrance length is 0.16 m and the flow will be parabolic for approximately 85% of the straight tube geometry. The uniform flow velocity profile is also defined by a constant velocity of 0.1 m/s at the inlet. The walls are defined as 0 shear stress boundary conditions, which help to maintain the velocity profile injected at the inlet throughout the geometry.

The particles run in the straight tube geometry to investigate the diffusion deposition mechanism are 1000 $kg/m^3$, or unit density. The particles utilized are between 3 and 800 nm, all within the inhalable and diffusion range. These particle sizes combined with the flow

conditions provide Δ values between 1E-5 and 0.06, which correspond to deposition efficiencies between 0% and 50% for the equations being investigated. Particles smaller than 3 nm, where deposition would be greater than 50%, were not investigated. This range of Δ values was determined to be sufficient for this research, since it is not until generation 16 that Δ reaches 0.1 for reasonable breathing conditions, see Section 3.2. Additionally, Fluent DPM reports 100% of particles smaller than 20 nm, or a Δ value less than 1.45E-3, for these flow conditions as evaporating or not being able to be tracked due to size, see Sections 2.2. For these flow conditions it is not likely that the particles are actually evaporating, but rather that the particles are too small to be tracked by Fluent DPM. Additionally, for values of Δ below 1.27E-5 (parabolic) and Δ below 1.06E-4 (uniform), Fluent DPM predicts 0 particles depositing. Fluent FPM will not allow particles 1 nm and smaller to be defined, as discussed in Section 2.2. Figure 6.1 shows the Δ values obtained for the particle diameters and flow conditions run in the straight tube geometry to evaluate the diffusion deposition mechanism.

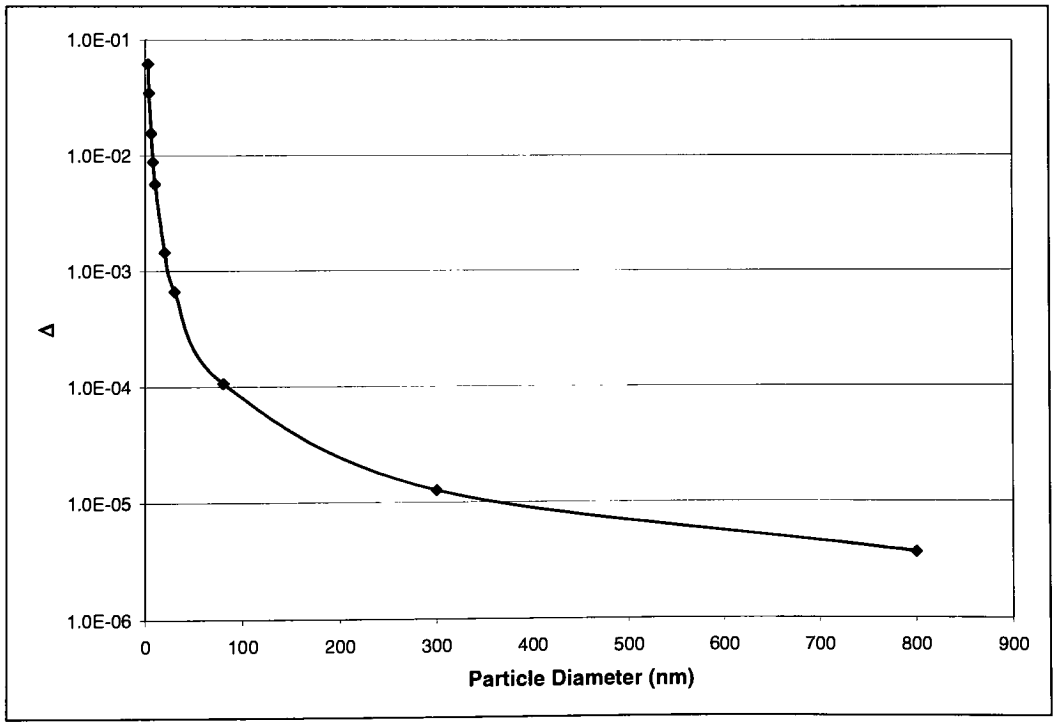


**Figure 6.1 Δ values for particle diameters and flow conditions run to evaluate the diffusion deposition mechanism in the straight tube geometry.**

As mentioned in Chapter 2, each software package generates particles differently. Fluent FPM automatically generates particles and injects them near the inlet. In Fluent, the particles are defined by an injection file created in J Builder from a Java script. In all the software packages the particles are randomly distributed. Fluent FPM is only capable of generating random particle distributions. The J Builder code used to generate the particles for Fluent DPM is written to obtain a random particle distribution. For the straight tube geometry in Fluent DPM the particles were injected at 0.1 mm from the inlet and no less than 0.5 mm from the walls, occupying 95% of the available radius.

### 6.2.2 Comparison of CFD Results and Analytical Equations

The CFD data obtained from Fluent DPM and Fluent FPM for diffusion in the straight tube geometry is compared to the analytical equations introduced in Section 6.1. The data is split into parabolic and uniform flow conditions. Ingham's (1975) diffusion equation for parabolic flow, Equation (6.1), is compared to the parabolic flow data from the CFD software packages in Section 6.2.2.1. Ingham's (1975) diffusion equation for uniform flow, Equation (6.4), is compared to the uniform flow data from the CFD software packages in Section 6.2.2.2. The straight tube utilized for both flow conditions is 1 m in length, has a radius of 0.01 m (10 mm), and flow is in the positive y-direction, see Section 4.1 for more detail.

#### 6.2.2.1 Parabolic Flow Conditions

The data obtained from Fluent DPM and Fluent FPM for diffusion from parabolic flow in the straight tube geometry is compared to Equation (6.1), Ingham (1975). The deposition efficiencies are compared in terms of $\Delta$, in Figure 6.2, and particle diameter, in Figure 6.3.

Figure 6.2 provides the deposition efficiency verses $\Delta$ for Fluent DPM, Fluent FPM, and Ingham's (1975) analytical equation for deposition by diffusion from a parabolic flow. For the values of $\Delta$, where Fluent DPM is capable of predicting deposition, the trend varies greatly from Ingham's (1975) prediction for parabolic flow. Fluent DPM predicts deposition twice as high as Ingham (1975) for $\Delta$ values between 1E-3 and 1E-4. Fluent FPM's predictions for both parabolic and developing flow conditions compares very well with Ingham's (1975) predictions for parabolic flow. For both flow conditions Fluent FPM under predicts Ingham's (1975) equation slightly. Fluent FPM's predictions for parabolic flow

conditions are never more than 2.5% under Ingham's (1975) predictions. Fluent FPM's predictions are slightly closer to Ingham's (1975) for the developing flow conditions, never more than 1.5% under Ingham's (1975) predictions. Both the Fluent FPM flow conditions match the shape of Ingham's (1975) equation. Because there are so few points available for Fluent DPM it is difficult to identify the true shape of the curve over a wide range of Δ, however for the data that could be obtained the curve is noticeably steeper and not a great match when compared to Ingham's (1975) parabolic equation.

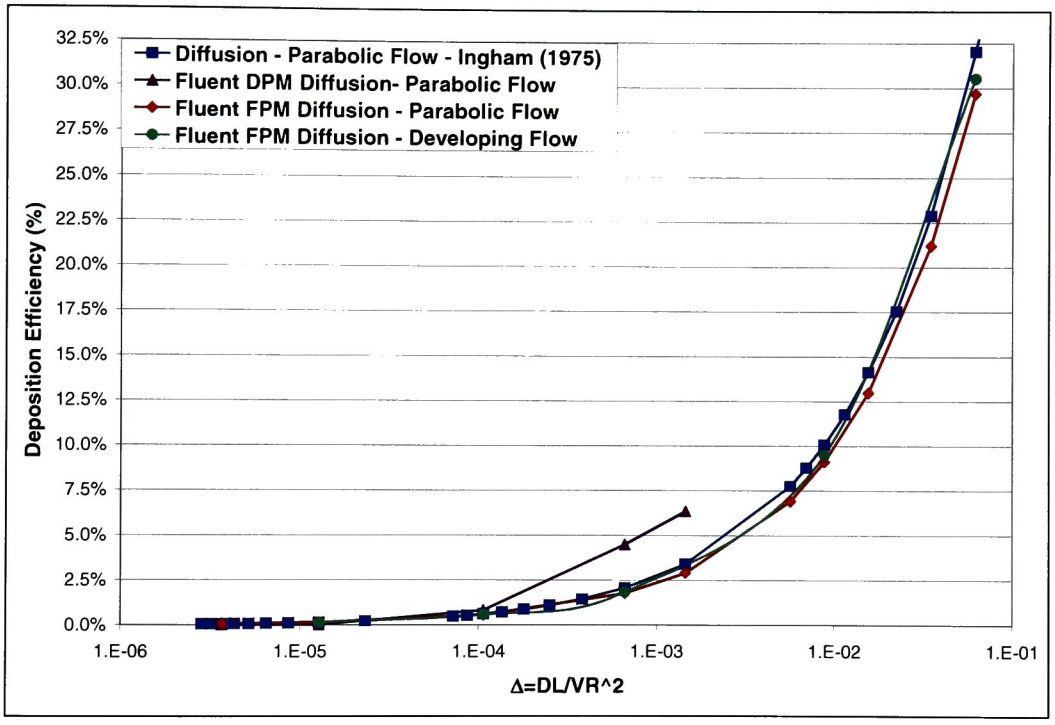


**Figure 6.2 Comparison of CFD data and analytical equations for diffusion from parabolic flow in a straight tube in terms of Δ. *Ingham (1975) is the same equation as Yeh and Schum (1980).**

Figure 6.3 provides deposition efficiency for the particle sizes that correspond to the Δ values in Figure 6.2, for the two software packages investigated and Igham's (1975) analytical equation for deposition by diffusion from uniform flow. For particles larger than 800 nm in these flow conditions, Fluent DPM returns 0 particles depositing. For particles between 20 and 80 nm in these flow conditions Fluent DPM predicts twice the deposition efficiency of Ingham's (1975) analytical equation. Fluent FPM for both parabolic and developing flow under predicts Ingham's (1975) analytical equation by only a few percent.

Fluent FPM is always within 2.5% of Ingham's (1975) equation for parabolic flow and 1.5% for developing flow. Fluent FPM matches the exponential shape of Ingham's analytic equation's curve almost exactly for both parabolic and developing flow conditions.

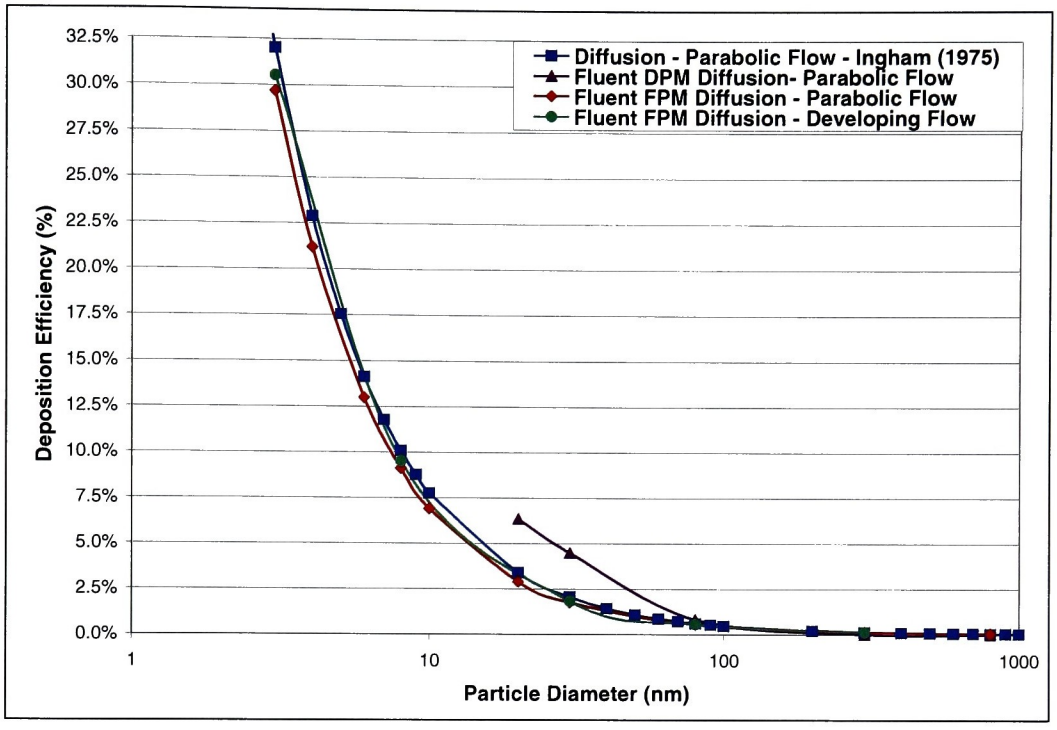


**Figure 6.3 Comparison of CFD data and analytical equations for diffusion from parabolic flow in a straight tube in terms of particle size. *Ingham (1975) is the same equation as Yeh and Schum (1980).**

In general, Fluent FPM is significantly better than Fluent DPM in predicting deposition by diffusion from parabolic flow. Additionally, developing flow predictions are very similar to the parabolic flow predictions. The agreement is expected since the entrance length for the developing flow indicts the flow will be fully developed by 0.15 m or for 85% of the total length. In fact, the developing flow conditions matched Ingham's (1975) analytical equation for parabolic flow slightly better than the actual parabolic flow condition.

### 6.2.2.2 Uniform Flow Conditions

The data obtained from Fluent DPM and Fluent FPM for diffusion from uniform flow in a straight tube is compared to Equation (6.4), Ingham (1975). The deposition efficiencies are compared in terms of $\Delta$, Figure 6.4, and particle diameter, Figure 6.5.

Figure 6.4 provides the deposition efficiency verses $\Delta$ for the two CFD software packages being investigated and Ingham's (1975) analytical equation for diffusion from

uniform flow. The few deposition efficiencies Fluent DPM is capable of predicting are between 2% and 5% under Ingham's (1975) predictions for uniform flow. These predictions are nearly a third of Ingham's (1975) predictions for the same values of Δ. The shape of curve predicted by Fluent DPM may be similar to Ingham's (1975) predictions, however with only three data points it is difficult to draw any conclusions about the curve shapes. Fluent FPM is significantly more accurate when compared to Ingham's (1975) predictions for diffusion from uniform flow. Fluent FPM under predicts Ingham (1975) for all values of Δ above 5.6E-3 and below 1.4E-4. For values of Δ between 1.4E-4 and 5.6E-3 Fluent FPM is always within 0.1% of Ingham's (1975) predictions. For all values of Δ Fluent FPM is within 2.5% of Ingham's (1975) predictions of deposition for diffusion from uniform flow. Fluent FPM matches the exponential curve shape generated by Ingham's (1975) analytical equations almost exactly.

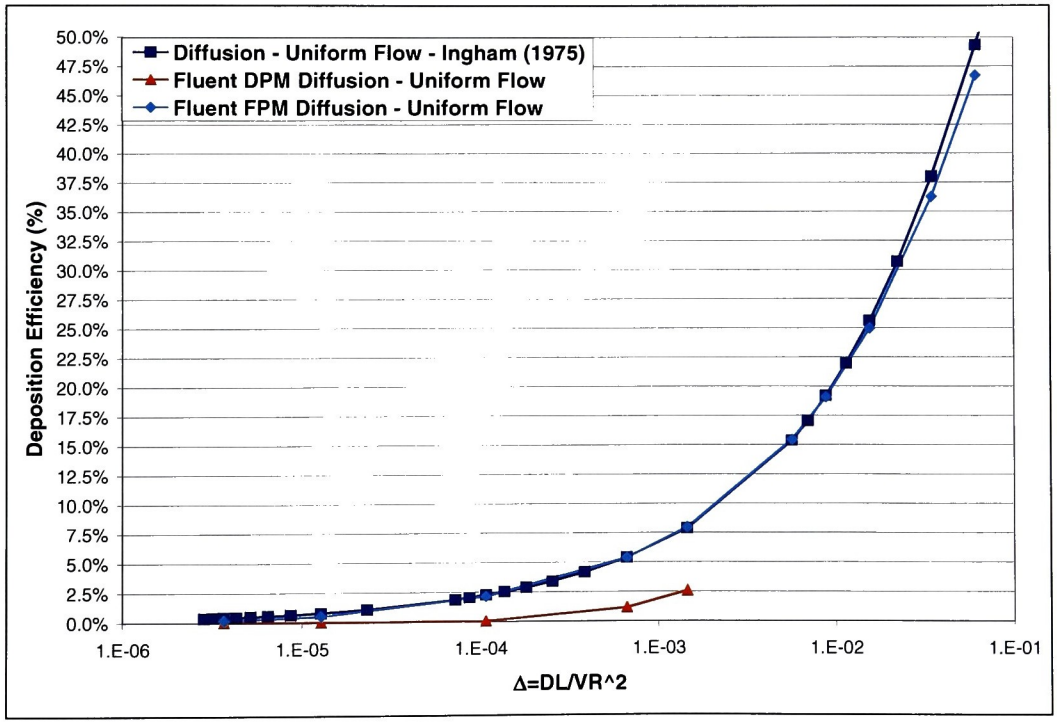


**Figure 6.4 Comparison of CFD data and analytical equations for diffusion from uniform flow in a straight tube in terms of Δ.**

Figure 6.5 provides the deposition efficiency for the particle sizes that correspond to the Δ values in Figure 6.4, for the two CFD software packages being investigated and

Ingham's (1975) analytical equation for deposition by diffusion from uniform flow. For particles greater than 80 nm Fluent DPM reports 0 particles depositing. As seen in Figure 6.4, Fluent DPM under predicts Ingham's (1975) analytical equation by nearly a third. Again with only three data points it is difficult to compare the shape of Fluent DPM's curve with Ingham's (1975) analytical equation. Fluent FPM predicts Ingham's (1975) analytical equation within 2.5% for all particle sizes investigated for these flow conditions. The curves produced by Ingham's (1975) analytical equation and Fluent FPM are nearly identical for all particle sizes investigated in these flow conditions.

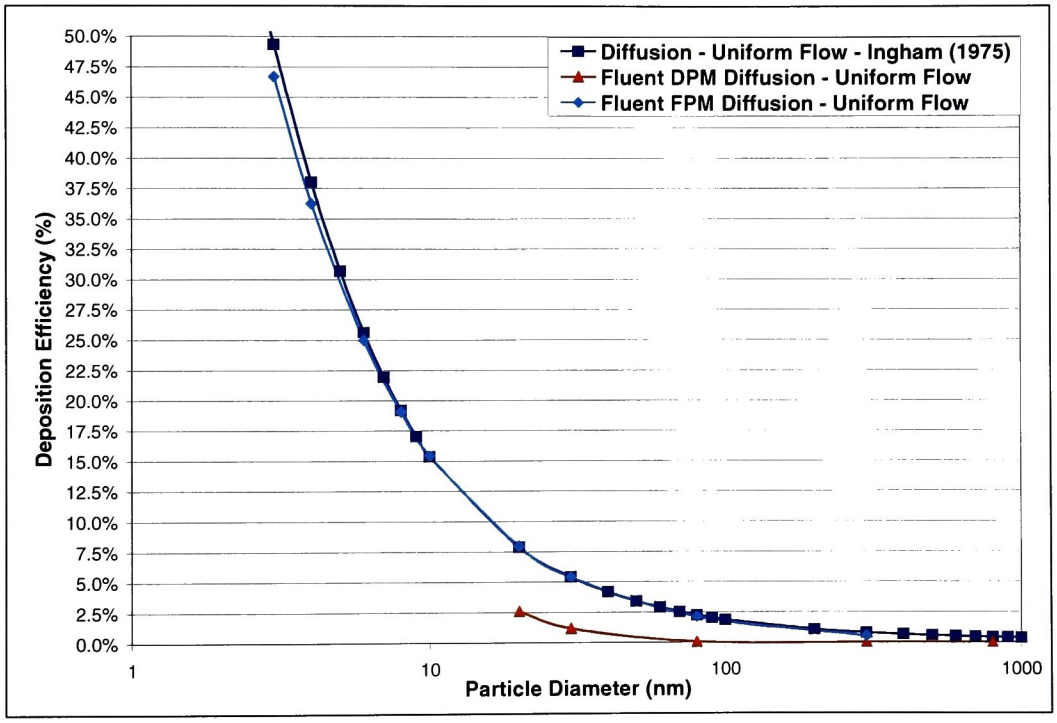


**Figure 6.5 Comparison of CFD data and analytical equation for diffusion from uniform flow in a straight tube in terms of particle size.**

### 6.2.3 Summary

The deposition efficiency predicted by each CFD software package and analytical equation for diffusion is provided in Table 6.2. As can be seen in Table 6.2, there is currently no published experimental data for isolated diffusion in a straight tube. This data could assist with improving understanding of both analytical and numerical predictions for the diffusion deposition mechanism.

When comparing to Ingham's (1975) analytical equation for parabolic flow, Fluent FPM for developing flow conditions is slightly more accurate than Fluent FPM for parabolic flow conditions, showing differences from analytical of 1.5% verses 2.5%, respectively. Both Fluent FPM flow conditions are significantly more accurate than Fluent DPM which more than doubles Ingham's (1975) prediction, or is 200% over analytical predictions. Additionally, Fluent DPM is only able to predict deposition efficiencies for a small range of particle sizes or Δ values, due to particles smaller than 20 nm evaporating or being too small to be tracked and deposition dropping to 0% prematurely.

**Table 6.2 Summary of deposition efficiencies observed in the straight tube geometry for diffusion for each flow condition and particle size.**

| Flow Rate (lpm) | Velocity Profile | Particle Size (μm) | Δ Value | Fluent DPM | Fluent FPM | Ingham (1975) Parabolic | Ingham (1975) Uniform | Experimental Data |
|---|---|---|---|---|---|---|---|---|
| 0.03 | Parabolic | 0.003 | 6.15E-02 | Evaporate | 29.68% | 32.03% | N/A | N/A |
| 0.03 | Parabolic | 0.004 | 3.47E-02 | Evaporate | 21.19% | 22.88% | N/A | N/A |
| 0.03 | Parabolic | 0.006 | 1.55E-02 | Evaporate | 12.99% | 14.14% | N/A | N/A |
| 0.03 | Parabolic | 0.008 | 8.77E-03 | Evaporate | 9.11% | 10.08% | N/A | N/A |
| 0.03 | Parabolic | 0.01 | 5.64E-03 | Evaporate | 6.91% | 7.76% | N/A | N/A |
| 0.03 | Parabolic | 0.02 | 1.45E-03 | 6.35% | 2.91% | 3.41% | N/A | N/A |
| 0.03 | Parabolic | 0.03 | 6.61E-04 | 4.49% | 1.76% | 2.07% | N/A | N/A |
| 0.03 | Parabolic | 0.08 | 1.06E-04 | 0.82% | 0.55% | 0.62% | N/A | N/A |
| 0.03 | Parabolic | 0.3 | 1.27E-05 | 0.02% | 0.15% | 0.15% | N/A | N/A |
| 0.03 | Parabolic | 0.8 | 3.66E-06 | 0.00% | 0.07% | 0.06% | N/A | N/A |
| 0.03 | Uniform | 0.003 | 6.15E-02 | Evaporate | 46.71% | N/A | 49.34% | N/A |
| 0.03 | Uniform | 0.004 | 3.47E-02 | Evaporate | 36.26% | N/A | 38.04% | N/A |
| 0.03 | Uniform | 0.006 | 1.55E-02 | Evaporate | 24.98% | N/A | 25.63% | N/A |
| 0.03 | Uniform | 0.008 | 8.77E-03 | Evaporate | 19.07% | N/A | 19.19% | N/A |
| 0.03 | Uniform | 0.01 | 5.64E-03 | Evaporate | 15.43% | N/A | 15.36% | N/A |
| 0.03 | Uniform | 0.02 | 1.45E-03 | 2.58% | 7.95% | N/A | 7.88% | N/A |
| 0.03 | Uniform | 0.03 | 6.61E-04 | 1.17% | 5.39% | N/A | 5.42% | N/A |
| 0.03 | Uniform | 0.08 | 1.06E-04 | 0.06% | 2.11% | N/A | 2.25% | N/A |
| 0.03 | Uniform | 0.3 | 1.27E-05 | 0.00% | 0.51% | N/A | 0.79% | N/A |
| 0.03 | Uniform | 0.8 | 3.66E-06 | 0.00% | 0.17% | N/A | 0.43% | N/A |

When comparing to Ingham's (1975) analytical equation for uniform flow, Fluent FPM is again significantly more accurate than Fluent DPM, which is under analytical by as much as three times or 300%. Fluent DPM is again only capable of predicting deposition for a small range of particle sizes or Δ values. Fluent FPM is always within 2.5% of Ingham's (1975) predictions for all values of Δ and particle sizes investigated in these flow conditions.

Of the three software packages being investigated, Fluent FPM is the only software package truly capable of predicting molecular diffusion over a range of Δ values. CFX only

predicts turbulent diffusion. Fluent DPM is not able to predict molecular diffusion for particles smaller than 20 nm, due to program limitations. Additionally, for the few values of $\Delta$ Fluent DPM is capable of predicting deposition by diffusion, the predictions are two or three times under or over Ingham's (1975) predictions. Fluent FPM has been able to predict molecular diffusion for particles as small as 3 nm in this research. Fluent FPM accurately predicts deposition by diffusion for both parabolic and uniform flow for all values of $\Delta$ investigated. Of the three packages, the only software that should be utilized for further diffusion research at this time is Fluent FPM.

# Chapter 7

# Impaction Deposition Mechanism

## 7.1 Impaction Theoretical Equations

There are numerous analytical and empirical equations that have been developed to predict deposition by impaction in the lung, bifurcating tubes, and bending tubes, as discussed in Section 1.3.3. The equations presented in the following sections have been utilized in the Trumpet Model, NCRP Model, and MPPD Model. These equations have been selected to evaluate the accuracy of the various CFD software packages in predicting deposition by the impaction mechanism based on their wide recognition and extensive peer review.

### 7.1.1 Yeh and Schum's Impaction Equation for a Bend (1980)

Yeh and Schum's (1980) impaction equation for a bend is utilized in the NCRP Model (United States National Council on Radiation Protection and Measurements, 1997). The equation is derived in Yeh (1974) based on the equation of motion of a particle rather than the stopping distance concept, and assuming a constant velocity profile. In the NCRP Model, the equations is attributed to Yeh and Schum (1980), this convention is followed in this research for ease of comparison by others in the aerosol deposition community. The equation is a general equation for inertial impaction in a bend, valid for constant velocity profiles and laminar flow. Although it is used in the NCRP code for all profiles and all flow conditions (personal correspondence). Yeh and Schum's (1980) equation is defined as,

$$\eta_i = 1 - \frac{2}{\pi}\cos^{-1}(\theta \bullet Stk) + \frac{1}{\pi}\sin\left[2\cos^{-1}(\theta \bullet Stk)\right], \qquad \textbf{Equation (7.1)}$$

for $\theta \bullet Stk < 1$,

and

$$\eta_i = 1, \qquad \textbf{Equation (7.2)}$$

for $\theta \bullet Stk \geq 1$.

In Equation (7.1) and Equation (7.2), $\eta_i$ is the deposition efficiency for impaction, $\theta$ is the bend or bifurcation angle in radians (half the internal angle of the bifurcation, if it is symmetric), and Stk is the Stokes number defined as,

$$Stk = \frac{\rho_p d_p^2 V C_c}{18 \mu D_p}, \qquad \textbf{Equation (7.3)}$$

for this research. In Equation (7.3) $\rho_p$ is the density of the particle, $d_p$ is the diameter of the particle, V is the average velocity of air in the generation entering the bifurcation, $C_c$ is the Cunningham slip correction factor defined by Equation (5.4), $\mu$ is the dynamic viscosity of air, and $D_p$ is the diameter of the generation entering the bifurcation.

Equation (7.1) is bounded by the product of the bend angle and the Stokes number. Equation (7.1) is only valid for positive values of $\theta$*Stk between 0 and 1. When the product of the bend angle and Stokes number is 0 there are 0% of the particles depositing. When the product of the bend angle and Stokes number is 1 there are 100% of the particles depositing.

Yeh and Schum's (1974) analytical equation for inertial impaction is utilized to evaluate the accuracy of the various CFD software packages in predicting deposition by impaction for parabolic, uniform, and developing flow conditions in Sections 7.3.2.1, 7.3.2.3, and 7.3.2.4.

### 7.1.2 Cai and Yu's Impaction Equations for Parabolic and Uniform Flow (1988)

Cai and Yu (1988) derived equations for impaction from parabolic and uniform flow. Cai and Yu's (1988) impaction equation for parabolic flow in a bifurcating tube is utilized the MPPD (Anjilvel and Asgharian, 1995). Cai and Yu's (1988) impaction equation for uniform flow in a bifurcating tube is currently not utilized in any of the models being focused on. This is largely due to the MPPD Model currently only utilizing equations for laminar or parabolic flow conditions. However, Cai and Yu's (1988) impaction equation for uniform flow is referenced and used for comparison by several research groups with good correlation and is therefore being presented and utilized in this research for completeness. Both of Cai and Yu's (1988) equations for impaction are derived from the stopping distance, velocity of the particles, and the geometry of the bifurcation. Gravity is neglected to isolate the impaction mechanism.

Cai and Yu's (1988) analytical equation for impaction from parabolic flow is defined by,

$$\eta_i = G(\theta, R_d/R_p) \bullet Stk, \qquad \textbf{Equation (7.4)}$$

where $\eta_i$ is the deposition efficiency for impaction, Stk is the Stokes number defined by Equation (7.3), and G is defined as,

$$G(\theta, R_d/R_p) = \frac{8\sin\theta\, f_1(\theta, R_d/R_p)}{\left(\frac{R_d}{R_p}\right) f_0(\theta, R_d/R_p)}. \qquad \textbf{Equation (7.5)}$$

In Equation (7.5), θ is the bifurcation angle in radians (half the internal angle of the bifurcation, if it is symmetric), $R_d$ is the radius of the daughter or generation following the bifurcation, $R_p$ is the radius of the parent or generation entering the bifurcation, $f_0$ is defined as,

$$f_0(\theta, R_d/R_p) = \pi\left[1 - \frac{1}{4}\left(\frac{R_d}{R_p}\right)^2\right] - \frac{4}{3}\left(\frac{15}{16}\pi - 2\right)\left(\frac{R_d}{R_p}\right)^2 \cos^2\theta, \qquad \textbf{Equation (7.6)}$$

and $f_1$ is defined as,

$$\begin{aligned} f_1(\theta, R_1/R_2) = 1 - \frac{1}{3}\left(\frac{R_d}{R_p}\right)^2 + \left(\pi - \frac{11}{3}\right)\left(\frac{R_d}{R_p}\right)^2 \cos^2\theta - \frac{1}{3}\left(\frac{R_d}{R_p}\right)^2 \sin\theta \\ + \left(\frac{2}{3} - \frac{\pi}{8}\right)\left(\frac{R_d}{R_p}\right)^4 \cos^2\theta + \frac{1}{5}\left(\frac{R_d}{R_p}\right)^4 \sin^2\theta + \\ \left(6 - \frac{15}{8}\pi\right)\left(\frac{R_d}{R_p}\right)^4 \cos^4\theta + \left(\frac{7}{15} - \frac{\pi}{8}\right)\left(\frac{R_d}{R_p}\right)^4 \sin^2\theta\cos^2\theta \end{aligned} \qquad \textbf{Equation (7.7)}$$

Cai and Yu's (1988) analytical equation for impaction from uniform flow is defined as,

$$\eta_i = F(\theta, R_d/R_p) \bullet Stk, \qquad \textbf{Equation (7.8)}$$

where F is defined as,

$$F(\theta, R_d/R_p) = \frac{4\sin\theta}{\pi\left(\frac{R_d}{R_p}\right)}. \qquad \textbf{Equation (7.9)}$$

Cai and Yu (1988) compared Equation (7.4) and Equation (7.8) to Chan and Lippmann's (1980) data for spherical particles deposition in hollow casts of the first six airways for Stokes numbers between 0.001 and 1.0. Cai and Yu (1988) achieved reasonable agreement with limited knowledge of the flow conditions and exact geometry tested. Due to the complex nature of Equation (7.4) and Equation (7.8), it is not possible to generate bounds for Equation (7.4) and Equation (7.8) that will hold true for all geometries and flow conditions. Once the geometry is selected bounds for Stokes number can very easily be generated.

Cai and Yu's (1988) analytical equations for deposition by impaction from parabolic and uniform flow are used to evaluate the accuracy of the various CFD software packages in predicting deposition by impaction for parabolic and uniform flow conditions, respectively, in Sections 7.3.2.1, 7.3.2.3, and 7.3.2.4.

### 7.1.3 Zhang, Asgharian, and Anjilvel's Impaction Equation for Parabolic and Uniform Flow (1997)

Zhang, et al.'s (1997) empirical equations for impaction for parabolic and uniform flow in a bifurcating tube have been utilized in the Trumpet Model (Robinson and Yu, 2001) since at least 1999. Before this time the Trumpet model utilized an empirical relation derived from experimental data for deposition in a bend (Yu, 1978; Schlesinger and Lippmann, 1972; Johnston, et al., 1977). Zhang, et al.'s (1997) equations were developed to fit numerically generated deposition data. This data was generated using flow fields generated in FIDAP, another CFD software package not investigated in this research, for parabolic and uniform inlet conditions in a bifurcating tube with various ratios of parent to daughter diameters and bifurcation angles. The particle deposition was calculated using an external program developed by Asgharian and Anjilvel (1994), which utilizes the fourth order Runge-Kutta method to solve the equation on motion. Zhang, et al. (1997) investigated several Reynolds numbers within the laminar range. Gravity and Brownian motion were turned off to isolate the impaction deposition mechanism. The walls were defined as no slip boundaries and uniform pressure was assumed at the outlets.

Zhang, et al.'s (1997) impaction equation for parabolic flow is split into two parts where for $Stk < 0.04$,

$$\eta_i = 0.000654\exp\left(55.7Stk^{0.954}\right)\mathrm{Re}^{1/3}\sin\theta, \qquad \textbf{Equation (7.10)}$$

and for $Stk \geq 0.04$,

$$\eta_i = \left[0.19 - 0.193\exp\left(-9.5Stk^{1.565}\right)\right]\mathrm{Re}^{1/3}\sin\theta. \qquad \textbf{Equation (7.11)}$$

In Equation (7.10) and Equation (7.11), $\eta_i$ is the deposition efficiency for impaction, Stk is the Stokes number defined by Equation (7.3), $\theta$ is the bifurcation angle in radians, measured clockwise from the vertical up to the left bifurcation (half the internal angle of the bifurcation, if it is symmetric), and Re is the Reynolds Number for air entering the bifurcation defined as,

$$\mathrm{Re} = \frac{\rho V D_p}{\mu}. \qquad \textbf{Equation (7.12)}$$

In Equation (7.12), $\rho$ is the density of air, V is the average velocity of the free stream air in the generation entering the bifurcation, $D_p$ is the diameter of the generation entering the bifurcation or parent, and $\mu$ is the dynamic viscosity of air.

Zhang, et al.'s (1997) impaction equation for uniform flow is a two part equation where for $Stk < 0.07$,

$$\eta_i = 0.000425\exp\left(22.7Stk^{0.832}\right)\mathrm{Re}^{1/3}\sin\theta, \qquad \textbf{Equation (7.13)}$$

and for $Stk \geq 0.07$,

$$\eta_i = \left[0.19 - 0.194\exp\left(-3.28Stk^{1.585}\right)\right]\mathrm{Re}^{1/3}\sin\theta. \qquad \textbf{Equation (7.14)}$$

In equations 7.10, 7.11, 7.13 and 7.14, $\eta_i$ is valid up to 1, since deposition efficiency cannot exceed 100%.

Zhang, et al. (1997) compared the equations for impaction from parabolic and uniform flow to experimental data from Johnston, et al. (1977), Schlesinger, et al. (1977), Gurman, et al. (1984), and Kim and Iglesias (1989). The equations for impaction from parabolic flow compared reasonably well to Gurman, et al. (1984) for Stokes numbers between 0.01 and 0.1. The other three studies had fair to poor correlation. The equations for impaction from uniform flow compared reasonably well to Schlesinger, et al. (1977) for Stokes numbers between 0.01 and 1.0. Zhang, et al.'s (1997) equation for uniform flow had fair to poor correlation with the other three studies. It should be noted that Zhang, et al.

(1997) normalized all these studies in terms of Stokes number, Reynolds number and bifurcation angle in order to compare with their impaction equation for parabolic flow. Of the studies, only Kim and Inglesias (1989) compared to a bifurcation and this geometry was altered significantly in Zhang, et al.'s (1997) study. The geometry utilized by Zhang, et al. (1997) focused on the bifurcation region and had very short parent and daughter generations. Additionally, there was a sharp bifurcation, rather than a filleted one and a long, gradual transition from the parent to daughter generations. As mentioned in Section 1.4, Johnston, et al. (1977) utilized a bend for his experiments and Schlesinger, et al. (1977) and Gurman, et al. (1984) utilized hollow cast of lung geometries.

Due to the multiple independent variables in Equation (7.10) and Equation (7.11) that effect deposition, it is not possible to determine a single or multiple variable bounds that will hold true for all flow conditions or geometries. Once the geometry is selected, bounds for Stokes number can very easily be generated.

Zhang, et al.'s (1997) empirical equations for impaction from parabolic and uniform flow are utilized to evaluate the accuracy of the various CFD software packages in predicting deposition by impaction from parabolic and uniform flow conditions, respectively, in Sections 7.3.2.1, 7.3.2.3, and 7.3.2.4.

## 7.2 Kim and Iglesias' Experimental Data (1989)

There are several experimental studies that investigate deposition in bends, bifurcating tubes, and series of bifurcating tubes, see Section 1.4. Kim and Iglesias' (1989) study has been selected to evaluate the various CFD software packages ability to predict deposition by impaction. Kim and Iglesias' (1989) was selected because the study examined deposition in a single bifurcation, explored multiple particles sizes and flow conditions, reported more than one data point for each particle size and flow condition, almost completely isolated the impaction mechanism at some of the flow conditions, and provided ample information to recreate the experiment computationally.

Kim and Iglesias (1989) explored deposition in symmetric and asymmetric bifurcations at several angles and ratios of flow through the daughter tubes. For this research only the symmetric bifurcation with a 30° half angle was utilized, the geometry is described in more detail in Section 4.2. Kim and Iglesias (1989) investigated three flow rates; 4 lpm, 8

lpm, and 12 lpm. For each flow rate investigated, Kim and Iglesias (1989) utilized three particle sizes; 3 μm, 5 μm, and 7 μm.

Kim and Iglesias (1989) broke the bifurcation geometry into seven sections to allow for local deposition to be investigated, shown in Figure 7.1. The data reported in Kim and Iglesias (1989) is for deposition in sections D1 and D2, which accounts for 88% ± 2% of the total deposition for Stk > 0.09 and 71% ± 7% of the total deposition for Stk < 0.05. The experimental data presented in this research reflects the estimated total deposition calculated from Kim and Iglesias's (1989) data using this information (see Table 7.1).

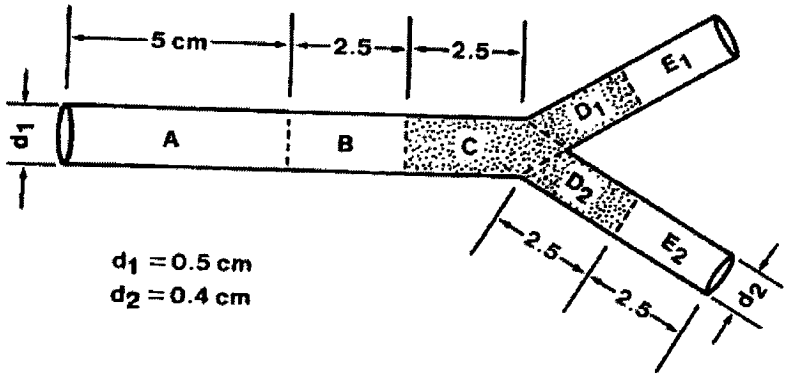


**Figure 7.1 Schematic of Kim and Iglesias' (1989) bifurcating tube showing individual sections used for local deposition.**

**Table 7.1 Kim and Igelsias' (1989) experimental data for Sections D1 and D2 and estimated total deposition.**

| Flow rate in Parent (liter/min) | Particle Size (μm) | Stokes Number | Deposition in Sections D1 and D2 | % of Total | Estimated Total Deposition (range of 2 runs) |
|---|---|---|---|---|---|
| 4 | 3 | 0.017 | 0.6% | 71% ± 7% | 0.77-0.94% |
| | 5 | 0.047 | 3.5-4.2% | 71% ± 7% | 4.49-6.56% |
| | 7 | 0.091 | 20.6-22.4% | 88% ± 2% | 22.89-26.05% |
| 8 | 3 | 0.034 | 1.8-2.2% | 71% ± 7% | 2.31-3.44% |
| | 5 | 0.093 | 21-24.1% | 88% ± 2% | 23.33-28.02% |
| | 7 | 0.18 | 46.3-50.2% | 88% ± 2% | 51.44-58.37% |
| 12 | 3 | 0.05 | 4.4-4.5% | 71% ± 7% | 5.64-7.03% |
| | 5 | 0.14 | 31.7-34.3% | 88% ± 2% | 35.22-39.88% |
| | 7 | 0.27 | 59.1-61.3% | 88% ± 2% | 65.67-71.28% |

In order to insure the impaction deposition mechanism was isolated in Kim and Iglesias (1989), the relative effect of each mechanism was explored. The presence of deposition by diffusion could quickly be eliminated, since the size of the particles being investigated, all larger than 1 μm, are at the upper limit for deposition by diffusion. To determine the effect of sedimentation it was necessary to know how Kim and Iglesias (1989) positioned the bifurcation relative to gravity. A schematic of the experimental set-up utilized by Kim and Iglesias (1989) is shown in Figure 7.2. Figure 7.2 indicates that the bifurcation is held in the horizontal position where gravity could cause deposition by sedimentation; this was confirmed through a personal communication. To examine the effect of impaction and sedimentation in the bifurcation for Kim and Iglesias' (1989) experimental conditions, the deposition efficiencies for all the impaction equations introduced in Section 7.1, Pich's (1972) sedimentation equation, and Yu, et al.'s (1977) sedimentation equation are plotted for all particle sizes and all flow conditions investigated. At the ε values present in the bifurcation Pich (1972), Wang (1975), and Yeh and Schum (1980) predict the same deposition efficiency for parabolic flow and Yu, et al. (1977) and Yeh and Schum (1980) for uniform flow (See Section 5.2.2). Therefore it is only necessary to explore one equation for each velocity profile. Pich (1972) and Yu, et al. (1977) were selected to evaluate the effect of sedimentation in the bifurcation geometry because each predicts the highest deposition efficiency for sedimentation for their respective velocity profile and provide predictions closest to those obtained from CFD in the straight tube (See Section 5.2.2). The impaction equations predict an array of deposition efficiencies, so each equation is plotted.

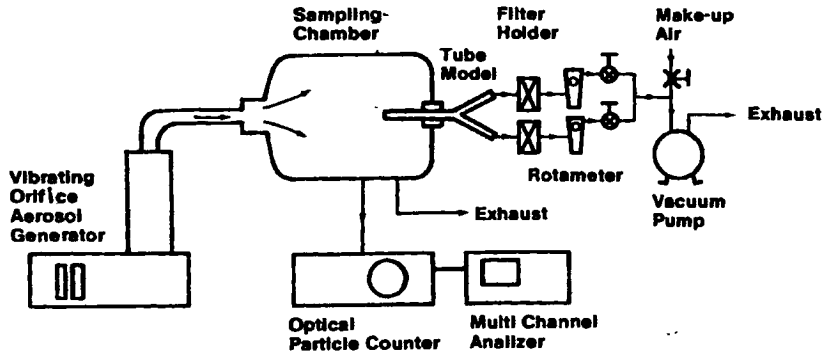


**Figure 7.2 Schematic of test set-up utilized by Kim and Iglesias (1989) to obtain experimental data for deposition by impaction in a bifurcating tube.**

Plots were created for each of the particle sizes as a function of flow rate to visualize the effect of sedimentation relative to impaction. Figure 7.3 shows this plot for the 3 μm particle size, where sedimentation represented the largest percent of the total deposition compared to the other two sizes. The plots for the 5 μm and 7 μm particle sizes are contained in Appendix F.

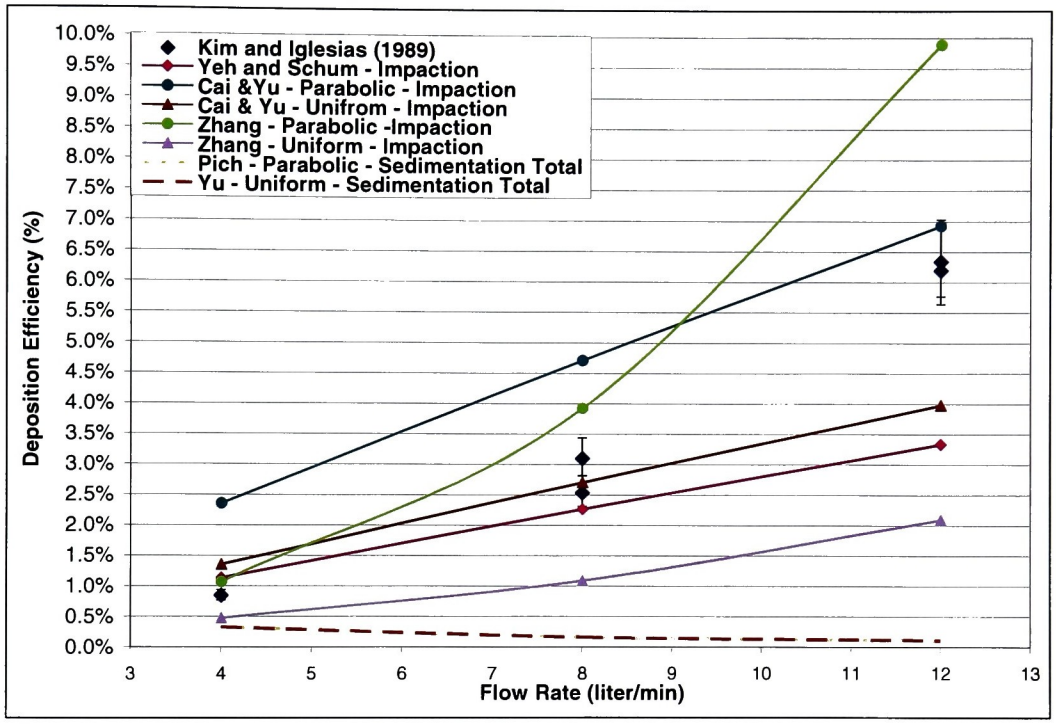


**Figure 7.3 Theoretical equations estimates of impaction and sedimentation in the bifurcating tube geometry for 3 μm particles at 4, 8, and 12 lpm flow rates.**

To determine which experimental cases are acceptable for isolating impaction, the maximum percent of the total deposition resulting from sedimentation is determined for each condition. If the percent attributed to sedimentation is less than 2%, impaction is considered sufficiently isolated. The total deposition by sedimentation in the parent and daughter airways is determined by,

$$dep_{tot} = dep_p + dep_d\left(1 - dep_p\right), \qquad \textbf{Equation (7.15)}$$

where $dep_{tot}$ is the total deposition, $dep_p$ is the deposition in the parent generation, and $dep_d$ is the deposition a daughter generation. Predictions for sedimentation in the parent, daughter,

and entire bifurcation geometry are included in Table 7.2 for Pich (1972), parabolic flow, and Table 7.3 for Yu, et al. (1977), uniform flow, for all flow rates and particle sizes.

**Table 7.2 Affect of sedimentation in the bifurcating tube for parabolic flow predicted by Pich (1972).**

| Flow rate in Parent (liter/min) | Particle Size (μm) | Stokes Number | Pich (1972) Sedimentation Parent | Pich (1972) Sedimentation in 1 Daughter | Pich (1972) Sedimentation Total | % of experimental (average of average) |
|---|---|---|---|---|---|---|
| 4 | 3 | 0.017 | 0.18% | 0.15% | 0.33% | 38.64% |
| | 5 | 0.047 | 0.50% | 0.40% | 0.90% | 16.66% |
| | 7 | 0.091 | 0.98% | 0.79% | 1.76% | 7.21% |
| 8 | 3 | 0.034 | 0.09% | 0.07% | 0.16% | 5.80% |
| | 5 | 0.093 | 0.25% | 0.20% | 0.45% | 1.77% |
| | 7 | 0.18 | 0.49% | 0.39% | 0.89% | 1.61% |
| 12 | 3 | 0.05 | 0.06% | 0.05% | 0.11% | 1.74% |
| | 5 | 0.14 | 0.17% | 0.13% | 0.30% | 0.81% |
| | 7 | 0.27 | 0.33% | 0.26% | 0.59% | 0.86% |

**Table 7.3 Affect of sedimentation in the bifurcating tube for uniform flow predicted by Yu, et al. (1977).**

| Flow rate in Parent (liter/min) | Particle Size (μm) | Stokes Number | Yu, et al. (1977) Sedimentation Parent | Yu, et al. (1977) Sedimentation in 1 Daughter | Yu, et al. (1977) Sedimentation Total | % of experimental (average of average) |
|---|---|---|---|---|---|---|
| 4 | 3 | 0.017 | 0.18% | 0.15% | 0.33% | 38.76% |
| | 5 | 0.047 | 0.51% | 0.40% | 0.91% | 16.75% |
| | 7 | 0.091 | 0.99% | 0.79% | 1.78% | 7.27% |
| 8 | 3 | 0.034 | 0.09% | 0.07% | 0.16% | 5.82% |
| | 5 | 0.093 | 0.25% | 0.20% | 0.45% | 1.77% |
| | 7 | 0.18 | 0.50% | 0.40% | 0.89% | 1.62% |
| 12 | 3 | 0.05 | 0.06% | 0.05% | 0.11% | 1.74% |
| | 5 | 0.14 | 0.17% | 0.13% | 0.30% | 0.81% |
| | 7 | 0.27 | 0.33% | 0.26% | 0.59% | 0.87% |

At the 4 lpm flow rate, sedimentation accounts for between 7.2% and 38.8% of the total deposition, depending on the particle size. Sedimentation is between 1.6% and 5.8% of the total deposition at the 8 lpm flow rate and 0.86% and 1.7% of the total deposition at the 12 lpm flow rate, depending on the particle size. The impaction mechanism is only isolated at the 12 lpm flow rate for all particle sizes, where sedimentation is theoretically less than 2% of the total observed deposition. Impaction is also isolated for the 5 μm and 7 μm particle sizes at the 8 lpm flow rate. At the 4 lpm flow rate, sedimentation theoretically accounts for a

significant amount of the total observed deposition; therefore combined impaction and sedimentation is investigated at this flow rate. The 8 lpm (5 μm and 7 μm only) and 12 lpm (all sizes) flow rates are only investigated for the isolated impaction mechanism in this research.

## 7.3 Results for Impaction in a Bifurcating Tube from Various CFD Software Packages

The impaction mechanism is evaluated in Fluent DPM and CFX. Fluent FPM is not evaluated due to the software being incapable of predicting deposition by impaction. For more information on Fluent FPM's tracking algorithms and inability to track particle deposition by impaction see Section 2.2.

### 7.3.1 Flow Conditions and Particle Properties

The flow conditions utilized in the bifurcating tube geometry to investigate the impaction deposition mechanism have been selected to allow for comparison to Kim and Iglesias' (1989) experimental data for nearly the identical bifurcation geometry. The flow conditions utilized in the various CFD software packages were calculated from the information provided by Kim and Iglesias (1989). The general flow conditions utilized for all flow rates are contained in Table 7.4 and the flow conditions dependent on flow rate are contained in Table 7.5 for the three flow rates investigated.

As seen in Table 7.5 both laminar and transitional flow conditions were investigated by Kim and Iglesias (1989). When investigating transitional flow there are options for the viscous solver, laminar or one of the turbulence models, since neither of the software packages investigated has a designated solver for transitional flow. The k-epsilon solver is the most commonly utilized turbulence model and was therefore selected for this research. It should be noted, that both CFX and Fluent DPM recommend the k-epsilon turbulence solver only be utilized for fully developed turbulent flow (Fluent Inc., 2003; ANSYS Inc., 2003) despite its common use for all Reynolds number flows in other research. The length scale and turbulence intensity option is utilized for the k-epsilon solver in both CFD packages. The length scale is defined as,

$$Ls = 0.07(D_p) \text{ (Fluent, 2003),} \qquad \textbf{Equation (7.16)}$$

where Ls is the length scale for a duct, $D_p$ is the diameter of the parent generation, the 0.07 factor is based on the maximum mixing length of fully developed turbulent pipe flow. For this research a length scale of 3. 5E-4 m is utilized and turbulence intensities of 1%, 5%, and 10% are investigated. To isolate the impaction deposition mechanism, Brownian diffusion and gravity are turned off.

**Table 7.4 Flow conditions run in the bifurcating tube for all flow rates to investigate the impaction deposition mechanism.**

| | |
|---|---|
| Viscosity (air STP) | 1.8E-5 $Ns/m^2$ |
| Air Density (STP) | 1.2 $kg/m^3$ |
| Mean Free Path | 0.066 μm |

**Table 7.5 Flow conditions run in the bifurcating tube dependent on flow rate to investigate the impaction deposition mechanism.**

| Flow Rate | Average Velocity in Parent | Reynolds Number | Entrance Length |
|---|---|---|---|
| 4 liter/min (6.67E-5 $m^3/s$) | 3.40 m/s | 1132 | 33.95 cm |
| 8 liter/min (1.33E-4 $m^3/s$) | 6.79 m/s | 2264 | 67.90 cm |
| 12 liter/min (2.00E-4 $m^3/s$) | 10.19 m/s | 3395 | 101.8 cm |

Three velocity profiles are utilized in the bifurcating tube to investigate the impaction deposition mechanism; parabolic, developing and uniform velocity profiles. Plots of the velocity profiles at the inlet, 9.5 cm down the parent section, 0.5 cm in the daughter section and 4.5 cm down the daughter section of the bifurcating tube are contained in Appendix D for Fluent DPM and CFX. For the parabolic velocity profile the walls are defined as no slip boundaries and the velocity profile is defined at the inlet by a user defined function in Fluent DPM and an expression in CFX. The parabolic velocity profile is defined by Equation (5.19) where constants A, B, and C are provided in Table 7.6 for the three flow rates investigated. The developing velocity profile is defined by a constant velocity at the inlet, which corresponds to the average velocities contained in Table 7.5 for each flow rate and no slip boundaries at the walls. The uniform velocity profile is defined by a constant velocity at the inlet, which also corresponds to the average velocity for each flow rate and free slip or 0 shear stress boundaries at the walls. All three profiles are evaluated for all three flow rates; even though Kim and Iglesias (1989) placed a tube (inner diameter 0.5 cm and length 20 cm) in front of the bifurcation, which would result in partially developed flow at these flow rates, see Table 7.5. It is necessary to explore all three profile shapes, since Kim and Iglesias

(1989) did not provide PIV (particle image velocimetry) measurements, pressure drop, or any other detailed information about the velocity profiles obtained during testing. Additionally, exploring multiple velocity profiles will provide more information on the nature of the algorithms utilized by the various CFD software packages.

**Table 7.6 Constants for parabolic flow velocity profile equation for investigating impaction in the bifurcating tube geometry.**

| Flow Rate | A | B | C |
|---|---|---|---|
| 4 liter/min | -1088000 $m^{-1}s^{-1}$ | -1088000 $m^{-1}s^{-1}$ | 6.8 m/s |
| 8 liter/min | -2172800 $m^{-1}s^{-1}$ | -2172800 $m^{-1}s^{-1}$ | 13.58 m/s |
| 12 liter/min | -3260800 $m^{-1}s^{-1}$ | -3260800 $m^{-1}s^{-1}$ | 20.38 m/s |

Kim and Iglesias (1994) utilized monodisperse oleic acid droplets tagged with uranine for their experiments. The dissolved oleic acid, which was aerosolized to create 3 μm, 5 μm, and 7 μm, had a density of 891 $kg/m^3$. The particles utilized to investigate the accuracy of the various CFD software packages are solid particles of sizes 3 μm, 5 μm, and 7 μm, with a density of 891 $kg/m^3$. The flow conditions and particle sizes utilized by Kim and Iglesias (1989) and this research provide Stokes numbers between 0.017 and 0.27; see Figure 7.4.

As mentioned in Chapter 2, each software package generates particles differently. CFX automatically generates particles and injects them near the inlet. In Fluent, the particles are defined by an injection file created in J Builder from a Java script. In all the software packages the particles are randomly distributed. In CFX, the random distribution is created by using the Uniform setting for the particles. The J Builder code used to generate the particles for Fluent DPM is written to obtain a random particle distribution. For the bifurcating tube geometry in Fluent DPM the particles were injected at 0.01 mm from the inlet and no less than 0.5 mm from the walls, occupying 98% of the available radius.

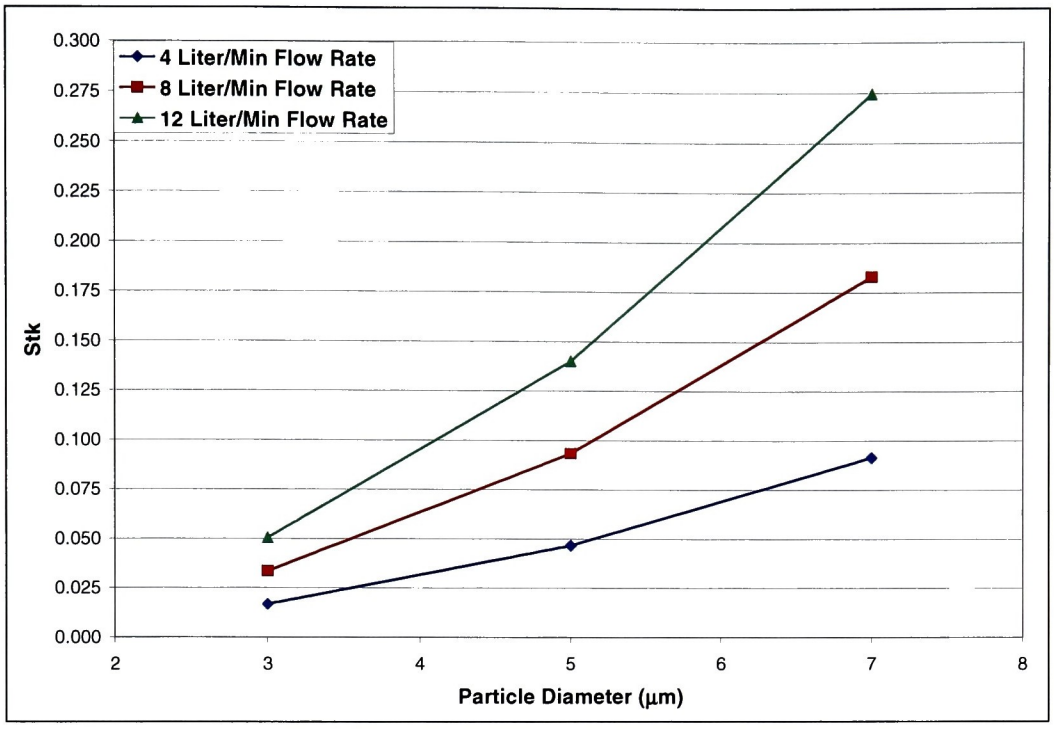


**Figure 7.4 Stokes numbers for particle diameter and three flow rates run to evaluate the impaction deposition mechanism in the bifurcating tube geometry.**

### 7.3.2 Comparison of CFD Results, Experimental Data, and Analytical Equations

The CFD data obtained from Fluent DPM and CFX for impaction in the bifurcating tube is compared to the analytical and empirical equations introduced in Section 7.1 and the experimental data obtained by Kim and Iglesias (1989) introduced in Section 7.2 and 7.3.1. Section 7.3.2.1 contains data for the 4 lpm flow conditions for impaction and combined impaction and sedimentation for parabolic, developing and uniform velocity profiles. Section 7.3.2.3 and Section 7.3.2.4 contains data for the 8 lpm and 12 lpm flow conditions, respectively, for impaction using the laminar and k-epsilon solvers in CFX and Fluent DPM for parabolic, developing, and uniform velocity profiles. In each Section, the parabolic flow conditions are compared to Equation (7.1), Yeh and Schum (1980), Equation (7.4), Cai and Yu (1988), and Equation (7.10), Zhang, et al. (1997). The uniform flow conditions are compared to Equation (7.1), Yeh and Schum (1980), Equation (7.8), Cai and Yu (1988), and

Equation (7.13), Zhang, et al. (1997). The developing flow conditions are compared to the uniform and parabolic data obtained from the CFD software packages.

### 7.3.2.1 Isolated Impaction at the 4 Liter/Min Flow Conditions

At the 4 lpm flow rate, particle deposition is investigated for the impaction and combined impaction and sedimentation mechanisms for parabolic, uniform and developing velocity profiles. The data generated by Fluent DPM and CFX is compared to experimental data from Kim and Iglesias (1989) and the analytical equations from Yeh and Schum (1980), Cai and Yu (1988), and Zhang, et al. (1997).

Isolated impaction is investigated to determine how Fluent DPM and CFX compare to the analytical equations for similar flow conditions and Kim and Iglesias' (1989) experimental data. It is known that sedimentation theoretically accounts for as much as 38.8% of the total deposition observed and correlation with experimental data could be poor, however, the presence of sedimentation should not affect the correlation between CFD results and analytical equations. At the 4 lpm flow rate, the velocity profile is expected to be 59% developed at the entrance to the bifurcation geometry based on Kim and Iglesias' (1989) experimental data; therefore an accurate depiction of the velocity profile is parabolic or developing. However, since detailed information about the velocity profiles was not provided, parabolic, uniform and developing velocity profiles are investigated. It is anticipated that the developing flow conditions will provide deposition efficiencies between those predicted by parabolic and developing flow.

Figure 7.5 provides the deposition efficiency verses Stokes number for parabolic flow with isolated impaction for the two CFD software packages, the three relevant impaction analytical equations, and Kim and Iglesias' (1989) experimental data. It is expected the parabolic flow conditions will over predict the deposition efficiencies at the 4 lpm, since the flow is roughly 59% developed at the bifurcation in Kim and Inglesias' (1989) experiment. However, the influence of sedimentation at the 4 lpm flow rate should result in the impaction theoretical predictions under estimating the experimental data where sedimentation theoretically has a deposition efficiency higher than a few percent.

The theoretical equations do not underestimate the experimental data, as is expected due to the presence of sedimentation, except for the 7 μm particles (Stk = 0.091). For the 5

μm particles (Stk = 0.50), Zhang, et al. (1997) and Cai and Yu (1988) predict higher deposition, and for the 3 μm particles (Stk = 0.017), all three impaction theoretical equations over predict the experimental data, Zhang, et al. (1997) by the largest amount, followed by Yeh and Schum (1980), and then Cai and Yu (1988). The over estimation of the experimental data by the theoretical equations could be attributed to the flow not being fully developed and theoretical deposition by sedimentation being less than 1% at these particle sizes. According to the theoretical predictions for sedimentation, as the particle size increases the more the theoretical impaction equations should under predict the experimental data, due to the sedimentation deposition efficiency increasing above 1%. This is in fact what is seen; at the 3 μm (Stk = 0.017) the theoretical equations are off by 0.5% to 1.5%, by the 7 μm (Stk = 0.091) the theoretical equations are off by 5% to 15%.

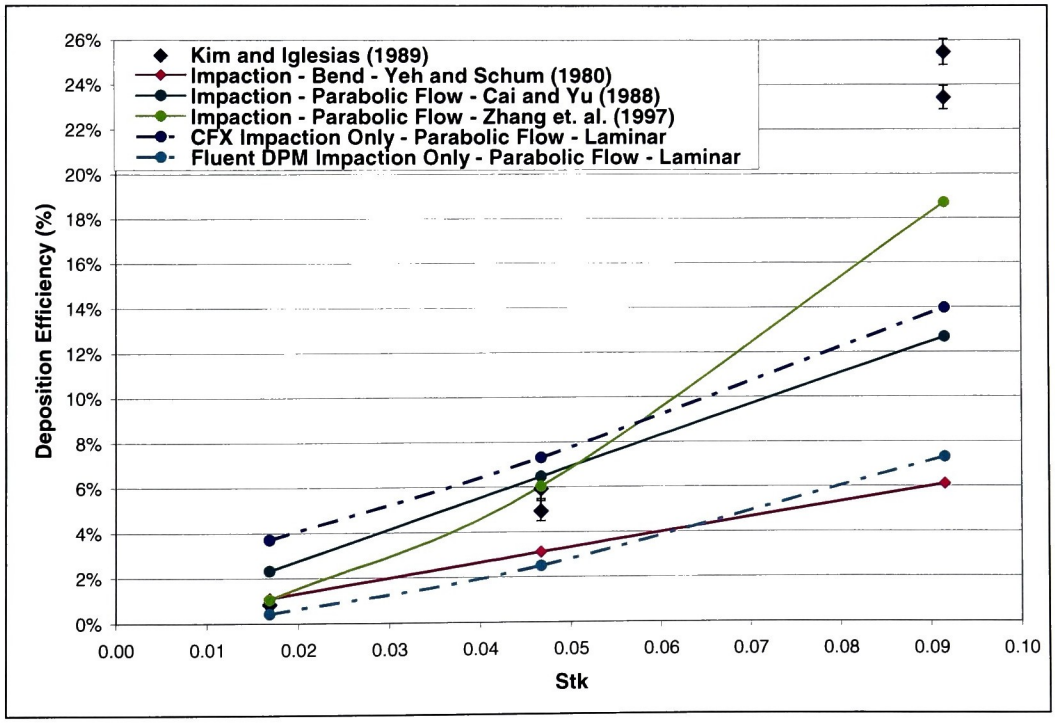


**Figure 7.5 Comparison of CFD data, analytical equations, and experimental data for isolated impaction in the bifurcating tube geometry for parabolic flow at a 4 lpm flow rate.**

Experimental data is between 7.5% and 16% greater than the CFD predictions at the 0.091 (7 μm) Stokes number, more than theoretically predicted (see Table 7.2 and Table 7.3). CFX's prediction agrees with experimental data at the 0.047 Stokes number (5 μm), while

over predicting at the 0.017 (3 μm) Stokes number and under predicting at the 0.091 (7 μm) Stokes number. This trend is unexpected, because sedimentation theoretically represents a larger percent of the total deposition at the 3 μm and 5 μm particles sizes than the 7 μm particles size (see Table 7.2). It would therefore be expected that CFD would under predict the experimental data by more at the lower Stokes numbers or smaller particle sizes. The trend could be attributed to the conflicting influence of sedimentation, which should cause predictions to be less than experimental data, and parabolic flow, which could over predict the experimental data for this flow condition. Of the CFD software packages tested, Fluent DPM has the curve shape closest to the experimental data, with a steeper incline from the 0.047 (5 μm) to 0.091 (7 μm) Stokes number. Fluent DPM under predicts the experimental data at all Stokes numbers.

CFX's prediction aligns closest with Cai and Yu (1988) and has a similar curve shape. CFX over predicts Cai and Yu (1988) by 1% to 2% for the Stokes number investigated. The deposition efficiencies predicted by Fluent DPM align closest with Yeh and Schum (1980), always within 1.5% for the Stokes numbers investigated. Fluent DPM is under Cai and Yu (1988) by 2% to 7% and Zhang, et al. (1997) by 1% to 13%.

Table 7.6 provides the deposition efficiency verses Stokes number for uniform flow with isolated impaction for the two CFD software packages, the three relevant impaction analytical equations, and Kim and Iglesias' (1989) experimental data. At the highest stokes number, 0.091 (7 μm), all analytical equations significantly under predict experimental data. This is likely because the uniform profile used in the analytical equations results in smaller deposition by impaction than the parabolic profile, which more closely matches the experimental conditions. As the sedimentation becomes more significant at lower Stokes numbers, the affect of the parabolic profile is reduced and better agreement is found between experimental and CFD. This is consistent with earlier findings that for sedimentation, uniform and parabolic flow conditions predict similar deposition efficiencies at small $\varepsilon$ values (See Section 5.2.2). Cai and Yu (1988) is within 2% of the experimental data at Stokes numbers of 0.017 (3 μm) and 0.5% at 0.047 (10 μm). Yeh and Schum (1980) is only slightly worse than Cai and Yu (1988) at these stokes numbers, while Zhang, et al. (1997) predicts as little as one fifth of the experimental deposition. Zhang, et al. (1997) has the

same exponential increase in deposition seen in the experimental data, while Cai and Yu (1988) and Yeh and Schum (1980) predict a more linear increase in deposition.

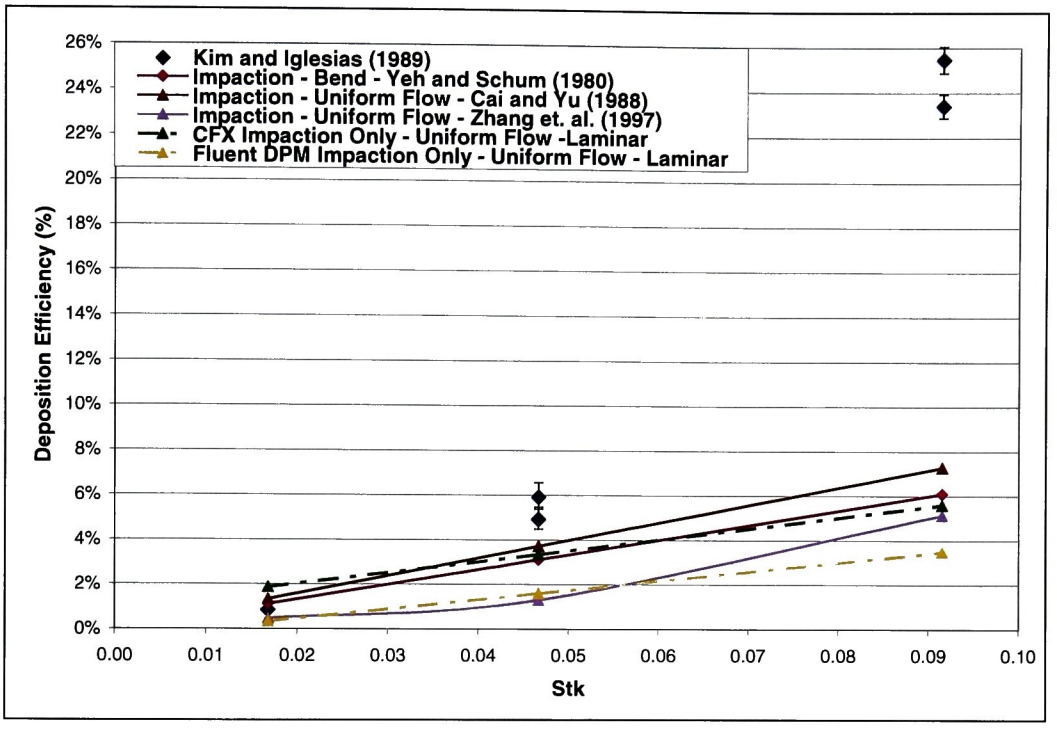


**Figure 7.6 Comparison of CFD data, analytical equations, and experimental data for isolated impaction in the bifurcating tube geometry for uniform flow at a 4 lpm flow rate.**

The CFD results significantly under predict experimental data at the highest Stokes number but agree better as the Stokes number decreases, similar to the trend found with theoretical predictions. Agreement between CFD and theoretical equations is between 0.5% and 4%, which is expected since both are using a uniform profile. However, there is a notable difference in the line trends. The slope of the theoretical curves of Cai and Yu (1988) and Yeh and Schum (1980) are slightly larger than the CFD results. In addition, it was expected that the behavior of Zhang, et al. (1997) would closely agree with the other CFD packages, since it is actually a numerical and not an analytical solution, using actually velocity profiles. However, Zhang, et al. (1997) shows an exponential rather than the linear curves seen in the CFD and other theoretical equations' prediction, which use constant velocity profiles.

Figure 7.7 provides the deposition efficiency verses Stokes number for isolated impaction for the two CFD software packages at parabolic, uniform and developing flow conditions and Kim and Iglesias' (1989) experimental data. At first glance, it is expected that the developing flow condition should provide impaction deposition efficiencies between the uniform and parabolic flow cases, since the center line flow is moving faster than the uniform flow conditions, and slower than the fully developed parabolic flow conditions. The faster the air is moving the more difficult it is for the particles to have sufficient time to change path and follow the free stream flow, so the faster the streamline velocity the higher the deposition efficiency by impaction is anticipated to be. However, the developing flow condition will actually have faster moving particles distal to the centerline compared to the parabolic case, so it is reasonable that in some conditions, developing flow would result in larger deposition efficiencies than parabolic flow. For both CFX and Fluent DPM at the lower Stokes numbers, developing flow results are between the uniform and parabolic cases, however at the 0.091 (7 μm) Stokes number the deposition efficiency is slightly higher for the developing flow condition. The developing flow condition in general provides deposition efficiencies closer to the parabolic flow condition than the uniform condition, which is expected for this flow rate where the parent tube is 30% of the entrance length and the profile is more parabolic than uniform (See Appendix D).

Although CFX provides higher deposition efficiencies for each flow condition than Fluent DPM, the curve shape at each flow condition is similar for the two CFD software packages. The slope of the uniform profile cases for CFD is significantly smaller than the parabolic or developing cases, so that the choice of velocity profile has a larger affect at higher Stokes numbers than at lower Stokes numbers. The slope of the developing profile cases are larger than the parabolic cases and slightly exponential in behavior, compared to the larger exponential behavior of the experimental data, yielding only a slightly better agreement, at the highest Stokes number, with experimental data compared to the parabolic case. The remaining difference between experimental and CFD data is likely due to the presence of sedimentation.

In general, for high Stokes number, the CFD and analytical equations have better agreement with the experimental data for the parabolic flow conditions at the 4 lpm flow rate. CFD software packages and analytical equations significantly under predict the experimental

data for uniform flow conditions at the 4 lpm flow rate at the high Stokes numbers. Developing flow predictions align closer with the parabolic flow than the uniform flow predictions for these flow conditions. For the 4 lpm flow condition it is fair to say the experimental flow is either parabolic or developing. The developing flow predictions fall between parabolic and uniform predictions, except at the 0.091 (7 μm) Stokes number, where developing flow predictions for deposition efficiency are slightly higher than the parabolic flow predictions. Zhang, et al. (1997) has the best agreement with the experimental data in shape and magnitude for all Stokes numbers compared to the other two theoretical equations. CFX always predicts higher deposition than Fluent for all flow conditions.

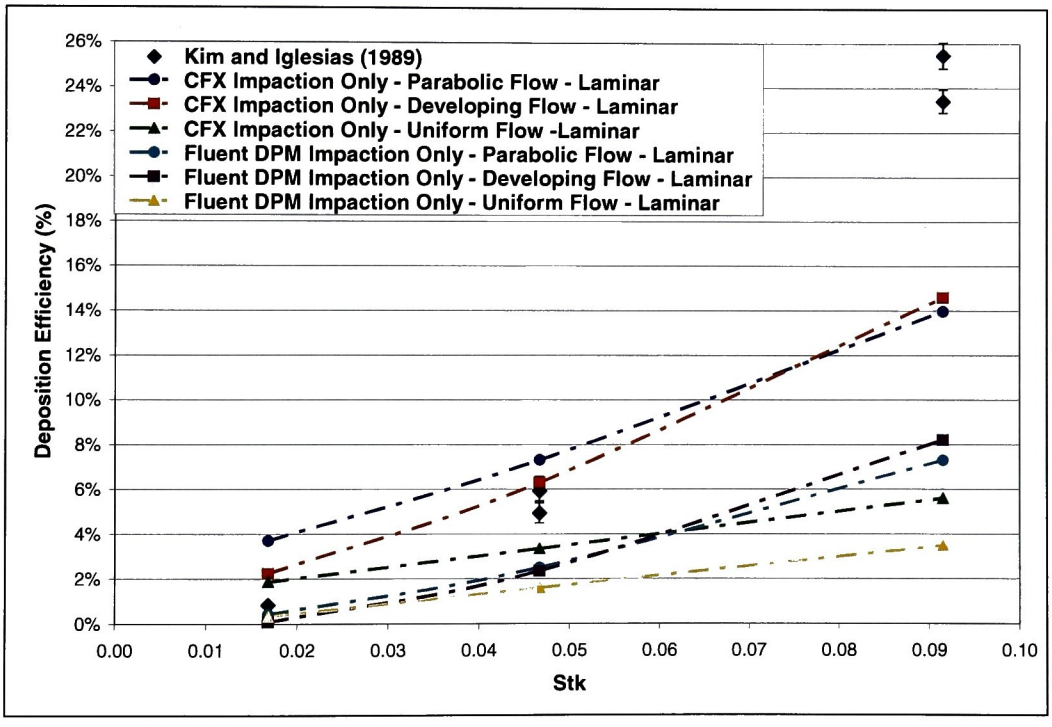


**Figure 7.7 Comparison of CFD data for developing flow to CFD data for parabolic and uniform flow and experimental data for isolated impaction in the bifurcating tube geometry at a 4 lpm flow rate.**

### 7.3.2.2 Combined Impaction and Sedimentation at the 4 Liter/Min Flow Condition

Combined impaction and sedimentation is investigated in the bifurcating tube at the 4 lpm flow rate because Pich (1972) and Yu, et al. (1997) predict sedimentation to account for

between 7.2% and 33.8% of the total experimental deposition for both parabolic and uniform flow, see Table 7.2 and Table 7.3. Parabolic, uniform and developing velocity profiles are all investigated to see the effect the addition of sedimentation has on each flow condition compared to isolated impaction.

Figure 7.8 provides the deposition efficiency verses Stokes number for parabolic flow with combined impaction and sedimentation for the two CFD software packages, and Kim and Iglesias' (1989) experimental data. When including deposition by sedimentation, the increases in deposition efficiencies for CFX and Fluent DPM were close, 7% at the 0.091 (7 μm) Stokes number, 3% and 4% at the 0.047 (5 μm) Stokes number, and 1% and 1.5% at the 0.017 (3 μm) Stokes number, respectively, for parabolic flow at the 4 lpm flow rate. These increases due to sedimentation are roughly four times the increase predicted by Pich (1972), see Table 7.2. However, this is consistent with the amount of error or difference between CFD and the three theoretical sedimentation equations found when testing isolated sedimentation in the straight tube (See section 5.2.2.1). This is shown in Table 7.7, where the percent reported for each geometry reflect the amount the software over (positive) or under (negative) predicts the sedimentation theoretical equations for parabolic flow. As can clearly be seen transition from the straight tube to the bifurcating tube had little effect on the accuracy of the CFD software package in predicting deposition by sedimentation.

The addition of sedimentation increases the agreement of Fluent DPM's predictions with experimental data for all Stokes numbers. CFX has better agreement with experimental data at the 0.091 (7 μm) Stokes number, but the addition of sedimentation significantly over predicts deposition at the lower Stokes number. The curve shape is basically the same as for isolated impaction for both CFD software packages, aside from a slightly steeper slope.

**Table 7.7 Deposition efficiencies for sedimentation from parabolic flow each software package predicts for the straight tube and bifurcating tube geometry. Note: The percent represents the amount the CFD package over or under the predicted theory. Positive values are over prediction, negative values are under predictions. Pich (1972) represents all parabolic sedimentation analytical equations.**

| ε Value | CFX | | Fluent DPM | | Sedimentation Theory (Pich 1972) |
|---|---|---|---|---|---|
| | Straight Tube | Bifurcation | Straight Tube | Bifurcation | |
| 0.002 | 2.5% | 1.5% | -0.32% | 1% | 0.33% |
| 0.005 | 4.4% | 4% | 2.4% | 3% | 0.90% |
| 0.01 | 8% | 7% | 6% | 7% | 1.76% |

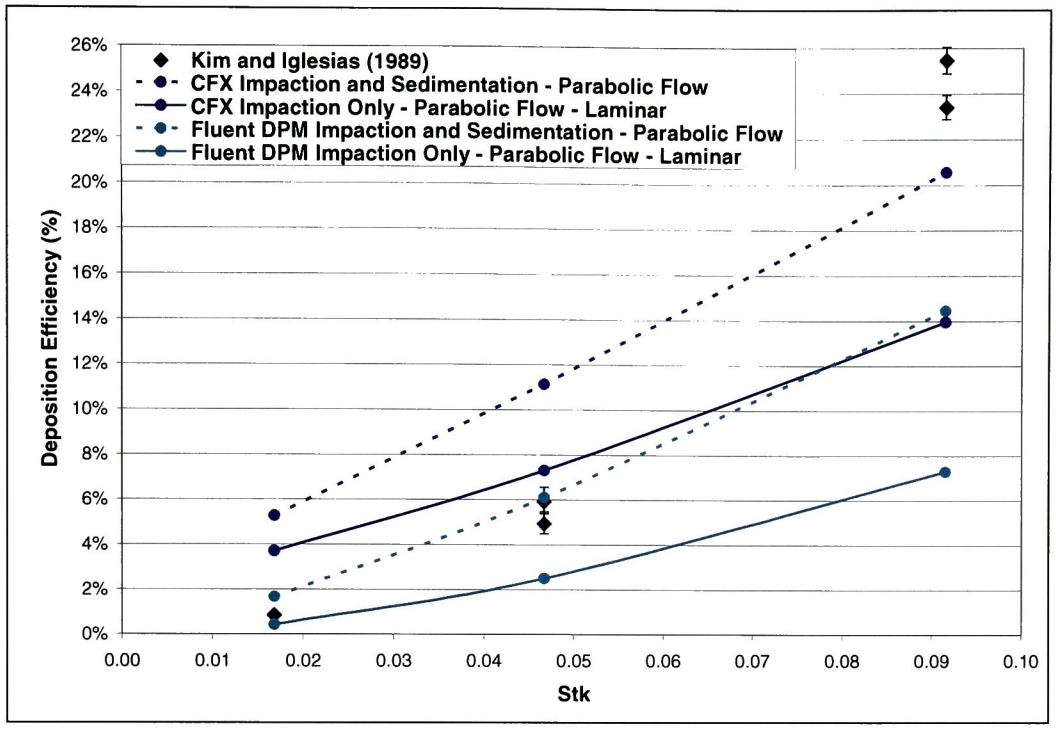


**Figure 7.8 Comparison of CFD data, analytical equations, and experimental data for combined impaction and sedimentation in the bifurcating tube geometry for parabolic flow at a 4 lpm flow rate.**

Figure 7.9 provides the deposition efficiency verses Stokes number for uniform flow with combined impaction and sedimentation for the two CFD software packages, and Kim and Iglesias' (1989) experimental data. When including deposition by sedimentation the deposition efficiency increases by less than 0.4% for both CFD software packages at all Stokes numbers for uniform flow. This is slightly less than predicted by Yu, et al. (1977) for the 0.047 (5 μm) and 0.091 (7 μm) Stokes numbers, see Table 7.3. The variation in analytical and CFD predictions for uniform flow conditions in the bifurcation are similar to those seen in the straight tube (see Table 7.8). The CFD predictions in the bifurcating tube slightly over predict Yu, et al. (1977) at these ε values, while in the straight tube CFD predictions had been just under Yu, et al. (1977) at these ε values. No more attention needs to be given to the uniform flow case at the 4 lpm flow rate, since the velocity profile in the experimental is clearly not uniform, even with the addition of sedimentation.

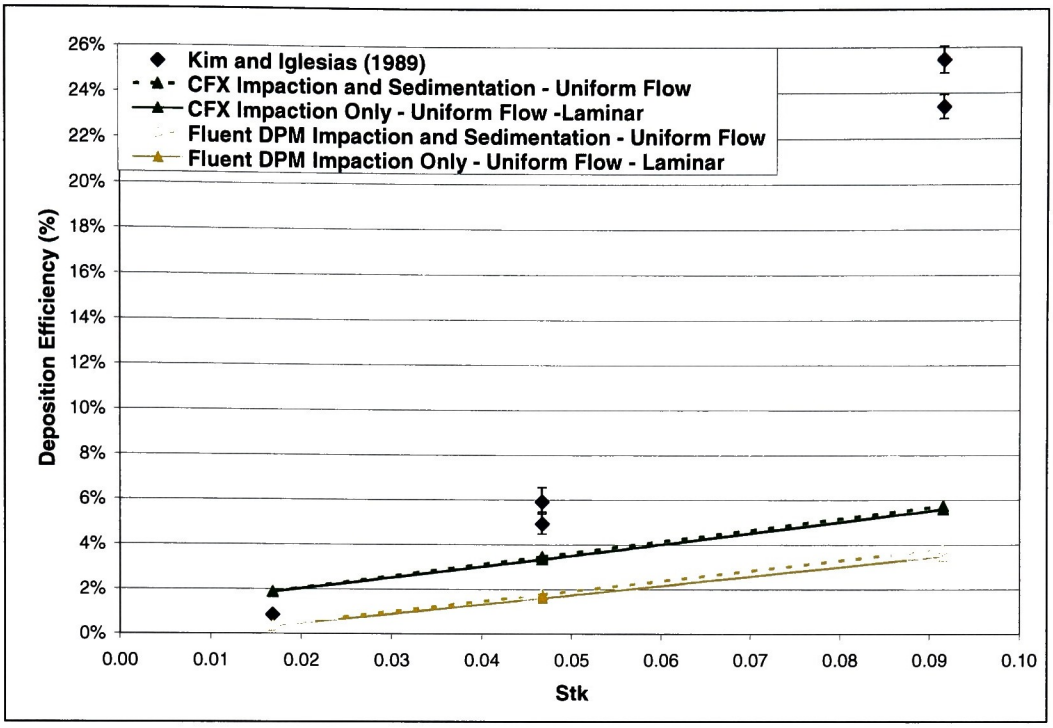


**Figure 7.9 Comparison of CFD data, analytical equations, and experimental data for combined impaction and sedimentation in the bifurcating tube geometry for uniform flow at a 4 lpm flow rate.**

**Table 7.8 Deposition efficiencies for sedimentation from uniform flow each software package predicts for the straight tube and bifurcating tube geometry. Note: The percent represents the amount the CFD package over or under the predicted theory. Positive values are over prediction, negative values are under predictions. Yu, et al. (1975) represents all parabolic sedimentation analytical equations.**

| ε Value | CFX | | Fluent DPM | | Sedimentation Theory (Yu, et al. 1977) |
|---|---|---|---|---|---|
| | Straight Tube | Bifurcation | Straight Tube | Bifurcation | |
| 0.002 | -0.18% | 1.54% | -0.33% | 0.00% | 0.33% |
| 0.005 | -0.07% | 2.43% | -0.91% | 0.69% | 0.91% |
| 0.01 | 0.20% | 3.82% | -1.78% | 1.70% | 1.78% |

Figure 7.10 provides the deposition efficiency verses Stokes number for developing flow with combined impaction and sedimentation and Kim and Iglesias' (1989) experimental data. When including deposition by sedimentation, the deposition efficiencies increase between 3.5% and 4% at the 0.091 Stokes number (7 μm), between 1% and 2% at the 0.047 (5 μm) Stokes number, and less than 0.5% at the 0.017 (3μm) Stokes number. This increase is less than the increase found for the parabolic flow case and could be due to the developing profile having faster moving particles distal to the centerline compared to the parabolic flow case. These faster moving particles will have a shorter residence time and smaller

sedimentation efficiencies than particles on the same streamline in the parabolic case. Like with the parabolic flow runs shown in Figure 7.8, the addition of sedimentation improves Fluent DPM's agreement with experimental data at all Stokes numbers investigated. CFX has improved agreement with experimental data at the 0.091 (7 μm) Stokes number, but over predicts experimental data by as much as 1.5% at the lower Stokes numbers.

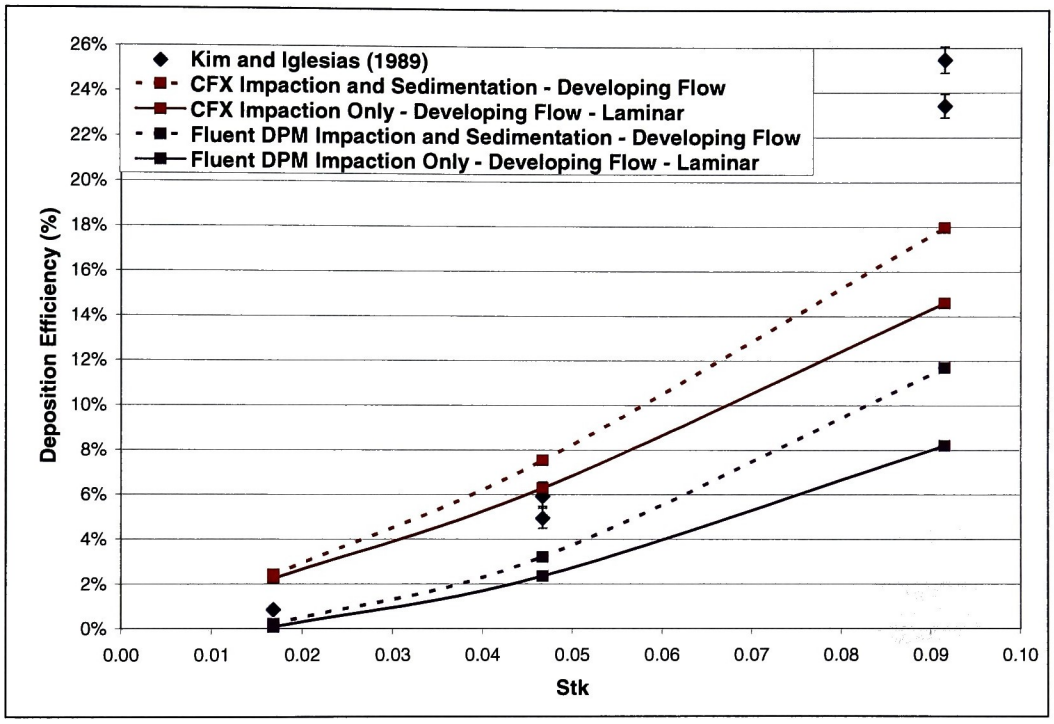


**Figure 7.10 Comparison of CFD and experimental data for combined impaction and sedimentation in the bifurcating tube geometry for developing flow at a 4 lpm flow rate.**

In general, the inclusion of sedimentation in CFD increases the deposition efficiency, which improves agreement with experimental data for the highest Stokes numbers in CFX and all Stokes numbers in Fluent DPM. The largest increase in deposition efficiency due to sedimentation for CFD is seen in the parabolic flow conditions. The increase in deposition efficiency due to sedimentation is closest to Pich (1972) and Yu, et al. (1977) at the developing flow conditions, but still too high at the 0.091 (7 μm) Stokes number. The error in theoretical and observed sedimentation for the parabolic velocity profile agrees with that was seen in the straight tube geometry in Section 5.2.2 for the same ε values. It is clear at the 4 lpm flow rate deposition is not solely governed by the impaction mechanism.

### 7.3.2.3 Isolated Impaction at the 8 Liter/Min Flow Conditions

At the 8 lpm flow rate, the laminar and k-epsilon solvers are utilized to investigate particle deposition for isolated impaction. Both the laminar and k-epsilon solvers are investigated for parabolic, uniform, and developing velocity profiles. The combined impaction and sedimentation mechanism is ignored, due to the relatively small effect of sedimentation predicted by Pich (1972) and Yu, et al. (1977), see Table 7.2 and Table 7.3, respectively; however impaction is only isolated at the 0.093 (5 μm) and 0.18 (9 μm) Stokes numbers. The predictions generated by Fluent DPM and CFX are compared to experimental data from Kim and Iglesias (1989) and the analytical equations from Yeh and Schum (1980), Cai and Yu (1988), and Zhang, et al. (1997).

The Reynolds number at the 8 lpm flow in the parent generation (Re = 2264, see Table 7.5) indicates the flow is right near the border of transitional flow, Reynolds number 2300. To determine if varying the turbulence intensity will affect the deposition efficiency at these flow conditions, turbulence intensities of 1%, 5%, and 10% are investigated for each velocity profile and CFD software package. Figure 7.11 provides the deposition efficiency verses Stokes number for the k-epsilon predictions from CFX and Fluent DPM for developing flow at the 8 lpm flow rate the three turbulence intensities investigated. There is less than 0.5% variation in either CFD software package's predictions of deposition efficiency due to varying the turbulence intensity at any of the Stokes numbers. This same trend is seen for uniform and parabolic flow conditions, found in Appendix G. CFX is unable to predict deposition when utilizing the k-epsilon solver for the uniform flow conditions at the 8 lpm flow rate, the solution just diverges, see Appendix G. In CFX, as the turbulence intensity increases the deposition efficiency increases for parabolic and developing flow. In Fluent, as the turbulence intensity increases so does the deposition efficiency, however the change is practically unnoticeable. Due to the minimal variation in deposition efficiency, only the predictions from the 5% (midpoint) turbulence intensity will be compared to the analytical predictions and experimental data.

Isolated impaction is investigated at the 8 lpm flow rate to determine the accuracy of CFX and Fluent DPM's predictions compared to analytical equations for similar flow conditions and Kim and Iglesias' (1989) experimental data in the bifurcating tube. According to the theoretical predictions impaction is isolated at the 0.093 (5 μm) and 0.18 (7

μm) Stokes numbers. The velocity profile is expected to be 29% developed at the entrance to the bifurcating geometry based on Kim and Iglesias' (1989) experimental data; therefore an accurate depiction of the velocity profile is uniform or developing. The parabolic, uniform, and developing velocity profiles are all investigated in this research, since no detailed information about the velocity profiles was provided by Kim and Iglesias (1989). It is also anticipated that the deposition efficiency predicted for the developing flow condition will fall between the parabolic and uniform predictions.

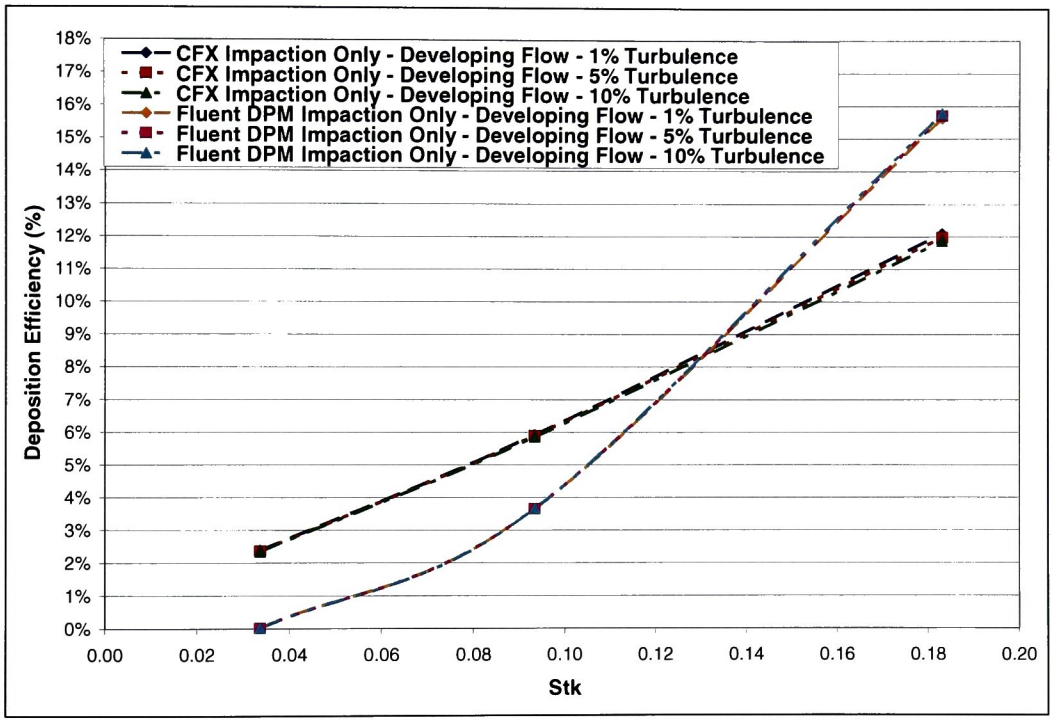


**Figure 7.11 CFD predictions for CFX and Fluent DPM for 1%, 5%, and 10% turbulence intensities for developing flow at the 8 lpm flow rate.**

Figure 7.12 provides the deposition efficiency verses Stokes number for isolated impaction for the two CFD software packages, the three relevant analytical equations, and Kim and Iglesias' (1989) experimental data for the parabolic flow conditions. Zhang, et al.'s (1997) analytical equation for parabolic flow provides the best agreement with Kim and Iglesias' (1989) experimental data, only slightly higher than experimental data at the 0.18 (7 μm) Stokes number. Cai and Yu (1988) and Yeh and Schum (1980) under predict the experimental data by roughly 12% and 19%, respectively at the 0.093 (5 μm) Stokes number

and 30% and 43%, respectively at the 0.18 (7 μm) Stokes number. All the analytical predictions have curve shapes similar to the experimental data at the 8 lpm flow rate. The curves are linear with a slightly steeper slope between the 0.093 (5 μm) and 0.18 (7 μm) Stokes numbers. The under prediction is expected due to the small presence of sedimentation. However, this under prediction by theoretical equations is not seen at the lowest Stokes number, 0.034 (3 μm) where the affect should be the largest.

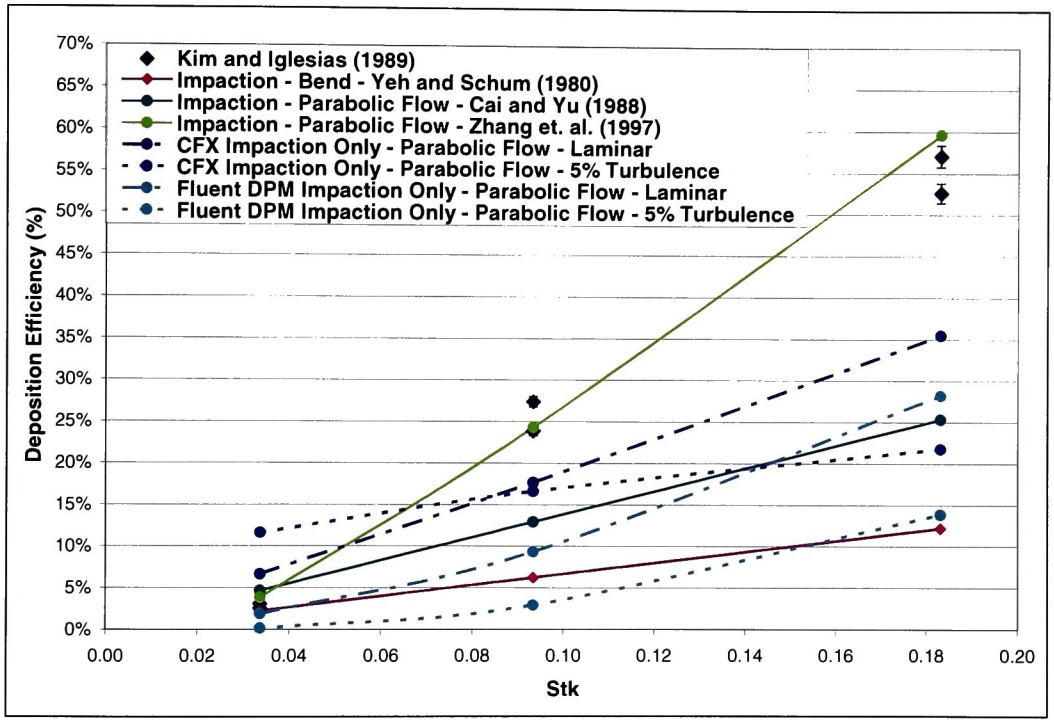


**Figure 7.12 Comparison of CFD data, analytical equation, and experimental data for isolated impaction in the bifurcating tube geometry for parabolic flow at the 8 lpm flow rate.**

Neither CFD software packages' predictions align well with any of the analytical equations or experimental data. CFX for the laminar solver has similar shape to the analytical curves and provides deposition efficiencies between Zhang, et al. (1997) and Cai and Yu (1988). CFX is higher than Zhang, et al. (1997), Cai and Yu (1988) and the experimental data at the 0.034 (3 μm) Stokes number, this difference is even more noticeable when the turbulence solver is utilized. This is unexpected since impaction is not isolated at the 0.034 (3 μm) Stokes number; therefore predictions should be lower than the experimental data. However, CFX significantly over predicts the experimental data at the 0.034 (3 μm)

Stokes number. This could be due to the experimental flow not being parabolic, however if this was the case it should over predict the experimental data for all Stokes numbers. In CFX, the turbulence solver flattens the curve and reduces alignment with the analytical equations and experimental data at all Stokes numbers investigated. Some of this change in deposition efficiency due to the addition of turbulence can be attributed to the changes in velocity profile associated with the addition of turbulence eddies which effect the rate at which the flow develops or disrupt fully developed flow (See Appendix D).

In Fluent DPM, the laminar and turbulent solvers have a steeper slope between the 0.093 (5 μm) and 0.18 (7 μm) Stokes number than any of the analytical equations. The deposition efficiencies predicted by Fluent DPM with the laminar solver are near Yeh and Schum's (1980) prediction and experimental data at the 0.034 (3 μm) Stokes number, by the 0.18 (7 μm) Stokes number Fluent over predicts Yeh and Schum (1980) by nearly 20% and under predicts the experimental data by as much as 25%. When the turbulence solver is utilized in Fluent DPM the deposition efficiency curve is shifted down and flattened slightly, but remains linear.

Figure 7.13 provides the deposition efficiency verses Stokes number for isolated impaction for the two CFD software packages, the three relevant analytical equations, and Kim and Iglesias' (1989) experimental data for the uniform flow conditions. All the analytical equations and CFD software packages significantly under predict the experimental data obtain by Kim and Iglesias (1989) for the 8 lpm flow rate in the bifurcating tube. It is likely that the flow conditions in Kim and Iglesias' (1989) experiment were not uniform for the 8 lpm flow rate, despite the entrance length calculations. Zhang, et al.'s (1997) prediction has the closest fit to the experimental curve shape of the analytical equations, despite being significantly lower than experimental data at all Stokes numbers. Fluent DPM and CFX predictions are within 3% of one another at all Stokes numbers investigated. The CFD software packages' predictions are lower than Cai and Yu (1988) and Yeh and Schum (1980), but have similar curve shapes. The addition of turbulence in Fluent DPM reduces the deposition efficiency less than 2% and does not affect the shape of the deposition efficiency curve. This variation can again be attributed to slight changes in the velocity profile due to the addition of turbulent eddies. The variation is less at for uniform flow, since the flow is

already not developing due to the 0 shear stress or free slip boundaries at the walls (See Appendix D).

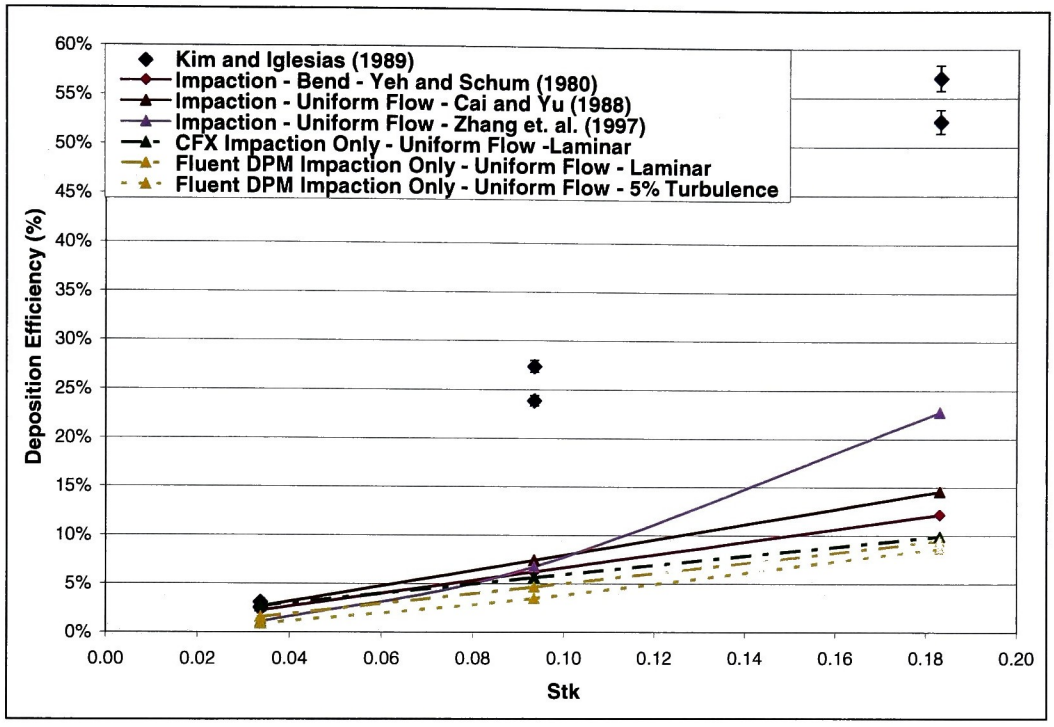


**Figure 7.13 Comparison of CFD data, analytical equation, and experimental data for isolated impaction in the bifurcating tube geometry for uniform flow at the 8 lpm flow rate.**

Figure 7.14 provides the deposition efficiency verses Stokes number for isolated impaction for the two CFD software packages for parabolic, uniform, and developing flow conditions and Kim and Iglesias' (1989) experimental data for the bifurcating tube at the 8 lpm flow rate. None of the CFD software packages agree well with experimental data at the higher Stokes numbers for any of the flow conditions, where impaction theoretically is isolated.

For the laminar CFD solvers, the developing flow conditions provide deposition efficiencies between the uniform and parabolic flow, as expected. The developing flow conditions provide predictions closer to the parabolic flow prediction than uniform. This is unexpected since the flow should only be 15% developed at the end of the parent tube, starting from uniform flow.

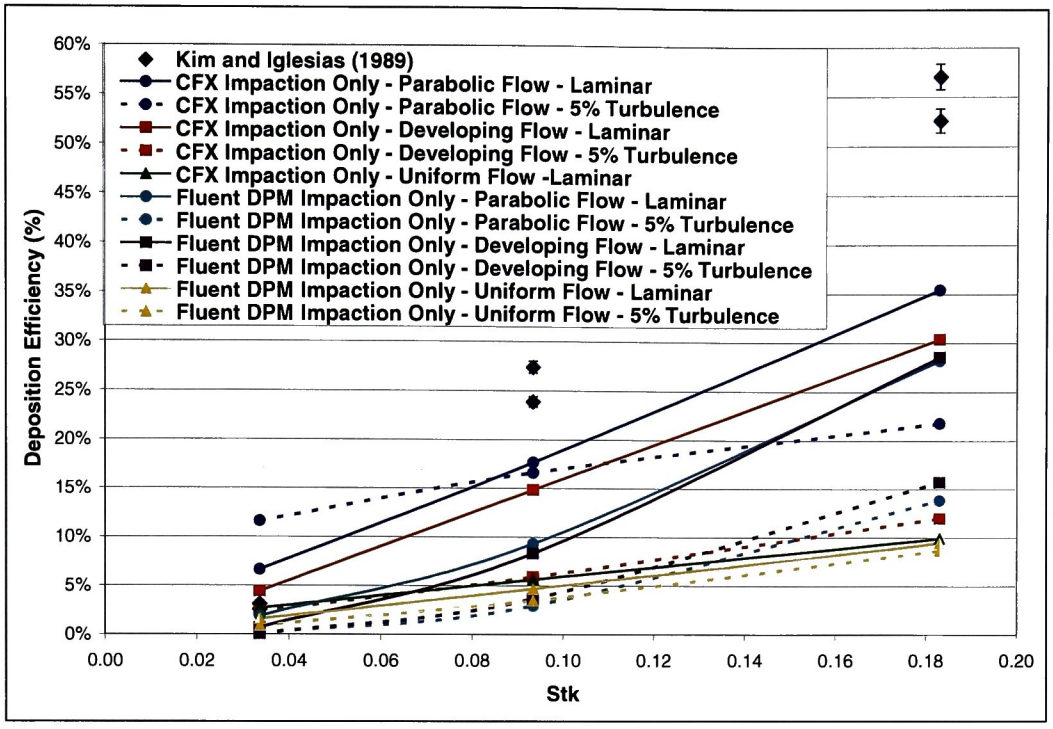


**Figure 7.14 Comparison of CFD data for developing flow to CFD data for parabolic and uniform flow and experimental data for isolated impaction in the bifurcating tube geometry at the 8 lpm flow rate.**

When turbulence is utilized in Fluent DPM the developing flow conditions provide a deposition efficiency 2% higher than parabolic flow at the 0.18 (7 μm) Stokes number. When the CFX turbulence solver is used, there is a significant reduction, as much as 17%, in deposition from the parabolic to developing flow conditions. In Fluent DPM, there is a larger decrease in the deposition efficiency for the parabolic and developing flow conditions when the turbulence solver is utilized, as much as 15%, compared to the uniform flow conditions which decrease no more than 2%. This can be attributed to the k-epsilon solver introducing turbulent eddies that interact with the velocity profile. These turbulent eddies prevent the flow from developing or make a developed flow turbulent or less developed. This is why less change is seen in the turbulent flow conditions, which are already not developing. The effect of the turbulent eddies can be seen in the velocity profiles for both the developing and parabolic velocity profiles near the bifurcation, which are flatter than when the laminar solver is utilized (see Appendix D). The velocity at the center of the parent generation is also reduced, which is likely the key factor affecting the deposition efficiency (See Appendix D).

In general, the parabolic flow conditions align the closest with the experimental data for the analytical equations and CFD software packages, despite the entrance length indicating the flow to be only 29% developed at the entrance to the bifurcation geometry. In general, the analytical equations and CFD predictions have the best agreement with experimental data at the 0.034 (3 μm) and 0.093 (5 μm) Stokes numbers. However, impaction is only isolated at the 0.093 (5 μm) and 0.18 (7 μm) Stokes, where it would be expected agreement with theory would be better. Zhang, et al.'s (1997) parabolic flow equation has the best agreement with the experimental data of any of the analytical equations. CFX provides deposition efficiencies closer to experimental data, but Fluent DPM more accurately predicts the curve shape of the experimental data. None of the CFD software packages have good agreement with the analytical equations for the various velocity profiles. Varying the intensity of the k-epsilon turbulence has no noticeable effect on the deposition efficiency at the 8 lpm flow conditions, where the flow is just within the transitional region, see Table 7.5. The use of the k-epsilon turbulence solver provides lower deposition efficiencies then those provided with the laminar solver in both CFX and Fluent DPM. Both CFD software packages have worse agreement with experimental data when the k-epsilon turbulence model is utilized. The poor correlation between the analytical equations, CFD predictions, and experimental data makes it difficult to conclude if any source of data is accurately predicting or observing what is taking place in the bifurcating tube geometry.

#### 7.3.2.4 12 Liter/Min Flow Conditions

At the 12 lpm flow rate, the laminar and k-epsilon solvers are utilized to investigate particle deposition for isolated impaction for parabolic, uniform, and developing velocity profiles. Both the laminar and k-epsilon solvers are investigated for the parabolic, uniform, and developing velocity profiles. The combined impaction and sedimentation mechanism is ignored, since impaction is isolated for all particle sizes at this flow rate, see Table 7.2 and Table 7.3, respectively. The predictions generated by Fluent DPM and CFX are compared to experimental data from Kim and Iglesias (1989) and the analytical equations from Yeh and Schum (1980), Cai and Yu (1988), and Zhang, et al. (1997).

The Reynolds number at the 12 lpm flow in the parent generation (Re = 3395, see Table 7.5) indicates the flow is in the transitional flow region, Reynolds number between

2300 and 4000 to 10000 (Fox and McDonald, 1998). The k-epsilon turbulent solver and laminar solver are investigated in Fluent DPM and CFX, since the flow is in the transition region. To determine the effect of varying the turbulence intensity on the deposition efficiency at these flow conditions, turbulence intensities of 1%, 5%, and 10% are investigated for each velocity profile and solver. Figure 7.15 provides the deposition efficiency verses Stokes number for the k-epsilon predictions from CFX and Fluent DPM for developing flow at the 12 lpm flow rate the three turbulence intensities investigated. Appendix G contains the plots for the uniform and parabolic velocity profiles. In Fluent DPM, the deposition efficiency changes by less than 0.5% as the turbulence intensity is varied for all velocity profiles and Stokes number investigated. In CFX, the largest variation in deposition efficiency as a result of changing the turbulence intensity is seen in the developing flow case, where there is as much as a 2.5% difference in the deposition efficiencies at the 0.27 Stokes number, see Figure 7.15. For the uniform and parabolic flow conditions there is around 1% variation in the deposition efficiencies as a result of changing the turbulence intensity in CFX, see Appendix G. In CFX for uniform and developing flow, the deposition efficiency increases with decreasing turbulence intensity. For parabolic flow in CFX, as the turbulence intensity increases so does the deposition efficiency. For both CFX and Fluent DPM, the change in deposition efficiency as a result of varying the turbulence intensity is minimal and only the 5% case (midpoint) will be compared to the analytical equations and experimental data.

Isolated impaction is investigated at the 12 lpm flow rate to determine the accuracy of CFX and Fluent DPM's predictions compared to analytical equations for similar flow conditions and Kim and Iglesias' (1989) experimental data in the bifurcating tube. This is the flow condition where Kim and Iglesias (1989) were able to almost completely isolate the impaction mechanism for all Stokes numbers, see Section 7.2. The velocity profile is expected to be 20% developed at the entrance to the bifurcating geometry for Kim and Iglesias' (1989) experimental data; therefore an accurate depiction of the velocity profile is uniform or developing. The parabolic, uniform, and developing velocity profiles are all investigated in this research, since no detailed information about the velocity profiles was provided by Kim and Iglesias (1989). It is also anticipated that the deposition efficiency

predicted for the developing flow condition will fall between the parabolic and uniform predictions.

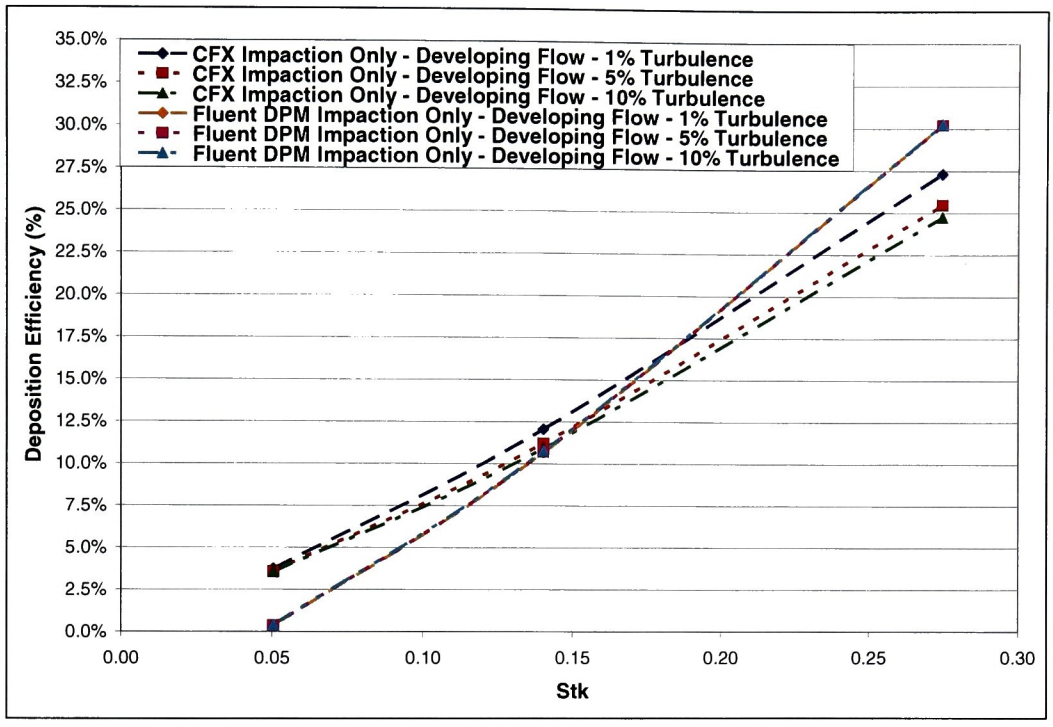


**Figure 7.15 CFD predictions for CFX and Fluent DPM for 1%, 5%, and 10% turbulence intensities for developing flow at the 12 lpm flow rate.**

Figure 7.16 provides deposition efficiency verses Stokes number for the parabolic flow with isolated impaction for the two CFD software packages, the three relevant analytical equations, and Kim and Iglesias' (1989) experimental data. The analytical equations agree fairly well with Kim and Iglesias' (1989) experimental data at the lowest Stokes number but diverge at the higher Stokes numbers. Zhang, et al. (1997) over predicts the experimental data, with larger differences at higher Stokes numbers. Cai and Yu (1988) agrees with the experimental data at the 0.05 (3 μm) Stokes number, but significantly under predicts the experimental data at higher Stokes numbers. Yeh and Schum (1980) under predict the experimental data at all Stokes numbers by more than Cai and Yu (1988).

For the laminar solver, CFX provides deposition efficiencies 5% to 10% higher than Fluent DPM. This makes CFX in better agreement with experimental data at the higher Stokes numbers, but Fluent DPM in better agreement at the 0.05 (3 μm) Stokes number.

Both Fluent DPM and CFX laminar results have similar curve shapes to the experimental data.

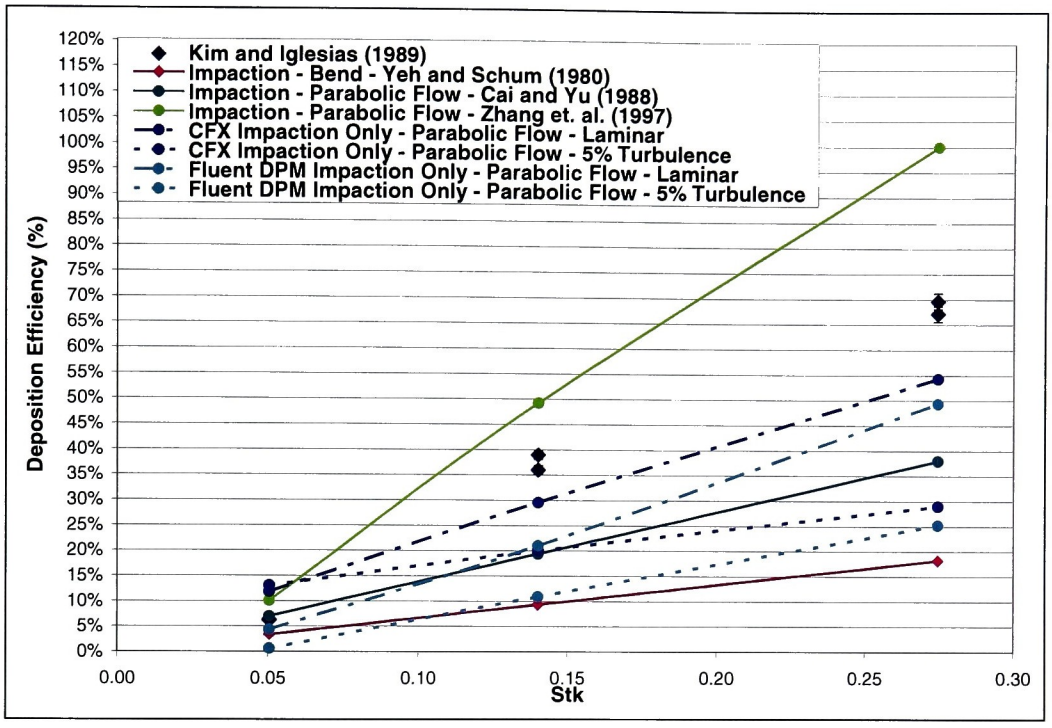


**Figure 7.16 Comparison of CFD data, analytical equations, and experimental data for isolated impaction in the bifurcating tube geometry for parabolic flow at the 12 lpm flow rate.**

The use of the k-epsilon turbulence solver reduces the deposition efficiency for both CFX and Fluent DPM from what was obtained with the laminar solver. In addition, both turbulent solver curves are significantly steeper than when the laminar solver was utilized.

The parabolic flow condition provides poor agreement with experimental data, as expected by the entrance length; however only Zhang, et al. (1997) over predicts the experimental data as expected if the flow was uniform or developing in Kim and Iglesias' (1989) experiment.

Figure 7.17 provides the deposition efficiency verses Stokes number for uniform flow with isolated impaction for the two CFD software packages, the three relevant analytical equations for impaction, and Kim and Iglesias' (1989) experimental data for deposition in a bifurcating tube at the 12 lpm flow rate. The analytical equations agree well with experimental data for the smallest Stokes numbers but diverge for the larger Stokes values.

Zhang, et al. (1997) more accurately predicts the curve shape of the experimental data than the other two theoretical equations, but the deposition efficiency values are below experimental data by more than 20% at the 0.27 (7 μm) Stokes number.

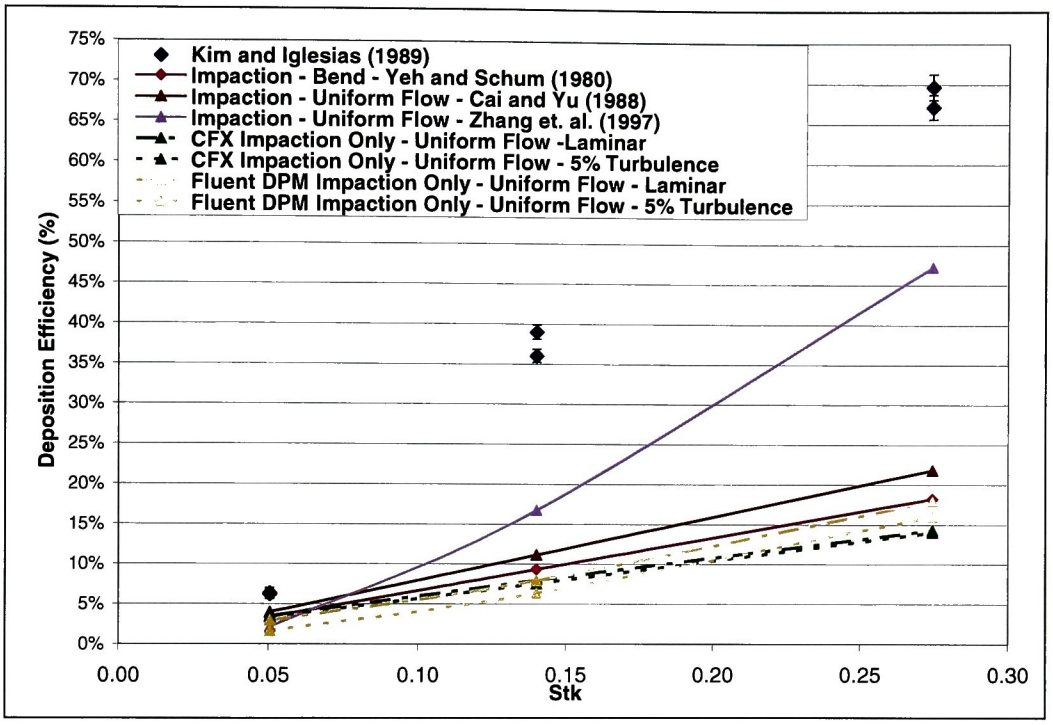


**Figure 7.17 Comparison of CFD data, analytical equations, and experimental data for isolated impaction in the bifurcation geometry for uniform flow at the 12 lpm flow rate.**

The CFD software packages agree with the theoretical predictions of Yeh and Schum (1980) and Cai and Yu (1988) at all Stokes numbers. CFD only agrees with Zhang, et al. (1997) at Stokes 0.05 (3 μm). As Stokes number increases, Zhang, et al. (1997) increases exponentially, while the CFD curves remains linear.

The CFD results agree with the experimental data only at the 0.05 (3 μm) Stokes number. The CFD curves are linear, while the experimental curves increase exponentially with Stokes, so that as Stokes number increases, the CFD results significantly under predicts the experimental data. The turbulence solver does not improve CFD's agreement with experimental data. There is roughly a 2% decrease in the deposition efficiency in Fluent DPM by utilizing the turbulent solver. The laminar and turbulence solver in CFX return nearly the same deposition efficiency for all Stokes numbers investigated. The CFD results for uniform flow indicate that the experimental conditions are more parabolic than uniform.

Figure 7.18 provides the deposition efficiency verses Stokes number for isolated impaction for the two CFD software packages for parabolic, uniform and developing velocity profiles and Kim and Iglesias' (1989) experimental data for the bifurcating tube geometry. When the laminar solver is utilized the developing flow conditions in both CFD software packages result in deposition efficiencies between parabolic and uniform flow predictions, as expected. When the turbulence solver is utilized Fluent DPM predicts a higher deposition efficiency at the 0.27 (7 μm) Stokes number for developing flow than parabolic. For CFX the developing flow prediction remains between the parabolic and uniform prediction. For the higher Stokes numbers all the CFD software packages significantly under predict the experimental data. At the 0.05 (3 μm) Stokes number CFX's developing flow prediction and Fluent DPM's parabolic flow prediction agree the best with the experimental data. As seen before, the turbulence solver changes the shape of the deposition efficiency curve for all flow rates and reduces the deposition efficiencies observed.

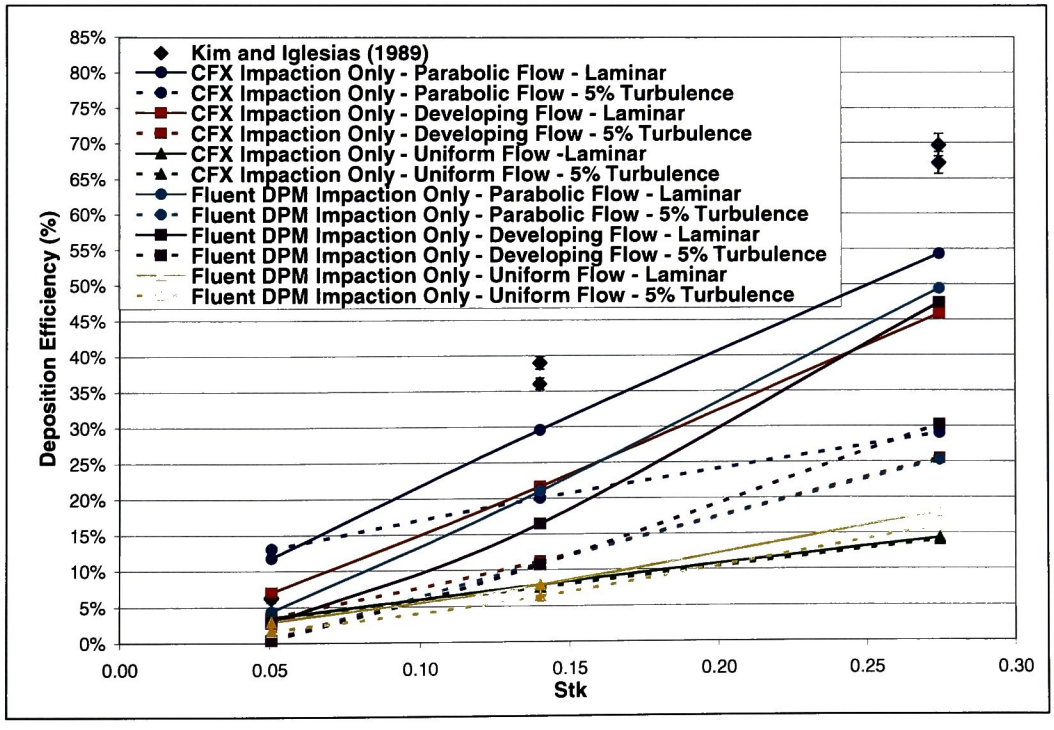


**Figure 7.18 Comparison of CFD data for developing flow to CFD data for parabolic flow and uniform flow and experimental data for isolated impaction in the bifurcating tube geometry at the 12 lpm flow rate.**

In general, the parabolic flow conditions for the CFD data provide the best agreement with experimental data, despite the entrance length only indicating that the flow should be 20% developed at the entrance to the bifurcating tube geometry. In fact, the uniform flow predictions still provide the worst agreement with experimental data. None of the analytical equations agree well with the experimental data at the 12 lpm flow rate, except for the lowest Stokes number 0.05 (0.3 μm.) Compared to the other two flow conditions, the 12 lpm should have the best agreement with experimental data since impaction is isolated for all Stokes numbers. However, for the 12 lpm case compared to 4 lpm case agreement is about the same. Varying the turbulence intensity in the k-epsilon solve has little effect on the deposition efficiency except at the higher Stokes numbers. The turbulence solver does reduce the deposition efficiency and change the shape of the curve for all flow conditions examined. The poor correlation between the analytical equations, CFD predictions, and experimental data makes it difficult to conclude which, if any, source of data is accurately predicting or observing what is taking place in the bifurcating tube geometry.

### 7.3.3 Summary

A summary of the numerical, analytical, and experimental deposition efficiency for impaction in the bifurcating tube is provided in Table 7.9. There are several impaction equations that have been developed over the years; however there is still substantial variation in the deposition efficiencies predicted even by the most prominent equations. The equations utilized in this research predicted deposition efficiencies that ranged up to 80% from one another, see Table 7.9. Some of the variation in the analytical predictions can be attributed to how each equation was derived. Yeh and Schum's (1980) equation was developed analytically for a bend, rather than a bifurcation. The equation assumes a parabolic velocity profile throughout the geometry, despite changes that will occur at and following the bend due to the change in flows path. Additionally, Yeh and Schum's (1980) equation when originally derived by Yeh (1974) was developed solely for parabolic flow, however in the NCRP Model (United States National Council on Radiation Protection and Measurements, 1997) and this research it is utilized for all flow conditions. Cai and Yu's (1988) analytical equations are both for flow through a bifurcation. The equations assume the same velocity profile throughout the geometry, either parabolic or uniform depending on the equation, the

derivation does not account for variations in the velocity profile at and after the bifurcation. The empirical equations developed by Zhang, et al. (1997) are based on CFD data for a bifurcation. In the CFD experiments a parabolic or uniform velocity profile was defined at the inlet, but allowed to change as it passed through the bifurcation, based on the changes in diameter and path. The equations developed by Zhang, et al. (1997) provide a more accurate representation of what could happen in a real fluid flow than the analytical equations examined. This could be explain why Zhang, et al. (1997) had better agreement with experimental data at most flow conditions.

It is difficult to isolate the impaction deposition mechanism in laboratory experiment while maintaining Reynolds numbers comparable to those found in the lung. The data obtained from Dr. Oldham in the other bifurcating geometry isolated the sedimentation deposition mechanism in his bifurcating tube geometry, see Appendix B. Kim and Iglesias (1989) were able to isolate the impaction deposition mechanism for one flow rate for all particle sizes examined and at this flow rate obtained Reynolds numbers higher then those found in the lung at normal breathing conditions, see Sections 3.2 and 7.2. The other flow rates investigated by Kim and Iglesias (1989) had at least one particle size that had theoretical deposition by sedimentation that represented more than 2% of the total deposition observed. At the 4 lpm flow rate, sedimentation theoretically counted for between 7% and 39% of the total deposition observed by Kim and Iglesias (1989), see Table 7.2 and Table 7.3.

When comparing to experimental data the uniform flow equations and CFD predictions had poor correlation for all flow rates examined, except the lowest Stokes number. At the 12 lpm and 8 lpm flow rate the flow should be less than 30% developed at the entrance to the bifurcating tube geometry according to the flow conditions provided by Kim and Iglesias (1989). However, the parabolic flow conditions provide better agreement with experimental for both CFD software packages. Some of this can be attributed to how quickly the velocity begins to resemble the parabolic velocity profile (See Appendix D). Cai and Yu's (1988) parabolic and uniform flow equations and Yeh and Schum (1980) had fair to poor correlation for all flow conditions and Stokes numbers investigated. Zhang, et al.'s (1997) parabolic flow equation had the best correlation with experimental data at the 4 and 8 lpm flow rates; however at the 12 lpm Zhang, et al. (1997) over predicted the experimental

data by as much as 27%. It is not surprising Zhang, et al. (1997) had the best agreement with the experimental data, since this experimental data had been used to help evaluate the accuracy of Zhang, et al.'s (1997) impaction equations. Yeh and Schum (1980) typically predicted the lowest deposition efficiency; this could be due to the equation being developed for a bend rather than a bifurcation. Of the CFD software packages, CFX typically had the best agreement with the experimental data; however neither software package agreed well for all Stokes numbers examined and should be researched further.

The addition of sedimentation in the CFD software packages increased the deposition efficiency at all flow rate. The increases in deposition efficiency were not as close for the various velocity profiles as predicted by the analytical equations; however the difference was consistent with straight tube model results. The largest increases in deposition with the addition of sedimentation were seen at the higher Stokes number or 7 μm particle size and parabolic velocity profile, which is unexpected since sedimentation makes up a larger percentage of deposition at lower Stokes numbers.

For the flow conditions examined, varying the turbulence intensity had minimal effect on the deposition efficiencies predicted by either CFD software package. At the 12 lpm flow rate there was some variance in the deposition efficiency, due to changing the turbulence intensity, but only at the higher Stokes numbers and still less than 2.5%. The use of the k-epsilon turbulence solver adds turbulent eddies to the flow which can flatten the profile and increase the distance required for the flow to develop. For both CFD software packages the changes in profile due to utilizing the turbulence solver reduces the deposition efficiency, which makes the agreement with the experimental data worse. The turbulence solver also alters the shape of the deposition efficiency curve, particularly in CFX for parabolic flow conditions. Based on this research, it does not appear that the turbulence solver should be utilized for transitional flow and the software manufactures recommendation of only using the turbulence solver for fully developed turbulent flow should be followed.

From this research it is obvious that there is still substantial learning that needs to be done into the impaction deposition mechanism both for analytical equations and CFD tracking algorithms. Until CFD and experimental data are obtained for the exact same geometry and flow conditions where the impaction mechanism is completely isolated, it will be difficult to determine which CFD software package and analytical equations are most

accurate. In the mean time it is necessary to continue utilizing all the equations and software packages in order to obtain the widest understanding of what could be occurring.

**Table 7.9 Summary of deposition efficiencies observed in the bifurcating tube for impaction for each flow condition and particle size.**

| Flow Rate (lpm) | Velocity Profile | Particle Size (μm) | Stokes Number | Fluent DPM (Turbulent) | CFX (Turbulent) | Yeh & Schum (1980) | Cai & Yu (1988) Parabolic | Cai & Yu (1988) Uniform | Zhang, et al. (1997) Parabolic | Zhang, et al. (1997) Uniform | Experimental Data |
|---|---|---|---|---|---|---|---|---|---|---|---|
| 4 | Parabolic | 3 | 0.017 | 0.43% | 3.71% | 1.12% | 2.33% | N/A | 1.05% | N/A | 0.77-0.94% |
| 4 | Parabolic | 5 | 0.047 | 2.50% | 7.31% | 3.11% | 6.47% | N/A | 6.03% | N/A | 4.49-6.56% |
| 4 | Parabolic | 7 | 0.091 | 7.30% | 13.97% | 6.10% | 12.68% | N/A | 18.71% | N/A | 22.89-26.05% |
| 4 | Uniform | 3 | 0.017 | 0.33% | 1.87% | 1.12% | N/A | 1.34% | N/A | 0.47% | 0.77-0.94% |
| 4 | Uniform | 5 | 0.047 | 1.60% | 3.34% | 3.11% | N/A | 3.72% | N/A | 1.30% | 4.49-6.56% |
| 4 | Uniform | 7 | 0.091 | 3.48% | 5.60% | 6.10% | N/A | 7.28% | N/A | 5.13% | 22.89-26.05% |
| 4 | Developing | 3 | 0.017 | 0.08% | 2.24% | 1.12% | N/A | N/A | N/A | N/A | 0.77-0.94% |
| 4 | Developing | 5 | 0.047 | 2.35% | 6.29% | 3.11% | N/A | N/A | N/A | N/A | 4.49-6.56% |
| 4 | Developing | 7 | 0.091 | 8.21% | 14.60% | 6.10% | N/A | N/A | N/A | N/A | 22.89-26.05% |
| 8 | Parabolic | 3 | 0.034 | 1.87% (0.12%) | 6.64% (11.62%) | 2.24% | 4.66% | N/A | 3.83% | N/A | 2.31-3.44% |
| 8 | Parabolic | 5 | 0.093 | 9.33% (2.92%) | 17.66% (16.60%) | 6.22% | 12.93% | N/A | 24.30% | N/A | 23.33-28.02% |
| 8 | Parabolic | 7 | 0.18 | 28.22% (13.86%) | 35.46% (21.78%) | 12.18% | 25.35% | N/A | 59.64% | N/A | 51.44-58.37% |
| 8 | Uniform | 3 | 0.034 | 1.57% (0.90%) | 2.69% | 2.24% | N/A | 2.67% | N/A | 1.08% | 2.31-3.44% |
| 8 | Uniform | 5 | 0.093 | 4.66% (3.48%) | 5.63% | 6.22% | N/A | 7.43% | N/A | 6.75% | 23.33-28.02% |
| 8 | Uniform | 7 | 0.18 | 9.43% (8.66%) | 9.93% | 12.18% | N/A | 14.56% | N/A | 22.76% | 51.44-58.37% |
| 8 | Developing | 3 | 0.034 | 0.69% (0.02%) | 4.42% (2.37%) | 2.24% | N/A | N/A | N/A | N/A | 2.31-3.44% |
| 8 | Developing | 5 | 0.093 | 8.33% (3.66%) | 14.85% (5.89%) | 6.22% | N/A | N/A | N/A | N/A | 23.33-28.02% |
| 8 | Developing | 7 | 0.18 | 28.57% (15.71%) | 30.42% (11.98%) | 12.18% | N/A | N/A | N/A | N/A | 51.44-58.37% |

| Flow Rate (lpm) | Velocity Profile | Particle Size (μm) | Stokes Number | Fluent DPM (Turbulent) | CFX (Turbulent) | Yeh & Schum (1980) | Cai & Yu (1988) Parabolic | Cai & Yu (1988) Uniform | Zhang, et al. (1997) Parabolic | Zhang, et al. (1997) Uniform | Experimental Data |
|---|---|---|---|---|---|---|---|---|---|---|---|
| 12 | Parabolic | 3 | 0.05 | 4.34% (0.59%) | 11.80% (13.08%) | 3.36% | 6.98% | N/A | 10.04% | N/A | 5.64-7.03% |
| 12 | Parabolic | 5 | 0.14 | 21.00% (10.91%) | 29.57% (20.02%) | 9.33% | 19.40% | N/A | 49.21% | N/A | 35.22-39.88% |
| 12 | Parabolic | 7 | 0.27 | 49.38% (25.23%) | 54.31% (29.00%) | 18.24% | 38.03% | N/A | 100.00% | N/A | 65.67-71.28% |
| 12 | Uniform | 3 | 0.05 | 2.95% (1.63%) | 3.51% (3.37%) | 3.36% | N/A | 4.01% | N/A | 2.12% | 5.64-7.03% |
| 12 | Uniform | 5 | 0.14 | 7.93% (6.32%) | 7.96% (7.56%) | 9.33% | N/A | 11.15% | N/A | 16.73% | 35.22-39.88% |
| 12 | Uniform | 7 | 0.27 | 17.93% (15.96%) | 14.32% (14.03%) | 18.24% | N/A | 21.84% | N/A | 47.25% | 65.67-71.28% |
| 12 | Developing | 3 | 0.05 | 2.78% (0.37%) | 7.00% (3.59%) | 3.36% | N/A | N/A | N/A | N/A | 5.64-7.03% |
| 12 | Developing | 5 | 0.14 | 16.46% (10.72%) | 21.65% (11.22%) | 9.33% | N/A | N/A | N/A | N/A | 35.22-39.88% |
| 12 | Developing | 7 | 0.27 | 47.39% (30.21%) | 45.83% (25.48%) | 18.24% | N/A | N/A | N/A | N/A | 65.67-71.28% |

# Chapter 8
# Deposition in the Three Generation Lung Geometry

## 8.1 Three Generation Lung Geometry Experimental Data

There are several experimental studies that investigate deposition in multi-generation lung geometries, see Section 1.4. Oldham, et al. (2000) was selected for this research because it is one of the few studies were identical experimental and numerical models of the geometry were available. Additionally, an existing research agreement between Dr. Robinson at Rochester Institute of Technology and Dr. Oldham at the University of California, Irvine, made it easy to obtain the numerical model and additional experimental data that has been gathered since 2000.

The hollow three generation lung cast utilized by Oldham, et al. (2000) represents generations 3, 4 and 5 of Weibel Model A, where generation 0 represents the trachea. The model is made from silicone rubber, see Section 4.3 for dimensions and mesh details. The experimental set up is similar to that described in Oldham, et al. (1997). Two casts were connected to a 2 inch copper T and tested simultaneously. The copper T has a 5.4 cm inside diameter. The distance from the centerline to the model connection is 7.5 cm. The hollow cast is connected by a 0.93 cm long, 0.57 cm inside diameter copper tube that is fitted inside the copper T by a brass connector.

Dr. Oldham has utilized the hollow three generation lung cast to investigate two flow rates; 1.5 lpm and 7.5 lpm at the entrance to the model or generation three. This is equivalent to tracheal flow rates of 12 lpm and 60 lpm in generation 0 of the Weibel Model A, for 1.5 lpm and 7.5lpm flow rates, respectively. For the 1.5 lpm flow rate, Dr. Oldham has obtained data for 3 μm and 10 μm particles, see Table 8.1, which were obtained by Rochester Institute of Technology through personal correspondence. For the 7.5 lpm flow rate, Dr. Oldham has

gathered data for 1 μm, 3 μm and 10 μm particles, see Table 8.2. The 1 μm and 10 μm particle results are published in Oldham, et al. (2000).

**Table 8.1 Experimental deposition in the three generation lung geometry at the 1.5 lpm flow rate (Oldham, et al., 2000) and personal correspondence.**

| Particle Size (μm) | Experimental Run #1 | Experimental Run #2 | Average Experimental Deposition |
|---|---|---|---|
| 3 | 1% | 2.1% | 1.55% |
| 10 | 45% | 42% | 43.5% |

**Table 8.2 Experimental deposition in the three generation lung geometry at the 7.5 lpm flow rate (Oldham, et al., 2000) and personal correspondence.**

| Particle Size (μm) | Experimental Run #1 | Experimental Run #2 | Average Experimental Deposition |
|---|---|---|---|
| 1 | 0.06% | --- | 0.06% |
| 3 | 1.5% | 3.4% | 2.45% |
| 10 | 85% | 81% | 83% |

Particle deposition in the three generation lung geometry was obtained by cutting the cast along the center line and dividing the model into top and bottom halves. Particle deposition in each half was counted using fluorescence microscopes and photographs. Particle deposition was counted by two individuals and complete agreement on deposition values was obtained (Oldham, et al., 2000).

Oldham, et al. (2000) ran the experiments with the three generation geometry in the horizontal position. This will affect the deposition mechanisms present in the geometry, which are discussed in Section 8.3.

## 8.2 Flow Conditions and Particle Properties

The flow conditions utilized in the three generation lung geometry have been selected to match experimental data previously gathered by Dr. Oldham at the University of California Irvine for the exact same geometry. Two flow rates were utilized by Dr. Oldham; 1.5 lpm and 7.5 lpm at the entrance to the three generation lung geometry, or generation three. The general flow conditions that are valid for all flow rates are provided in Table 8.3. Table 8.4 provides the flow conditions calculated in each generation of the three generation lung geometry based on Dr. Oldham's data for the two flow rates.

**Table 8.3 Flow conditions run in the three generation geometry for all flow rates.**

| | |
|---|---|
| Viscosity (air STP) | 1.789E-5 $Ns/m^2$ |
| Air Density (STP) | 1.225 $kg/m^3$ |
| Mean Free Path | 0.066 μm |

**Table 8.4 Flow conditions in the various generations of the three generation geometry for the two flow rates investigated.**

| Flow Rate at entrance to Generation 3 | 1.5 liter/min (2.5E-5 $m^3/s$) | 7.5 liter/min (1.25 E-5 $m^3/s$) |
|---|---|---|
| Average Velocity in Generation 3 | 1.01 m/s | 5.04 m/s |
| Reynolds Number in Generation 3 | 388 | 1939 |
| Entrance Length for Generation 3 | 0.130 m | 0.653 m |
| Average Velocity in Generation 4 | 0.803 m/s | 4.02 m/s |
| Reynolds Number in Generation 4 | 245 | 1224 |
| Entrance Length for Generation 4 | 0.065 m | 0.327 m |
| Average Velocity in Generation 5 | 0.645 m/s | 3.22 m/s |
| Reynolds Number in Generation 5 | 155 | 775 |
| Entrance Length for Generation 5 | 0.033 m | 0.163 m |

Three different velocity profiles are utilized to investigate the various deposition mechanisms; parabolic, developing and uniform velocity profiles (see Table 1.8 for exact conditions used for each mechanism and software package). Plots of the velocity profiles for each of the three flow conditions at the inlet to each generation and right before each bifurcation region are provided in Appendix D. The parabolic velocity profile is defined by Equation (5.19) where constants A, B, and C are provided in Table 8.5 for each of the flow rates investigated. As discussed previously, for parabolic runs the walls are defined as no slip boundaries and the velocity profile is defined by an expression or user defined function depending on the software package being utilized. In the uniform velocity profile runs, the walls are defined as free slip or 0 shear stress boundaries with a constant velocity profile at the inlet, which corresponds to the average velocity in generation three, see Table 8.4. The developing velocity profile runs are defined by no slip boundaries at the walls and a constant velocity profile, which again corresponds to the average velocity in generation three, see Table 8.4. The velocity profiles used to investigate each flow conditions will be discussed in Section 8.3.

**Table 8.5 Constants utilized in parabolic flow velocity profile equation for flow rates investigated in the three generation geometry.**

| Flow Rate | A | B | C |
|---|---|---|---|
| 1.5 liter/min | -257089 $m^{-1}s^{-1}$ | -257089 $m^{-1}s^{-1}$ | 2.03 m/s |
| 7.5 liter/min | -1285392 $m^{-1}s^{-1}$ | -1285392 $m^{-1}s^{-1}$ | 10.1504 m/s |

Dr. Oldham utilized monodisperse fluorescent polystyrene latex particles to investigate deposition in the three generation lung geometry. Three particles sizes were utilized; 1 μm, 3 μm, and 10 μm. The particles were purchased from various suppliers and had densities of approximately 1000 kg/m$^3$, or unit density. The particles were aerosolized using a modified nebulizer. For the CFD analysis in this research, a 0.44 μm particle size is also investigated in addition to the 1 μm, 3 μm, and 10 μm particle sizes. In the CFD analysis, the particles are solid and have a density of 1000 kg/m$^3$, or unit density.

In Fluent DPM, the particles are defined by a file and are injected 1E-19 m from the inlet and no less than 0.01 mm from the walls, occupying 99.6% of the available radius. In CFX and Fluent FPM, the internal random particle generation is utilized.

## 8.3 Dominant Deposition Mechanisms and Software Packages Utilized for Each Mechanism

When comparing to experimental data it is imperative to understand which deposition mechanisms are present before setting up CFD analysis. For the three generation geometry it is necessary to investigate the effect of impaction, sedimentation, and diffusion for each of the flow rates examined by Dr. Oldham. The relative influence of the impaction mechanism is investigated due to the presence of the bifurcations. The experiments were conducted with the three generation lung geometry in the horizontal position where gravity could cause deposition by sedimentation. The particle sizes tested were 1 μm, 3 μm and 10 μm particles where the diffusion mechanism should be negligible; however the addition of the 0.44 μm particle size in the CFD analysis necessitates the quantification of the diffusion mechanism.

To determine the influence of each mechanism the most accurate analytical equations from Chapters 5, 6, and 7 will be utilized. For sedimentation from parabolic flow at the ε values present in the three generation lung model (See Table 8.9 and Table 8.15), Pich (1972), Wang (1975) and Yeh and Schum (1980) predict the same deposition efficiency, and are represented here by Pich (1972). Fluent FPM is the only software package in close agreement with the analytical equations at all ε values present in the three generation lung geometry for sedimentation from parabolic flow. For sedimentation from uniform flow at these ε values (See Table 8.9 and Table 8.15), Yu, et al. (1977), and Yeh and Schum (1980) predict the same deposition efficiency, and are represented here by Yu, et al. (1977). Fluent

DPM predicts zero deposition; Fluent FPM and CFX are within 1% above and below the analytical equations, respectively, for sedimentation from uniform flow.

Ingham's (1975) equations are used to determine the theoretical deposition by diffusion, since these were the only equations for diffusion investigated in Chapter 6. Although, the Ingham (1975) equation was not evaluated at these low Δ values (see Table 8.7 and Table 8.13), the lowest value tested, 1E-5, yielded a deposition efficiency of 0.15% for both Ingham (1975) parabolic and Fluent FPM parabolic, with similar trends approaching observed for other small values of Δ. Fluent FPM developing flow predicted the same deposition as parabolic at these Δ values. For uniform flow, Fluent FPM and Ingham (1975) respectively predict 0.5% and 0.8% efficiencies and as smaller Δ values are approached, the 0.3% difference is expected to continue.

The total theoretical deposition efficiency for the sedimentation and diffusion mechanisms is calculated by,

$$dep_{tot} = dep_{gen3} + dep_{gen4}\left(1 - dep_{gen3}\right) + dep_{gen5}\left(1 - dep_{gen3} - \left[dep_{gen4}\left(1 - dep_{gen3}\right)\right]\right), \qquad \textbf{Equation (8.1)}$$

where $dep_{tot}$ is the total deposition efficiency, $dep_{gen3}$ is the deposition efficiency in generation three, $dep_{gen4}$ is the deposition in generation four, and $dep_{gen5}$ is the deposition in generation five.

To determine the theoretical deposition by impaction, Yeh and Schum (1980), Cai and Yu (1988), and Zhang, et al. (1997) are all utilized due to the substantial variance in predictions between these equations and lack of correlation between the analytical equations, CFD predictions, and experimental data in Chapter 7. Of the Stokes numbers present in the three generation lung model (see Table 8.11 and Table 8.17), only Stokes values from 1.7E-2 to 2.75E-1 were tested against the CFD software packages in Chapter 7 due to the limited available experimental data. However, additional work should be done to make an accurate comparison between CFD and theory for isolated impaction at the Stokes numbers present in the three generation lung geometry. The total theoretical deposition efficiency for the impaction mechanism is calculated by,

$$dep_{tot} = dep_{bif3} + dep_{bif4}\left(1 - dep_{bif3}\right), \qquad \textbf{Equation (8.2)}$$

where $dep_{tot}$ is the total deposition efficiency, $dep_{bif3}$ is the deposition efficiency in the bifurcation between generation three and four, and $dep_{bif4}$ is the deposition efficiency in the bifurcation between generation four and five.

The theoretical affect of each mechanism at the 1.5 lpm and 7.5 lpm flow rates is presented in Section 8.3.1 and Section 8.3.2, respectively.

### 8.3.1 1.5 Liter/Min Flow Rate

Figure 8.1 shows the theoretical deposition efficiency predictions for the three deposition mechanisms present in the three generation lung geometry at the 1.5 lpm flow rate. The theoretical total deposition efficiencies in all three generations due to diffusion predicted by Ingham (1975) are provided in Table 8.6. Table 8.7 contains the Δ values in each generation and particle size at the 1.5lpm flow rate. At the 1.5 lpm flow rate, diffusion will theoretically provide deposition efficiencies less than 0.5% at all particle sizes. Diffusion theoretically will not have a noticeable affect on the total deposition efficiency, except at the 3 μm particle size if the flow is uniform, where diffusion is theoretically 6.9% of the total deposition observed by Dr. Oldham, see Table 8.6. Since there is no experimental data for the 1 μm and 0.44 μm particles sizes, where diffusion should have the greatest affect, diffusion is investigated with CFD in the three generation lung geometry in Section 8.4.1.

**Table 8.6 Affect of diffusion in the three generation lung geometry at the 1.5 lpm flow rate.**

| Particle Diameter (μm) | Diffusion Ingham (1975) - 1.5lpm – Uniform Flow | % of Experimental | Diffusion Ingham (1975) - 1.5lpm - Parabolic Flow | % of Experimental |
|---|---|---|---|---|
| 0.44 | 0.316% | --- | 0.029% | --- |
| 1 | 0.193% | --- | 0.015% | --- |
| 3 | 0.106% | 6.9% | 0.007% | 0.4% |
| 10 | 0.057% | 0.1% | 0.003% | 0.01% |

**Table 8.7 Δ values in each generation of the three generation lung geometry at the 1.5l pm flow rate.**

| Particle Diameter (μm) | Δ in Generation 3 | Δ in Generation 4 | Δ in Generation 5 | Average Δ Value |
|---|---|---|---|---|
| 0.44 | 7.28E-8 | 2.43E-7 | 4.10E-7 | 2.41E-7 |
| 1 | 2.71E-8 | 9.03E-8 | 1.52E-7 | 8.98E-8 |
| 3 | 8.21E-9 | 2.74E-8 | 4.62E-8 | 2.72E-8 |
| 10 | 2.38E-9 | 7.93E-9 | 1.34E-8 | 7.90E-9 |

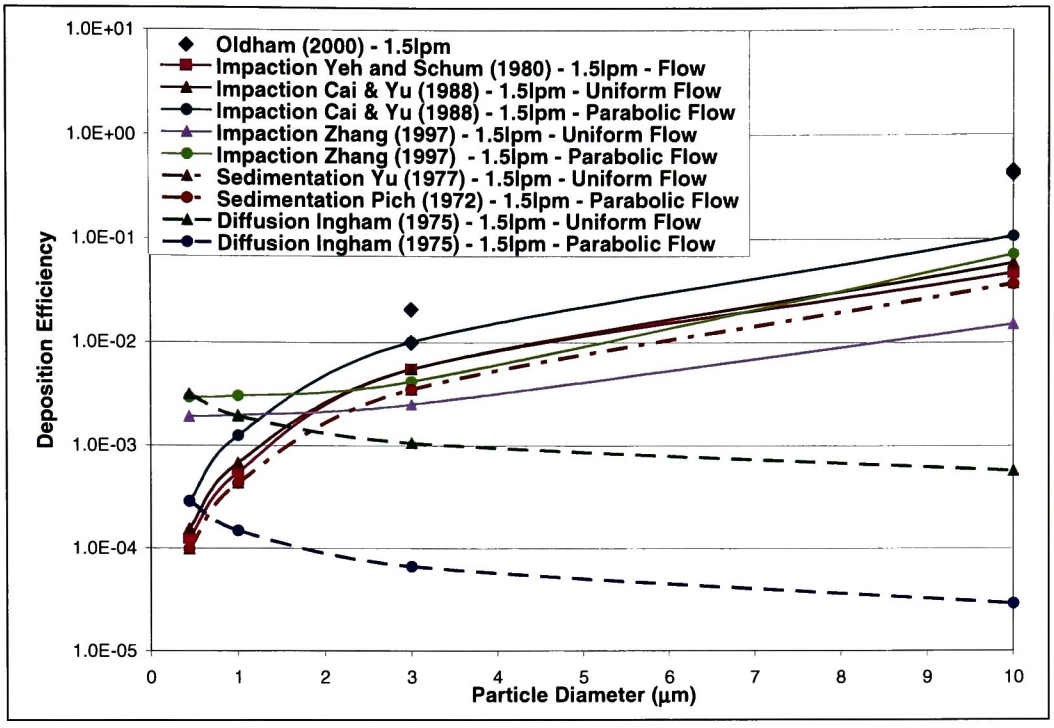


**Figure 8.1 Theoretical predictions of impaction, sedimentation, and diffusion in the three generation lung geometry at the 1.5 lpm flow rate.**

Based on the results obtained in Chapter 6, only Fluent FPM is capable of accurately predicting deposition by diffusion and is therefore, the only CFD software package utilized in this research (see Section 6.2.2.1 and 6.2.2.2). Only the developing velocity profile is investigated in this research.

Theoretical deposition efficiencies for sedimentation in all three generations predicted by Pich (1972), for parabolic flow, and Yu, et al. (1977), for uniform flow, are provided in Table 8.8. The ε values in each generation of the three generation lung geometry at the 1.5 lpm flow rate are provided in Table 8.9. At the 1.5 lpm flow rate, sedimentation is predicted to have the greatest effect on the total deposition efficiency at the 3 µm particle size. At the 3 µm particle size sedimentation theoretically has a deposition efficiency of 0.35%, which accounts for 23% of the total deposition (43.5%) observed by Dr. Oldham (see Table 8.1 and Table 8.8). The 10 µm particle size theoretically provides a deposition efficiency of 3.5%, but only accounts for 8.5% of the total deposition (1.55%) observed by Dr. Oldham (see Table 8.1 and Table 8.8). Sedimentation theoretically contributes significantly to the total deposition and is explored with the CFD software packages in Section 8.4.3.

Due to the nature of the three generation lung geometry and the software packages, sedimentation is not able to be isolated and is presented as a combined impaction and sedimentation mechanism in Section 8.4.3 for Fluent DPM and CFX. Sedimentation is not investigated in Fluent FPM, despite it having the best correlation with all three analytical equations for these ε values for parabolic flow, because Fluent FPM is not capable of predicting deposition by impaction. In future work, sedimentation could be predicted by Fluent FPM and combined with the impaction deposition efficiency from either Fluent DPM or CFX.

**Table 8.8 Affect of sedimentation in the three generation lung geometry at the 1.5 lpm flow rate.**

| Particle Diameter (μm) | Sedimentation Yu, et al. (1977) - 1.5lpm - Uniform Flow | % of Experimental | Sedimentation Pich (1972) - 1.5lpm - Parabolic Flow | % of Experimental |
|---|---|---|---|---|
| 0.44 | 0.01% | --- | 0.01% | --- |
| 1 | 0.04% | --- | 0.04% | --- |
| 3 | 0.35% | 23% | 0.35% | 23% |
| 10 | 3.74% | 8.6% | 3.69% | 8.5% |

**Table 8.9 ε values in each generation of the three generation lung geometry at the 1.5 lpm flow rate.**

| Particle Diameter (μm) | ε in Generation 3 | ε in Generation 4 | ε in Generation 5 | Average ε Value |
|---|---|---|---|---|
| 0.44 | 8.11E-6 | 2.14E-5 | 2.85E-5 | 1,93E-5 |
| 1 | 3.54E-5 | 9.35E-5 | 1.24E-4 | 8.43E-5 |
| 3 | 2.90E-4 | 7.65E-4 | 1.02E-3 | 6.92E-4 |
| 10 | 3.11E-3 | 8.21E-3 | 1.09E-2 | 7.41E-3 |

The theoretical deposition efficiency predicted by each analytical equation for the impaction mechanism in the three generation lung geometry at the 1.5 lpm flow rate is provided in Table 8.10. Table 8.11 provides the Stokes number at each bifurcation in the three generation lung geometry for the 1.5lpm flow rate. The impaction equations continue to predict the wide range of deposition efficiencies, seen in Chapter 7. It should be noted that at the 1.5 lpm flow rate in the three generation lung geometry, Cai and Yu's (1988) parabolic flow equation predicts the highest deposition efficiency, while Zhang, et al.'s (1997) uniform flow equation predicts the lowest deposition efficiency.

The CFD software packages predictions for deposition by impaction in the three generation lung geometry are presented in Section 8.4.2 for isolated impaction and Section

8.4.3 for combined sedimentation and impaction in Fluent DPM and CFX. In both Sections impaction is investigated for parabolic and uniform velocity profiles.

**Table 8.10 Affect of impaction in the three generation lung geometry at the 1.5 lpm flow rate.**

| Particle Diameter (μm) | Impact Zhang, et al. (1997) 1.5lpm Par. Flow | % of Exp. | Impact Zhang, et al. (1997) 1.5lpm Uni. Flow | % of Exp. | Impact Cai & Yu (1988) 1.5lpm Uni. Flow | % of Exp. | Impact Cai & Yu (1988) 1.5lpm Par. Flow | % of Exp. | Impact Yeh and Schum (1980) 1.5lpm Flow | % of Exp. |
|---|---|---|---|---|---|---|---|---|---|---|
| 0.44 | 0.29% | --- | 0.19% | --- | 0.02% | --- | 0.03% | --- | 0.01% | --- |
| 1 | 0.30% | --- | 0.20% | --- | 0.07% | --- | 0.12% | --- | 0.05% | --- |
| 3 | 0.42% | 27% | 0.25% | 16% | 0.55% | 36% | 1.02% | 66% | 0.55% | 36% |
| 10 | 7.16% | 16% | 1.51% | 3.5% | 5.85% | 13% | 10.66% | 24% | 4.73% | 11% |

**Table 8.11 Stokes numbers values at each bifurcation of the three generation lung geometry at the 1.5 lpm flow rate.**

| Particle Diameter (μm) | Stk Bifurcation from 3 to 4 | Stk Bifurcation from 3 to 4 | Average Stokes Number |
|---|---|---|---|
| 0.44 | 1.47E-4 | 1.48E-4 | 1.48E-4 |
| 1 | 6.43E-4 | 6.47E-4 | 6.45E-4 |
| 3 | 5.27E-3 | 5.30E-3 | 5.29E-3 |
| 10 | 5.65E-2 | 5.68E-2 | 5.67E-2 |

At the 1.5 lpm flow rate, impaction theoretically accounts for between 16% and 66% of the total deposition observed by Dr. Oldham at the 3 μm particle size. It should be noted that under some conditions, when the theoretical sedimentation and impaction are added, a significant portion of the experimental deposition is still unaccounted for. For the 1.5 lpm parabolic flow with 3 μm particles, sedimentation accounts for 23% and impaction accounts for between 27% and 66% of the 43.5% experimental deposition efficiency. Combining the theoretical sedimentation and impaction deposition efficiency results in a total deposition of 50% to 89%, depending on the theoretical impaction equation utilized. As a result between 11% and 50% of the experimental deposition is not accounted for with theoretical predictions. At the 10 μm particle size impaction theoretically is between 3.5% and 24% of the total deposition observed by Dr. Oldham. At the 1.5 lpm flow rate, none of the deposition mechanisms theoretically predict even a quarter of the deposition observed by Dr. Oldham at the 10 μm particle size. Combining sedimentation and impaction theoretically only accounts for 11% to 32% of the total experimental deposition. This is an unexpected trend, it is expected theory would account for roughly the same amount of the total

deposition at all particles sizes, since the same equations are being utilized. However, since the dimensionless parameters (Δ, ε, and Stk) vary with particle size and the accuracy of each equation can vary as the dimensionless parameters change (See Chapters 5, 6, and 7); it is possible the combined theory could account for different amounts of the total deposition at various particle sizes.

### 8.3.2 7.5 Liter/Min Flow Rate

Figure 8.2 shows the theoretical deposition efficiency predictions for the three deposition mechanisms present in the three generation lung geometry at the 7.5 lpm flow rates. The theoretical deposition by diffusion predicted by Ingham in the three generation geometry at the 7.5 lpm flow rate is provided in Table 8.12. Table 8.13 provides the Δ values for each generation of the three generation lung geometry at the 7.5 lpm flow rate. At the 7.5 lpm flow rate, data is actually available for a particle size where deposition by diffusion is possible. Diffusion theoretically should provide less than 0.2% deposition efficiency for any of the particle sizes investigated in this research. Since the experimental deposition is also small for the 1 μm particle size, diffusion is theoretically between 8.4% and 144% of the total deposition observed by Dr. Oldham, depending on the velocity profile, see Table 8.12. With the 1 μm particle being tested at the 1.5 lpm flow rate it is difficult to determine if the deposition at the 7.5 lpm flow rate for the 1 μm particle size is a result of diffusion. If experimental data was available for the 1 μm particle at both flow rates, it could be determined if diffusion was in fact contributing this significantly to the deposition at the 1 μm particle size. The deposition efficiency at the 1.5 lpm flow rate for the 1 μm was larger than was has been measured at the 7.5 lpm flow rate it would be safe to say diffusion was dominate, since deposition by diffusion increases with increasing resistance time. The other particle sizes where experimental data exist are not within the diffusion range, and deposition by diffusion is theoretically less than 2%, as expected.

Diffusion in the three generation lung geometry is investigated in CFD in Section 8.4.1. Based on the results obtained in Chapter 6, only Fluent FPM was capable of accurately predicting deposition by diffusion and is therefore, the only CFD software package utilized in this research (see Section 6.2.2.1 and 6.2.2.2). Like the 1.5 lpm flow rate only the developing velocity profile is investigated.

**Table 8.12 Affect of diffusion in the three generation lung geometry at the 7.5 lpm flow rate.**

| Particle Diameter (μm) | Diffusion Ingham (1975) - 7.5lpm - Uniform Flow | % of Experimental | Diffusion Ingham (1975) - 7.5lpm - Parabolic Flow | % of Experimental |
|---|---|---|---|---|
| 0.44 | 0.141% | --- | 0.010% | --- |
| 1 | 0.086% | 144% | 0.005% | 8.4% |
| 3 | 0.048% | 1.9% | 0.002% | 0.09% |
| 10 | 0.026% | 0.03% | 0.001% | 0.001% |

**Table 8.13 Δ values in each generation of the three generation lung geometry at the 7.5l pm flow rate.**

| Particle Diameter (μm) | Δ in Generation 3 | Δ in Generation 4 | Δ in Generation 5 | Average Δ Value |
|---|---|---|---|---|
| 0.44 | 1.46E-8 | 4.86E-8 | 8.20E-8 | 4.84E-8 |
| 1 | 5.41E-9 | 1.81E-8 | 3.05E-8 | 1.80E-8 |
| 3 | 1.64E-9 | 5.48E-9 | 9.24E-9 | 5.45E-9 |
| 10 | 4.76E-10 | 1.59E-9 | 2.68E-9 | 1.58E-9 |

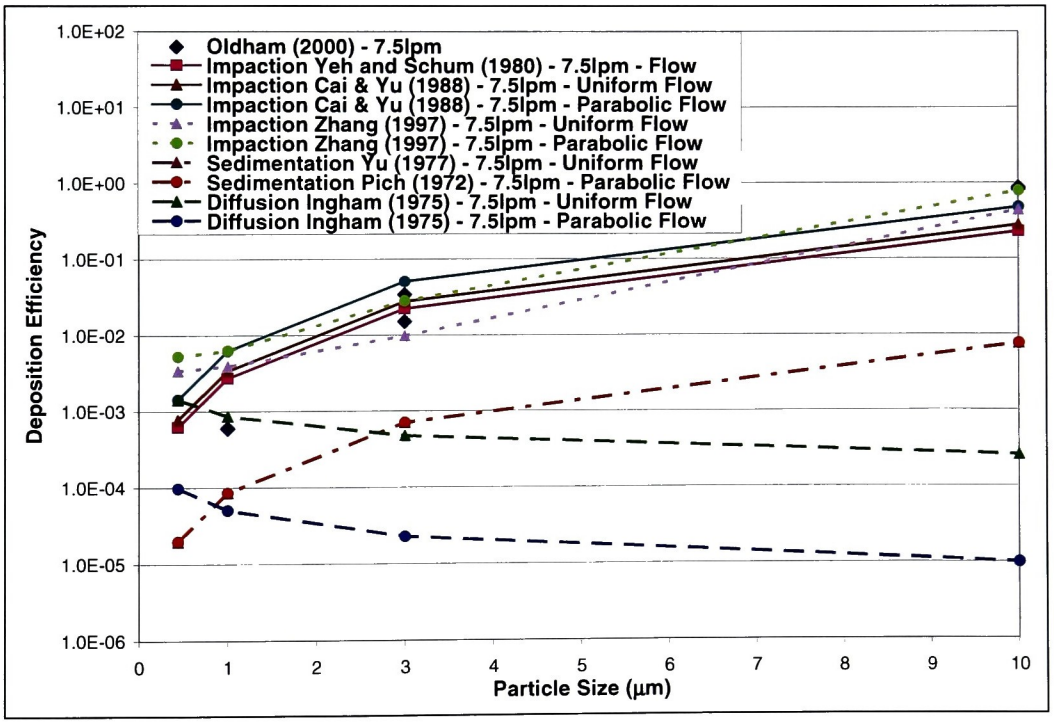


**Figure 8.2 Theoretical predictions of impaction, sedimentation, and diffusion in the three generation lung geometry at the 7.5 lpm flow rate.**

Theoretical deposition efficiencies for sedimentation in the three generation lung geometry at the 7.5 lpm flow rate are provided in Table 8.14. Table 8.15 provides the ε values for each generation of the three generation lung geometry for the 7.5 lpm flow rate. The sedimentation mechanism theoretically results in deposition efficiencies less than 1% for

all particle sizes investigated at the 7.5 lpm flow rate. At the 1 μm and 3 μm particle sizes, sedimentation is theoretically 14% and 2.9% of the total deposition (0.06% and 2.45%, respectively) observed by Dr. Oldham, respectively. At the 10 μm particle size, sedimentation is theoretically 0.9% of the total experimental deposition (83%) observed by Oldham (2000).

**Table 8.14 Affect of sedimentation in the three generation lung geometry at the 7.5 lpm flow rate.**

| Particle Diameter (μm) | Sedimentation Yu, et al. (1977) - 7.5lpm - Uniform Flow | % of Experimental | Sedimentation Pich (1972) - 7.5lpm - Parabolic Flow | % of Experimental |
|---|---|---|---|---|
| 0.44 | 0.00% | --- | 0.00% | --- |
| 1 | 0.01% | 14% | 0.01% | 14% |
| 3 | 0.07% | 2.9% | 0.07% | 2.9% |
| 10 | 0.75% | 0.9% | 0.75% | 0.9% |

**Table 8.15 ε values in each generation of the three generation lung geometry at the 7.5 lpm flow rate.**

| Particle Diameter (μm) | ε in Generation 3 | ε in Generation 4 | ε in Generation 5 | Average ε Value |
|---|---|---|---|---|
| 0.44 | 1.62E-6 | 4.28E-6 | 5.71E-6 | 3.87E-6 |
| 1 | 7.08E-6 | 1.87E-5 | 2.49E-5 | 1.69E-5 |
| 3 | 5.80E-5 | 1.53E-4 | 2.04E-4 | 1.38E-4 |
| 10 | 6.22E-4 | 1.64E-3 | 2.19E-3 | 1.48E-3 |

According to theoretical prediction sedimentation contributes noticeably to the total deposition in the three generation lung geometry at the 7.5 lpm flow rate and is therefore explored with CFD in Section 8.4.3. Due to the nature of the three generation lung geometry and the software packages, sedimentation is not able to be isolated and is presented as a combined impaction and sedimentation mechanism in Section 8.4.3 for Fluent DPM and CFX, since Fluent FPM is unable to model deposition by impaction. Like the 1.5 lpm flow rate only the parabolic and uniform velocity profiles are investigated in this research. Theoretical deposition efficiencies for the impaction mechanism in the three generation lung geometry are provided in Table 8.16. Table 8.17 provides the Stokes number at each bifurcation in the three generation lung geometry at the 7.5 lpm flow rate. As seen at the 1.5 lpm flow rate, the impaction equations continue to predict the wide range of deposition efficiencies, seen in Chapter 7. At the 1 μm particle sizes, impaction theoretically contributes more than 100% of the total deposition observed by Oldham, et al. (2000) for all of the

analytical equations investigated. Additionally, impaction is predicted to theoretically represent between 39% and 206% of the total deposition (2.45%) observed by Dr. Oldham for the 3 μm particle size. Some of the range of deposition efficiency can be attributed to the equations predicting deposition from both uniform and parabolic flow. At the 10 μm particle size, impaction is theoretically responsible for between 27% and 94% of the total deposition observed by Oldham, et al. (2000). At the 7.5 lpm flow rate, Zhang, et al.'s (1997) parabolic flow equation predicts the highest deposition efficiency, while Yeh and Schum's (1980) equation predicts the lowest deposition efficiency.

**Table 8.16 Affect of impaction in the three generation lung geometry at the 7.5 lpm flow rate.**

| Particle Diameter (μm) | Impact Zhang, et al. (1997) 7.5lpm Par. Flow | % of Exp. | Impact Zhang, et al. (1997) 7.5lpm Uni. Flow | % of Exp. | Impact Cai & Yu (1988) 7.5lpm Uni. Flow | % of Exp. | Impact Cai & Yu (1988) 7.5lpm Par. Flow | % of Exp. | Impact Yeh and Schum (1980) 7.5lpm Flow | % of Exp. |
|---|---|---|---|---|---|---|---|---|---|---|
| 0.44 | 0.52% | --- | 0.34% | --- | 0.08% | --- | 0.14% | --- | 0.06% | --- |
| 1 | 0.62% | 1041% | 0.39% | 649% | 0.34% | 563% | 0.62% | 1037% | 0.27% | 454% |
| 3 | 2.80% | 114% | 0.97% | 39% | 2.75% | 112% | 5.04% | 206% | 2.22% | 91% |
| 10 | 77.76% | 94% | 43.59% | 53% | 27.51% | 33% | 47.29% | 57% | 22.47% | 27% |

**Table 8.17 Stokes number in each bifurcation in the three generation lung geometry at the 7.5 lpm flow rate.**

| Particle Diameter (μm) | Stk Bifurcation from 3 to 4 | Stk Bifurcation from 3 to 4 | Average Stokes Number |
|---|---|---|---|
| 0.44 | 7.37E-4 | 7.42E-4 | 7.40E-4 |
| 1 | 3.21E-3 | 3.24E-3 | 3.23E-3 |
| 3 | 2.63E-2 | 2.65E-2 | 2.64E-2 |
| 10 | 2.83E-1 | 2.84E-1 | 2.84E-1 |

The CFD software packages predictions for deposition by impaction in the three generation lung geometry are presented in Section 8.4.2 for isolated impaction and Section 8.4.3 for combined sedimentation and impaction in Fluent DPM and CFX. Only the parabolic and uniform velocity profiles are examined in this research.

It should be noted that at the 7.5 lpm flow rate, both impaction and diffusion theoretically represent more than 100% of total deposition observed by Dr. Oldham at the 1 μm particle size. Impaction could theoretically represent 100% or more of the total deposition observed by Dr. Oldham at the 3 μm and 10 μm particle sizes and be the only

deposition mechanism present in the three generation geometry at the 7.5lpm. At the 10 μm particle size, the sedimentation and diffusion theoretically account for less than 1% of the total (83%) experimental deposition efficiency. Therefore impaction could theoretically be the only mechanism contributing to the deposition of the 10 μm particles at the 7.5 lpm flow rate.

## 8.4 Comparison of CFD Result and Analytical Equations to Experimental Data for Total Deposition in the Three Generation Geometry

Deposition in the three generation model is evaluated in CFD for diffusion, Section 8.4.1, impaction, Section 8.4.2, and combined impaction and sedimentation, Section 8.4.3, mechanisms. These mechanisms have been selected for investigation based on the dominate deposition mechanisms in the three generation lung geometry at the 1.5 and 7.5 lpm flow rates discussed in Sections 8.3.1 and 8.3.2, respectively. Deposition efficiencies are compared to particle diameter in the three generation lung geometry rather than ε, Δ, and Stokes number because these dimensionless parameters vary with both particle size and generation or bifurcation; therefore in the three generation lung geometry there are multiple values for these dimensionless parameters at a size particle diameter unlike Chapters 5, 6, and 7 (See Tables in Section 8.3).

### 8.4.1 Diffusion

Ingham's (1975) equations for parabolic and uniform velocity profiles are compared to the developing velocity profile in Fluent FPM. Both of Ingham's (1975) diffusion equations are plotted to provide the range of theoretical results for the experimental flow conditions. The experimental velocity profiles have not been visualized experimentally for these conditions, but Fluent FPM (See Appendix D) indicates the velocity profile is developing as it enters the bifurcation between generation three and four, even when starting from a constant velocity profile at the inlet. As explained in Section 8.3, results for Fluent FPM developing and parabolic profiles are expected to be the same at these Δ values.

Section 8.4.1.1 provides data for the isolated diffusion deposition mechanism in the three generation lung geometry at the 1.5 lpm flow rate. Section 8.4.1.2 provides data for the

isolated diffusion deposition mechanism in the three generation lung geometry at the 7.5 lpm flow rate. Section 8.4.1.3 summarizes the diffusion deposition mechanism in the three generation lung geometry.

### 8.4.1.1 Diffusion at 1.5 Liter/Min Flow Rate

Figure 8.3 provides the deposition efficiency verses particle diameter for isolated diffusion in the three generation lung geometry for Fluent FPM and Ingham's (1975) analytical equations at the 1.5 lpm flow rate. Fluent FPM predicts deposition efficiencies lower than Ingham's (1975) predictions for parabolic and uniform velocity profiles, as seen in the straight tube (see Section 6.2.2). In fact, when comparing to parabolic flow Fluent FPM is an order of magnitude lower in its prediction. It should be noted, the deposition efficiency is under 0.4%, where an order of magnitude is minimal change in deposition efficiency. $\Delta$ values between 4E-7 and 8E-9 were not investigated in the straight tube geometry, since only particle sizes within the diffusion range were investigated (see Figure 6.1 and Table 8.7). The lack of data at these $\Delta$ values make it impossible to determine if the increased error in Fluent FPM's predictions compared to Ingham's (1975) analytical equations is a function or the $\Delta$ values or the more complicated geometry. In the single bifurcation geometry at the 1E-5 $\Delta$ value Ingham's (1975) parabolic equation and Fluent FPM predict the same deposition efficiency. However, the particle sizes being investigated in the three generation lung geometry are all larger than 0.1 μm, where diffusion typically becomes measurable for most flow conditions. The variation in deposition efficiency is unnoticeable when compared to magnitude of the experimental data.

At the 0.44 μm and 1 μm particle sizes, where diffusion should have noticeable affect on deposition, there is no experimental data from Dr. Oldham to compare with Fluent FPM's predictions and Ingham's (1975) analytical equations. At the larger particle sizes, where experimental data is available, Fluent FPM's predictions agree well with the analytical equations, despite noticeable differences in deposition efficiency in Figure 8.3. Without experimental data it is not possible to determine if Fluent DPM or the analytical equations are more accurately predicting what is happening in the three generation lung model for particle sizes at the upper limit of the diffusion range. Either way this information will have

little impact on the total deposition efficiency at the 3 μm and 10 μm particle sizes, where experimental data is currently available.

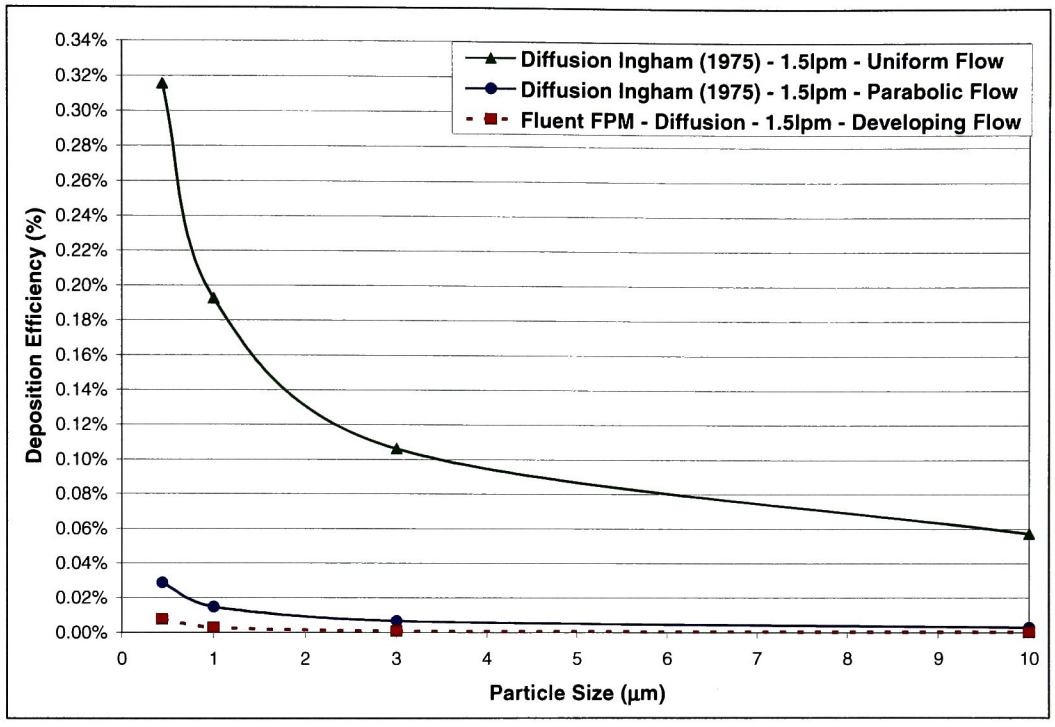


**Figure 8.3 Comparison of Fluent FPM's prediction and Ingham's analytical equations for isolated diffusion in the three generation lung geometry at the 1.5 lpm flow rate.**

### 8.4.1.2 Diffusion at 7.5 Liter/Min Flow Rate

Figure 8.4 provides the deposition efficiency verses particle diameter for isolated diffusion in the three generation lung geometry for Fluent FPM and Ingham's (1975) analytical equations at the 7.5 lpm flow rate. Fluent FPM again predicts deposition efficiencies lower than Ingham's (1975) predictions for parabolic and uniform velocity profiles, as seen in the straight tube (see Section 6.2.2). When comparing Fluent FPM to Ingham's (1975) parabolic flow equation, Fluent FPM is an order of magnitude lower in its prediction. It should be noted, the deposition efficiency is under 0.15%, where an order of magnitude is minimal change in deposition efficiency. However, the difference between Ingham (1975) and Fluent FPM is actually less than the 0.3% observed in the straight tube at the 1E-5 Δ value.

As encountered at the 1.5 lpm flow rate, Δ values between 9E-8 and 4E-10 were not evaluated in the straight tube geometry (see Figure 6.1 and Table 8.13). These values of Δ were not explored in the straight tube because they correspond to particle diameters too large for diffusion to be a measurable mechanism. Therefore, it is not possible to determine if the variation in correlation with theory is due to the Δ value or the multi-generation geometry.

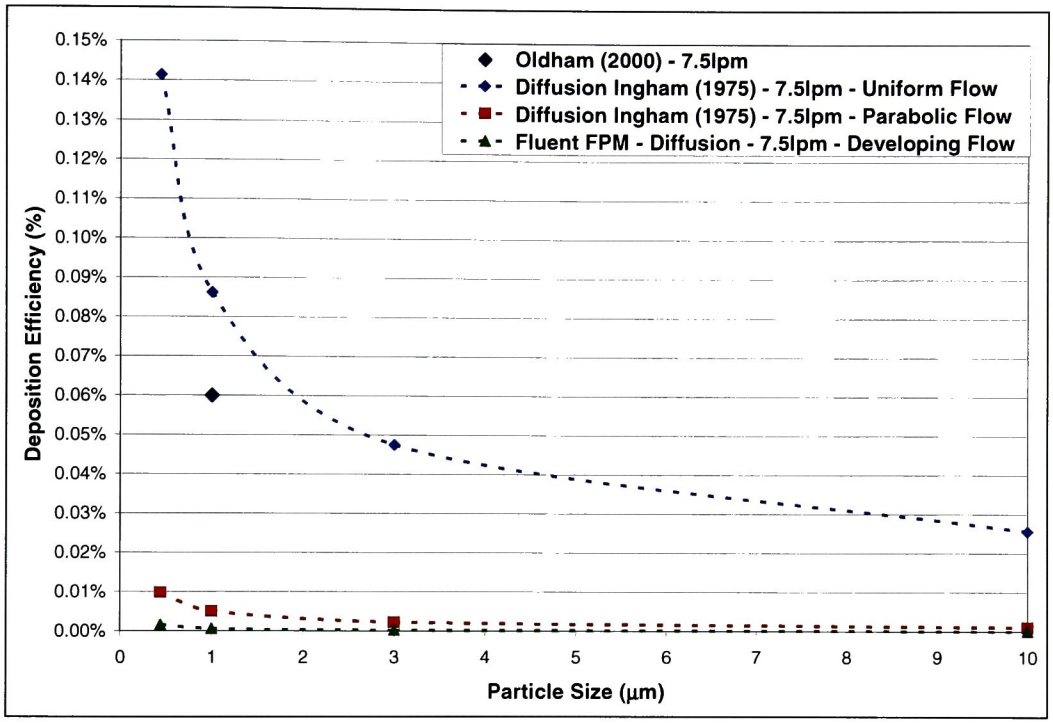


**Figure 8.4 Comparison of Fluent FPM's prediction for isolated diffusion, Ingham's analytical equations, and Oldham's experimental data in the three generation lung geometry at the 7.5 lpm flow rate.**

At the 1 μm particle size, experimental data obtained by Oldham, et al. (2000) is between Ingham's (1975) analytical equations for uniform and parabolic flow. As discussed in Section 8.3.2, diffusion is not the only deposition mechanism providing a significant theoretically contribution to the total deposition, given this fact it is likely the parabolic flow equation is a better representation of what is occurring. Especially, since Ingham's (1975) uniform flow equation predictions a deposition efficiency 144% of the total experimental deposition (0.06%) for the 1 μm particle size. The parabolic flow equation predicts 8.4% of the experimental deposition, while Fluent FPM predicts 1% of the experimental deposition.

At the 3 μm and 10 μm particle sizes Fluent FPM's predictions of deposition by diffusion agree well with the analytical equations, varying less than 0.05%.

### 8.4.1.3 Diffusion Summary for the Three Generation Lung Geometry

Fluent FPM is predicting lower deposition efficiencies than Ingham's (1975) analytical equations. A similar trend is observed in the straight tube in Section 6.2.2 for uniform flow, however, parabolic and developing flow Fluent FPM predictions were the same as theory in the straight tube for Δ values slightly larger than these. However, since Δ values on the order of magnitude present in the three generation lung geometry at the 1.5 lpm and 7.5 lpm flow rates were not investigated in the straight tube, it cannot be concluded whether the variation in Fluent FPM's accuracy is due to the Δ value or the more complicated geometry. At the flow conditions and particle sizes investigated in this research less than 1% of all particles injected are deposited by the diffusion deposition mechanism. The slight or even order of magnitude variations between theoretical predictions and Fluent FPM's predictions do not have a substantial effect on the total particle deposition.

Without more than one data point in the diffusion range it difficult to know if either Fluent FPM or Ingham's (1975) analytical equations are accurately representing what is occurring in the three generation model. Additionally, unless diffusion is the only mechanism present it will still be difficult to make this distinction. In a bifurcating geometry, like the three generation lung, the only way to reduce the influence of the impaction deposition mechanism is to utilize smaller particles, where inertia is less of a factor. Currently, Ultrafine particles as small as 40 nm have been able to be studied in hollow cast (Cohen, 1987; Cohen, et al., 1990). It is still difficult to obtain particles smaller than this for physical experiments with reasonable consistency in the particle diameters. Even with particles as small as 40 nm, diffusion is not completely isolated. Impaction still has some contribution to total deposition, although considerably less than diffusion at most flow rates (Cohen and Asgharian, 1990; Broday, 2004).

### 8.4.2 Impaction

When investigating the isolated impaction mechanism in the three generation lung geometry Yeh and Schum's (1980), Cai and Yu's (1988), and Zhang, et al.'s (1997) theoretical equations for uniform and parabolic velocity profile are compared to Dr. Oldham's experimental data and CFX and Fluent DPM for parabolic and uniform flow. All the impaction theoretical equations are included due to the large variation observed in Section 7.3. Additionally, the parabolic and uniform velocity profiles are investigated in CFD due to the large variation in deposition efficiencies observed by the two velocity profiles in Section 7.3.

Section 8.4.2.1 provides data for the isolate impaction deposition mechanism in the three generation lung geometry at the 1.5 lpm flow rate. Section 8.4.2.2 provides data for the isolated impaction deposition mechanism in the three generation lung geometry at the 7.5 lpm flow rate. Section 8.4.2.3 summarizes the impaction deposition mechanism in the three generation lung model.

#### 8.4.2.1 Impaction at 1.5 Liter/Min Flow Rate

Figure 8.5 provides the deposition efficiency verses particle diameter for isolated impaction from a parabolic velocity profile in the three generation lung geometry for the two CFD software packages, the three relevant theoretical equations, and Dr. Oldham's experimental data at the 1.5 lpm flow rate. At the 10 μm particle sizes, all the theoretical equations predict less than a quarter of the experimental deposition. However, at the 3 μm particle size the analytical equations predict between 66% and 27% of the total experimental deposition, see Table 8.10. The large variation in the influence of impaction between the 3 μm and 10 μm particle sizes could be attributed to an increase in the affect of sedimentation, since larger particles are inclined to settle faster than smaller ones.

Fluent DPM predicts deposition efficiencies for isolated impaction in the three generation lung geometry from parabolic flow at the 1.5 lpm flow rate, with a curve shape similar to Cai and Yu (1988). However, the deposition efficiencies are 10% to 15% higher at each particle size. CFX predicts deposition efficiencies for isolated impaction in the three generation lung geometry from parabolic flow at the 1.5 lpm flow rate, with a curve shape similar to Zhang, et al. (1997). Zhang, et al. (1997) has a lightly steeper slope between the 3

μm and 10 μm particle sizes than predicted by CFX. The deposition efficiencies predicted by CFX are between 3% and 4% higher than Zhang, et al. (1997).

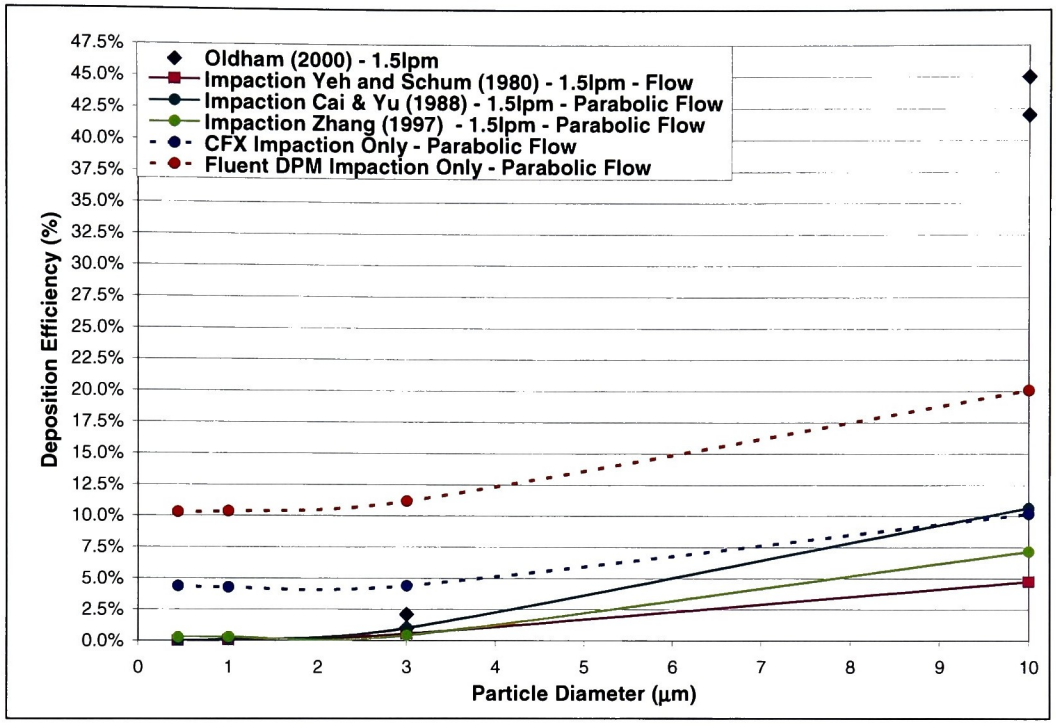


**Figure 8.5 Comparison of CFD data, analytical equations, and experimental data for isolated impaction in the three generation lung geometry for parabolic flow at the 1.5 lpm flow rate.**

The Stokes numbers at the bifurcations in the three generation lung geometry are significantly smaller than the Stokes number explored in the single bifurcation geometry, in Chapter 7. However, at the lowest Stokes numbers examined in the single bifurcation geometry, CFX continually over predicts all analytical equations, as it does in the three generation geometry at the 1.5 lpm flow rate. Fluent DPM's predictions for parabolic flow in the single bifurcation geometry are typically several percent lower than CFX and all the analytical equations. However, Fluent DPM is over predicting CFX and the analytical equations in the three generation model, an unexplainable change from the bifurcation predictions. The CFD software packages agree with different analytical equations for parabolic flow in the three generation geometry than in the single bifurcation geometry. In the single bifurcation geometry, CFX agrees closest with Cai and Yu (1988), while Fluent DPM aligns with Yeh and Schum (1980) for Stokes numbers less than 0.05 (See Figure 7.5,

Figure 7.12, and Figure 7.16). Neither of the CFD software packages agreed well with Zhang, et al. (1997) for parabolic flow at Stokes numbers less than 0.05 in the single bifurcation.

Both CFX and Fluent DPM over predict the deposition observed Dr. Oldham at the 3 μm particle size, CFX by 3% and Fluent DPM by 10%. While at the 10 μm particle size both CFX and Fluent DPM under predict the experimental data by 33% and 23%, respectively. In the single bifurcation geometry, it was usual for CFX to over predict Kim and Iglesias' (1989) experimental data at Stokes numbers less than 0.05 for parabolic flow conditions (See Figure 7.5, Figure 7.12, and Figure 7.16). However, Fluent DPM always under predicts Kim and Iglesias' (1989) experimental data for Stokes numbers less than 0.05.

Figure 8.6 provides the deposition efficiency verses particle diameter for isolated impaction from a uniform velocity profile in the three generation lung geometry for the two CFD software packages, the three relevant analytical equations, and Dr. Oldham's experimental data at the 1.5 lpm flow rate. There is again better correlation between the analytical equations and the experimental data at the 3 μm particle size than the 10 μm particle size. Since this large variation in analytical and experimental data is seen in both parabolic and uniform velocity profiles at the 10 μm particle size, it is likely that at the 1.5 lpm flow condition impaction is not the only deposition mechanism contributing to deposition in the experimental data.

CFX and Fluent DPM both predict deposition efficiencies with similar curve shape to Zhang, et al. (1997) and Yeh and Schum (1980). The deposition efficiencies predicted by CFX and Fluent are within 0.5% of one another. Both are roughly 1% higher than Yeh and Schum's (1980) predictions and 1% to 5% higher than Zhang, et al.'s (1997) predictions. In the single bifurcation geometry, CFX regularly over predicted the uniform flow equations at Stokes numbers less than 0.05. However, Fluent DPM never over predicted CFX or the analytical equations at Stokes numbers less than 0.05 in the uniform velocity profile runs (See Figure 7.6, Figure 7.13, and Figure 7.17).

Both CFX and Fluent DPM's predictions are more than 35% under the experimental data at the 10 μm particle size. At the 3 μm particle size, CFX and Fluent DPM fit right in between the two experimental data points observed by Dr. Oldham. Trends in CFD predictions of experimental data in the three generation lung model at the 1.5lpm flow rate

for isolated impaction do not agree with what was observed in the single bifurcation geometry in Chapter 7 for Stokes numbers less than 0.05. In the single bifurcation geometry at the 0.017 Stokes numbers, CFX is over predicting Fluent DPM and Kim and Iglesias' (1989) experimental data for the uniform velocity profile. For Stokes number greater 0.02, CFX under predicts experimental data in the bifurcation tube geometry. At the same Stokes numbers, Fluent DPM is predicting deposition efficiencies closer to those observed by Kim and Igelsias (1989). It is important to remember, Stokes numbers as small as those present at the bifurcations in the three generation model for the 1.5 lpm flow rate were not examined in the single bifurcation geometry. It is therefore difficult to say if the variations are due to the change in geometry or the small Stokes numbers.

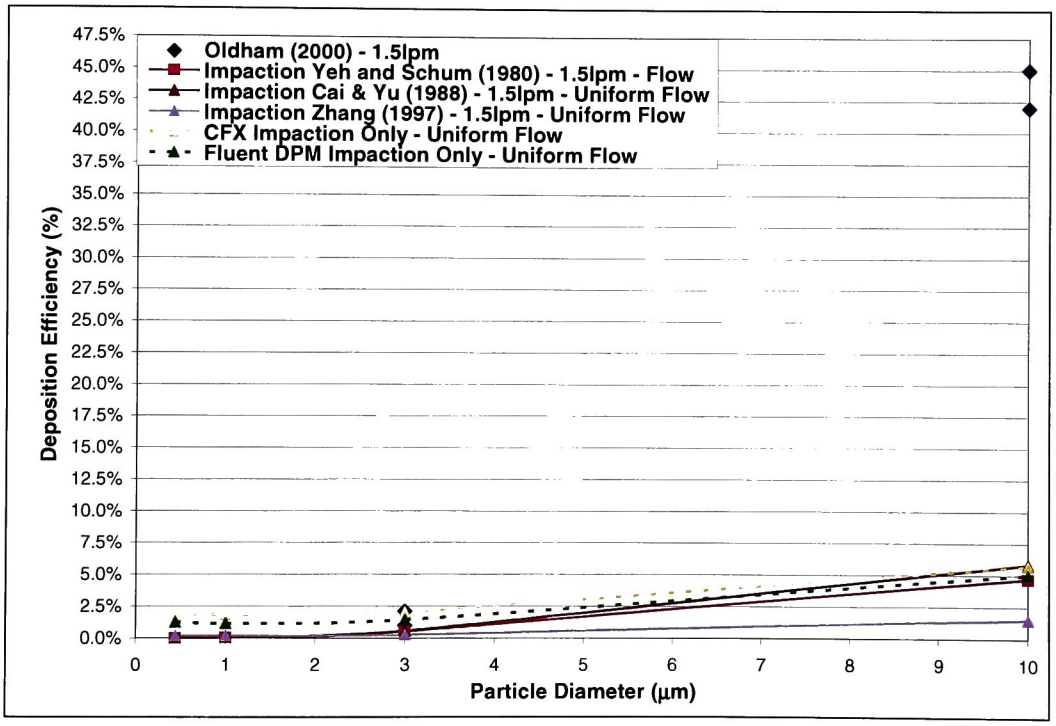


**Figure 8.6 Comparison of CFD data, analytical equations, and experimental data for isolated impaction in the three generation lung geometry for uniform flow at the 1.5 lpm flow rate.**

## 8.4.2.2 Impaction at 7.5 Liter/Min Flow Rate

Figure 8.7 provides the deposition efficiency verses particle diameter for isolated impaction from a parabolic velocity profile in the three generation lung geometry for the two CFD

software packages, the three relevant analytical equations, and Dr. Oldham's experimental data at the 7.5 lpm flow rate. Zhang, et al. (1997) has the best agreement with the experimental data of the analytical equations, predicting deposition efficiencies within 1% to 4% of Dr. Oldham's experimental data at all particle diameters. This corresponds to what was seen in the bifurcation at Stokes numbers less than 0.15 in the single bifurcation in Chapter 7. However, in the single bifurcation geometry, Zhang, et al.'s agreement with Kim and Iglesias' (1989) experimental data breaks down at Stokes numbers greater than 0.15 to 0.20 depending on the flow rate (see Figure 7.12 and Figure 7.16). Zhang, et al.'s (1997) predictions indicate that impaction is the dominate mechanism at the 7.5 lpm flow rate if the flow is parabolic for all particle sizes. The other analytical equations agree impaction is a dominate mechanism at the 1 μm and 3 μm particle sizes; however leave room for the influence of other deposition mechanisms at the 10 μm particle size. This is again similar to what was seen in the single bifurcation for parabolic flow at all Stokes numbers, where Zhang, et al. (1997) regularly over predicted all the other analytical equations for parabolic flow (See Figure 7.5, Figure 7.12, and Figure 7.16). There is a 55% range of deposition efficiencies predicted by the analytical equations at the 10 μm particle size for a parabolic velocity profile at the 7.5 lpm flow rate. At the 1 μm and 3 μm particle sizes the analytical equations are as much as ten times the experimental data, however the range of deposition efficiencies is less than 1% and not substantial when compared to the total experimental deposition efficiency.

CFX and Fluent DPM both over predict all the analytical equations at the 0.44 μm particle sizes. At the 10 μm particle size, both CFD software packages provide deposition efficiencies within the range predicted by the various analytical equations. CFX is with in 2.5% of Zhang, et al. (1997) at the 10 μm particle size. Fluent DPM under predicts Zhang, et al. (1997) by 15% and over predicts Cai and Yu (1988) by roughly 17% at the 10 μm particle size. The curve shape predicted by CFX and Fluent DPM is similar to Cai and Yu (1988). Fluent DPM is between 5% and 15% higher than Cai and Yu's (1988) predictions, while CFX is between 10% and 25% higher.

In the single bifurcation geometry in Chapter 7, CFX over predicted Cai and Yu (1988) while having a similar curve shape, as seen here for parabolic flow. Fluent DPM was typically closer to the Yeh and Schum's (1980) predictions in the single bifurcation for

Stokes numbers less than 0.05 and Cai and Yu (1988) for Stokes numbers greater than 0.15. Additionally, in the single bifurcation geometry CFX and Fluent DPM's predictions are closer in value as the Stokes number increases for parabolic flow, which is the opposite of what is being seen in the three generation geometry.

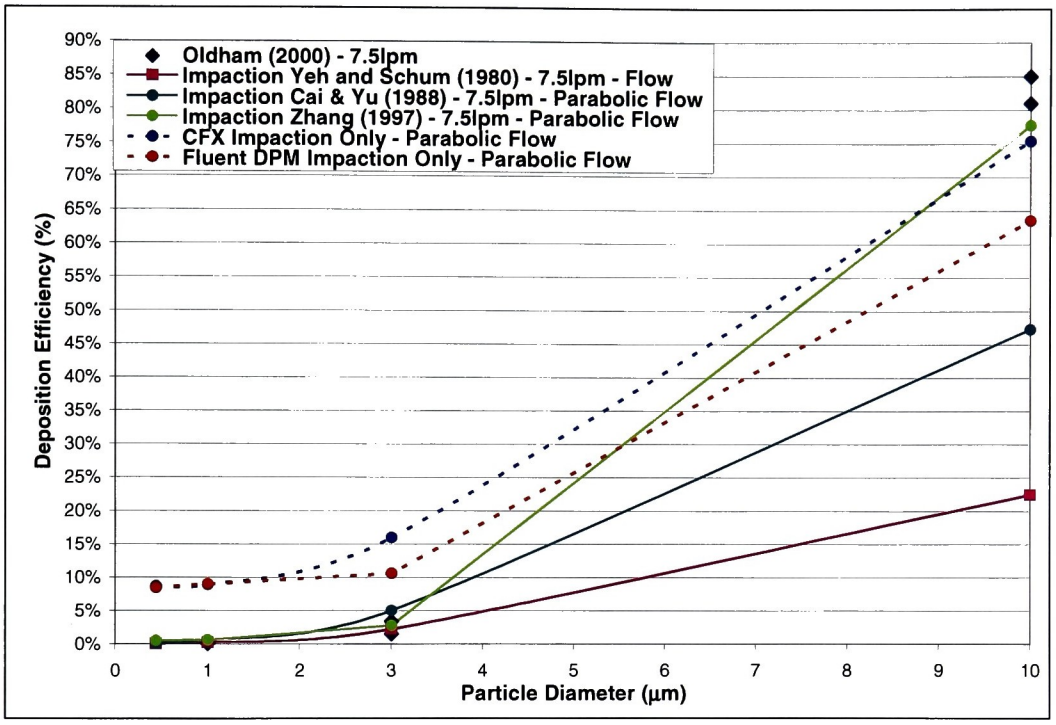


**Figure 8.7 Comparison of CFD data, analytical equations, and experimental data for isolated impaction in the three generation lung geometry for parabolic flow at the 7.5 lpm flow rate.**

CFD predictions for deposition from parabolic flow in the three generation lung model at the 7.5 lpm flow rate agree well with experimental data at the 10 µm particle size. This is expected, since impaction is theoretically isolated at the 10 µm particle size for these flow conditions. However, at the 1 µm and 3µm particle sizes, where sedimentation should theoretically have an affect on deposition, both CFD software packages predict deposition by impaction as much as ten times greater than the deposition observed by Dr. Oldham. In the single bifurcation geometry, CFX over predict the experimental data at Stokes numbers less than 0.05, while Fluent DPM under predicts experimental data. The entrance length for these flow conditions could account for why deposition is being over predicted by parabolic flow at the 7.5 lpm rate, see Table 8.4. However, it is not clear why the same trend is not seen at the 10 µm particle size if the issue is the velocity profile.

Figure 8.8 provides the deposition efficiency verses particle diameter for isolated impaction from a uniform velocity profile in the three generation lung geometry for the two CFD software packages, the three relevant analytical equations, and Dr. Oldham's experimental data at the 7.5 lpm flow rate. All analytical equations predict more than 100% of the experimental deposition observed at the 1 μm particle size. At the 3 μm particle size, Cai and Yu (1988) and Yeh and Schum (1980) still predict nearly 100% of the deposition observed by Dr. Oldham to be attributed to impaction. Zhang, et al. (1997) only predicts 39% of the observed deposition to be attributed to impaction. In the single bifurcation geometry in Chapter 7, at the 0.017 Stokes numbers (1 μm particle size in the three generation geometry) Cai and Yu (1988) and Yeh and Schum (1980) over predict Kim and Iglesias' (1989) experimental data (see Figure 7.6, Figure 7.13, and Figure 7.17), while in the three generation geometry they are several percent under Dr. Oldham's observations. By the 0.05 Stokes number all analytical equations are under predicting Kim and Iglesias' (1989). At the 10 μm particle size, deposition by impaction is theoretically 53% to 27% of the deposition observed by Dr. Oldham at the 7.5 lpm flow rate, with Zhang, et al. (1997) predicting the highest deposition efficiency. This too agrees with what was seen in Chapter 7 for uniform flow in the bifurcation tube geometry at Stokes numbers greater than 0.10.

CFX and Fluent DPM predict deposition efficiency within 1% to 7% of Cai and Yu (1988) for all particle sizes. Deposition efficiencies from both CFX and Fluent DPM over predict Cai and Yu (1988) and Yeh and Schum (1980) at all particle sizes. In the single bifurcation geometry, CFD aligns closest with Cai and Yu (1988), but under predicted both Cai and Yu (1988) and Yeh and Schum (1980) at Stokes numbers greater than 0.05. This is the opposite of what is being seen in the three generation geometry for uniform flow at similar Stokes numbers. The CFD predictions over estimating Cai and Yu (1988) and Yeh and Schum (1980) in the three generation lung geometry could be due to the increase in the number of bifurcations.

For the 1 μm and 3 μm particle sizes, both CFX and Fluent DPM over predict Dr. Oldham's data. This agrees with what was observed in the bifurcation tube geometry at Stokes number less than 0.02 for CFX, but not Fluent DPM. At the 10 μm particle size, CFD predicts less than 50% of the experimental deposition observed by Dr. Oldham for uniform

flow conditions. This also agree with the bifurcation tube geometry observations for Stokes numbers greater than 0.10.

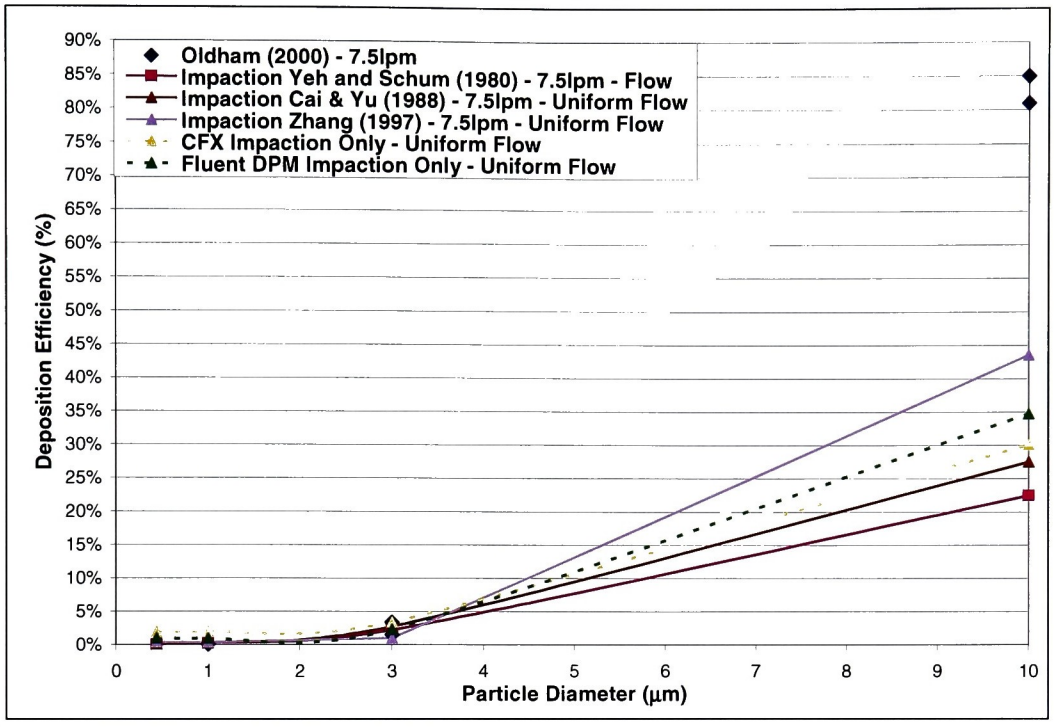


**Figure 8.8 Comparison of CFD data, analytical equations, and experimental data for isolated impaction in the three generation lung geometry for uniform flow at the 7.5 lpm flow rate.**

### 8.4.2.3 Summary of Impaction in the Three Generation Lung Geometry

In general, the parabolic velocity profile predicts higher deposition efficiencies than the uniform velocity profile for both the theoretical equations and CFD predictions. This agrees with what was observed in the single bifurcation geometry in Chapter 7. There is still substantial variation in the analytical equations predictions, which also agrees with what was seen in Chapter 7 for the impaction deposition mechanism.

At the 1.5 lpm flow rate, both the parabolic and uniform velocity profiles have reasonable agreement between the CFD prediction, theoretical equations and experimental data at the 3 µm particle size. However, at the 10 µm particle size, CFD predictions and theoretical equations provide deposition efficiencies for isolated impaction at least 21% below, or half of the experimental deposition measure by Dr. Oldham. Exploring the developing velocity profile may help improve agreement at the 1.5 lpm flow rate.

At the 7.5pm flow rate, Fluent DPM and CFX provide similar deposition efficiencies. Fluent DPM is over predicting CFX, particularly at the 3 μm and 10 μm particle sizes. This is opposite of what was seen in the single bifurcation geometry in Chapter 7 for impaction at similar Stokes numbers. The CFD predictions are more accurate at the 3 μm particle size for uniform flow, while at the 10 μm particle size CFD agrees closer with parabolic predictions. It is known that the uniform flow conditions are not a realistic representation of the physical flow in the experiments based on the velocity profiles from CFD, which show the developing velocity profile starting to take on a parabolic profile by the first bifurcation at this flow rate. Exploring the developing velocity profile at the 7.5 lpm flow rate may improve correlation with experimental data at all particle sizes.

### 8.4.3 Combined Impaction and Sedimentation

When investigating the sedimentation mechanism in the three generation lung geometry, it has to be combined with impaction due to the nature of the CFD software packages. Based on the dominate mechanism analysis, the combined impaction and sedimentation deposition mechanism should provide the most accurate representation of the conditions present within the three generation lung geometry during the experimental runs conducted by Dr. Oldham.

Deposition predicted by combined impaction and sedimentation is compared to the CFD data obtained for isolated impaction and Dr. Oldham's experimental data. Only the parabolic and uniform velocity profiles are investigated for comparison purposes. Section 8.4.3.1 provides data for the 1.5 lpm flow rate, Section 8.4.3.2 provides data for the 7.5 lpm flow rate, and Section 8.4.3.3 provides the summary of deposition by combined impaction and sedimentation.

#### 8.4.3.1 Combined Impaction and Sedimentation at 1.5 Liter/Min Flow Rate

Figure 8.9 provides the deposition efficiency verses particle diameter for Dr. Oldham's experimental data and the various CFD software packages at the 1.5 lpm flow rate for parabolic flow for both isolated impaction and combined impaction and sedimentation. The addition of sedimentation in both CFD software packages significantly increases the deposition efficiency at all particle sizes. In Fluent DPM, the addition of sedimentation increases deposition by 5% to 15% depending on the particle size. Fluent DPM, is indicating

sedimentation is the dominate deposition mechanism at all particle sizes for the 1.5lpm flow rate, despite theoretical predictions. CFX experiences a smaller increase in deposition with the addition of sedimentation, especially at the smaller particle sizes. CFX still predicts sedimentation to be the dominate deposition mechanism particularly at the 10 um particle size. However at the 3 μm particle size sedimentation is only roughly 40% of the combined deposition efficiency in CFX, where in Fluent DPM it is nearly 90% of the combined deposition efficiency.

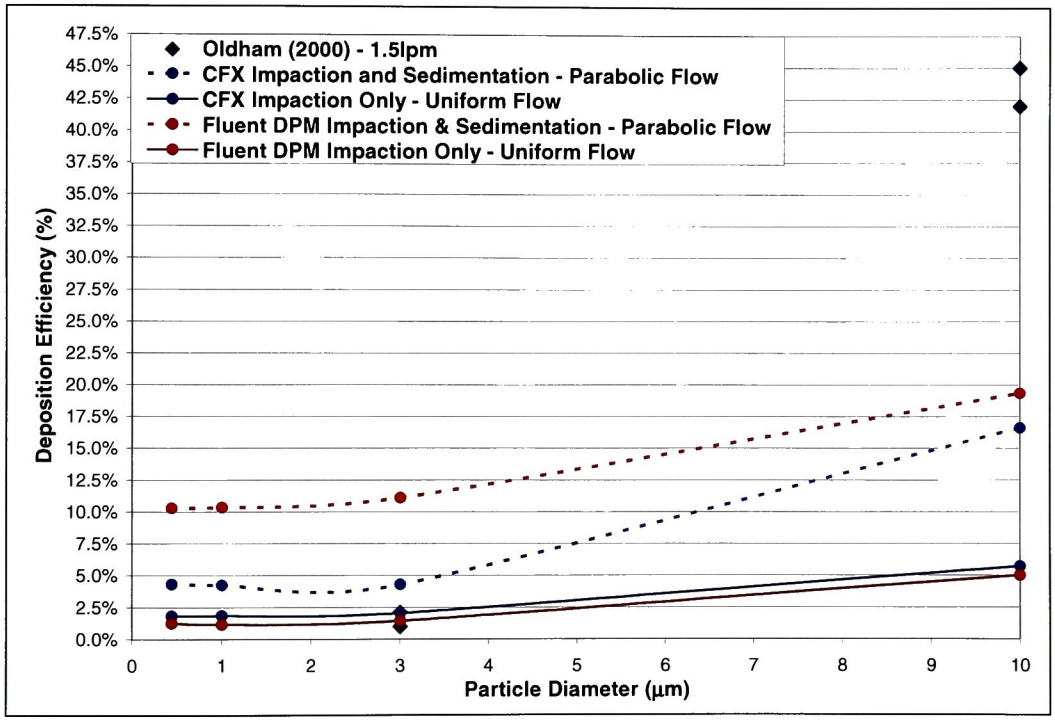


**Figure 8.9 Comparison of CFD and experimental data for combined impaction and sedimentation in the three generation lung geometry for parabolic flow at the 1.5 lpm flow rate.**

When comparing to experimental data. Both CFD software packages over predict the experimental data at the 3 μm particle size. At the 10 μm particle size both CFD software packages under predict the experimental data, by more than half. The over prediction at 3 μm could be attributed to the flow not being fully developed yet, however this then does not explain the under prediction at the 10 μm particle size.

Figure 8.10 provides the deposition efficiency verses particle diameter for Dr. Oldham's experimental data and the various CFD software packages at the 1.5 lpm flow rate

for uniform flow for both isolated impaction and combined impaction and sedimentation. The addition of sedimentation has much less affect in both software packages for the uniform velocity profile compared to the parabolic velocity profile discussed previously. In fact, CFX is not even showing a noticeable increase in deposition efficiency due to the addition of sedimentation. Fluent DPM is only showing a noticeable increase in deposition efficiency at the 10 μm particle size. At the 10 μm particle size, theoretically there should be a 3.5% increase in deposition efficiency; Fluent DPM is only predicting a 1% increase.

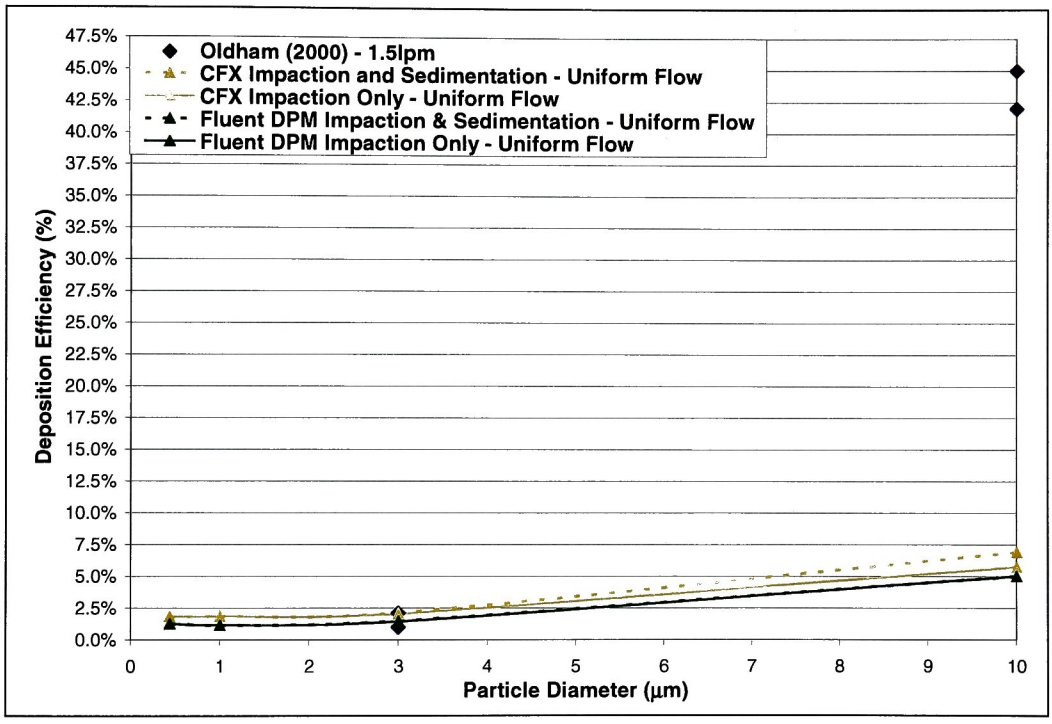


**Figure 8.10 Comparison of CFD and experimental data for combined impaction and sedimentation in the three generation lung geometry for uniform flow at the 1.5 lpm flow rate.**

When comparing to Dr. Oldham's experimental data both CFD software packages align better at the 3 μm particle size than the 10 μm particle size. Based on the CFD predictions at the 3 μm particle size it would appear the flow is uniform in the experimental runs. However, when examining the 10 μm particle size it appears the flow is developed. It is known that the uniform flow condition is an unrealistic representation of the physical flow in the three generation lung geometry at the 1.5 lpm flow rate. Researching the developing

velocity profile could improve correlation between CFD predictions and Dr. Oldham's experimental data.

### 8.4.3.2 Combined Impaction and Sedimentation at 7.5 Liter/Min Flow Rate

Figure 8.11 provides the deposition efficiency verses particle diameter for Dr. Oldham's experimental data and the various CFD software packages at the 7.5 lpm flow rate for parabolic flow for both isolated impaction and combined impaction and sedimentation. For CFX, there is less than a 1% increase in the deposition efficiency with the addition of sedimentation at all particle sizes. This agrees well with the theoretical calculation for sedimentation at the 7.5 lpm flow rate in Table 8.15. Fluent DPM has less than 1% increase in the deposition efficiency at all particle sizes except 10 μm. At the 10 μm particle size, Fluent DPM's deposition efficiency increases by 5%; more than five times what is theoretically expected. Given the ε values present in the three generation geometry at both flow rates, it is not surprising Fluent DPM is over predicting theoretical predictions, based on the data for the straight tube in Chapter 5.

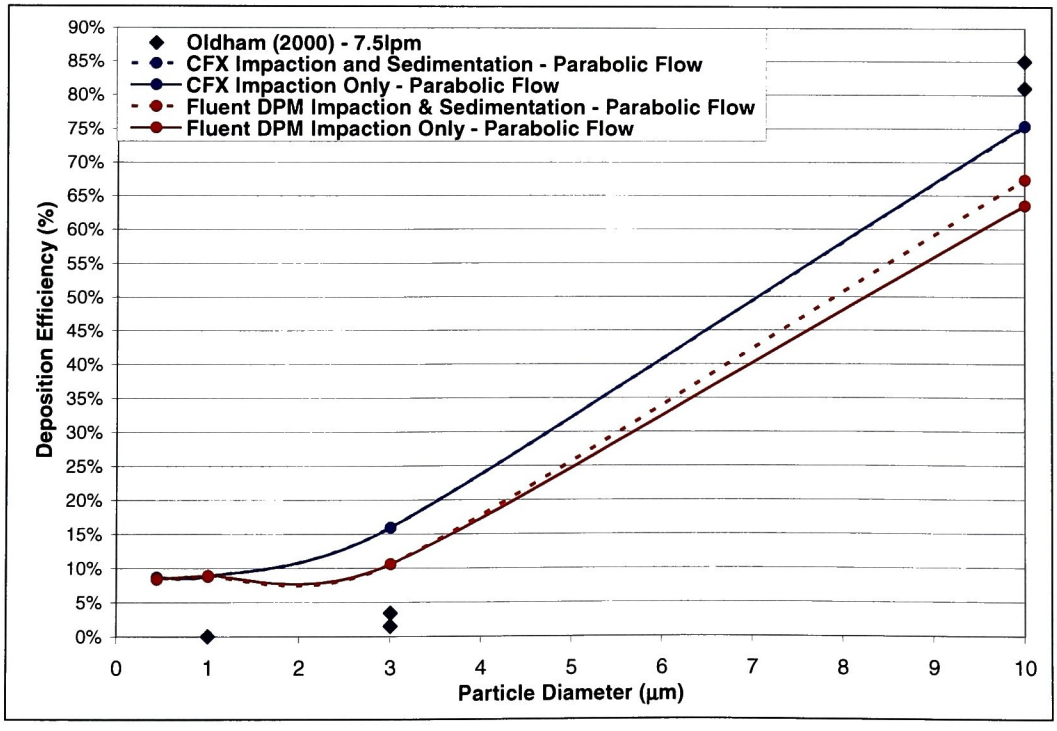


**Figure 8.11 Comparison of CFD and experimental data for combined impaction and sedimentation in the three generation lung geometry for parabolic flow at the 7.5 lpm flow rate.**

When comparing to the experimental data, both Fluent DPM and CFX have better agreement at the 10 μm particle size for parabolic flow conditions. CFX is only 5% less than the experimental data at the 10 μm particle size, but at least 13% higher at the 3 μm particle size. Fluent DPM is roughly 13% less than the experimental data at the 10 μm particle size and at least 7% higher at the 3 μm particle size.

Figure 8.12 provides the deposition efficiency verses particle diameter for Dr. Oldham's experimental data and the various CFD software packages at the 7.5 lpm flow rate for parabolic flow for both isolated impaction and combined impaction and sedimentation. Both CFX and Fluent DPM are seeing minimal increase in deposition efficiency at all particle sizes. Fluent DPM has the greatest increase at the 10 μm particle size, where sedimentation adds less than 1% to the total deposition efficiency. The increases due to sedimentation agree well with theoretical predictions at the 7.5 lpm flow rate for the three generation geometry.

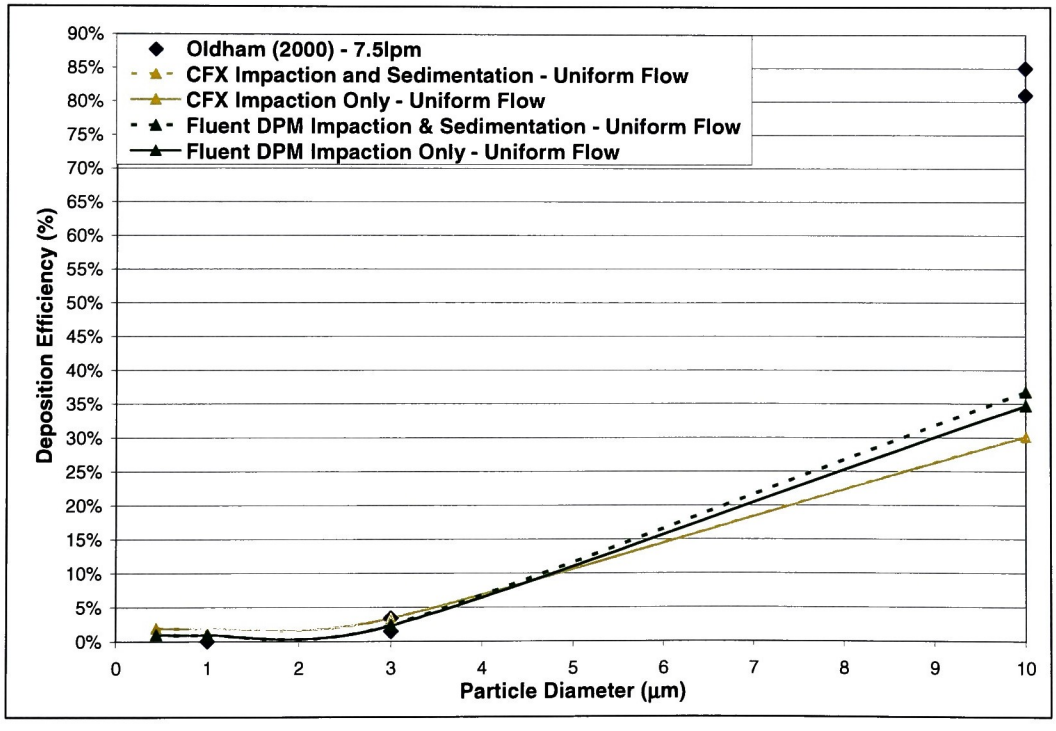


**Figure 8.12 Comparison of CFD and experimental data for combined impaction and sedimentation in the three generation lung geometry for uniform flow at the 7.5 lpm flow rate.**

When comparing to the experimental data, both Fluent DPM and CFX have better agreement at the 3 μm particle size. CFD predictions are less than half of the experimental deposition at the 10 μm particle size. There is once again not a single velocity profile which accurately predicts the experimental data at all flow conditions.

#### 8.4.3.3 Summary of Combined Impaction and Sedimentation in the Three Generation Lung Geometry

At both the 1.5 lpm and 7.5 lpm flow rates combined impaction and sedimentation predictions from CFD have better agreement with experimental data for the uniform velocity profile at the 3 μm particle size, compared to parabolic flow and isolated impaction. However, at the 10 μm particle size the parabolic velocity profile prediction agree better with experimental data, compared to the uniform velocity profile. Given this fact it is difficult to know which velocity profile truly represents what is occurring in the experimental runs. Although, developing flow profiles in CFD suggest uniform flow is not an accurate representation of the experimental flow conditions. It does not make sense that one profile can have good agreement at one particle size and terrible at another particle size.

CFX's predictions for the addition of sedimentation agree better with theoretical predictions compared to Fluent DPM. Fluent DPM predicts significantly more deposition by sedimentation then theoretically predicted at all particle sizes. Given the ε values present in the three generation geometry at both flow rates, it is not surprising Fluent DPM is over predicting theoretical predictions, based on the data for the straight tube in Chapter 5. However at the small ε values present in the three generation lung geometry CFX was actually over estimating the theoretical predicting by more in the straight tube.

### 8.4.4 Summary of Total Deposition in the Three Generation Lung Geometry

Analytical equations and CFD predictions from Fluent FPM accurately predict the relative affect of the diffusion deposition mechanism at all particles sizes. Discrepancies between CFD and theoretical predictions in straight tube and three generation lung geometry are similar for the diffusion deposition mechanism. Based on this information, simple straight

tube geometry results can be used to ascertain the uncertainty in CFD predictions for more complicated geometries.

The uniform velocity profile is not an accurate representation of the physical flow conditions present in the experiments. Velocity profiles from Fluent FPM show that even a uniform velocity profile allowed to develop, will began taking on a parabolic profile before the first bifurcation (See Appendix D). As a result the conclusions for the impaction and combined impaction and sedimentation deposition mechanism are only presented in these conclusions.

CFD and analytical predictions more accurately predict the experimental data at the 7.5 lpm flow rate. For 10 μm particles at the 1.5 lpm flow rate, only no more than 89% of the deposition is theoretically accounted for. At the 3 μm particle size, as little as 11% of the experimental deposition can be accounted for theoretically. At the 7.5 lpm flow rate Zhang, et al. (1997) provides the theoretical prediction which has the best agreement with the experimental data.

CFD predictions for isolated impaction for both software packages over predict the experimental deposition at the 1 μm and 3 μm particle sizes for both the 1.5 lpm and 7.5 lpm flow rates. At the 10 μm particle size, both Fluent DPM and CFX under predict Dr. Oldham's experimental data by 50% for parabolic flow conditions at the 1.5 lpm flow rate. At the 7.5 lpm flow rate, CFX predicts deposition by isolated impaction within 5% of the experimental data, which is excellent since impaction is isolated for this particle size and flow rate.

Discrepancies between CFD and theoretical predictions in straight tube and three generation lung geometry are similar for the sedimentation deposition mechanism. Based on this information, simple straight tube geometry results can be used to ascertain the uncertainty in CFD predictions for more complicated geometries. At the 1.5 lpm flow rate, both CFD software packages predict sedimentation to be the dominate deposition mechanism, which does not agree with theoretical predictions. At the 7.5 lpm flow rate the CFD predictions for sedimentation agree well with theoretical predictions. Fluent DPM is still over predicting theoretical predictions as was seen in the straight tube and single bifurcation geometries. There is minimal increase in CFX's predictions with the addition of sedimentation.

Combined impaction and sedimentation in CFX at the 7.5 lpm flow rate is able to accurately predict experimental date at the 10 μm particles. Currently accurate predictions of the other experimental data points have not been obtain by either CFD software package. Developing flow conditions could help to improve correlation with experimental data. If impaction predictions in CFX and Fluent DPM were not significantly over predicting experimental data at the 1 μm and 3 μm particle sizes the combined deposition efficiency could be determined by adding the most accurate predictions for each deposition mechanism outside of CFD to obtain total deposition.

## 8.5 Comparison of CFD Result and Experimental Data for Local Deposition in the Three Generation Lung Geometry

Local deposition in the three generation lung geometry was examined for the experimental data gathered by Dr. Oldham and CFD data. The shading scheme used to analysis the local deposition was the same for the experimental and CFD data and is provided in Figure 8.13. The deposition efficiencies are based on the percentage of total particles deposited not the total number of particles injected for reference.

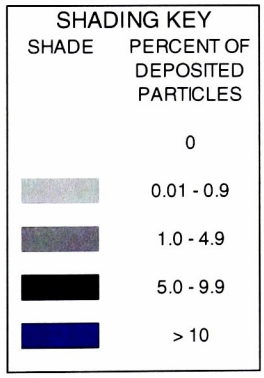


**Figure 8.13 Shading scheme used to examine local deposition for the experimental and local deposition in the 3 generation geometry.**

Experimental local deposition was obtained by Dr. Oldham at the University of California Irvine for 1 μm, 3μm, and 10μm particle sizes at the 7.5lpm flow rate and 3 μm and 10 μm particle sizes at the 1.5lpm flow rate. CFD data was obtained for Fluent DPM for the parabolic velocity profile for deposition by combined impaction and sedimentation. Data

has been gathered, but not processed for uniform flow conditions for deposition by combined impaction and sedimentation data in Fluent DPM.

Additionally, research has been done into how to obtain local deposition data from CFX. Rochester Institute of Technology has been working with CFX to develop and implement an external script that is played in CFX. This script will report the end position and velocity of particles intercepting a defined boundary to a text file. At this point no data has been obtained, due to computer limitations. ANSYS estimates that the computers being utilized at Rochester Institute of Technology only have enough memory to process the end locations for 2,000 to 4,000 particles, since they have been able to track 10,000 particles on their machines, which have 3GB of RAM. The computers being utilized at Rochester Institute of Technology have 1.25 GB and depending on how this memory is allocated will affect the maximum number of end locations that can be processed before all the memory has been used. Unfortunately, when reducing the number of particles injected into the three generation lung geometry from 50,000 to 2,000 the total deposition efficiencies changes by 4% to 9%, see Table 8.18. Due to these large discrepancies in deposition efficiencies, the script has not run to test local deposition capabilities for 2,000 particles at Rochester Institute of Technology. Therefore, it has not yet been determine if the machines currently being utilized Rochester Institute of Technology can in fact track 1000 to 2000 particles end locations in CFX without locking or crashing the computers. Additionally, it is not know what the minimum number of particles required to stabilize the deposition efficiency in CFX is for the three generation lung geometry. Dr. Robinson conducted a study in Fluent DPM, which determine 50,000 particles were required in the three generation lung geometry to stabilize the deposition efficiency (Robinson, et al., 2005). This value is utilized for all geometries and software packages in this research after personal correspondence with Chimera Technologies Inc. and ANSYS confirmed that 50,000 particles would be more than sufficient to stabilize the deposition efficiency in Fluent FPM and CFX, respectively.

**Table 8.18 Change in deposition efficiency for combined impaction and sedimentation from parabolic flow in CFX when going from 50,000 to 2,000 particles.**

| Flow Rate (Liter/Min) | Particle Size (μm) | Deposition Efficiency for 50,000 Particles | Deposition Efficiency for 2,000 Particles |
|---|---|---|---|
| 1.5 | 3 | 11.11% | 4.50% |
| 1.5 | 10 | 19.36% | 15.19% |

| | | | |
|---|---|---|---|
| 7.5 | 1 | 8.80% | 0% |
| 7.5 | 3 | 10.58% | 14.89% |
| 7.5 | 10 | 67.39% | 74.45% |

### 8.5.1 Local Deposition for 10 μm Particles at Each Flow Rate Investigated

Local deposition was obtained for both the 7.5 lpm and 1.5 lpm flow rates for the 10 μm particles size. Two runs of experimental data were gathered for each flow rate. CFD data is obtained from Fluent DPM for the parabolic velocity profile for deposition by combined impaction and sedimentation for each flow rate.

Local deposition in the three generation lung geometry obtained from experimental data for 10 μm particles at the 7.5 lpm flow rate is displayed in Figure 8.14. Local deposition obtained from Fluent DPM for 10 μm particles at the 7.5 lpm flow rate with a parabolic velocity profile is displayed in Figure 8.15. Additionally, Figure 8.16 shows where each particle deposits for the Fluent DPM data. As can be seen when comparing Figure 8.14 and Figure 8.15 the deposition patterns are fairly similar, both have the maximum deposition at the first bifurcation and another area of elevated deposition at the bifurcations between generation four and five.

The data obtained from Fluent DPM has slightly higher deposition at the bifurcation between generation three and four. Additionally, the Fluent DPM data indicates a substantial amount of deposition near the inlet to generation three that is not seen in either of the experimental casts. This increased deposition in generation three is likely due to the flow being fully developed and therefore have a very low velocity near the wall and much faster velocity in the center. The slow moving air near the wall is going to allow the particles injected on the lower half of the geometry and near the walls to settle out quickly, resulting in this increased deposition by sedimentation. In future work, comparing the top and bottom deposition with the experimental measurements will help to determine if this deposition is solely a result of sedimentation. In the experimental data, if the flow was still developing or had been tripped at the connector it could explain why there is less deposition in generation three in the experimental local deposition data than Fluent DPM's parabolic prediction.

Local deposition in the three generation lung geometry obtained from experimental data for 10 μm particles at the 1.5 lpm flow rate is shown in Figure 8.17. Local deposition obtained from Fluent DPM for 10 μm particles at the 1.5 lpm flow rate for the parabolic velocity profile is shown in Figure 8.18. Additionally, a plot of where each particle deposited for the Fluent DPM data is shown in Figure 8.19.

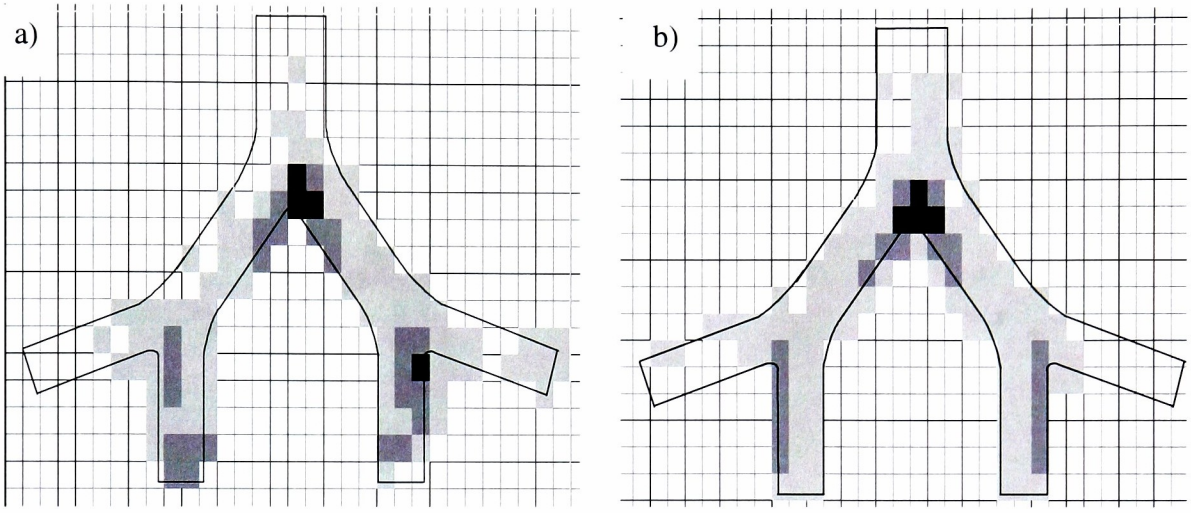


**Figure 8.14 Local deposition for 10 μm particles in 7.5 lpm flow obtained from experimental data in the 3 generation geometry a) 1st cast (4614 particles deposited) b) 2nd cast (2316 particles deposited). Each rectangle is 2.05 mm x 1.4 mm. The shading scheme is shown in Figure 8.13.**

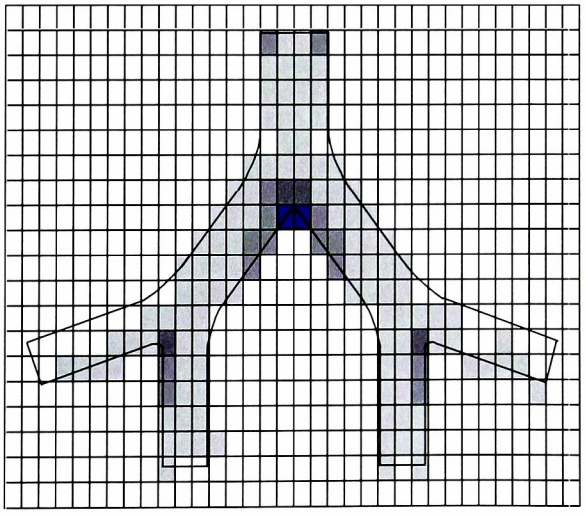

**Figure 8.15 Local deposition for 10 μm particles in 7.5 lpm parabolic flow obtained from Fluent DPM in the 3 generation geometry (33,696 particles deposited). Each rectangle is 2.05 mm x 1.4 mm. The shading scheme is shown in Figure 8.13.**

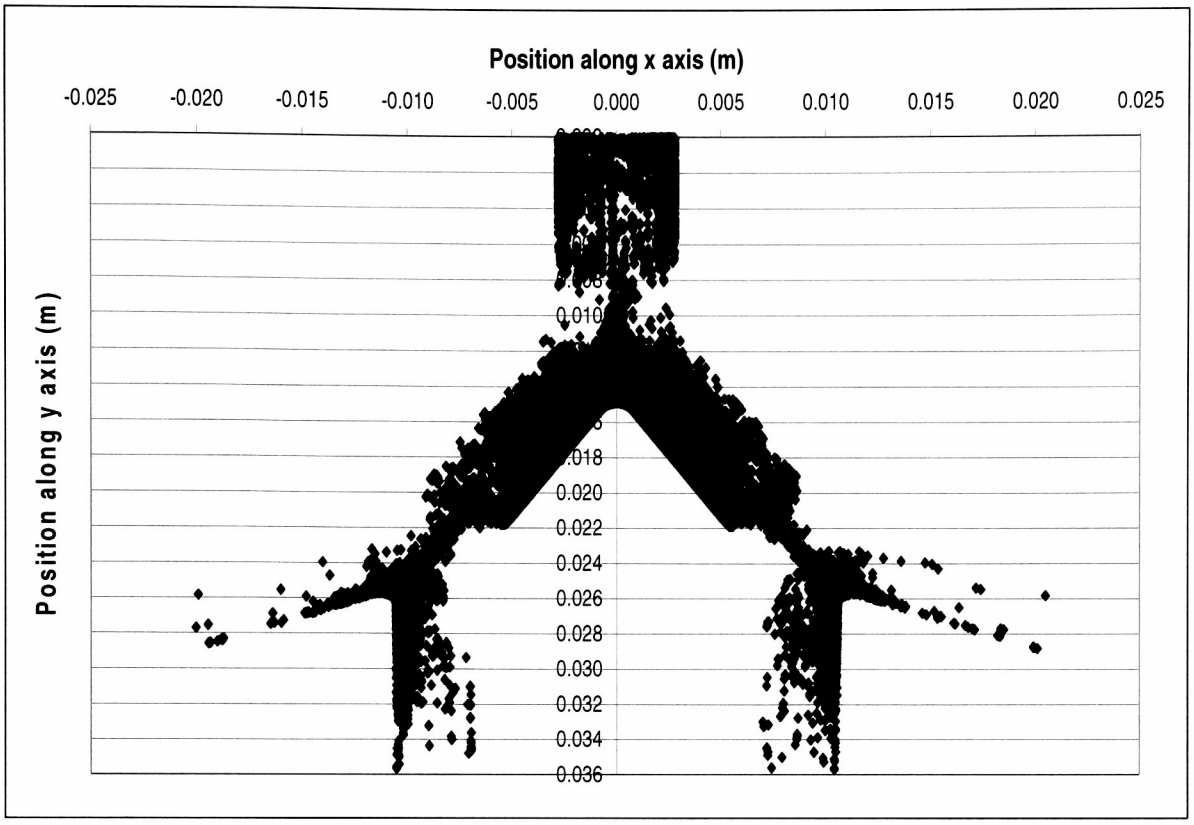


**Figure 8.16 Plot of each particles deposition for 10 μm particles in 7.5 lpm parabolic flow obtained from Fluent DPM in the 3 generation geometry (33,696 particles deposited).**

When comparing experimental deposition for the 7.5 lpm and 1.5lpm flow rates both have maximum deposition at the bifurcation between generations three and four with another "hot spot" at the bifurcation between generations four and five. The 7.5 lpm flow conditions have more deposition in generation three, while the 1.5 lpm flow conditions have more deposition in generations four and five. This is not quite what would be expected, since particles should settle from the slower moving fluid sooner. Additionally, the deposition efficiency at the bifurcation would be expected to be higher for the faster moving fluid since the particles should have more difficulty turning with the free stream, which is opposite of what was observed.

As far as the local deposition obtained from Fluent DPM, the results are noticeably different than the experimental data at the 1.5 lpm flow rate. The highest deposition efficiencies in Fluent DPM are near the inlet. The deposition at the bifurcation between generation three and four is only between 1% and 5% for Fluent DPM's local deposition prediction where it is between 5% and 9.9% and over 10% for the experimental data, for run

a and b respectively. Deposition in the generations four and five is not all that much different than what was seen in the experimental data.

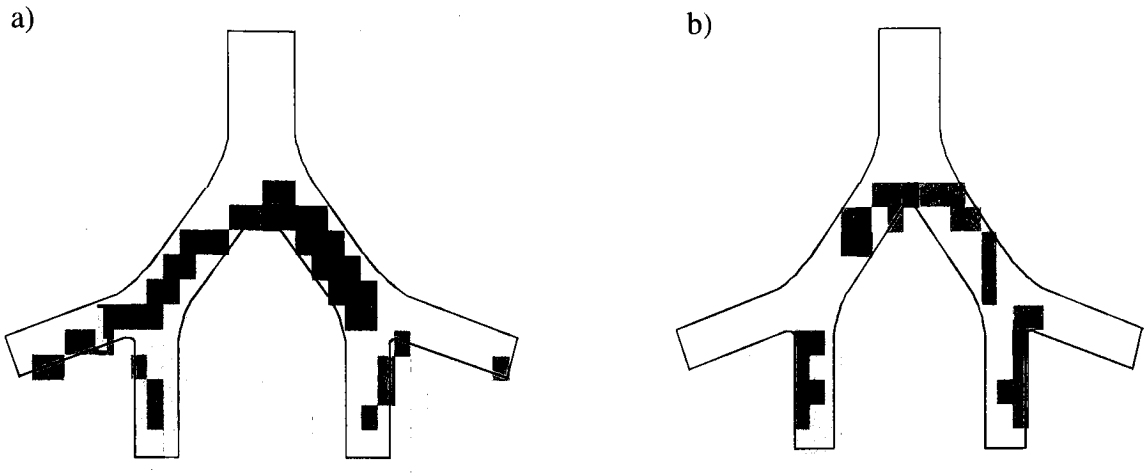


**Figure 8.17 Local deposition for 10 μm particles in 1.5 lpm flow obtained from experimental data in the 3 generation geometry a) 1st cast (1423 particles deposited) b) 2nd cast (1756 particles deposited). Each rectangle is 2.05 mm x 1.4 mm. The shading scheme is shown in Figure 8.13.**

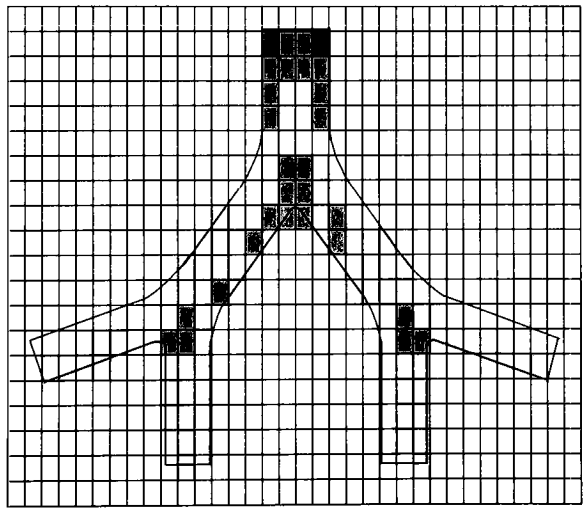

**Figure 8.18 Local deposition for 10 μm particles in 1.5 lpm parabolic flow obtained from Fluent DPM in the 3 generation geometry (9,681 particles deposited). Each rectangle is 2.05 mm x 1.4 mm. The shading scheme is shown in Figure 8.13.**

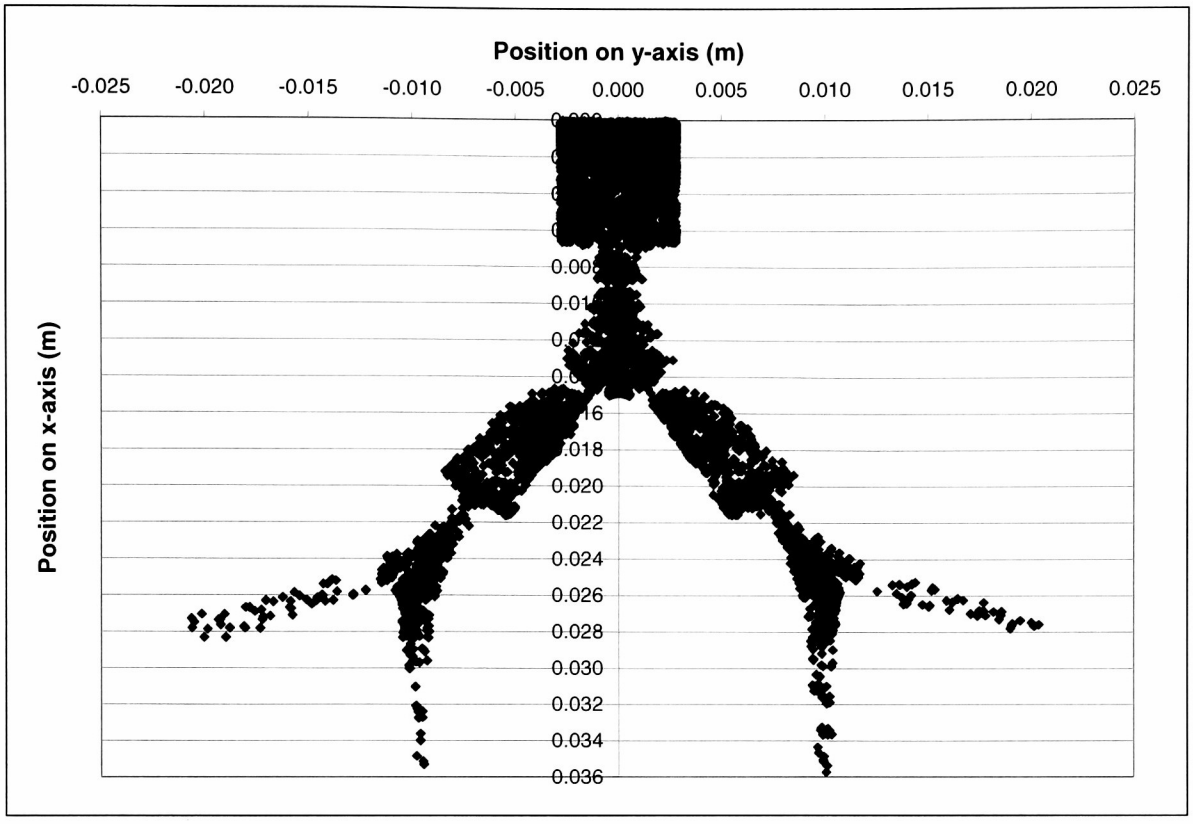


**Figure 8.19 Plot of each particles deposition for 10 μm particles in 1.5 lpm parabolic flow obtained from Fluent DPM in the 3 generation geometry (9,681 particles deposited).**

## 8.5.2 Local Deposition for 3 μm Particles at Each Flow Rate Investigated

Local deposition was obtained for both the 7.5 lpm and 1.5 lpm flow rates for the 3 μm particles size. Two runs of experimental data were gathered for each flow rate. CFD data is obtained from Fluent DPM for parabolic flow conditions with impaction and sedimentation for each flow rate.

Local deposition in the three generation lung geometry for 3 μm particles at the 7.5 lpm flow rate obtain from experimental data is displayed in Figure 8.20. Local deposition obtained from Fluent DPM for 3 μm particles at the 7.5 lpm flow rate with a parabolic velocity profile for deposition by combined impaction and sedimentation is displayed in Figure 8.21. Figure 8.22 provides a plot of where each particle deposited in the three generation lung geometry for the Fluent DPM data. It should be noted that there is significant variation in the number of particles which deposited in the two experimental casts. There are also substantial differences in where these particles deposited in the two

experimental casts and at what concentrations, see Figure 8.20. In the first experimental cast, the particles are concentrated in the bifurcations with smaller deposits in the generations. For the second experimental cast, the concentrations at the bifurcations are not as high as in the first cast and there is more deposition near the entrance and throughout each generation. It should be noted in the first cast 1.5% of the particles deposited while in the second cast 3.4% of the particles deposit. The second cast had twice the deposition seen in the first.

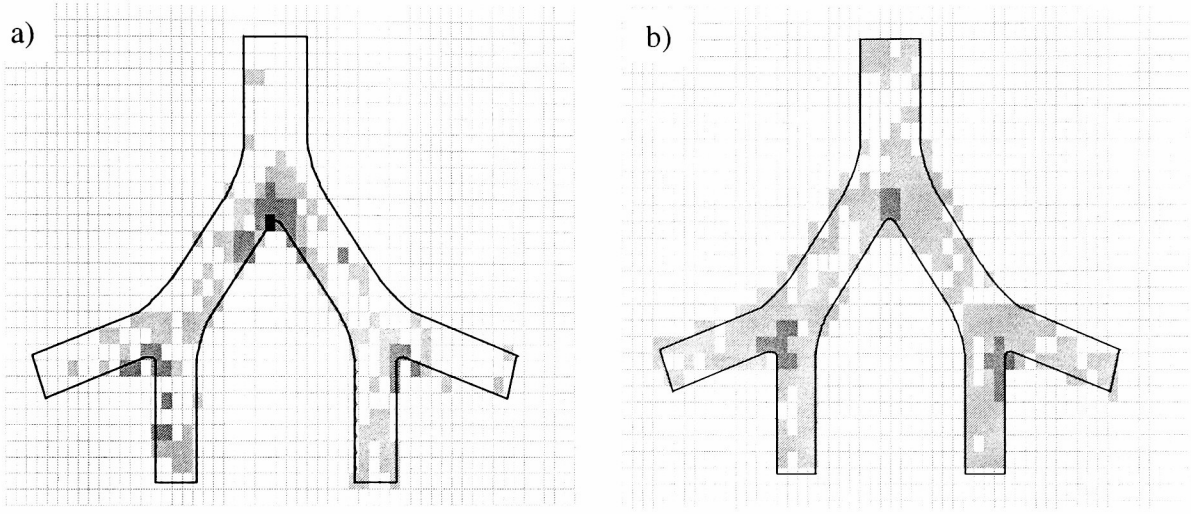


**Figure 8.20 Local deposition for 3 μm particles in 7.5 lpm flow obtained from experimental data in the 3 generation geometry a) 1st run (408 particles deposited) b) 2nd run (1,179 particles deposited). Each rectangle is 1.4 mm x 0.95 mm. The shading scheme is shown in Figure 8.13.**

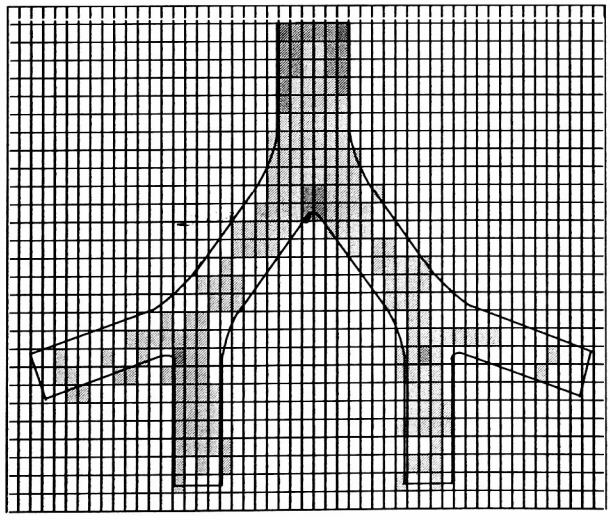

**Figure 8.21 Local deposition for 3 μm particles in 7.5 lpm parabolic flow obtained from Fluent DPM in the 3 generation geometry (5290 particles deposited). Each rectangle is 1.4 mm x 0.95 mm. The shading scheme is shown in Figure 8.13.**

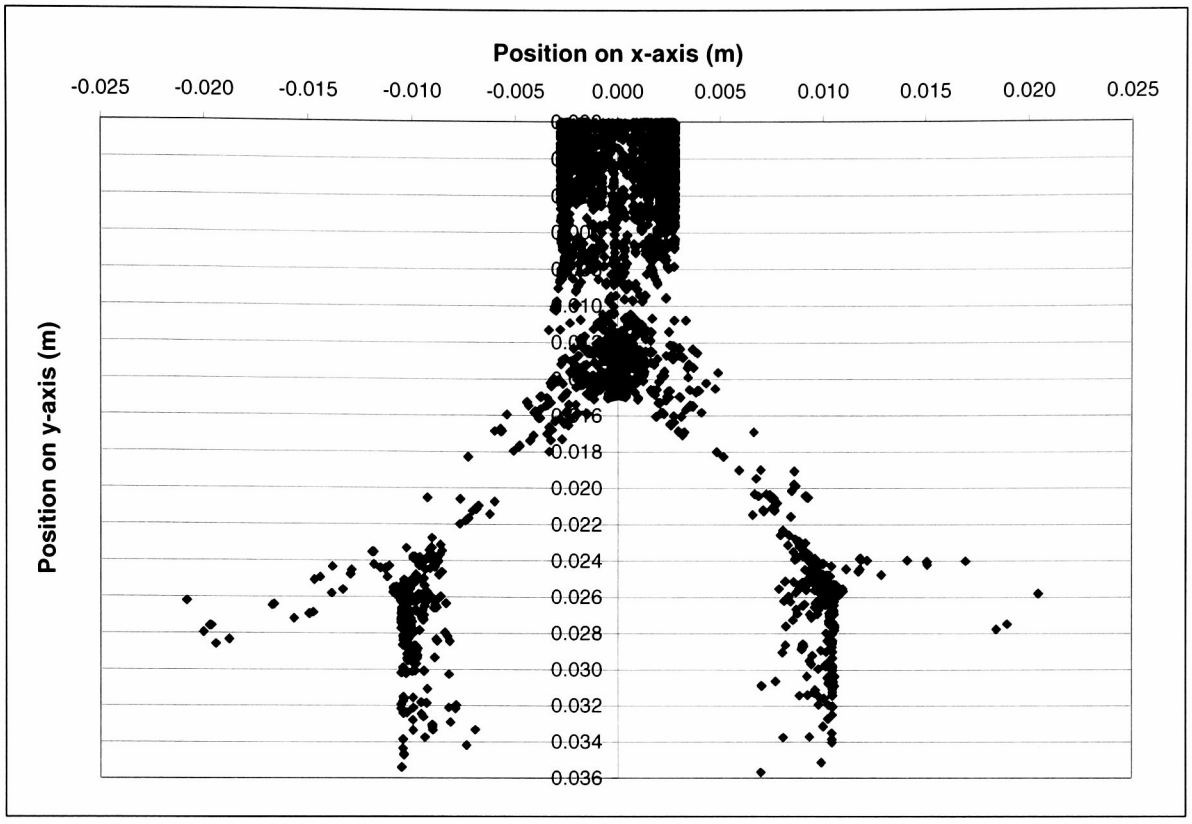


**Figure 8.22 Plot of each particles deposition for 3 μm particles in 7.5 lpm parabolic flow obtained from Fluent DPM in the 3 generation geometry (5290 particles deposited).**

When examining the local deposition from Fluent DPM it more closely resembles the results from the second experimental cast. There is higher deposition at the bifurcations than in the generations. However, the Fluent DPM data also has a significant number of particles depositing just after the inlet that is not seen to the same extent in either of the experimental run. As mentioned previously, this is due to the slower air velocities near the walls that allow the particles injected in the lower half of the bifurcation to settle quickly and deposit near the inlet. This could be checked by examining how the top and bottom percentages from Fluent DPM compare to data provided by Dr. Oldham. The two experimental casts were run simultaneously from opposite ends of a copper T. Given this set-up it is unclear why there is more deposition in one of the cast than the other.

Local deposition in the three generation lung geometry for 3 μm particles at the 1.5 lpm flow rate obtained from experimental data is displayed in Figure 8.23. Local deposition in the same three generation lung geometry obtained from Fluent DPM for 3 μm particles at the 1.5 lpm flow rate for a parabolic velocity profile is displayed in Figure 8.24. Figure 8.25

provides a plot of where each particle deposited in the three generation geometry for the Fluent DPM data for the 3 μm particle at the 1.5 lpm flow rate. It should be noted that there is again significant variation in the number of particles deposited in the two experimental casts, 1% verses 2.1%. There are also substantial differences in where particles deposited in the two experimental casts and at what concentrations, see Figure 8.23. In the first experimental cast, the deposition is concentrated around the bifurcations; there is some deposition in the generations, but most is near the bifurcations. In the second run, there is between 0.01% and 0.99% deposition throughout the entire three generation lung geometry.

The local deposition data obtained from Fluent DPM for 3 μm particles at the 1.5 lpm flow rates has the highest deposition near the inlet, which would be characteristic of fully developed parabolic flow. There are also slightly higher concentrations of particles at the bifurcations. Aside from this particles seem to depositing along the center of the generations. The local deposition is in the range of what was observed by Dr. Oldham in the experimental data.

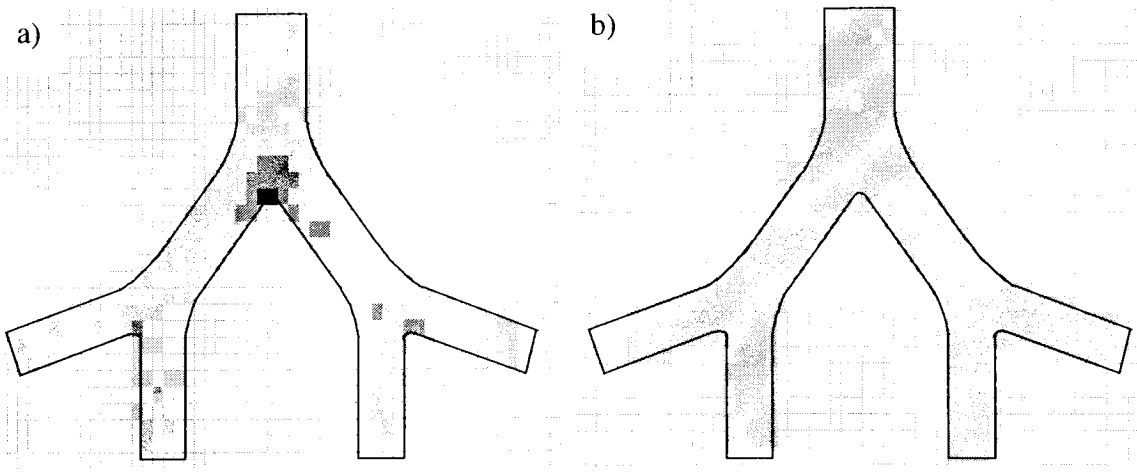


**Figure 8.23 Local deposition for 3 μm particles in 1.5 lpm flow obtained from experimental data in the 3 generation geometry a) 1st cast (678 particles deposited) b) 2nd cast (3,520 particles deposited). Each rectangle is 1.4 mm x 0.95 mm. The shading scheme is shown in Figure 8.13.**

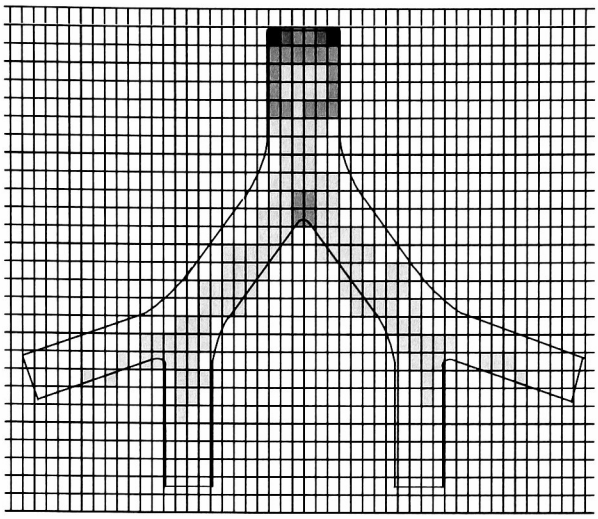

**Figure 8.24 Local deposition for 3 μm particles in 1.5 lpm parabolic flow obtained from Fluent DPM in the 3 generation geometry (5554 particles deposited). Each rectangle is 1.4 mm x 0.95 mm. The shading scheme is shown in Figure 8.1.**

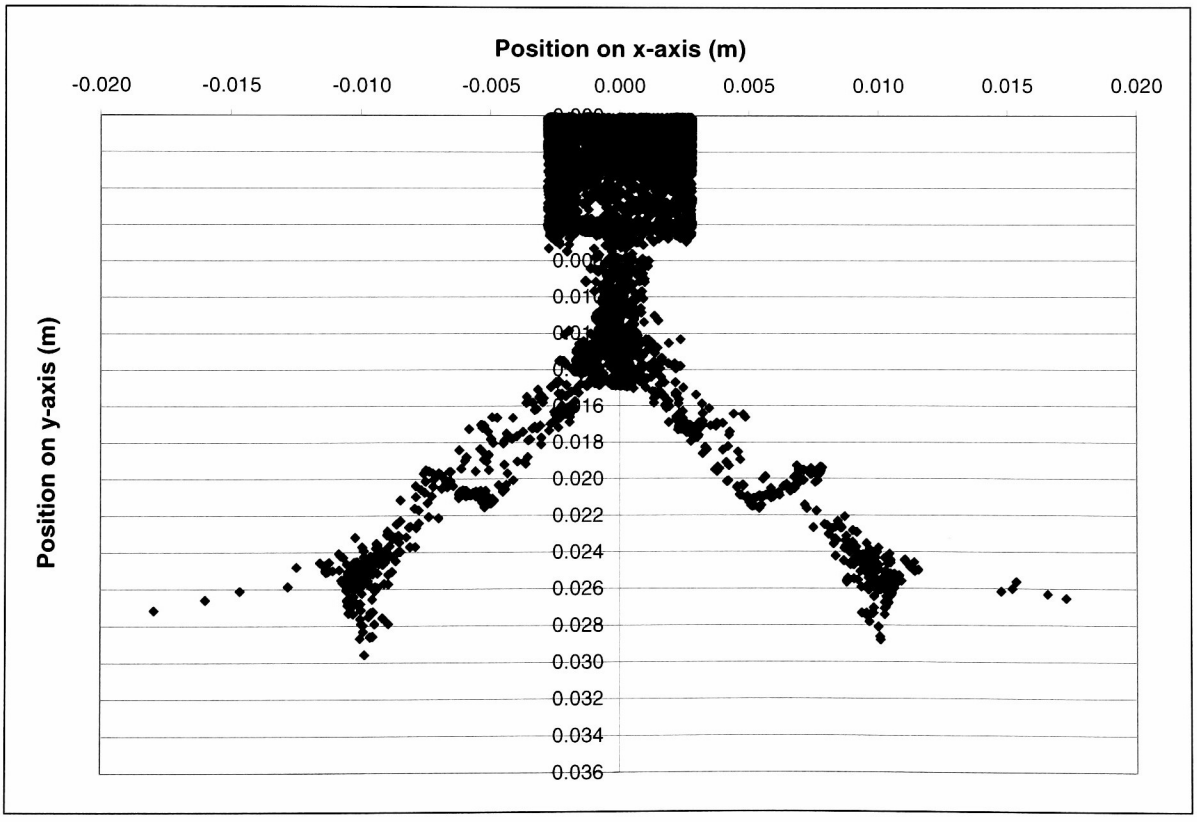


**Figure 8.25 Plot of each particles deposition for 3 μm particles in 1.5 lpm parabolic flow obtained from Fluent DPM in the 3 generation geometry (5554 particles deposited).**

### 8.5.3 Local Deposition for 1 μm Particles at 7.5 Liter/Min Flow Rate

Local deposition was obtained for the 7.5 lpm flow rates for the 1 μm particles size. One run of experimental data were gathered for the 7.5 lpm flow rate. CFD data was obtained from Fluent DPM for the parabolic velocity profile with deposition by combined impaction and sedimentation at the 7.5 lpm flow rate.

Local deposition in the three generation lung geometry obtained from experimental data for the 1 μm particles at the 7.5 lpm flow is displayed in Figure 8.26. Local deposition in the same three generation lung geometry obtained from Fluent DPM for the 1 μm particles at the 7.5 lpm flow is shown in Figure 8.27. The locations of where each particle deposits in the three generation lung geometry for the Fluent DPM data for 1 μm particles at the 7.5 lpm flow rate can be seen in Figure 8.28. For the experimental data, the maximum deposition occurs at the bifurcation between generation three and four, see Figure 8.26. There is deposition of less than 1.0% throughout most of the three generation lung geometry for the 1 μm particles.

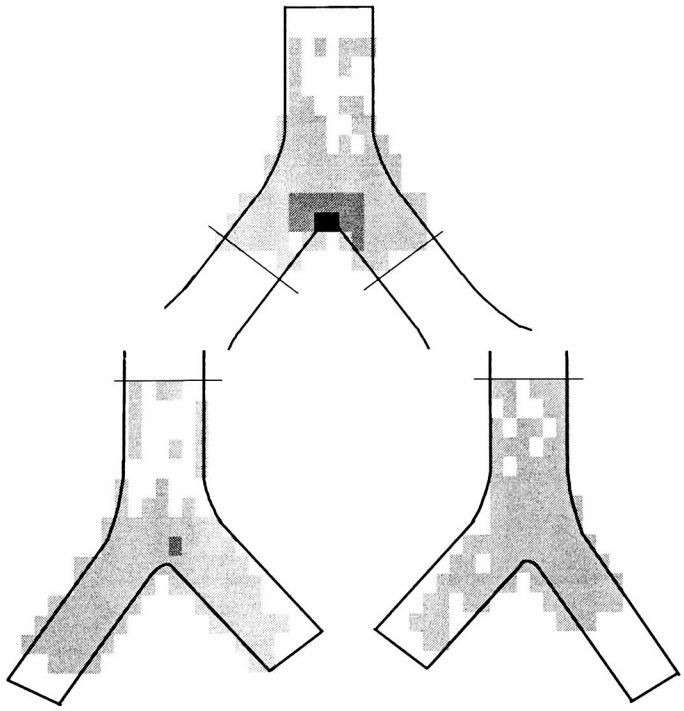

**Figure 8.26 Local deposition for 1 μm particles in 7.5 lpm flow obtained from experimental data in the 3 generation geometry. Each rectangle is 1.4 mm x 0.95 mm. The shading scheme is shown in Figure 8.13.**

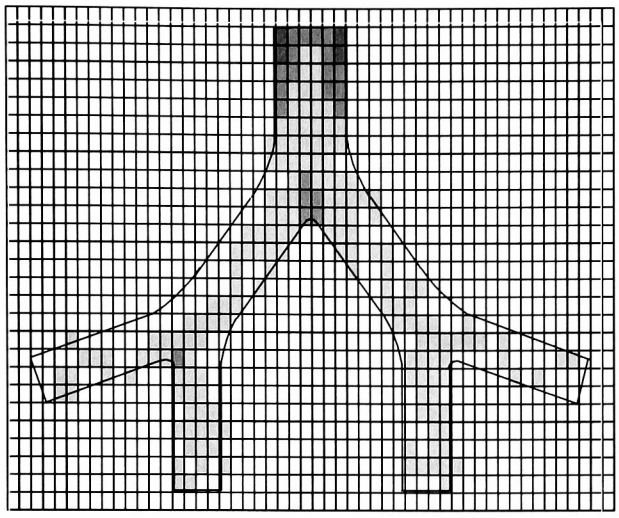

**Figure 8.27 Local deposition for 1 μm particles in 7.5 lpm parabolic flow obtained from Fluent DPM in the 3 generation geometry (4401 particles deposited). Each rectangle is 1.4 mm x 0.95 mm. The shading scheme is shown in Figure 8.13.**

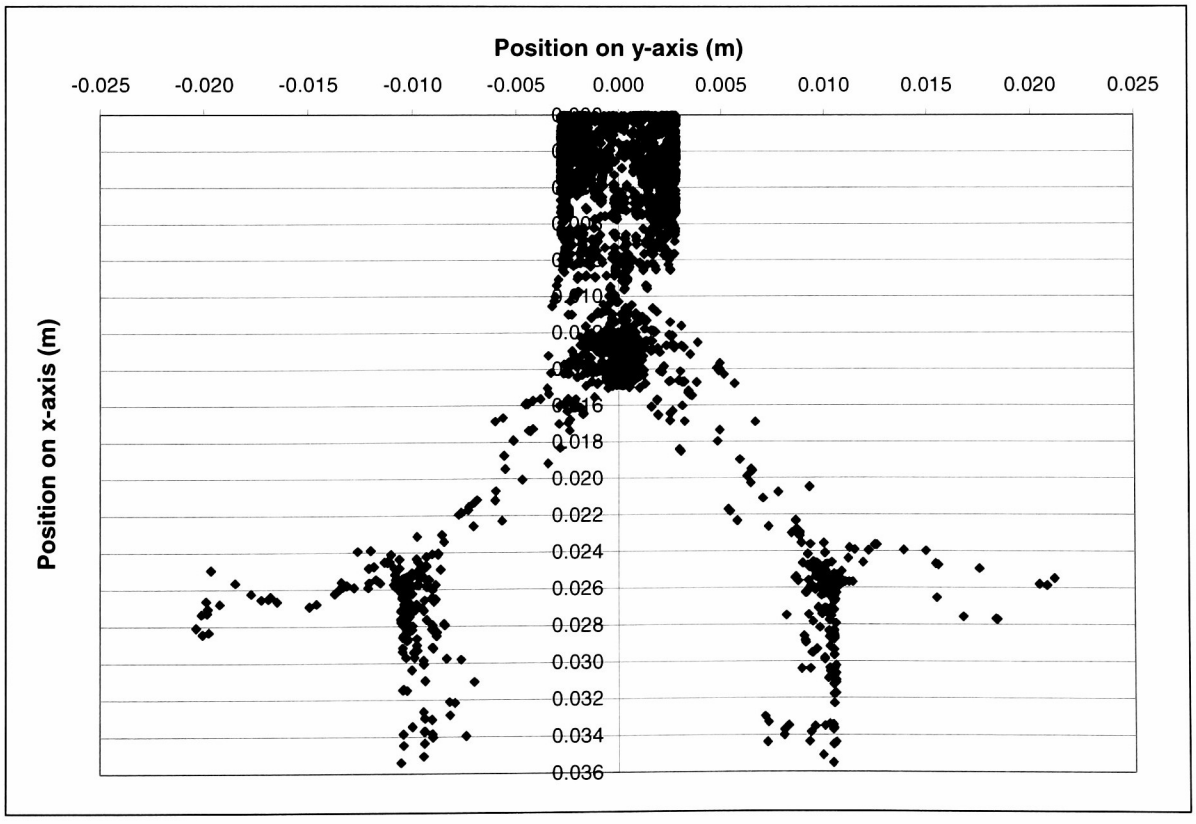


**Figure 8.28 Plot of each particles deposition for 1 μm particles in 7.5 lpm parabolic flow obtained from Fluent DPM in the 3 generation geometry (4401 particles deposited).**

The results from Fluent DPM are slightly different. There is more deposition at higher rates in generation three, again likely due to the parabolic flow conditions that have been described previously. Additionally, there is less deposition at the bifurcation between generation three and four, between 5.0% and 9.0% for experimental and 1.0% to 4.9% for Fluent DPM. The Fluent DPM local deposition also has less deposition throughout the generations than the experimental data.

### 8.5.4 Summary of Local Deposition in the Three Generation Lung Geometry

In all cases, Fluent DPM predicts higher deposition at the inlet for each particle size and flow rate investigated. As discussed throughout Section 8.5, the higher deposition the Fluent DPM local deposition predictions is likely due to particles injected near the wall in the lower half of the bifurcation settling out quickly due to the slower air velocity near the walls in fully developed flow. Knowing this it is possible that the experimental flow conditions were either still developing or could have been tripped by the connector at the entrance. This could be investigated by examining the deposition on the top and bottom half in Fluent DPM and comparing results to experimental data provide by Dr. Oldham.

For the 10 μm particle size, the experimental casts provide similar deposition patterns at both flow rates. The highest deposition occurs at the bifurcations, indicating impaction is the dominate deposition mechanism. The Fluent DPM prediction for local deposition also has elevated deposition at the bifurcation, but the highest deposition is at the inlet, likely due to the parabolic flow case being investigated.

The experimental data obtained for the 3 μm particle size varies greatly from one run to the other at both flow rates. The deposition efficiencies in the three generation lung geometry vary by 1.1% at the 1.5 lpm flow rate and 1.9% at the 7.5lpm flow rate. This is significant variation since the deposition efficiencies at the 3 μm particle size is less than 5% at both flow rates. In one cast deposition is higher at the bifurcations, while in the other cast there is just a constant level of deposition throughout the geometry. It is difficult to determine what the dominate mechanism is with the large variation in experimental data. The prediction for Fluent DPM is within the range of the experimental data, but additional

experimental runs would be helpful to better characterize the deposition and flow characteristics at the 3 μm particle size.

There is not good agreement at the 1 μm particle size between the experimental data and Fluent DPM's prediction. However, with only one experimental data point it is difficult to conclude what is actually happening given the large variation seen in the 3 μm particle size experimental runs.

The local deposition is a valuable tool and can help to explain some of the variation seen in the total deposition data in Section 8.4. However, the current process of obtaining local deposition in both CFD and physical experiments is very time consuming and tedious for the amount of information obtained from each test.

## 8.6 Summary

A summary of the numerical, analytical, and experimental deposition efficiencies in the three generation lung geometry are provided in Table 8.19. During this research it has been determined that analytical equations are a good predictor of the relative affect of each deposition mechanism in a multi-generation geometry as well as the simple geometries they were originally derived for. The analytical equations do not exactly predict deposition, but they do provide a good range to work with. There is still a lot of variation in the predictions generated by the impaction equations and further investigation at the experimental, analytical, and numerical could help to improve these analytical equations.

The diffusion deposition mechanism had little effect on the total deposition efficiency in the three generation lung geometry for the particle sizes and flow conditions investigated. The CFD predictions from Fluent FPM exhibit similar trends to what was observed in the straight tube geometry in Chapter 6. It would be useful to have straight tube data for the $\Delta$ values present in the three generation geometry at the 1.5 lpm flow rate, to confirm that Fluent FPM has the same accuracy for the straight tube geometry and more complicated geometries like the three generation lung model. However, theses $\Delta$ values are small and should predict very small deposition by diffusion. They also typically correspond to particle sizes outside the diffusion range for most flow rates and are therefore not really necessary.

Impaction is the dominate mechanism in the three generation lung geometry for the particle sizes and flow conditions investigated in this research. There is still substantial

variation in the impaction predictions from the CFD software packages and the analytical equations. This variation and the dominance of impaction could account for the poor overall agreement between CFD predictions and experimental data. At the 7.5 lpm flow rate, trends in the CFD software packages' and analytical equations' predictions are similar to those seen in the single bifurcation geometry for Stokes numbers within the same range. The Stokes numbers that are present in the three generation geometry at the 1.5 lpm flow are significantly lower than those investigated in the single bifurcation. The CFD software packages' and analytical equations' predictions did not agree well with trends from the single bifurcation at small Stokes numbers. There is a need for more studies that analyze the impaction deposition mechanism analytically, numerically, and experimentally at all Stokes numbers, in order to begin improving correlation and understanding. Especially since impaction is the dominate deposition mechanism within the tracheobroncial region of the lung.

Sedimentation is having the largest affect on total deposition at the 1.5 lpm flow rate, which agrees with theoretical predictions. The addition of sedimentation increases the deposition efficiency significantly more in Fluent DPM than CFX, particularly at the 7.5 lpm flow rate where CFX sees no noticeable change by the addition of sedimentation. Sedimentation increases deposition more at the 1.5 lpm flow rate compared to the 7.5 lpm flow rate, which is expected since lower flow rates allow more time for the particles to settle.

Local deposition data helped to confirm the dominance of the deposition mechanism, particular at the 10 μm particle size, where the majority of the deposition occurs at the bifurcation. Future work should include a comparison with the top and bottom deposition pattern to investigate sedimentation deposition mechanism. Local deposition also provided insight into some reasons why CFD and analytical equations may be experiencing difficulty correlating with experimental data. There is a large variation in local deposition patterns at the 3 μm particle size. The local deposition data indicated that the flow in the experimental runs was not yet fully developed, as expected by the experimental set up. More local deposition studies will significantly improve the understanding of deposition in multi-generation geometries despite their substantial time investment.

**Table 8.19 Summary of deposition efficiencies observed in the three generation lung geometry for each flow condition and particle size.**

| Flow Rate (lpm) | Velocity Profile | Particle Size (μm) | Diffusion | | | Impaction | | | | | | | Sedimentation | | Combined Impact & Sed | | Exp. Data |
|---|---|---|---|---|---|---|---|---|---|---|---|---|---|---|---|---|---|
| | | | Fluent FPM | Ingham Par. | Ingham Uni. | Fluent DPM | CFX | Yeh & Schum | Cai & Yu Par. | Cai & Yu Uni. | Zhang, et al. Par. | Zhang, et al. Uni. | Pich Par. | Yu, et al. Uni. | Fluent DPM | CFX | |
| 1.5 | Parabolic | 0.44 | N/A | 0.029% | N/A | 10.29% | 4.35% | 0.01% | 0.03% | N/A | 0.29% | N/A | 0.01% | N/A | 10.30% | 4.34% | N/A |
| 1.5 | Parabolic | 1 | N/A | 0.015% | N/A | 10.36% | 4.28% | 0.05% | 0.12% | N/A | 0.30% | N/A | 0.04% | N/A | 10.36% | 4.26% | N/A |
| 1.5 | Parabolic | 3 | N/A | 0.007% | N/A | 11.17% | 4.41% | 0.55% | 1.02% | N/A | 0.42% | N/A | 0.35% | N/A | 11.11% | 4.29% | 1%, 2.1% |
| 1.5 | Parabolic | 10 | N/A | 0.003% | N/A | 20.08% | 10.18% | 4.73% | 10.66% | N/A | 7.16% | N/A | 3.69% | N/A | 19.36% | 16.64% | 45%, 42% |
| 1.5 | Uniform | 0.44 | N/A | N/A | 0.316% | 1.25% | 1.83% | 0.01% | N/A | 0.02% | N/A | 0.19% | N/A | 0.01% | 1.27% | 1.82% | N/A |
| 1.5 | Uniform | 1 | N/A | N/A | 0.193% | 1.16% | 1.85% | 0.05% | N/A | 0.07% | N/A | 0.20% | N/A | 0.04% | 1.16% | 1.85% | N/A |
| 1.5 | Uniform | 3 | N/A | N/A | 0.106% | 1.45% | 2.06% | 0.55% | N/A | 0.55% | N/A | 0.25% | N/A | 0.35% | 1.48% | 2.12% | 1%, 2.1% |
| 1.5 | Uniform | 10 | N/A | N/A | 0.057% | 5.02% | 5.73% | 4.73% | N/A | 5.85% | N/A | 1.51% | N/A | 3.74% | 5.02% | 6.91% | 45%, 42% |
| 1.5 | Develop | 0.44 | 0.008% | N/A | N/A | N/A | N/A | 0.01% | N/A | N/A | N/A | N/A | N/A | N/A | N/A | N/A | N/A |
| 1.5 | Develop | 1 | 0.003% | N/A | N/A | N/A | N/A | 0.05% | N/A | N/A | N/A | N/A | N/A | N/A | N/A | N/A | N/A |
| 1.5 | Develop | 3 | 0.001% | N/A | N/A | N/A | N/A | 0.55% | N/A | N/A | N/A | N/A | N/A | N/A | N/A | N/A | 1%, 2.1% |
| 1.5 | Develop | 10 | 0.000% | N/A | N/A | N/A | N/A | 4.73% | N/A | N/A | N/A | N/A | N/A | N/A | N/A | N/A | 45%, 42% |
| 7.5 | Parabolic | 0.44 | N/A | 0.010% | N/A | 8.44% | 8.70% | 0.06% | 0.14% | N/A | 0.52% | N/A | 0.00% | N/A | 8.39% | 8.70% | N/A |
| 7.5 | Parabolic | 1 | N/A | 0.005% | N/A | 8.97% | 8.88% | 0.27% | 0.62% | N/A | 0.62% | N/A | 0.01% | N/A | 8.80% | 8.89% | 0.06% |
| 7.5 | Parabolic | 3 | N/A | 0.002% | N/A | 10.60% | 15.96% | 2.22% | 5.04% | N/A | 2.80% | N/A | 0.07% | N/A | 10.58% | 15.97% | 1.5%, 3.4% |
| 7.5 | Parabolic | 10 | N/A | 0.001% | N/A | 63.55% | 75.40% | 22.47% | 47.29% | N/A | 77.76% | N/A | 0.75% | N/A | 67.39% | 75.33% | 85%, 81% |
| 7.5 | Uniform | 0.44 | N/A | N/A | 0.141% | 1.00% | 1.94% | 0.06% | N/A | 0.08% | N/A | 0.34% | N/A | 0.00% | 1.00% | 1.94% | N/A |
| 7.5 | Uniform | 1 | N/A | N/A | 0.086% | 0.98% | 1.98% | 0.27% | N/A | 0.34% | N/A | 0.39% | N/A | 0.01% | 0.98% | 1.97% | 0.06% |
| 7.5 | Uniform | 3 | N/A | N/A | 0.048% | 2.31% | 3.42% | 2.22% | N/A | 2.75% | N/A | 0.97% | N/A | 0.07% | 2.40% | 3.40% | 1.5%, 3.4% |
| 7.5 | Uniform | 10 | N/A | N/A | 0.026% | 34.72% | 30.09% | 22.47% | N/A | 27.51% | N/A | 43.59% | N/A | 0.75% | 36.73% | 30.14% | 85%, 81% |

| Flow Rate (lpm) | Velocity Profile | Particle Size (μm) | Diffusion | | | Impaction | | | | | | | Sedimentation | | Combined Impact & Sed | | Exp. Data |
|---|---|---|---|---|---|---|---|---|---|---|---|---|---|---|---|---|---|
| | | | Fluent FPM | Ingham Par. | Ingham Uni. | Fluent DPM | CFX | Yeh & Schum | Cai & Yu Par. | Cai & Yu Uni. | Zhang, et al. Par. | Zhang, et al. Uni. | Pich Par. | Yu, et al. Uni. | Fluent DPM | CFX | |
| 7.5 | Develop | 0.44 | 0.002% | N/A | N/A | N/A | N/A | 0.06% | N/A | N/A | N/A | N/A | N/A | N/A | N/A | N/A | N/A |
| 7.5 | Develop | 1 | 0.001% | N/A | N/A | N/A | N/A | 0.27% | N/A | N/A | N/A | N/A | N/A | N/A | N/A | N/A | 0.06% |
| 7.5 | Develop | 3 | 0.000% | N/A | N/A | N/A | N/A | 2.22% | N/A | N/A | N/A | N/A | N/A | N/A | N/A | N/A | 1.5%, 3.4% |
| 7.5 | Develop | 10 | 0.000% | N/A | N/A | N/A | N/A | 22.47% | N/A | N/A | N/A | N/A | N/A | N/A | N/A | N/A | 85%, 81% |

# Chapter 9

# Conclusions and Future Work

## 9.1 Conclusions

The breadth of this research has provided substantial learning. Much of this learning will help to move CFD modeling of particle deposition in the lung forward at Rochester Institute of Technology. This research has quantified the relative accuracy of various analytical equations with respect to one another, with CFD predictions and in the case of impaction, with experimental data, for each isolated deposition mechanism.

When examining deposition by the sedimentation mechanism, CFD predictions for uniform flow typically have better agreement compared to parabolic flow conditions with analytical equations at all ε values. Of the CFD software packages, Fluent FPM has the best agreement with the parabolic flow equations from Pich (1972) and Wang (1975) for ε values less than 0.2 compared to Fluent DPM and CFX. Fluent FPM is also the only CFD package which predictions provide an S-shaped curve like the analytical equations. For uniform flow conditions both Fluent DPM and CFX agree well with analytical predictions from Yu, et al. (1977). At ε values less than 0.1, all parabolic flow equations provide the same deposition efficiency predictions; above 0.1 Pich (1972) and Wang (1975) provide the same predictions, while Yeh and Schum (1980) is as much as 20% lower in its predictions. For uniform flow conditions Yu, et al. (1977) and Yeh and Schum (1980) the same deposition efficiency predictions for ε values less than 0.1, by 1 Yeh and Schum (1980) is 20% less than Yu, et al. (1977). Experimental data for isolated sedimentation in a straight tube geometry is still necessary to better understand the sedimentation mechanism.

Of the three software packages, only Fluent FPM is able to accurately predict Ingham's (1975) analytical equations for deposition by diffusion. Fluent FPM has slightly better agreement with Ingham's (1975) analytical equation for uniform flow than parabolic flow. In both flow conditions Fluent FPM's predictions are never more than 2.5% less than

Ingham's (1975) equation for the same flow conditions. Fluent DPM is unable to track particles smaller than 20 nm in the straight tube and has poor correlation with Ingham's (1975) analytical equations for the data points that could be obtained. CFX is currently only able to track turbulent diffusion which was not researched. Experimental data for isolated diffusion in a simple straight tube is needed to evaluate the analytical equations and gain a better understanding of diffusion.

There is substantial variation in the analytical equations and CFD predictions for impaction in the bifurcating tube geometry. Of the impaction theories, Zhang, et al.'s (1997) parabolic flow equation has the best agreement with Kim and Iglesias' (1989) experimental data at most flow conditions. Cai and Yu (1988) and Yeh and Schum (1980) predict a more linear trend with respect to the deposition efficiencies then what is seen in the experimental. Cai and Yu's (1988) equation for parabolic flow over estimates experimental data for Stokes numbers less than 0.05 and significantly under estimates experimental data all other Stokes numbers. Cai and Yu's uniform equation under estimates experimental data at all Stokes numbers examined except 0.017, where is it slightly higher. Yeh and Schum's (1980) uniform and parabolic equations both under estimate experimental data at all Stokes numbers examined. Zhang, et al.'s (1997) uniform flow equation under estimates the experimental data for all Stokes number investigated. Fluent DPM's predictions typically align better with Yeh and Schum's (1980) equations, while CFX aligns closer with Cai and Yu's (1988) predictions. Parabolic and developing velocity profiles in the bifurcation provide a more realistic representation of physical flow conditions and have the best agreement with Kim and Iglesias' (1989) experimental. There is limited experimental data, where the impaction deposition mechanism has been isolated. At this point only one study has been located, Kim and Iglesias (1989), and impaction was not isolated for all particle sizes and flow rates investigated. In order to better understand the impaction deposition mechanism and improve analytical and CFD predictions more experimental studies are necessary.

Discrepancies between CFD and theoretical predictions in straight tube and three generation lung geometry are consistent for the sedimentation and diffusion deposition mechanism. Based on this information, simple straight tube geometry results can be used to ascertain the uncertainty in CFD predictions for more complicated geometries. In the three generation lung geometry, CFD predictions were able to accurately predict experimental data

at the 7.5 lpm flow rate for 10 μm particles with combined impaction and sedimentation and the parabolic velocity profile. CFX was lower by 5% and Fluent DPM lower by 13% than the experimental value of 83%. Fair correlation was obtained for the 3 μm particle sizes at 1.5 lpm with CFX. For 3 μm particle size and 1.5 lpm flow, CFX is 2% higher, while Fluent DPM is 9% higher than experimental value of 1.55%. Poor correlation was found for the 10 μm particle sizes at the 1.5 lpm flow rate and 1 μm and 3 μm particle sizes at the 7.5 lpm flow rate. For the 10 μm particle size at the 1.5 lpm flow rate, CFX is 26% lower and Fluent DPM is 23% lower than experimental the experimental value of 43.5%. For the 1 μm particle size at the 7.5 lpm flow rate, CFX and Fluent DPM are both 8% higher than experimental the experimental value of 0.06%. For the 3 μm particle size at the 7.5lpm flow rate, CFX is 12% higher and Fluent DPM is 7% higher than experimental the experimental value of 2.45%.

Exploring deposition efficiencies for combined impaction and sedimentation using the developing velocity profile could improve agreement with experimental data in the three generation geometry. After examining velocity profiles in the three generation lung geometry, it can be concluded that the uniform flow conditions are not an accurate representation of the physical flow conditions within the lung. The developing flow conditions have already developed 40% in generation three at the 1.5 lpm flow rate, according to CFD. Additionally, the parabolic and developing velocity profiles experience substantial skew in their profiles after the bifurcations that are not seen in the uniform or parabolic flow conditions.

Correlation between theoretical predictions and experimental is only good for the 10 μm particle size at the 7.5 lpm flow rate, and even here there is a range of theoretical predictions. For the 10 μm particle at the 7.5 lpm flow rate theoretical predictions for impaction range from 94% for Zhang, et al.'s (1997) parabolic flow equation to 27% for Yeh and Schum's (1980) impaction equation. Both sedimentation and diffusion theoretical equations predict less than 1% deposition efficiencies, for a combined deposition efficiency of 95% to 28% for the 10 μm particle size at the 7.5 lpm flow rate. At the 7.5 lpm flow rate, both impaction and diffusion theoretically represent more than 100% of the total deposition observed by Dr. Oldham at the 1 μm particle size. Impaction could theoretically represent 100% or more of the total deposition observed by Dr. Oldham at the 3 μm particle sizes. At

the 1.5 lpm flow rate, none of the deposition mechanisms theoretically predict even a quarter of the deposition observed by Dr. Oldham at the 10 μm particle size. Combining sedimentation and impaction theoretically only accounts for 11% to 32% of the total experimental deposition for the 10 μm particle at the 1.5 lpm flow rate. At the 3 μm particle size combined impaction and sedimentation could theoretically account for 50% to 89% of the particle deposition observed by Dr. Oldham.

Local deposition patterns in the three generation lung geometry for all five particle sizes reveal that flow within the geometry during experimental testing could not be fully developed. The large quantity of particles depositing near the inlet the of the three generation lung geometry is a characteristic of parabolic flow predictions that is not mimicked in the experimental data. Aside from this local deposition patterns for parabolic flow compare well to experimental data with "hot spots" at the bifurcation for the higher flow rate and larger particle sizes.

## 9.2 Future Work

This research is just one step in developing improved CFD models for particle deposition in the lung. There are still many more steps that will need to be taken before a complete 23 generation lung model of an ideal or replica lung geometry can be obtained. These recommendations focus on things that can be done in the coming years to improve CFD predictions and understanding of the various deposition mechanisms.

The next step in this research would be to examine the local deposition for the uniform and developing velocity profile in the three generation lung model. This will help determine the effect of flow conditions in the three generation model during the experiments conducted by Dr. Oldham.

Obtaining local deposition from CFX is a priority of Dr. Robinson's currently. The first step in this process is to conduct a study to determine the minimum number of particles needed to stabilize deposition in the three generation lung geometry. Once this is known, efforts should be made to work with CFX to develop a script capable of providing local deposition for this minimum number of particles with the current computing resources at Rochester Institute of Technology. It may also be useful to look into other more powerful computing options available for this research.

The three generation lung model could be remeshed with a hex and boundary layer mesh to determine if mesh affects agreement with experimental data. It is expected some variation will be seen just based on how the CFD software packages solve the equations of motion over a hex and tet element.

As has been seen in this research, there is still substantial research that needs to be done into the impaction deposition mechanism, particularly with respect to conducting experimental and numerical experiments with identical geometries. This information is essential to accurately predicting particle deposition in the tracheobroncial region of the lung, where impaction is the dominate deposition mechanism. Table 9.1 contains theoretical predictions for impaction and total sedimentation in the Y-bifurcation utilized by Kim and Iglesias (1989) at several particle diameters and flow rates. Particles sizes of 1, 3, 5, 7, and 10 μm have been selected because all are commonly utilized in experimental studies and can be obtained from supply companies. A density of 891 $kg/m^3$ is assumed as in the original experiments conducted by Kim and Iglesias (1989). This table focuses on parabolic flow, because, as the research has shown, it is the more realistic flow condition. Cai and Yu's (1988) theoretical predictions for impaction are utilized to represent a worst case, or lowest possible deposition by impaction. Although Yeh and Schum (1980) predicts lower deposition for all Stokes numbers in this research the equation was developed for a bend rather then a bifurcation, of the two equations for a bifurcation Cai and Yu (1988) typically provided the lower deposition efficiency. The influence of sedimentation is determined by dividing the sedimentation deposition efficiency by the sum on the impaction and sedimentation deposition efficiencies. Diffusion is neglected in the combined deposition calculations because it should be negligible at these particle sizes (all larger than 0.1 μm where diffusion starts to be noticeable.) Impaction is considered isolated if the sedimentation deposition efficiency is less that 2% of the combined theoretical impaction and sedimentation deposition efficiency. As can be seen in Table 9.1, for the Y bifurcation utilized by Kim and Iglesias (1989) this is only true at the 12 lpm flow rate where the flow is within the transitional flow regime (highlighted in yellow). It appears in this single bifurcation impaction cannot be isolated while remaining in the laminar flow regime. Other bifurcation geometries exist and should be investigated similarly. Additionally, a full analysis of all

theoretically impaction equations would be necessary before selecting final flow conditions to isolate impaction.

**Table 9.1 Theoretical effect of sedimentation and impaction in the Y-bifurcation utilized by Kim and Iglesias (1989). Note: Conditions highlighted in yellow represent transitional or turbulent flow.**

| Particle Size | Flow rate in Parent (liter/min) | Re in Parent | Stk | Cai &Yu Parabolic Impaction | Pich Parabolic Sedimentation Total | Sedimentation % of Combined Impaction and Sedimentation |
|---|---|---|---|---|---|---|
| 10 | 4 | 1132 | 0.187 | 25.87% | 3.56% | 12.09% |
| 10 | 5 | 1415 | 0.233 | 32.34% | 2.86% | 8.12% |
| 10 | 6 | 1698 | 0.280 | 38.80% | 2.39% | 5.79% |
| 10 | 7 | 1981 | 0.327 | 45.27% | 2.05% | 4.33% |
| 10 | 8 | 2264 | 0.373 | 51.74% | 1.80% | 3.35% |
| 10 | 12 | 3395 | 0.560 | 77.61% | 1.20% | 1.52% |
| 7 | 4 | 1132 | 0.091 | 12.61% | 1.76% | 12.25% |
| 7 | 5 | 1415 | 0.114 | 15.84% | 1.41% | 8.18% |
| 7 | 6 | 1698 | 0.137 | 19.01% | 1.18% | 5.83% |
| 7 | 7 | 1981 | 0.160 | 22.18% | 1.01% | 4.36% |
| 7 | 8 | 2264 | 0.180 | 24.93% | 0.89% | 3.43% |
| 7 | 12 | 3395 | 0.270 | 37.40% | 0.59% | 1.56% |
| 5 | 4 | 1132 | 0.047 | 6.51% | 0.90% | 12.18% |
| 5 | 5 | 1415 | 0.058 | 8.08% | 0.72% | 8.21% |
| 5 | 6 | 1698 | 0.070 | 9.70% | 0.60% | 5.86% |
| 5 | 7 | 1981 | 0.082 | 11.32% | 0.52% | 4.37% |
| 5 | 8 | 2264 | 0.093 | 12.88% | 0.45% | 3.40% |
| 5 | 12 | 3395 | 0.140 | 19.39% | 0.30% | 1.54% |
| 3 | 4 | 1132 | 0.017 | 2.35% | 0.33% | 12.18% |
| 3 | 5 | 1415 | 0.021 | 2.91% | 0.26% | 8.24% |
| 3 | 6 | 1698 | 0.025 | 3.49% | 0.22% | 5.87% |
| 3 | 7 | 1981 | 0.029 | 4.07% | 0.19% | 4.38% |
| 3 | 8 | 2264 | 0.034 | 4.71% | 0.16% | 3.36% |
| 3 | 12 | 3395 | 0.050 | 6.93% | 0.11% | 1.55% |
| 1 | 4 | 1132 | 0.002 | 0.26% | 0.04% | 12.33% |
| 1 | 5 | 1415 | 0.002 | 0.32% | 0.03% | 8.26% |
| 1 | 6 | 1698 | 0.003 | 0.39% | 0.02% | 5.89% |
| 1 | 7 | 1981 | 0.003 | 0.45% | 0.02% | 4.39% |
| 1 | 8 | 2264 | 0.004 | 0.52% | 0.02% | 3.40% |
| 1 | 12 | 3395 | 0.006 | 0.78% | 0.01% | 1.54% |

Finally, in the interest of moving toward a numerical model of the entire lung, it is the recommendation of this research that focus be placed on the pulmonary and alveolar regions of the lung. The software packages currently being utilized have very good agreement with

analytical predictions for the sedimentation and diffusion deposition mechanisms, which are dominate in these regions of the lung.

# Work Cited


1. American Lung Association. Estimated Prevalence and Incidence of Lung Disease By Lung Association Territory. 2004. [a]
2. American Lung Association. Trends in Tobacco Use. 2004. [b]
3. Anjilvel, S. and B. Asgharian. A Multiple-Path Model of Particle Deposition in the Rat Lung. *Fund. and App. Toxicology*. 28:41-50, 1995.
4. ANSYS Inc. CFX 5.7.1 User's Guide, 2003
5. Arde, L. and B. Westergren. Beta Mathematics Handbook. 2nd Edition, CRC Press Inc. Florida 1992, P. 243.
6. Asgharian, B., W. Hofmann, R. Bergmann. Particle Deposition in a Multiple-Path Model of the Human Lung. *Aerosol Sci. Tech.* 34:332-339, 2001.
7. Asgharian, B. and S. Anjilvel. Inertial and Gravitational Deposition of Particles in a Square Cross Section Bifurcating Airway. *Aerosol Sci. and Tech.* 20:1777-193, 1994.
8. Bailey, W. H. and R. J. Robinson. Deposition of Charged Particles In The Respiratory Tract With Special Reference To Particles Downwind Of High-Voltage AC Transmission Lines. Submitted to *J. Environmental Research.* March 2005.
9. Balashazy, I., W. Hofmann, and A. Farkas. Numerical Modeling of Deposition of Inhaled Particles in Central Human Airways. *Ann. Occup. Hyg.* 46(1):353-357, 2002.
10. Balashazy, I., T. Heistracher, and W. Hofmann. Air Flow and Particle Deposition Patterns in Bronchial Airway Bifurcation Patterns in Bronchial Airway Bifurcations: The Effect of Different CFD Models and Bifurcation Geometries. *J. Aerosol Medicine.* 9(3):287-301, 1996.
11. Balashazy, I. and W. Hofmann. Particle Deposition in Airway Bifurcations-I Inspiratory Flow. *J. Aerosol Sci.* 24(6):745-772, 1993. [a]
12. Balashazy, I. and W. Hofmann. Particle Deposition in Airway Bifurcations-II Expiratory Flow. *J. Aerosol Sci.* 24(6):773-786, 1993. [b]
13. Broday, D. M. Deposition of Ultrafine Particles at Carinal Region of the Upper Bronchial Airways. *Aerosol Sci. and Tech.* 38:991-1000, 2004.
14. Cai, F. S. and C.P Yu. Inertial and Interceptional Deposition of Spherical Particles and Fibers in a Bifurcating Airway. *J. Aerosol Sci.* 19(6):679-688, 1988.

15. Chan, T. L. and M. Lippmann. Experimental Measurements and Empirical Modeling of the Regional Deposition of Inhaled Particles in Humans. *Am. Ind. Hyg. Assoc. J.* 41:399-409, 1980.

16. Chen, Y. K. and C. P. Yu. Particle Deposition from Duct Flows by Combined Mechanisms. *J. Aerosol Sci. and Tech.* 19:389-395, 1993.

17. Cohen, B. S., R. G. Sussman, and M. Lippmann. Ultrafine Particle Deposition in a Human Tracheobronchial Cast. *Aerosol Sci. and Tech.* 12:1082-1091, 1990.

18. Cohen, B. S. and B. Asgharian. Deposition of Ultrafine Particles in the Upper Airways: An Empirical Analysis. *J. Aerosol Sci.* 6:789-797, 1990.

19. Cohen, B. S. Deposition of Ultrafine Particles in the Human Tracheobroncial Tree; A Determinant of the Dose from Radon Daughters. In Radon and Its Decay Products Chapter 14 (Edited by Hopke, P. H.), American Chemical Society, Washington DC, 1987. P. 475-486.

20. Comer, J. K., C. Kleinstreuer, S. Hyun, and C. S. Kim. Aerosol Transport and Deposition In Sequentially Bifurcating Airways. *Trans. of ASME.* 122:152-157, 2000.

21. Crystal, R. G., J. B. West, P. J. Barnes, and E. R. Weibel. The Lung: Scientific Foundations (Two Volume Set). Lippincott Williams & Wilkins Publishers. Philadelphia 1997.

22. Dendo, R. I., R. F. Phalen, R. C. Mannix, and M. J. Oldham. Effects of Breathing Parameters on Sidestream Cigarette Smoke Deposition in a Hollow Tracheobronchial Model. *Am. Ind. Hyg. Assoc. J.* 59:381-387, 1998.

23. Ferron, G. A. Deposition of Polydisperse Aerosols in Two Glass Models Representing the Upper Human Airways. *J. Aerosol Sci.* 8:409-427, 1977.

24. Fluent Inc. Fluent 6.1 User's Guide, Jan. 2005

25. Fox, R. W. and A. T. McDonald. Introduction to Fluid Mechanics. 5th Edition, John Wiley & Sons, Inc. New York 1998, P. 349+.

26. Gurman, J. L., M. Lippmann, and R. B. Schlesinger. Particle Deposition in Replica Casts of the Human Upper Tracheobroncial Tree Under Constant and Cyclic Inspiratory Flow: I. Experimental. *Aerosol Sci. and Tech.* 10:245-252, 1984.

27. Hammersley, J. R. and D. E. Olsen. Physical Models of the Smaller Pulmonary Airways, *J. Appl. Physiology.* 72:2402-2414, 1992.

28. Heistracher, T. and W. Hofmann. Physiologically Realistic Models of Bronchial Airway Bifurcations. *J. Aerosol Sci.* 26(3):497-509, 1995.

29. Heistracher, T. and W. Hofmann. Flow and Deposition Patterns in Successive Airway Bifurcations. *Ann. Occup. Hyg.* 41(Suppl. 1):537-542, 1997.

30. Hinds, William C. Aerosol Technology John Wiley & Sons, Inc. New York 1999, P. 42-73.

31. Hofmann, W., R. Golser, and I. Balashazy. Inspiratory Deposition Efficiency of Ultrafine Particles in a Human Airway Bifurcation Model. *Aerosol Sci. Tech.* 37:988-994, 2003.

32. Horsfield, K. G. Dart, D. E. Olsen, G. F. Filley, G. Cumming. Models of the Human Bronchial Tree. *J. Appl. Physiology.* 31:207-217, 1971.

33. Ingham, D. B. Diffusion of Aerosols in the Entrance Region of a Smooth Cylindrical Pipe. *J. Aerosol Sci.* 22(3):253-257, 1991.

34. Ingham, D. B. Diffusion of Aerosol from a Stream Flowing through a Short Cylindrical Pipe. *J. Aerosol Sci.* 15(5):637-641, 1984.

35. Ingham, D. B. Diffusion of Aerosols from a Stream Flowing Through a Cylindrical Tube. *J. Aerosol Sci.* 6:125-132, 1975.

36. International Commission on Radiological Protection. Human Respiratory Tract Model for Radiological Protection. Pergamon, New York, 1993.

37. Johnston, J. R., K. D. Isles, D. C. F. Muir. Inertial Deposition of Particles in Human Branching Airways. In W. H. Walton, Inhaled Particles IV, Part I. Unwin, Woking, 1977. P. 61-73.

38. Kim, C. S. and D. M. Fisher. Deposition Characteristics of Aerosol Particles in Sequentially Bifurcating Airway Models. *Aerosol Sci. and Tech.* 31:198-220, 1999.

39. Kim, C. S. and A. J. Iglesias. Deposition of Inhaled Particles in Bifurcating Airway Models: I. Inspiratory Deposition. *J. Aerosol Med.* 2:1-14, 1989. [a]

40. Kim, C. S. and A. J. Iglesias. Deposition of Inhaled Particles in Bifurcating Airway Models: II. Expiratory Deposition. *J. Aerosol Med.* 2:15-27, 1989. [b]

41. Koblinger, L. and W. Hofmann. Monte Carlo Modeling of Aerosol Deposition in Human Lungs. Part I: Simulation of Particle Transport in a Stochastic Lung Structure. *J. Aerosol Sci.* 21(5):661-674, 1990.

42. Landahl, H. D. On the Removal of Air-Borne Droplets by the Human Respiratory Tract: I. The Lung. *Bull. on Math. Biophys.* 12:43-56, 1950.

43. Lee, J. W., J. H. Goo, and M. K. Chung. Characteristics of Inertial Deposition in a Double Bifurcation. *J. Aerosol Sci.* 27(1):119-138, 1996.

44. Lee, J. W. and J. H. Goo. Numerical Simulation of Air Flow and Inertial Deposition of Particles in a Bifurcating Channel of Square Cross Section. *J. Aerosol Med.* 5(3):131-154, 1992.

45. Martin, D. and W. Jacobi. Diffusion Deposition of Small Sized Particles in the Bronchial Tree. *Health Phys.* 23:23-29, 1972.

46. Oldham, M. J., R. F. Phalen, and T. Heistracher. Computational Fluid Dynamic Predictions and Experimental Results for Particle Deposition in an Airway Model. *Aerosol Sci. and Tech.* 32:61-71, 2000.

47. Oldham, M. J., R. C. Mannix, and R. F. Phalen. Deposition of Monodisperse Particles in Hollow Models Representing Adult and Child Size Tracheobronchial Airways. *Health Phys.* 72:827-834, 1997.

48. Phalen, R., M. J. Oldham, R. Mannix, and G. M. Schum. Cigarette Smoke Deposition in the Tracheobronchial Tree: Evidence for Colligative Effects. *Aerosol Sci. and Tech.* 20:215-236, 1994.

49. Pich, J. Theory of Gravitational Deposition of Particles From Laminar Flows in Channels. *J. Aerosol Sci.* 3:351-361, 1972.

50. Pruyne, A. The Mapping of Velocity Profiles in a Three Generation Lung Model Using Particle Image Velocimetry Flow Analysis Techniques. Masters Thesis, Rochester Institute of Technology, Sept. 2004.

51. Rai, P. K. Simulating Particle Deposition in a Human Replica Lung Model. Masters Thesis, Rochester Institute of Technology, Feb. 2004.

52. Robinson, R.J., M.J. Oldham, R.E. Clinkenbeard and P. Rai. Experimental and numerical analysis of a 7 generation human replica tracheobronchial model. Submitted to Annuals of BMES. Aug, 2005.

53. Robinson R. J. and C. P. Yu. Deposition of Cigarette Smoke Particles in the Human Respiratory Tract." *J. Aerosol Sci. and Tech.* 34(2): 202-215, 2001.

54. Schlesinger, R. B. D. E. Bohing, T. L. Chan, and M. Lippmann. Particle Deposition in a Hollow Cast of the Human Tracheobronchial Tree. *J. Aerosol Sci.* 8:429-225, 1977.

55. Schlesinger, R. B. and M. Lippmann. Particle Deposition in the Trachea: In Vivo and in Hollow Cast. *Thorax.* 31:678-784, 1976.

56. Schlesinger, R. B. and M. Lippmann. Particle Deposition in Casts of the Human Upper Tracheobronchial Tree. *Am. Ind. Hyg. Assoc. J.* 33(4):237-251, 1972.

57. Sebel, P., D. Stoddart, R. Waldhorn, C. Waldmann, P. Whitfield Respiration: The Breath of Life. Tostar books Inc., New York, NY. 1985.

58. Shi, H., C. Kleinstreuer, Z. Zhang, and C. S. Kim. Nanoparticle Transport and Deposition in Bifurcating Tubes with Different Inlet Conditions. *Phys. of Fluids.* 16(7):2199-2213, 2004.

59. Smith, S., Y. S. Cheng, H. C. Yeh. Deposition of Ultrafine Particles in Human Tracheobronchial Airways of Adults and Children. *Aerosol Sci. and Tech.* 35:697-709, 2001.

60. United States. Environmental Protection Agency. Review of the National Ambient Air Quality Standards for Particulate Matter: Policy Assessment of Scientific and Technical Information. North Carolina: GPO, 2005.

61. United States. National Council on Radiation Protection and Measurements. Deposition, Retention, and Dosimetry of Inhaled Radioactive Substances. Bethesda, MD: GPO, 1997, P. 50-79+.

62. Wang, C. S. Gravitational Deposition of Particles from Laminar Flows in Inclined Channels. *J. Aerosol Sci.* 6:191-204, 1975.

63. Weibel, E. R Morphometry of the Human Lung. New York Academic Press, Springer-Verlag, 1963.

64. Whitby, E., F. Stratmann, and M. Wilck. Fine Particle Model (FPM) for Fluent, July, 2003.

65. Yeh, H. C. and G. M. Schum. Models of Human Lung Airways and Their Application to Inhaled Particle Deposition. *Bull. of Math. Bio.* 42:461-480, 1980.

66. Yeh, H. C. Use of a Heat Transfer Analogy for a Mathematical Model of Respiratory Tract Deposition. *Bull. of Math. Bio.* 36:105-116, 1974.

67. Yu, C. P. Exact Analysis of Aerosol Deposition during Steady Breathing. *Powder Technology*. 21:55-62, 1978.

68. Yu, C. P, C. S. Lui, and D. B. Taulbee. Simultaneous Diffusion and Sedimentation of Aerosols in a Horizontal Cylinder. *J. Aerosol Sci.* 8:309-316, 1977.

69. Yu, G., Z. Zhang, and R. Lessmann. Computer Simulation of the Flow Field and Particle Deposition by Diffusion in a 3-D Human Airway Bifurcation. *Aerosol Sci. Tech.* 25:338-352, 1996.

70. Zhang, L., B. Asharian, and S. Anjilvel. Inertial Deposition of Particles in the Human Upper Airway Bifurcations. *J. Aerosol Sci. Tech.* 26:97-110, 1997.

# Appendix A

# Overview of CFD Articles

**Table ( A.1 Overview of CFD articles examining particle deposition in the Tracheobronchial region or bifurcating tubes. Articles are organized by research group.**

| Authors (Year) | Software Package | Geometry | Deposition Mechanisms Investigated | Flow Conditions / Particle Diameters | Compared with Experimental Data | Conclusions |
|---|---|---|---|---|---|---|
| Asgharian and Anjilvel (1994) | FIDAP (flow) External Code (particles) | Square bifurcation | Impaction and Sedimentation | Re=100 & 1000 uniform & parabolic flow $10^{-3}$<Stk<$10^{1}$ | Kim and Iglesias (1989) Pui, et al. (1987) | Sedimentation losses agreed with existing theory. Impaction losses were on the same order of magnitude as other experimental data. |
| Hoffman, et al. (2003) | FIRE (flow) Monte Carlo Code (particles) | PRB model (Gen 3-4) | Impaction, Sedimentation, & Brownian Diffusion | 1.25, 7.5, and 15 lpm 1 to 500 nm | | Particle and flow transport equations must be solved simultaneously for diffusion in non-laminar flow or when the flow changes direction. It is not until particles are smaller than 10 nm that diffusion becomes dominate. |
| Balashazy, et al. (2002) | Fluent (flow) Monte Carlo Code (particles) | Ideal narrow bifurcation & PRB model (Gen 3-6) | | 0.01, 1, and 10 μm 10 to 120 lpm inspiratoy and expiratory flow | | Hot spot at the carina region. Deposition dependant on mesh, geometry, flow rate and particle sizes. |
| Balashazy, et al. (1996) [I] | FIRE (flow) Monte Carlo Code (particles) | Ideal narrow bifurcation & PRB model (Gen 3-4) | Impaction, Sedimentation, & Brownian Diffusion | Re=851 0.01 μm, 10 μm Stk=1.03E-5, 5.37E-1 | | Less skew in the PRB model. Secondary flow affects particle deposition in both Models. |

| | | | | | | |
|---|---|---|---|---|---|---|
| Balashazy and Hofmann (1993) [a] | Personal code using finite difference method (flow) Monte Carlo Code (particles) | Bifurcation similar to Kim and Iglesias (1989) (Ideal narrow bifurcation) and Wide bifurcation | Impaction, Sedimentation, Brownian Diffusion, & Interception | Re=568, 1784 and 1.25lpm uniform & parabolic flow 1000 random particles from 0.01 to 14 μm inspiratory flow | Kim and Iglesias (1989) and Johnson, et al. (1977) | Poor agreement with Kim (1989) at higher stokes were deposition was less than observed, otherwise values on same order of magnitude |
| Balashazy and Hofmann (1993) [b] | Personal code using finite difference method (flow) Monte Carlo Code (particles) | Bifurcation similar to Kim and Iglesias (1989) (Ideal narrow bifurcation) | Impaction, Sedimentation, Brownian Diffusion, & Interception | Re=178, 568, and 1066 1.25, 4, and 7.5 lpm 1000 random particles sizes 0.01 and 10 μm expiratory flow | Kim and Iglesias (1989) | Secondary flow is more important in expiratory deposition than inspriatory. Less deposition for expiratory flow. Hot spot on top and bottom of parent tube. Claimed agreement with Kim (1989) although exact conditions not compared. |
| Shi, et al. (2004) | CFX 4.4 (user defined function for diffusion) | Straight tube, 90° bend, and bifurcation with both planar and nonplanar configurations (Gen 3-5). | Impaction and Diffusion | Straight tube Re=200, 500, and 1000 5, 10, 20, 50, 100, and 150 nm Bend Re=251, 1000 5 and 12 μm Gen 3-5 Re=200, 500, and 1000. 1nm<$d_p$<150 nm parabolic, uniform, & "realistic" velocity profiles | Wang, et al. (2002) (Bend) Kim, C. S (2002) (for Gen 3-5) | Comparison with Kim difficult since different flow conditions was run. Theory and observed agree for straight tube diffusion. Bend data agrees with experimental for most particle sizes. Nonplanar has a minor effect on deposition. Inlet conditions will change deposition. |

| | | | | | | |
|---|---|---|---|---|---|---|
| Zhang, and Kleinstreuer (2001) | CFX | Ideal lung geometry (Gen 3-5) | | 500<Re<2000<br>0.02<Stk<0.12<br>7356 particles | Kim and Fisher (1999) | Compared with experimental good except at Stk >.1<br>Regardless of distribution particles injected near the center of the tube deposit at 1st bifurcation.<br>Position has less effect at later bifurcations, due to secondary flow. |
| Comer, et al. (2000) | CFX 4.2 with user defined functions | Ideal lung geometry (Gen 3-5) w/ in-plane and out-of-plane bifurcation | | Re=500, 1000, 1500, and 2000<br>Stk=0.037 to 0.23<br>3, 5, 7 μm particles | Kim and Fisher (1999) | Deposition varied 5-15% over range of Re, Kim and Fisher (1999) typically observed higher deposition.<br>Deposition varies significantly with geometry. |
| Lee, et al. (1996) | FIDAP | 2D and 3D double bifurcation geometry with 45° symmetric and asymmetric bifurcations | | Re=500<br>Stk=0.02-0.12<br>4 μm | Kim, et al (1994) | Compared single and double bifurcation data, reasonable agreement at some Stk values.<br>Deposition in 1st bifurcation for 3D almost the same as single bifurcation model, despite variations in flow and particle trajectory.<br>Deposition is highest in out-of-plane configuration. |

| | | | | | | |
|---|---|---|---|---|---|---|
| Lee and Goo (1992) | | 2D and 3D models Bifurcating square duct | Impaction | Re=500 and 1170 uniform and parabolic velocity profiles | Kim and Iglesias (1989) | Compare to theory based on Stk, same flow conditions and geometry are not utilize in both studies, agreement with experimental is good despite these variations. Secondary flow and velocity profile have a major impact on deposition. |
| Yu, et al. (1996) | PHOENICS | Ideal lung (Gen 0-1) | Diffusion and Impaction | Re=1000-2000 0.005 and 0.05μm | Zhao, et al. (1992) | 8.7% to 18.2% difference in efficiency compared to experimental. Inlet and outlet boundary conditions can effect flow and deposition. Diffusion has larger effect at lower Re. |

# Appendix B

# Other Bifurcation Geometry Data

The second bifurcation geometry research was purchased from Dyna Lab. Dyna Lab's part number for the Y-bifurcation is 2255-0000. The manufacture's part number is TS465 or 465 depending on the manufacturing date.

As part of this research, the Y-bifurcations were molded and characterized, so an identical numerical model could be created. The molds were created with instruction from Dr. Caranno in the Industrial Engineering Department. The molds were made with a two part polystyrene material, which was guided into the bifurcations with needles. The molds were left to set for 1 to 2 hours and then removed with razor blades, a process which destroyed the original Y-bifurcation. Figure B.1 show a bifurcation mold after being removed and the split Y-bifurcation. Several bifurcations and variations on the process were tied to determine how to create the highest quality bifurcations. 25 bifurcations were measured, molded, and characterized. Of these 25 bifurcations only 13 survived the molding and removal process. The surviving bifurcations were measured with calipers for diameters and lengths and the magnifier in the Industrial Engineering Department for angles. Table B.1 contains the measurements for the Y-bifurcations purchased from Dyna Lab. Table B.2 contains the measurements for the bifurcation models created in this research. It should be noted that because the bifurcations were injected molded by the manufacture, there are noticeable variations in the bifurcation angles and placements. This can be seen in Figure B.2, all the bifurcations have been imaged, but not all overset measurements were gathered, due to this geometry no longer using utilized.

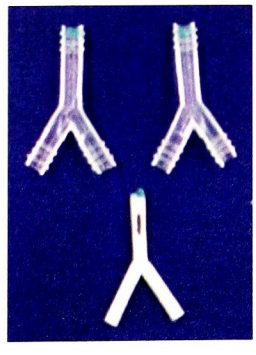

**Figure B.1 Bifurcation mold after removal**

**Table B.1 Bifurcation measurements for parts from Dyna Lab.**

| | Bifurcation Measurements | | | | | | | |
|---|---|---|---|---|---|---|---|---|
| Bifurcation ID | Parent Length | Daughter 1 Length | Daughter 2 Length | Parent Diameter | Daughter 1 Diameter | Daughter 2 Diameter | Maximum Length | Maximum Width |
| 1 | 0.780 | 0.605 | 0.607 | 0.124 | 0.128 | 0.127 | 1.400 | 0.795 |
| 2 | 0.798 | 0.607 | 0.606 | 0.128 | 0.127 | 0.128 | 1.385 | 0.797 |
| 3 | 0.756 | 0.632 | 0.615 | 0.127 | 0.128 | 0.129 | 1.382 | 0.812 |
| 4 | 0.762 | 0.611 | 0.625 | 0.128 | 0.128 | 0.127 | 1.408 | 0.820 |
| 5 | 0.795 | 0.600 | 0.602 | 0.129 | 0.128 | 0.128 | 1.387 | 0.792 |
| 6 | 0.758 | 0.611 | 0.629 | 0.126 | 0.128 | 0.128 | 1.383 | 0.824 |
| 7 | 0.743 | 0.617 | 0.629 | 0.124 | 0.127 | 0.129 | 1.376 | 0.818 |
| 8 | 0.747 | 0.619 | 0.635 | 0.122 | 0.125 | 0.126 | 1.378 | 0.814 |
| 9 | 0.759 | 0.605 | 0.631 | 0.121 | 0.128 | 0.128 | 1.377 | 0.811 |
| 10 | 0.757 | 0.615 | 0.627 | 0.123 | 0.127 | 0.128 | 1.371 | 0.817 |
| 11 | 0.754 | 0.611 | 0.618 | 0.124 | 0.128 | 0.128 | 1.383 | 0.826 |
| 12 | 0.739 | 0.611 | 0.631 | 0.122 | 0.125 | 0.126 | 1.374 | 0.814 |
| 13 | 0.750 | 0.615 | 0.628 | 0.124 | 0.125 | 0.125 | 1.373 | 0.811 |
| 14 | 0.754 | 0.614 | 0.633 | 0.122 | 0.124 | 0.126 | 1.373 | 0.801 |
| 15 | 0.746 | 0.619 | 0.636 | 0.122 | 0.126 | 0.125 | 1.371 | 0.807 |
| 16 | 0.752 | 0.615 | 0.626 | 0.124 | 0.126 | 0.126 | 1.380 | 0.815 |
| 17 | 0.748 | 0.612 | 0.628 | 0.122 | 0.126 | 0.126 | 1.379 | 0.822 |
| 18 | 0.755 | 0.615 | 0.631 | 0.122 | 0.125 | 0.125 | 1.388 | 0.817 |
| 19 | 0.744 | 0.616 | 0.630 | 0.121 | 0.125 | 0.125 | 1.383 | 0.821 |
| 20 | 0.757 | 0.622 | 0.625 | 0.122 | 0.125 | 0.127 | 1.383 | 0.824 |
| 21 | 0.748 | 0.625 | 0.632 | 0.122 | 0.126 | 0.126 | 1.384 | 0.822 |
| 22 | 0.748 | 0.628 | 0.631 | 0.123 | 0.126 | 0.126 | 1.379 | 0.821 |
| 23 | 0.747 | 0.620 | 0.627 | 0.122 | 0.126 | 0.127 | 1.380 | 0.820 |
| 24 | 0.749 | 0.620 | 0.630 | 0.122 | 0.126 | 0.126 | 1.384 | 0.820 |
| 25 | 0.758 | 0.626 | 0.624 | 0.122 | 0.125 | 0.126 | 1.382 | 0.823 |
| Maximum | 0.798 | 0.632 | 0.636 | 0.129 | 0.128 | 0.129 | 1.408 | 0.826 |
| Minimum | 0.739 | 0.600 | 0.602 | 0.121 | 0.124 | 0.125 | 1.371 | 0.792 |
| Average | 0.756 | 0.616 | 0.625 | 0.124 | 0.126 | 0.127 | 1.382 | 0.815 |
| Median | 0.754 | 0.615 | 0.628 | 0.122 | 0.126 | 0.126 | 1.382 | 0.817 |
| Standard Deviation | 0.015 | 0.008 | 0.009 | 0.002 | 0.001 | 0.001 | 0.008 | 0.009 |

**Table B.2 Measurements for the bifurcation models.**

| Bifurcation ID | Mold Measurements | | | | | | | | |
|---|---|---|---|---|---|---|---|---|---|
| | Parent Diameter | | Daughter 1 Diameter | | Daughter 2 Diameter | | Angle in Bifurcation | Angle Parent to Daughter 1 | Angle Parent to Daughter 2 |
| | Calipers | Magnifier | Calipers | Magnifier | Calipers | Magnifier | | | |
| 1 | 0.121 | 0.1229 | 0.121 | 0.124 | 0.121 | 0.1223 | 60° 35' | 148° 16' | 149° 28' |
| 2 | 0.123 | 0.1225 | 0.122 | 0.1231 | 0.124 | 0.1226 | 59° 21' | 150° 10' | 148° 19' |
| 3 | 0.122 | 0.1215 | 0.121 | 0.124 | 0.122 | 0.1254 | 59° 26' | 148° 39' | 149° 37' |
| 4 | 0.119 | 0.1208 | 0.122 | 0.1236 | 0.12 | 0.1268 | 59° 19' | 148° 41' | 150° 20' |
| 5 | 0.118 | 0.1212 | 0.119 | 0.1252 | 0.121 | 0.1226 | 59° 14' | 147° 26' | 150° 17' |
| 6 | Broke Removing From Model | | | | | | | | |
| 7 | Too Much Air in the Mold | | | | | | | | |
| 8 | Too Much Air in the Mold | | | | | | | | |
| 9 | Too Much Air in the Mold | | | | | | | | |
| 10 | Too Much Air in the Mold | | | | | | | | |
| 11 | 0.119 | 0.1226 | 0.121 | 0.1254 | 0.124 | 0.1252 | 59° 6' | 148° 0' | 150° 34' |
| 12 | 0.122 | 0.1222 | 0.123 | 0.1263 | 0.121 | 0.1264 | 58° 50' | 148° 44' | 150° 33' |
| 13 | 0.12 | 0.1214 | 0.125 | 0.1258 | 0.121 | 0.1267 | 59° 6' | 148° 40' | 150° 34' |
| 14 | 0.121 | 0.1215 | 0.124 | 0.1259 | 0.123 | 0.1283 | 58° 55' | 148° 51 | 150° 11' |
| 15 | 0.12 | 0.1219 | 0.122 | 0.1263 | 0.123 | 0.1271 | 58° 51' | 149° 11' | 149° 55' |
| 16 | Too Much Air in the Mold | | | | | | | | |
| 17 | Too Much Air in the Mold | | | | | | | | |
| 18 | Too Much Air in the Mold | | | | | | | | |
| 19 | Too Much Air in the Mold | | | | | | | | |
| 20 | Too Much Air in the Mold | | | | | | | | |
| 21 | 0.122 | 0.1216 | 0.123 | 0.1257 | 0.124 | 0.1259 | 58° 50' | 148° 46' | 150° 46' |
| 22 | 0.122 | 0.1219 | 0.126 | 0.1255 | 0.125 | 0.1279 | 58° 50' | 148° 54' | 149° 55' |
| 23 | 0.122 | 0.123 | 0.125 | 0.1244 | 0.125 | 0.1266 | 59° 22' | 148° 30' | 150° 19' |
| 24 | Broke Removing From Model | | | | | | | | |
| 25 | Too Much Air in the Mold | | | | | | | | |
| Maximum | 0.123 | 0.1230 | 0.126 | 0.1263 | 0.125 | 0.1283 | | | |
| Minimum | 0.118 | 0.1208 | 0.119 | 0.1231 | 0.120 | 0.1223 | | | |
| Average | 0.121 | 0.1219 | 0.123 | 0.1250 | 0.123 | 0.1257 | | | |
| Median | 0.121 | 0.1219 | 0.122 | 0.1254 | 0.123 | 0.1264 | | | |
| Standard Deviation | 0.002 | 0.0007 | 0.002 | 0.0011 | 0.002 | 0.0020 | | | |

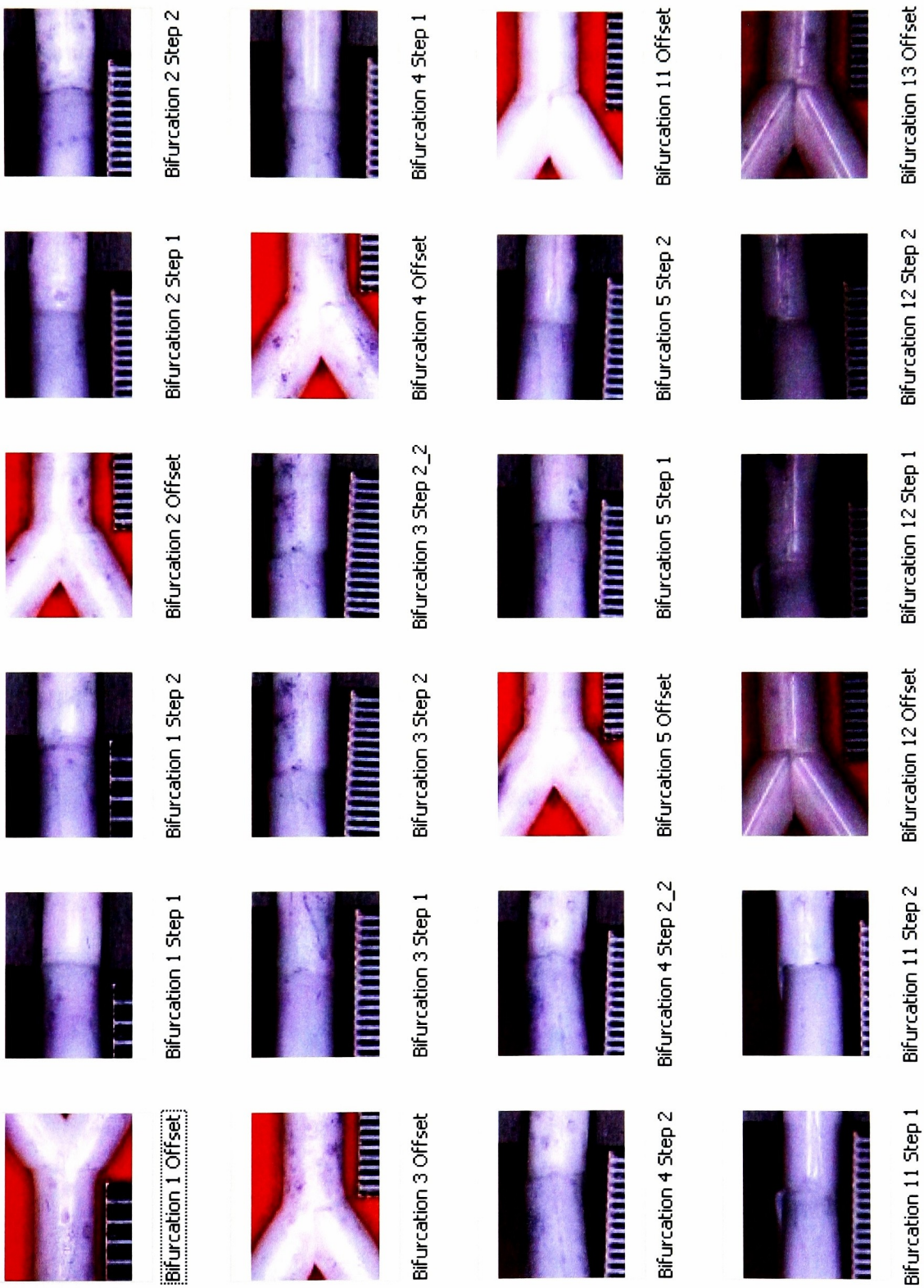


**Figure B.2 Images of variation in bifurcation molds.**

To measure deposition in the bifurcation geometry Dr. Oldham attached two of the Y-bifurcations as shown in Figure B.3. This configuration was utilized to limit the risk of losing particles since there was one inlet and one outlet.

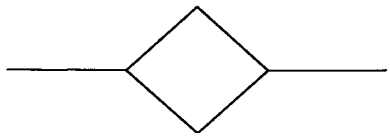

**Figure B.3 Bifurcation geometry tested by Dr. Oldham.**

Dr. Oldham ran several tide velocity at the 18 breaths/min frequency. In all test, 1 μm unit density particles were utilized. The experimental data obtained by Dr. Oldham is contained in Table B.3. The dominate mechanisms for this data were evaluated and as can be seen in Figure B.4, sedimentation is clearly the dominate deposition mechanism for the flow rates investigated by Oldham. It is not until at least 600 cc/min that impaction becomes the dominate deposition mechanism in this geometry. For this reason this data was not utilized to investigate impaction in a bifurcating tube.

**Table B.3 Experimental data obtained for Dr. Oldham's bifurcation geometry.**

| Frequency (breaths/min) | Tidal Volume (cc) | Flow rate (cc/min) | Deposition Efficiency |
|---|---|---|---|
| 18 | 5.6 | 100.8 | 2.05% |
| 18 | 1.7 | 30.6 | 22.20% |
| 18 | 0.6 | 10.8 | 76.00% |
| 18 | 0.06 | 1.08 | 100.00% |

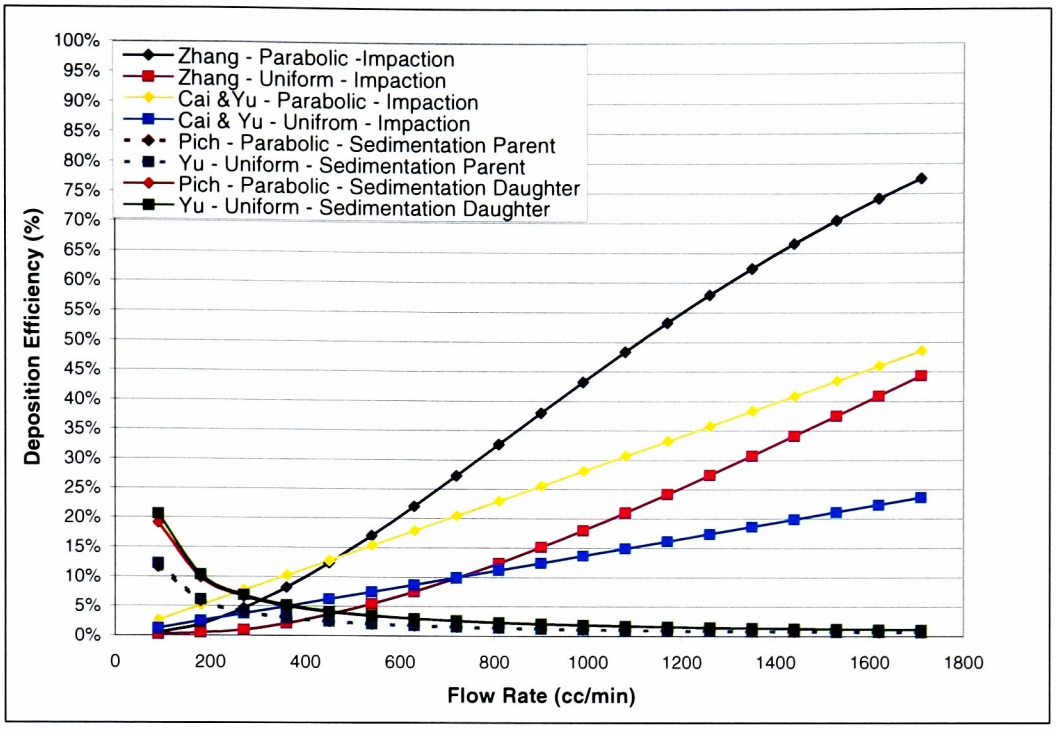


**Figure B.4 Dominate deposition mechanism in the bifurcation at various flow rates.**

# Appendix C

# Check of Wang's Derivation for Horizontal Flow Conditions

Wang's (1975) sedimentation equation for fully developed flow a straight tube circular tube is given as,

$$\eta_s = \frac{2}{\pi}\left[\varepsilon^{1/3}\left(1-\varepsilon^{2/3}\right)^{1/2}\left(2\varepsilon^{2/3}-1\right)+\sin^{-1}\varepsilon^{1/3}\right]. \tag{C.1}$$

Wang's general sedimentation equation is defined as,

$$\eta_s = 1-P-O, \tag{C.2}$$

where P is defined as,

$$P = \frac{2}{\pi}\left[\gamma^{1/2}(1-\gamma)^{1/2}(1-2\gamma)+\sin^{-1}(1-\gamma)^{1/2}\right]. \tag{C.3}$$

In (C.3), γ is defined in Chapter 5 by Equation (5.12), and is defined as,

$$\gamma = \frac{\left(\frac{3V_{ts}L}{8VR}\cos\phi\right)^{2/3}}{\left(1-\frac{V_{ts}}{2V}\sin\phi\right)}. \tag{C.4}$$

When $\phi = 0$, (C.4) simplifies to,

$$\gamma = \left(\frac{3V_{ts}L}{8VR}\right)^{2/3} = \varepsilon^{2/3}, \tag{C.5}$$

making (C.3),

$$P = \frac{2}{\pi}\left[\varepsilon^{1/3}\left(1-\varepsilon^{2/3}\right)^{1/2}\left(1-2\varepsilon^{2/3}\right)+\sin^{-1}\left(1-\varepsilon^{2/3}\right)^{1/2}\right]. \tag{C.6}$$

In (C.2), O is defined as,

$$O = 1-\frac{1}{\pi}\left[3\sigma^{1/2}(1-\sigma)^{1/2}+\sin^{-1}(1-\sigma)^{1/2}+\left(1-9\sigma^2\right)\sin^{-1}\left(\frac{1-\sigma}{1+3\sigma}\right)^{1/2}\right], \tag{C.7}$$

where σ, is defined in Chapter 5 by Equation (5.11), and is defined as,

$$\sigma = \frac{\frac{V_{ts}}{6V}\sin\phi}{\left(1-\frac{V_{ts}}{2V}\sin\phi\right)}. \qquad \textbf{(C.8)}$$

When $\phi = 0$, (C.8) simplifies to 0, making (C.7),

$$\begin{aligned} O &= 1-\frac{1}{\pi}\left[\sin^{-1}\sqrt{1}+\sin^{-1}\sqrt{1}\right] \\ &= 1-\frac{2}{\pi}\sin^{-1}\sqrt{1} \end{aligned} \qquad \textbf{(C.9)}$$

Substituting (C.6) and (C.9) into (C.2) provides,

$$\begin{aligned} \eta_s = 1-\frac{2}{\pi}\Bigg[\varepsilon^{1/3}\left(1-\varepsilon^{2/3}\right)^{1/2}\left(1-2\varepsilon^{2/3}\right)+\sin^{-1}\left(1-\varepsilon^{2/3}\right)^{1/2}\Bigg], \\ -\left[1-\frac{2}{\pi}\sin^{-1}\sqrt{1}\right] \end{aligned} \qquad \textbf{(C.10)}$$

which simplifies to,

$$\eta_s = \frac{2}{\pi}\left[\varepsilon^{1/3}\left(1-\varepsilon^{2/3}\right)^{1/2}\left(2\varepsilon^{2/3}-1\right)-\sin^{-1}\left(1-\varepsilon^{2/3}\right)^{1/2}+\sin^{-1}\sqrt{1}\right]. \qquad \textbf{(C.11)}$$

(C.11) is not equal to (C.1) when $\phi = 0$. The difference in (C.1) and (C.11) results in a 10% difference in deposition efficiency for all values of $\varepsilon$, see Figure C.1. Due to Wang's miscalculation, his equation for uphill parabolic flow can not be utilized for horizontal tubes.

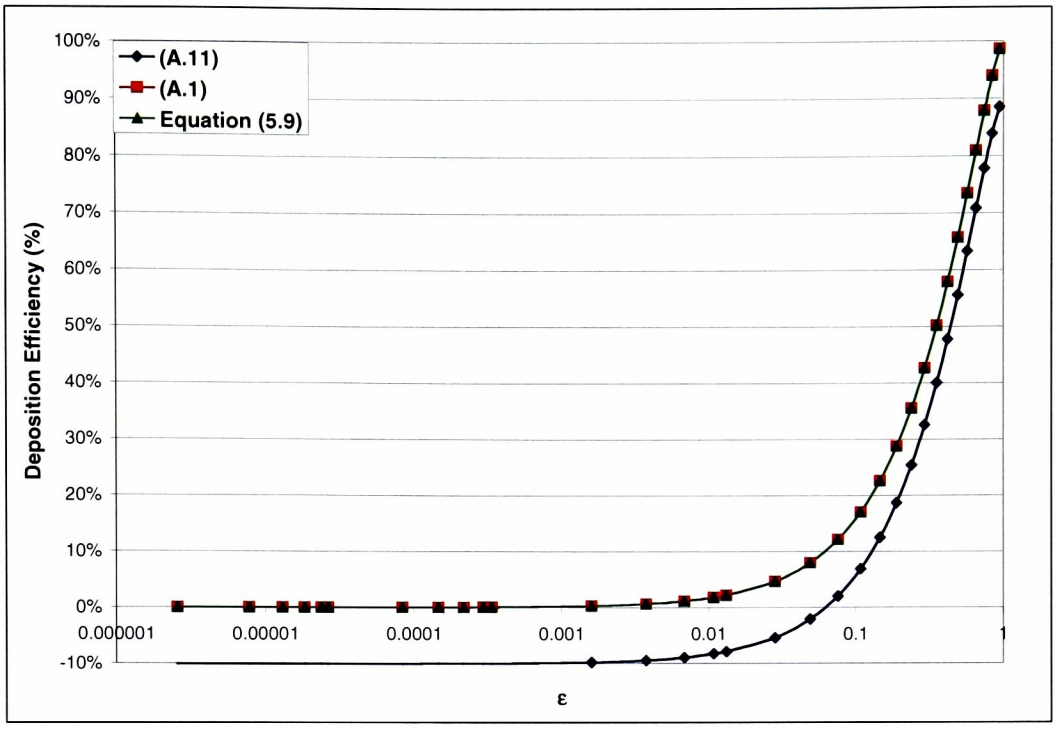


**Figure C.1 Comparison of Wang's different equations for sedimentation from parabolic flow in a horizontal circular tube.**

# Appendix D

# Velocity Profiles in the Various Geometries

## D.1 Straight Tube Velocity Profiles

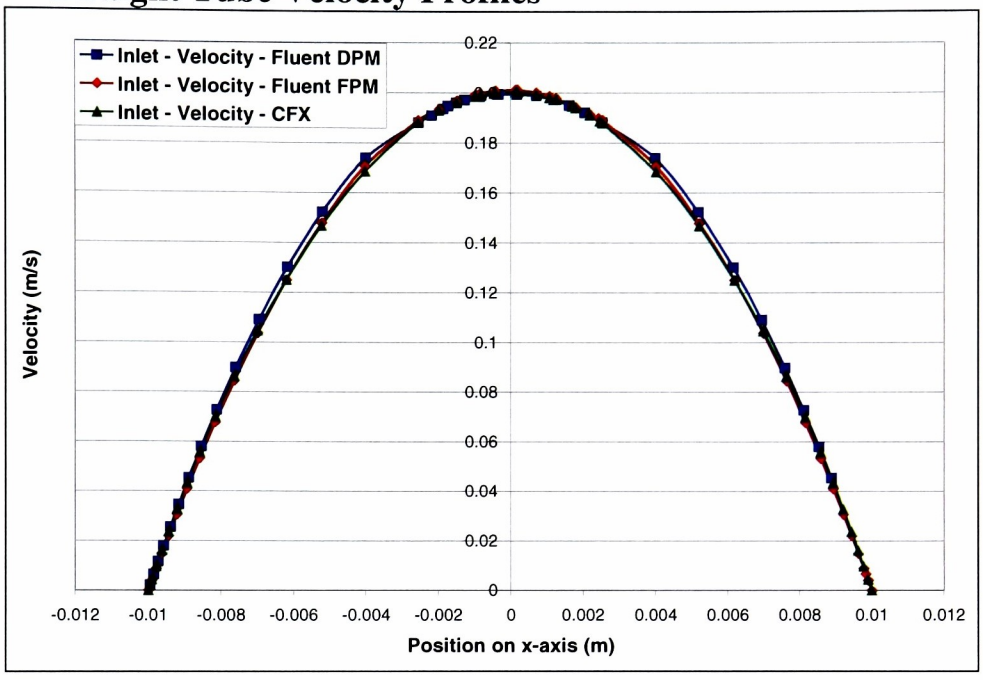


**Figure D.1 Parabolic velocity profile 1 mm from the inlet of the straight tube for sedimentation runs.**

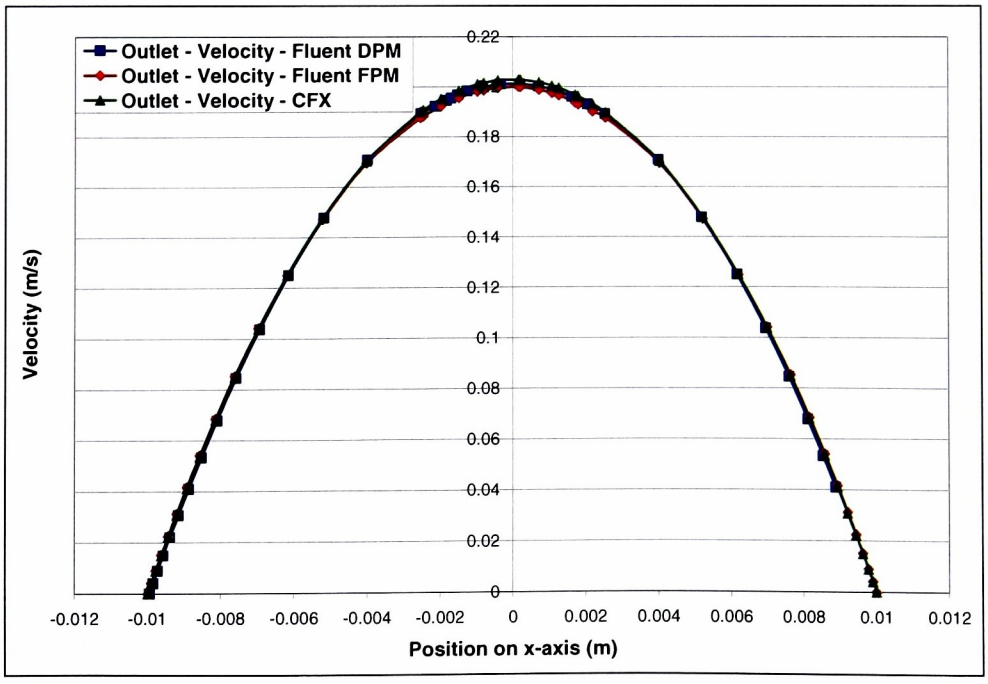


**Figure D.2 Parabolic velocity profile 10 mm from the outlet of the straight tube for sedimentation runs.**

The slight variation seen in Figure D.1 and Figure D.2 is due to the software packages sampling at different locations.

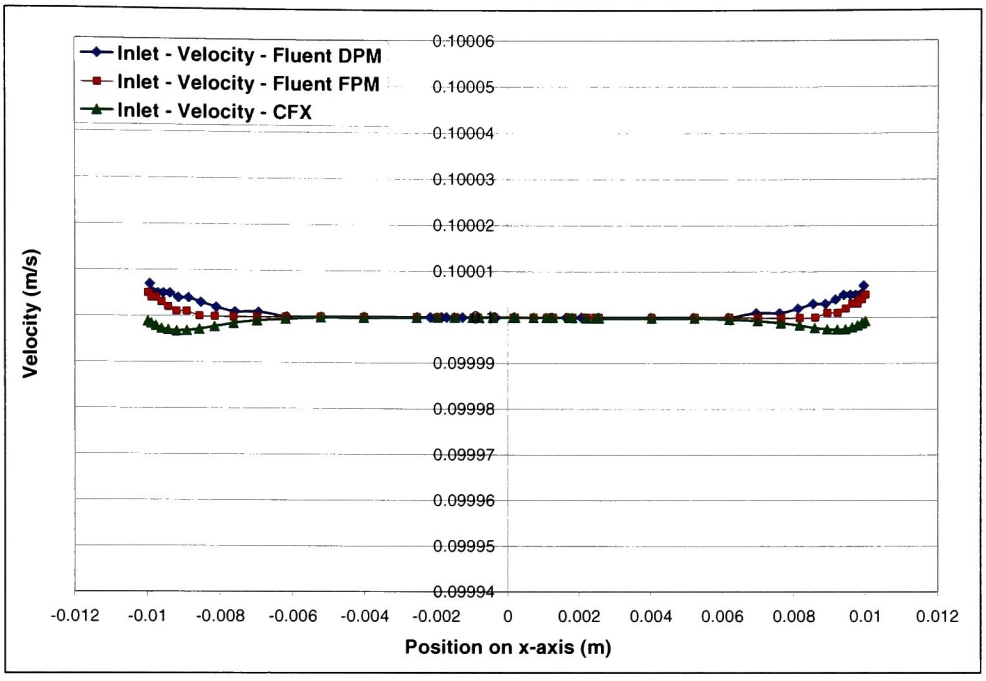


**Figure D.3 Uniform velocity profile 1 mm from the inlet of the straight tube for sedimentation runs.**

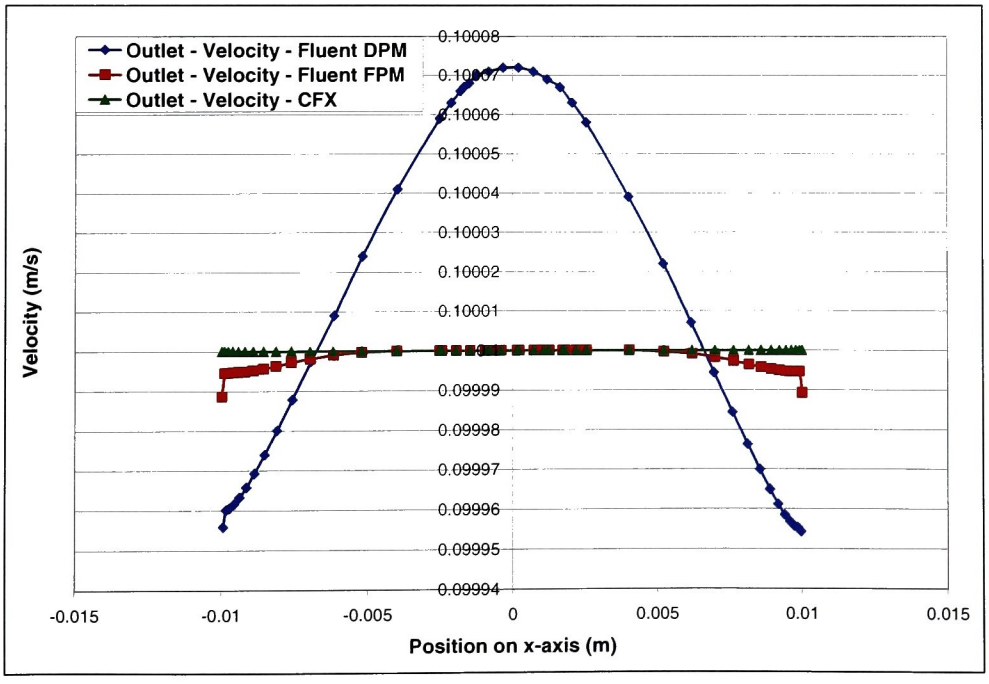


**Figure D.4 Uniform velocity profile 10 mm for the outlet of the straight tube for sedimentation runs.**

In Figure D.3 and Figure D.4, the variation in velocity profiles is on the order of 0.01 mm/s when compared to the parabolic profiles the uniform profiles are flat.

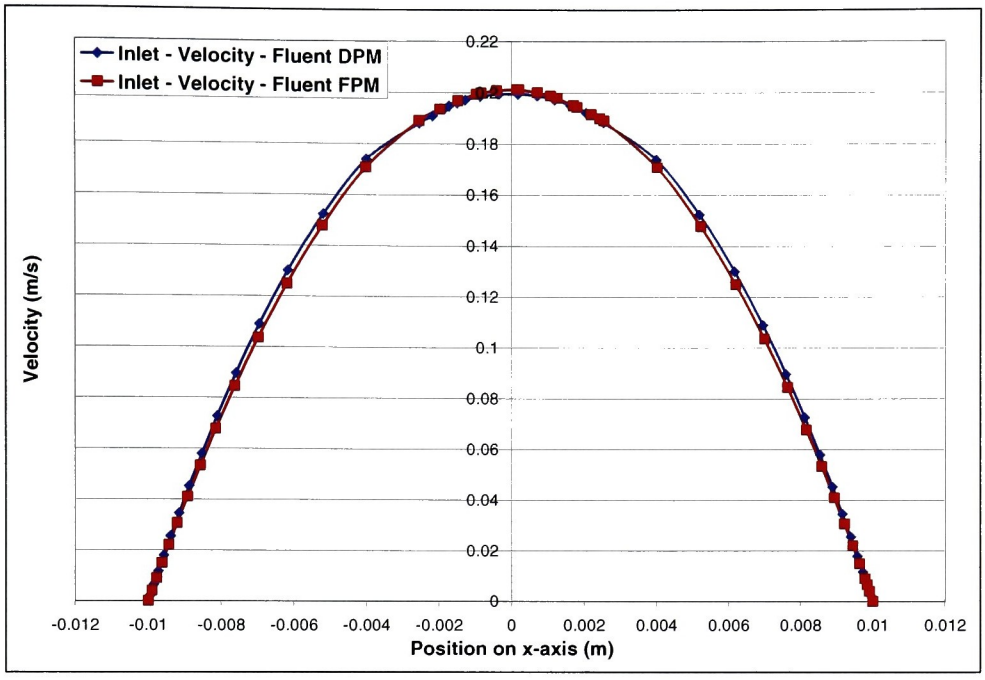


**Figure D.5 Parabolic velocity profile 1 mm from the inlet of the straight tube for diffusion runs.**

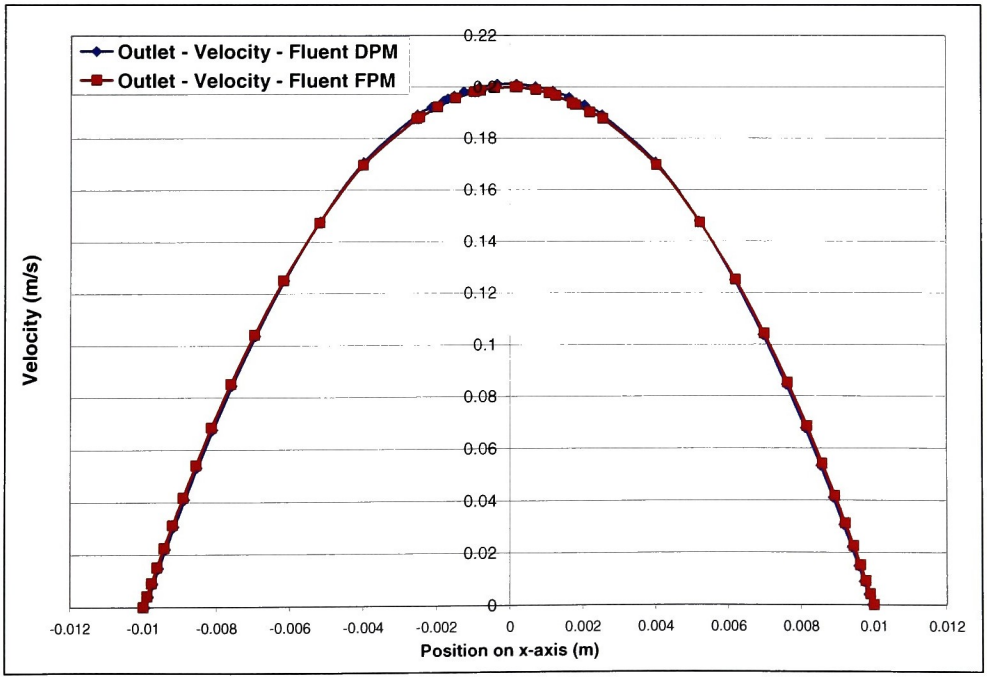


**Figure D.6 Uniform velocity profile 1 mm from the inlet of the straight tube for diffusion runs.**

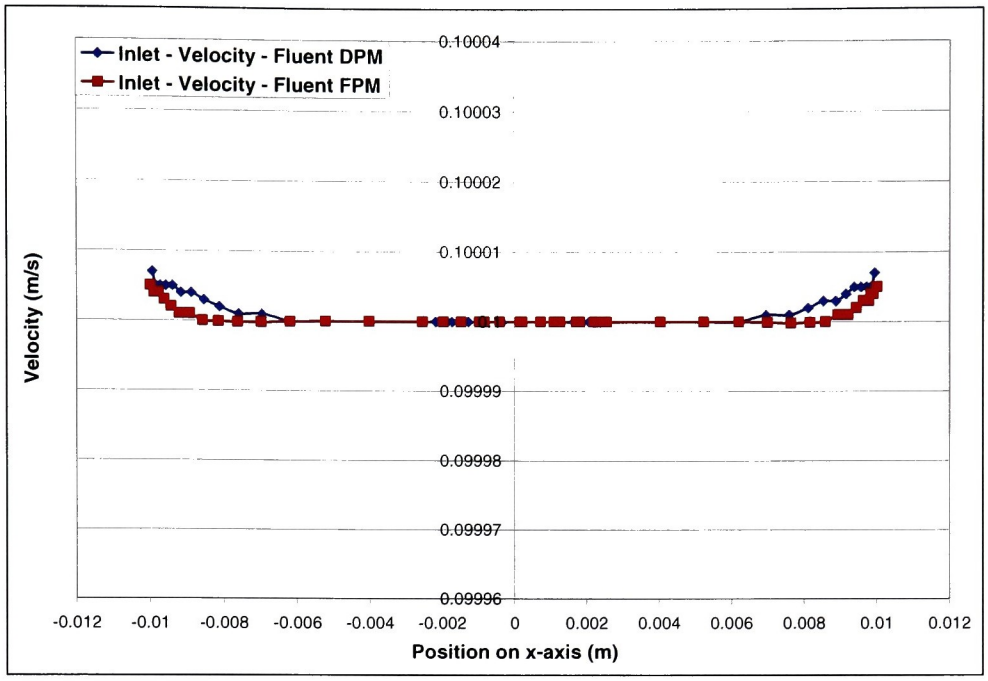


**Figure D.7 Uniform velocity profile 1 mm from the inlet of the straight tube for diffusion runs.**

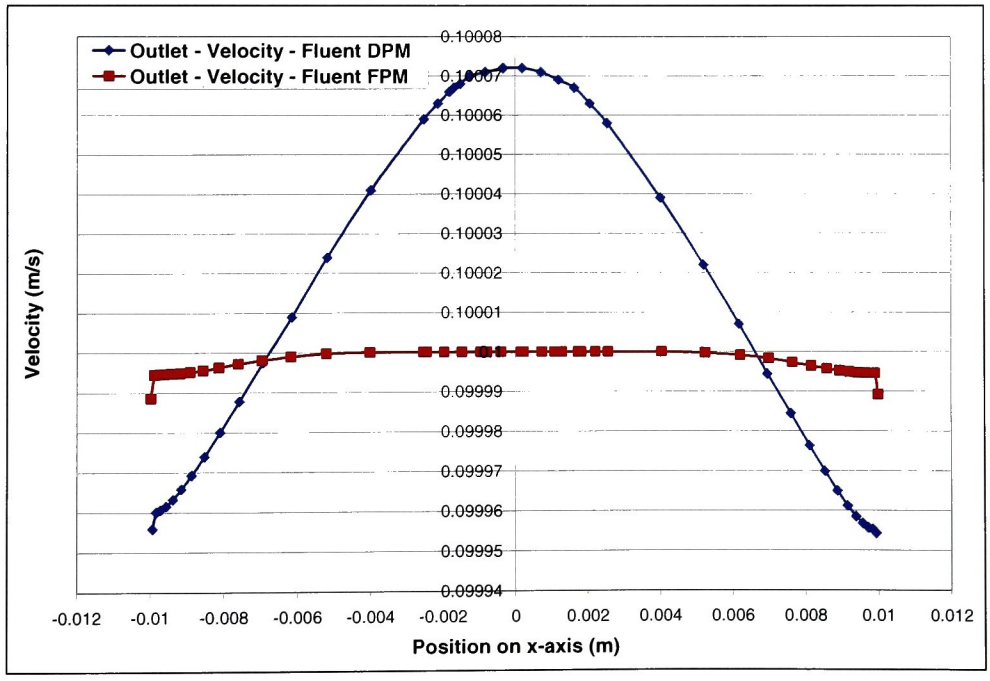


**Figure D.8 Uniform velocity profile 10 mm for the outlet of the straight tube for diffusion runs.**

## D.2 Bifurcating Tube Velocity Profiles

CFX is not capable of generating velocity profiles along cuts in terms of the cut plane length; therefore only Fluent DPM data is presented in the flowing graphs.

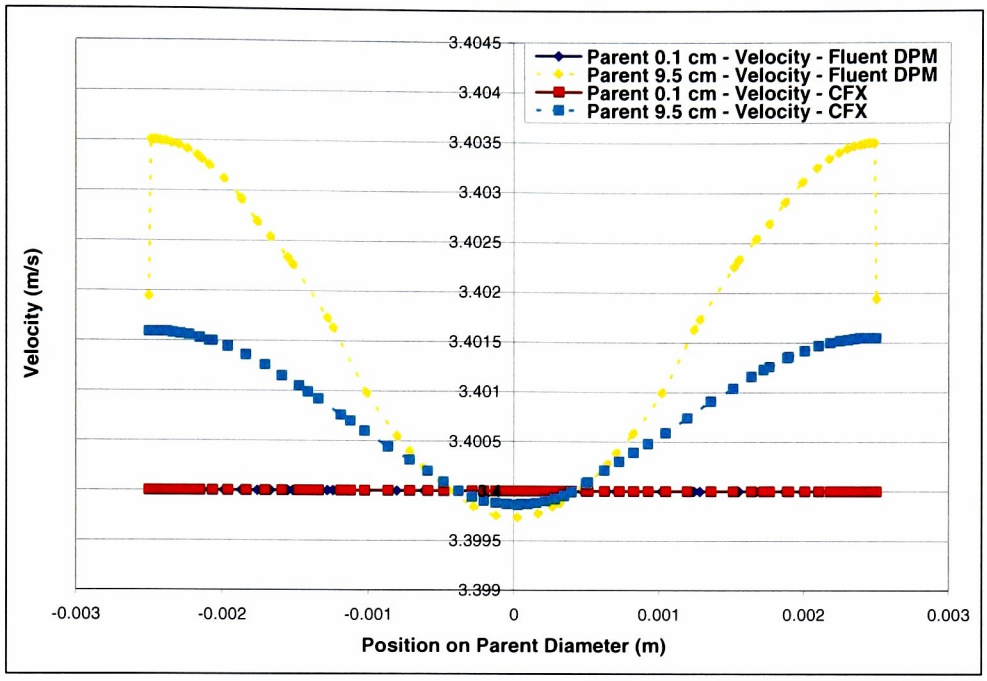


**Figure D.9 Uniform velocity profile at 4 lpm flow rate in the parent generation of the bifurcating tube for impaction runs.**

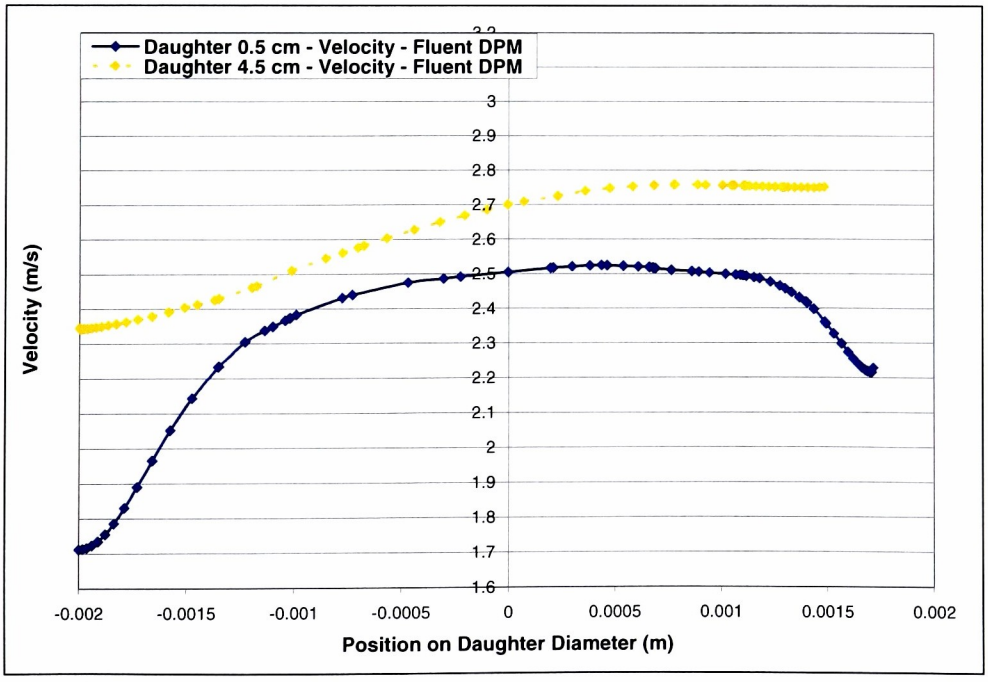


**Figure D.10 Uniform velocity profile at 4 lpm flow rate in the daughter generation of the bifurcating tube for impaction runs.**

Additionally, although all profiles were visual examine in both CFX and Fluent DPM, due to the immense time requirement to get data out of CFX only Fluent DPM's profiles are presented at some flow conditions.

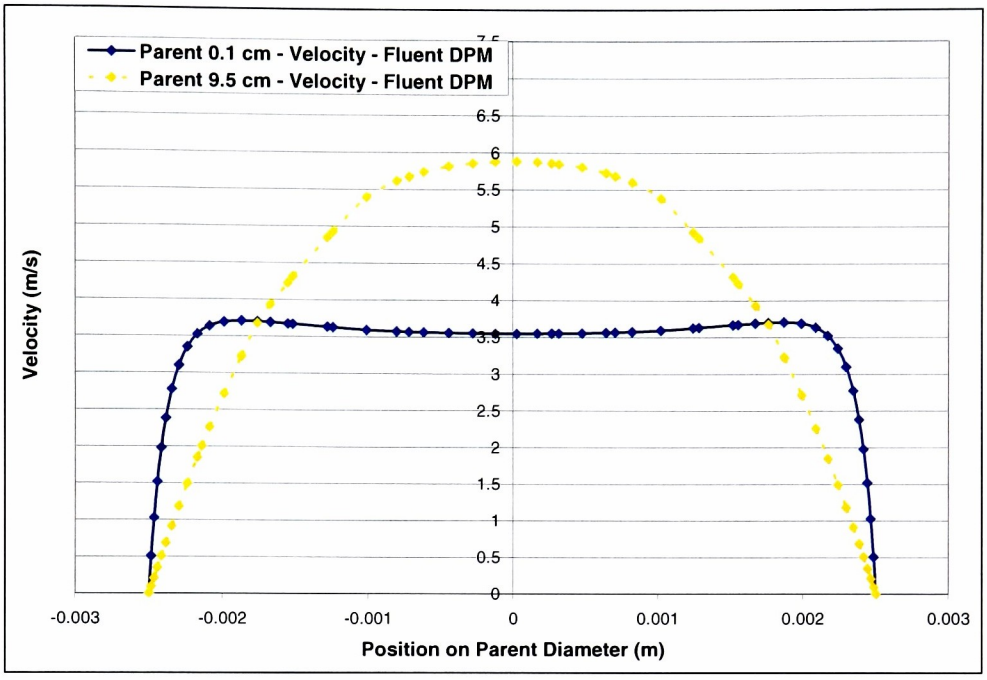


**Figure D.11 Developing velocity profile at 4 lpm flow rate in the parent generation of the bifurcating tube for impaction runs.**

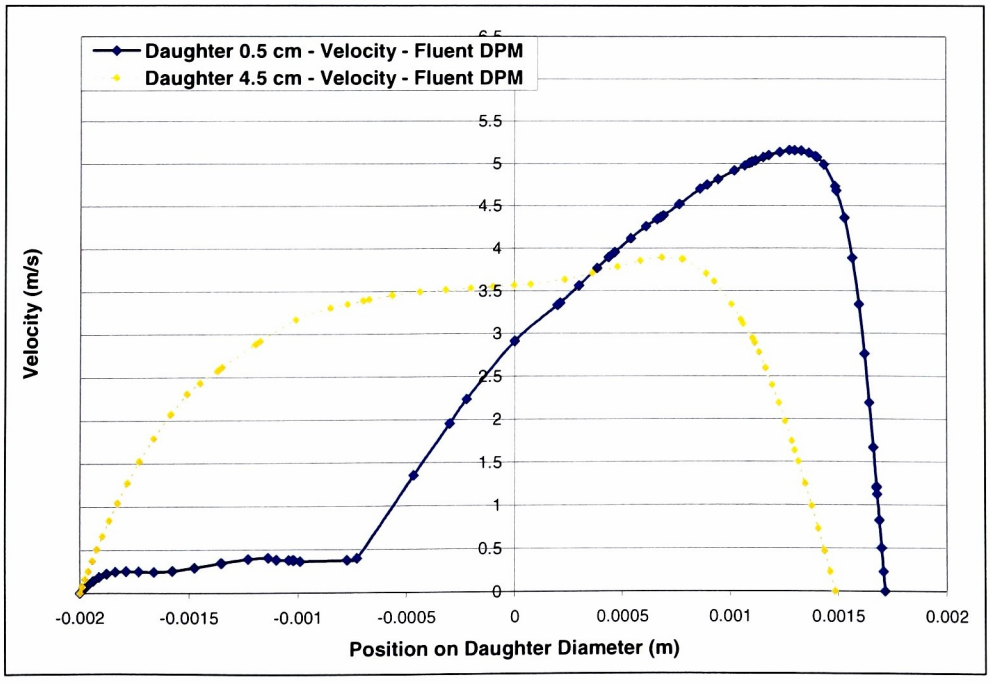


**Figure D.12 Developing velocity profile at 4 lpm flow rate in the daughter generation of the bifurcating tube for impaction runs.**

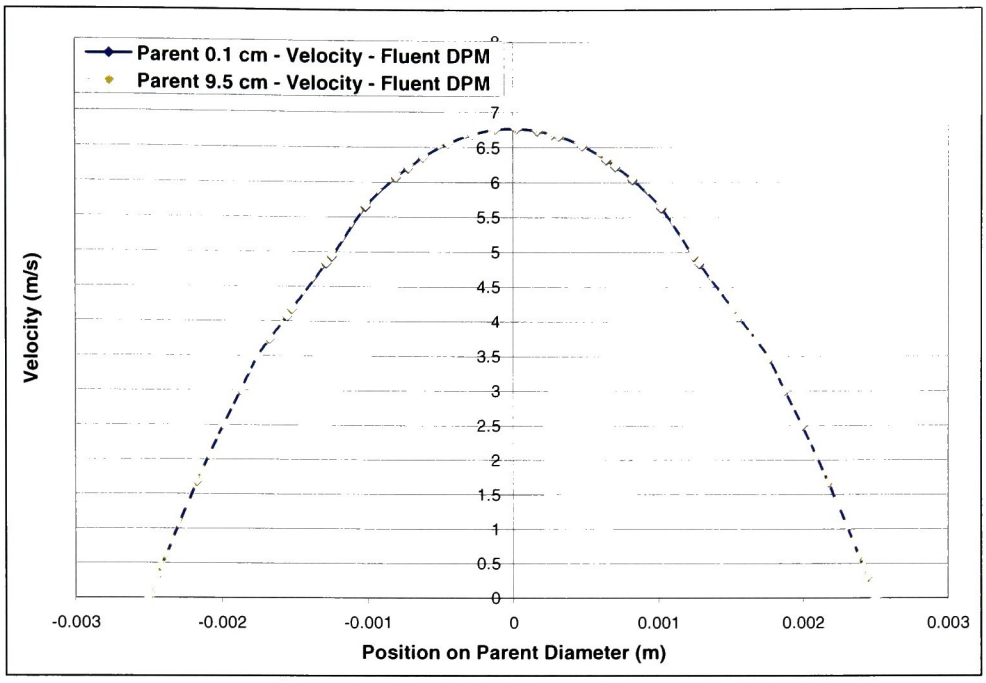


**Figure D.13 Parabolic velocity profile at 4 lpm flow rate in the parent generation of the bifurcating tube for impaction runs.**

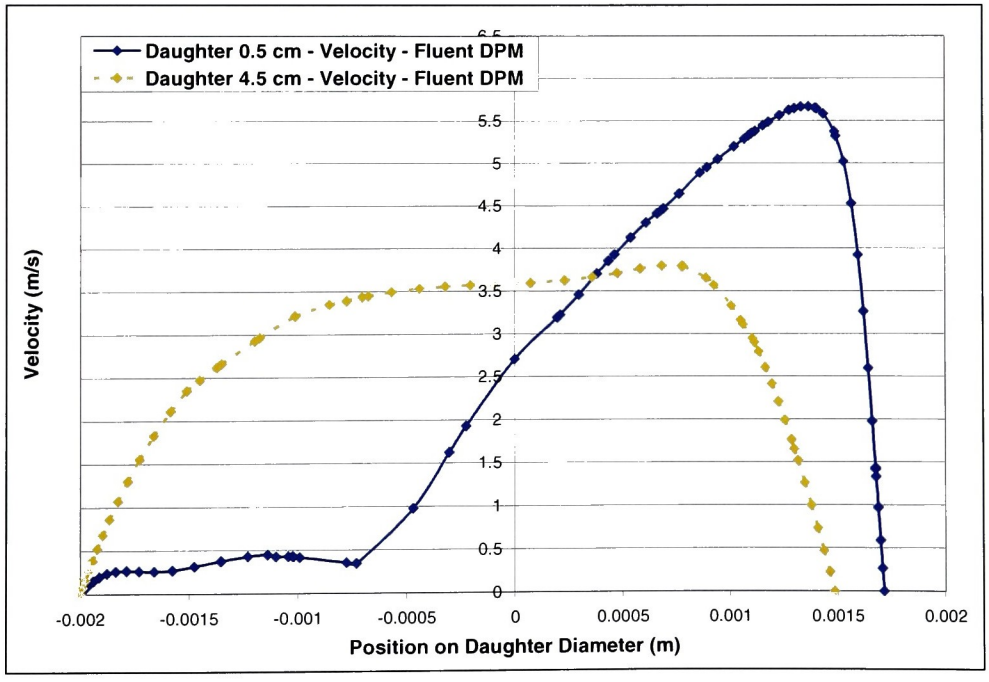


**Figure D.14 Parabolic velocity profile at 4 lpm flow rate in the daughter generation of the bifurcating tube for impaction runs.**

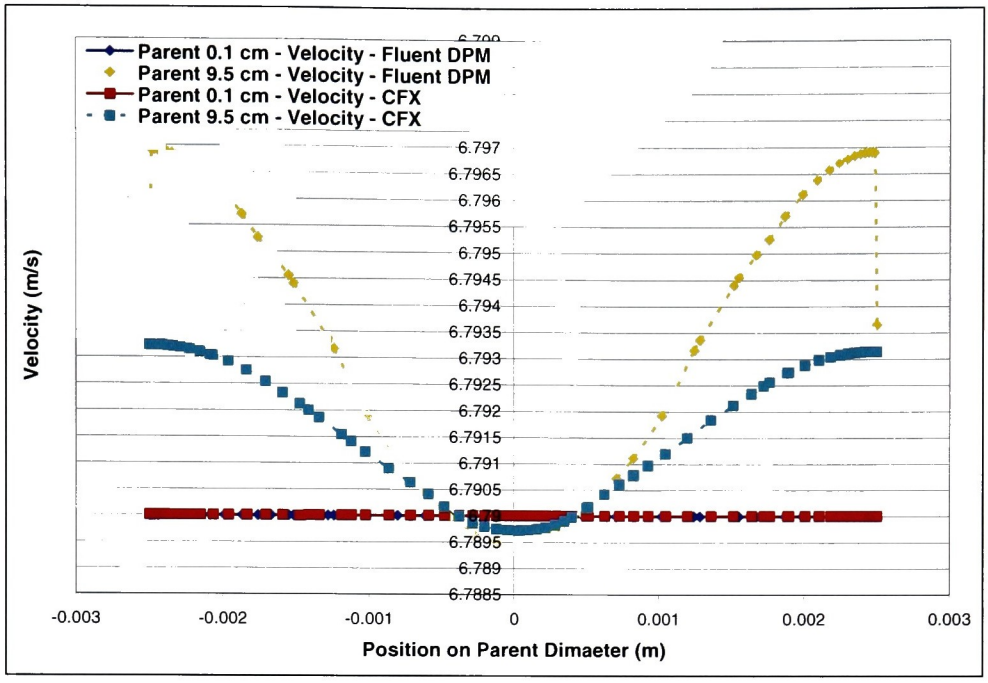


**Figure D.15 Uniform velocity profile at 8 lpm flow rate in the parent generation of the bifurcating tube for impaction runs.**

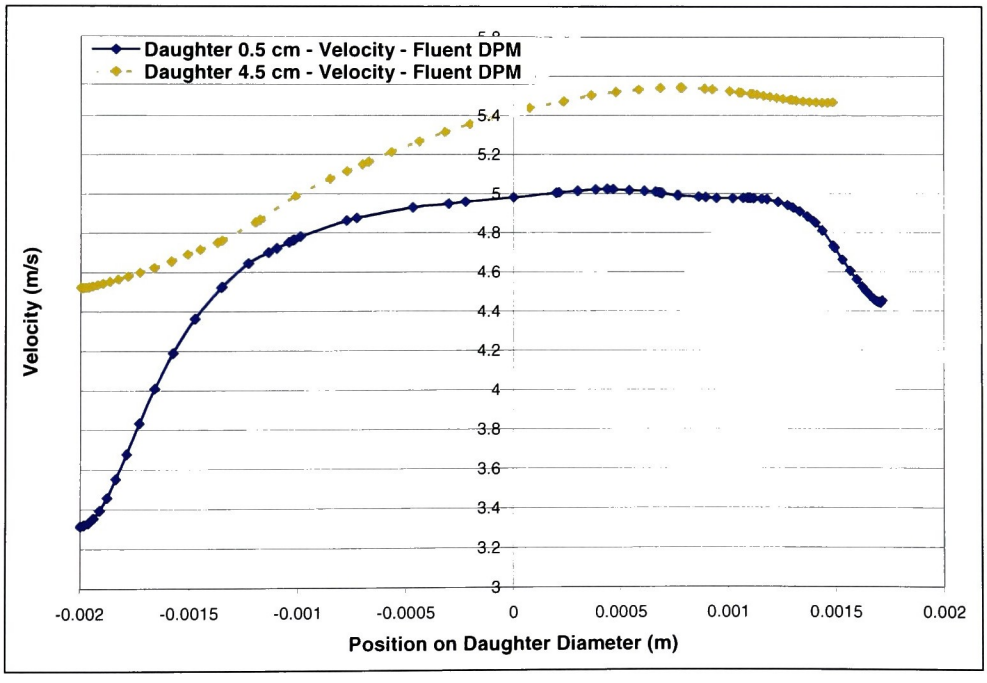


**Figure D.16 Uniform velocity profile at 8 lpm flow rate in the daughter generation of the bifurcating tube for impaction runs.**

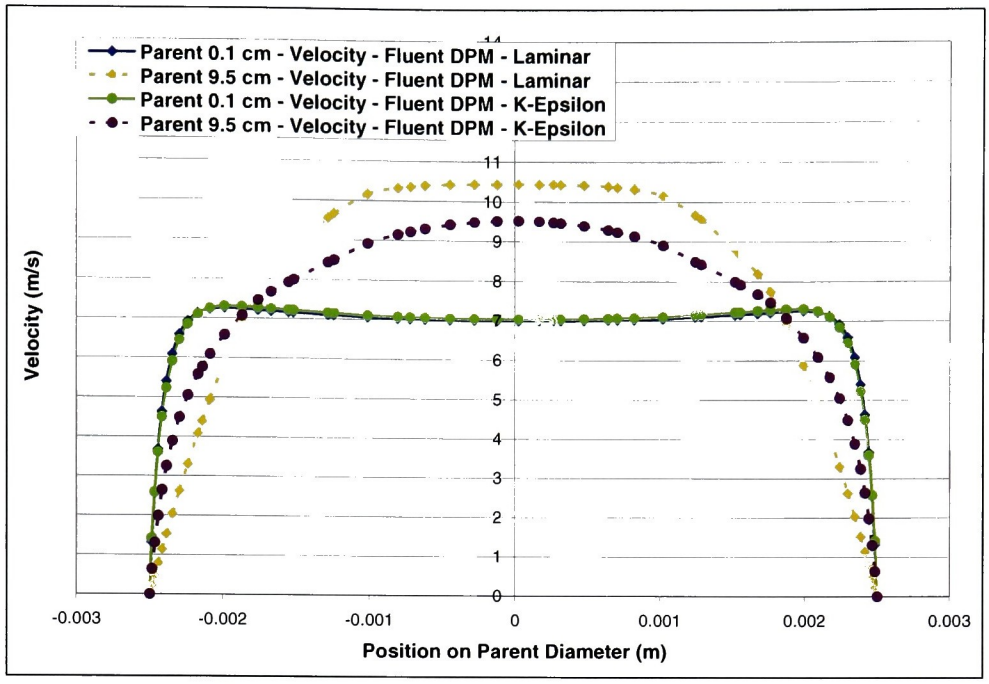


**Figure D.17 Developing velocity profile at 8 lpm flow rate in the parent generation of the bifurcating tube for impaction runs.**

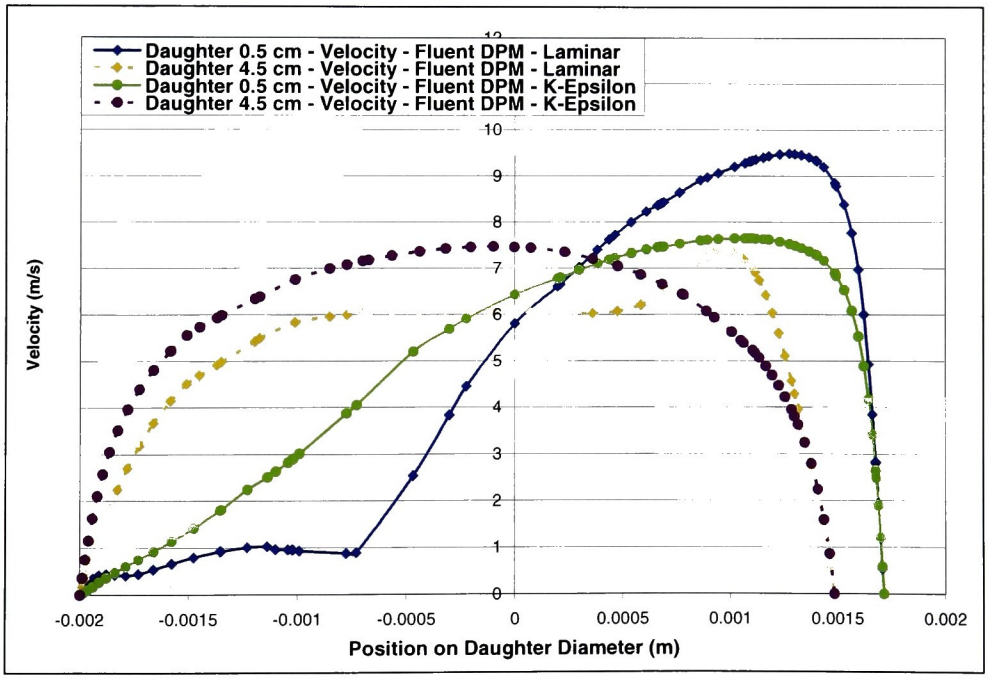


**Figure D.18 Developing velocity profile at 8 lpm flow rate in the daughter generation of the bifurcating tube for impaction runs.**

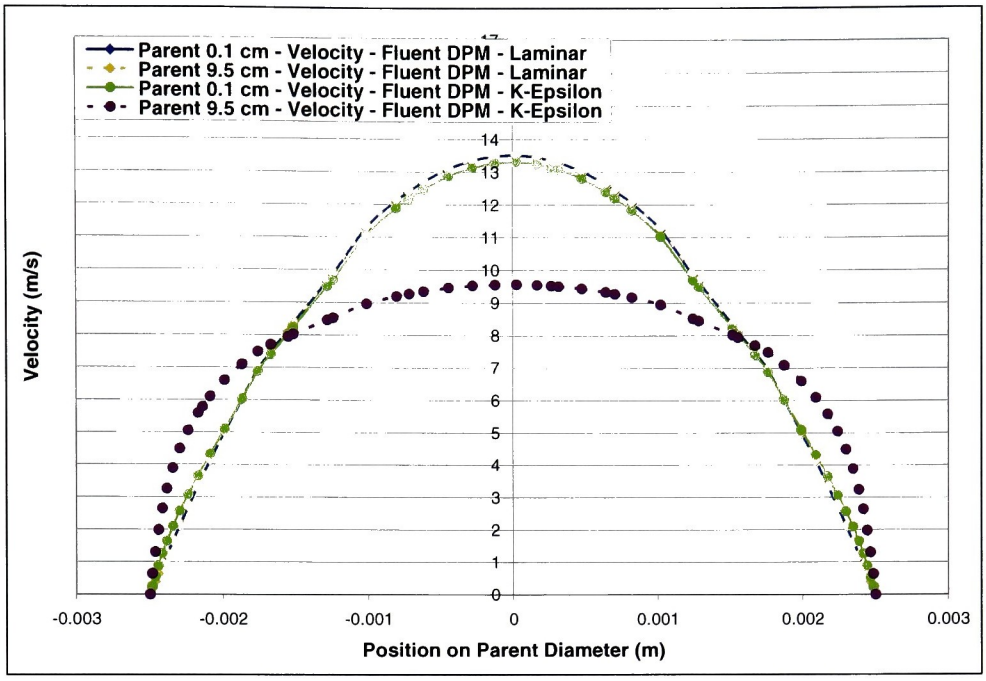


**Figure D.19 Parabolic velocity profile at 8 lpm flow rate in the parent generation of the bifurcating tube for impaction runs.**

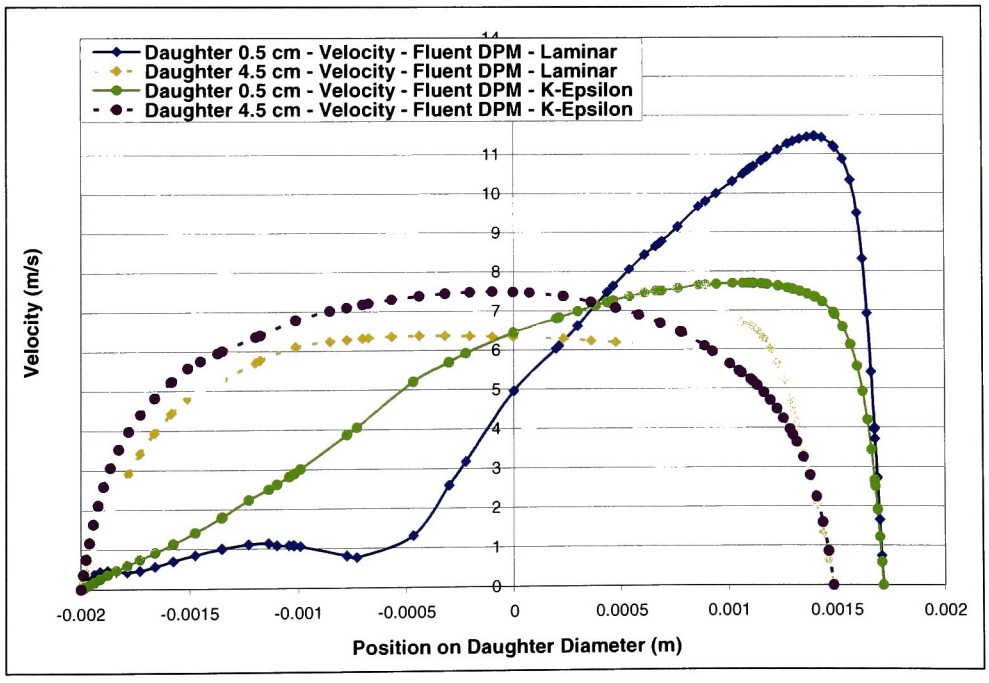


**Figure D.20 Parabolic velocity profile at 8 lpm flow rate in the daughter generation of the bifurcating tube for impaction runs.**

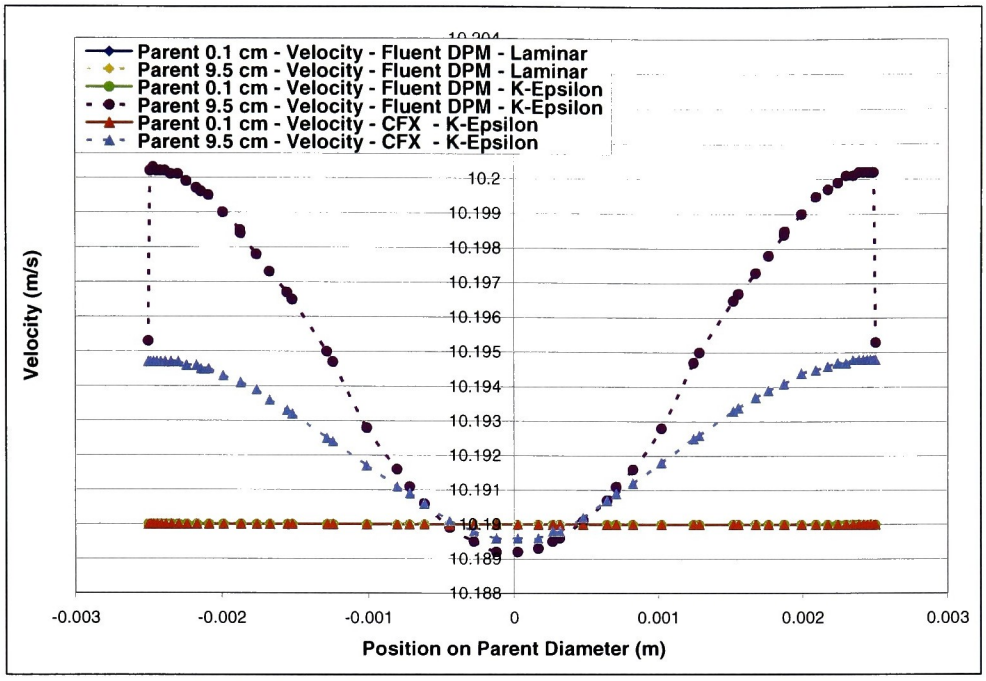


**Figure D.21 Uniform velocity profile at 12 lpm flow rate in the parent generation of the bifurcating tube for impaction runs.**

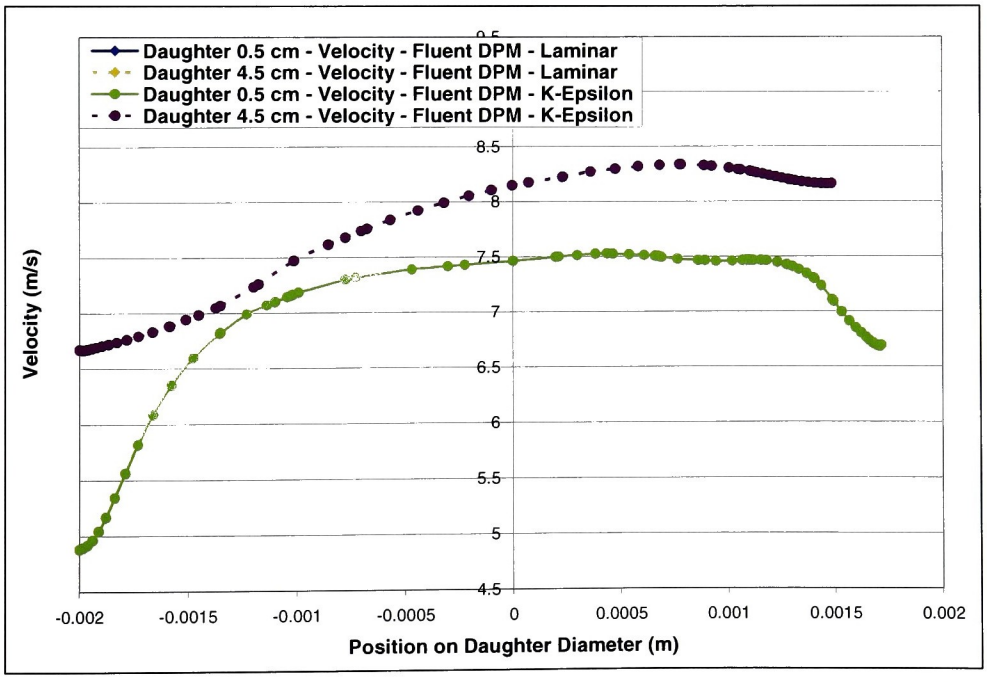


**Figure D.22 Uniform velocity profile at 12 lpm flow rate in the daughter generation of the bifurcating tube for impaction runs.**

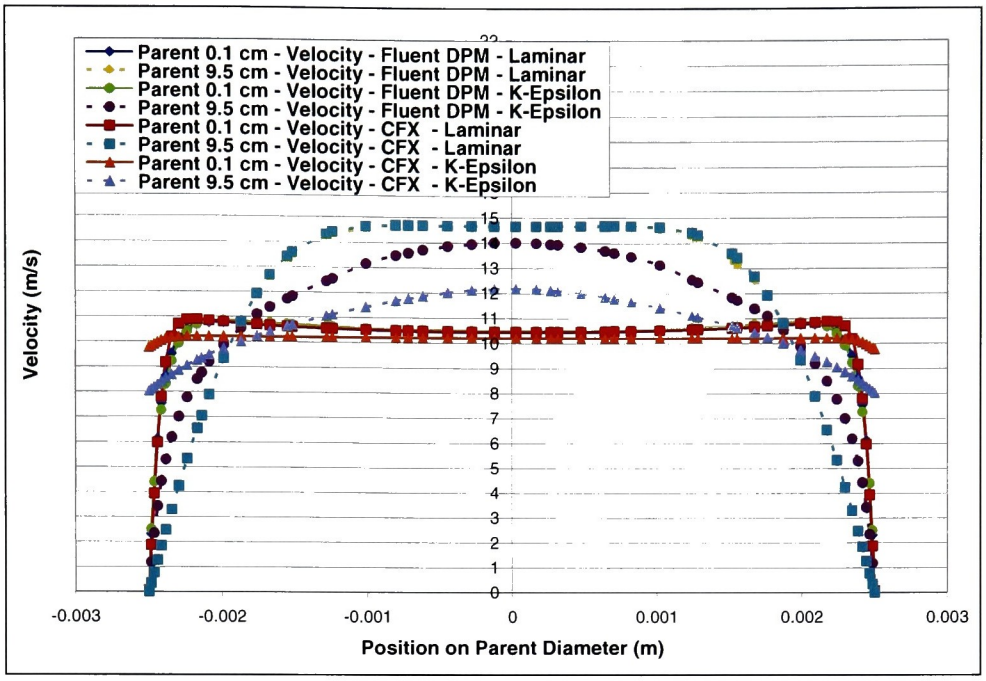


**Figure D.23 Developing velocity profile at 12 lpm flow rate in the parent generation of the bifurcating tube for impaction runs.**

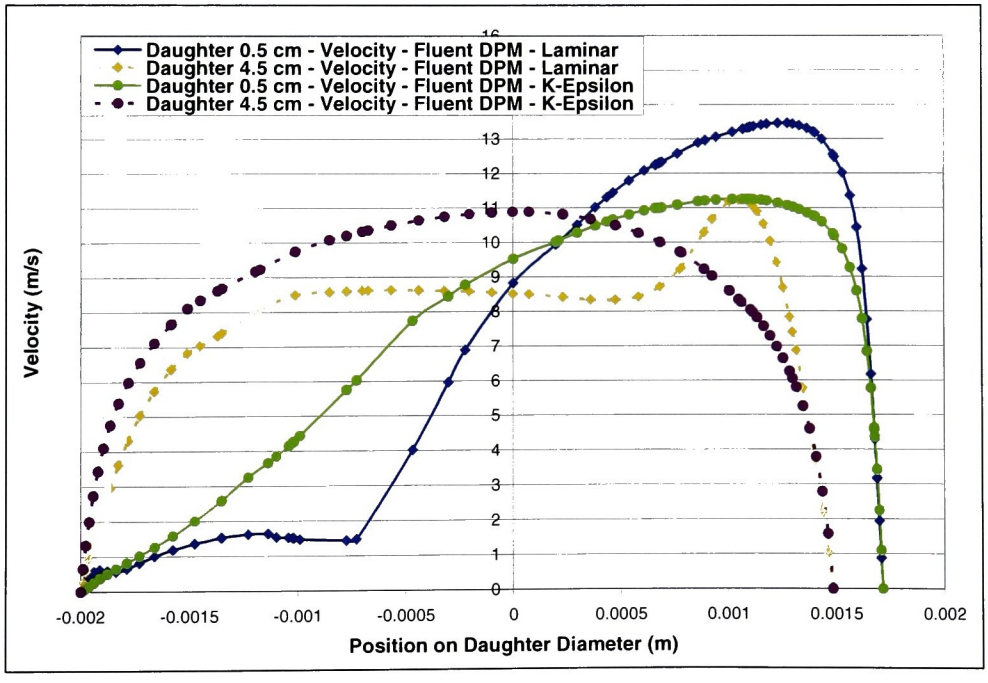


**Figure D.24 Developing velocity profile at 12 lpm flow rate in the parent generation of the bifurcating tube for impaction runs.**

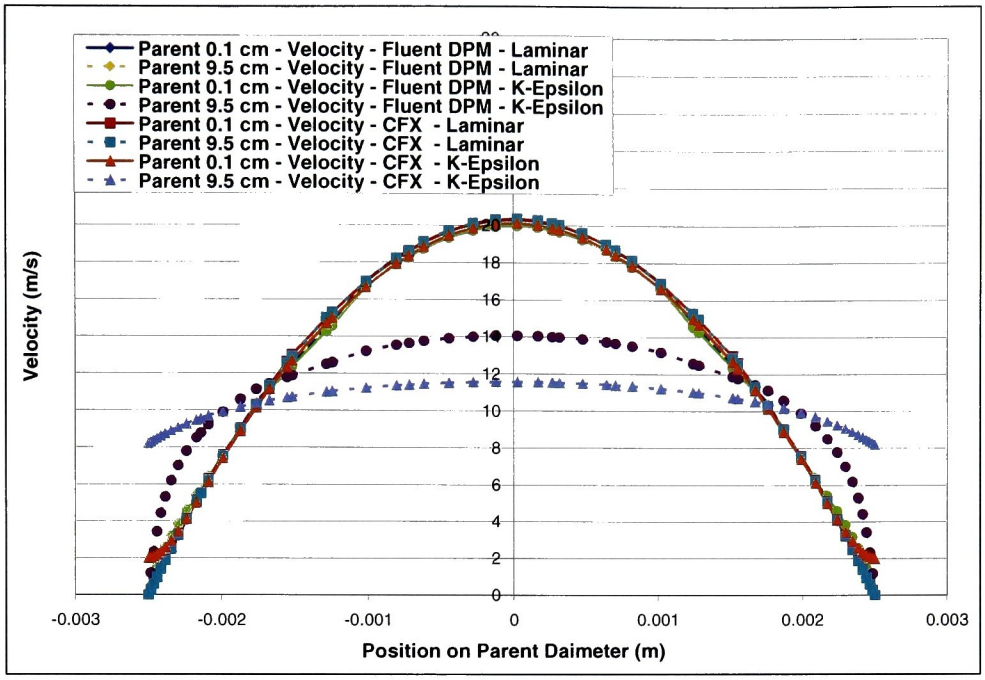


**Figure D.25 Parabolic velocity profile at 12 lpm flow rate in the parent generation of the bifurcating tube for impaction runs.**

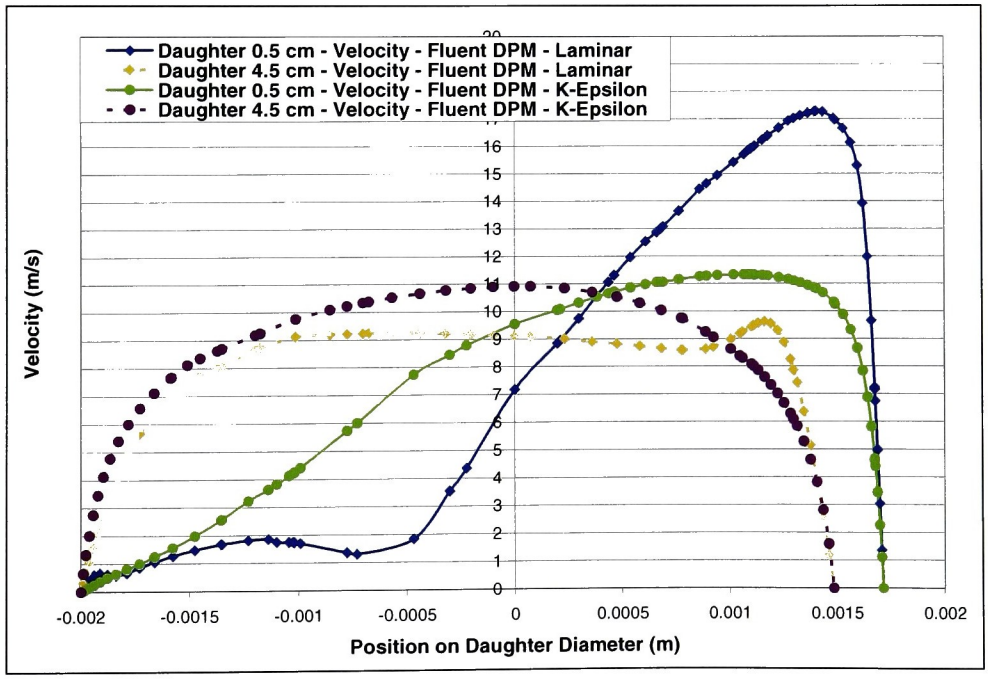


**Figure D.26 Parabolic velocity profile at 12 lpm flow rate in the daughter generation of the bifurcating tube for impaction runs.**

## D.3 Three Generation Lung Geometry Velocity Profiles

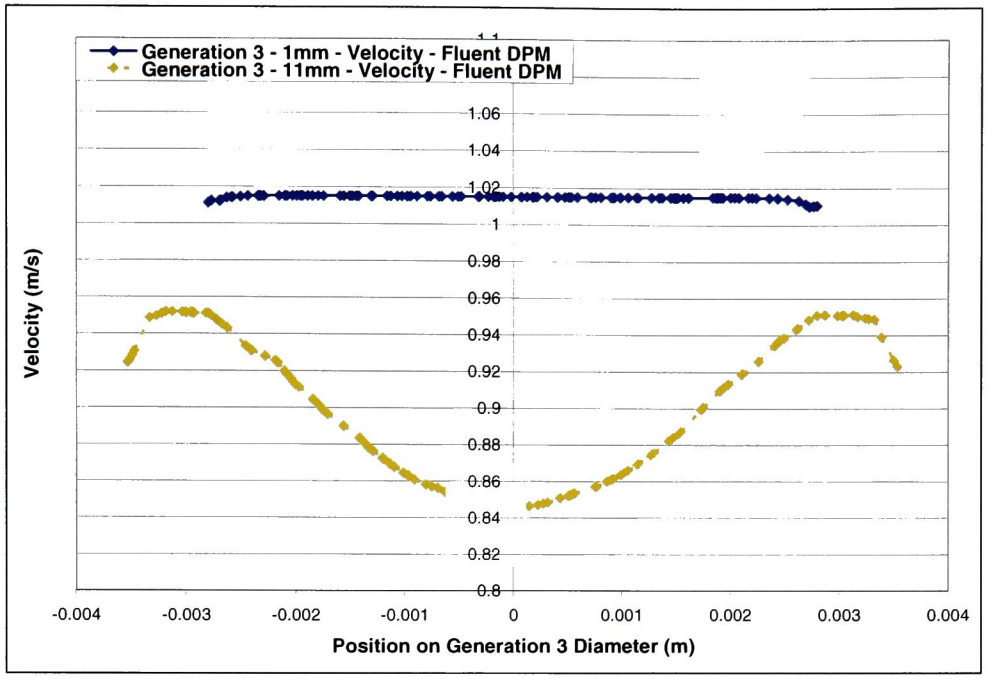


**Figure D.27 Uniform velocity profile at 1.5 lpm flow rate in generation three of the three generation lung geometry.**

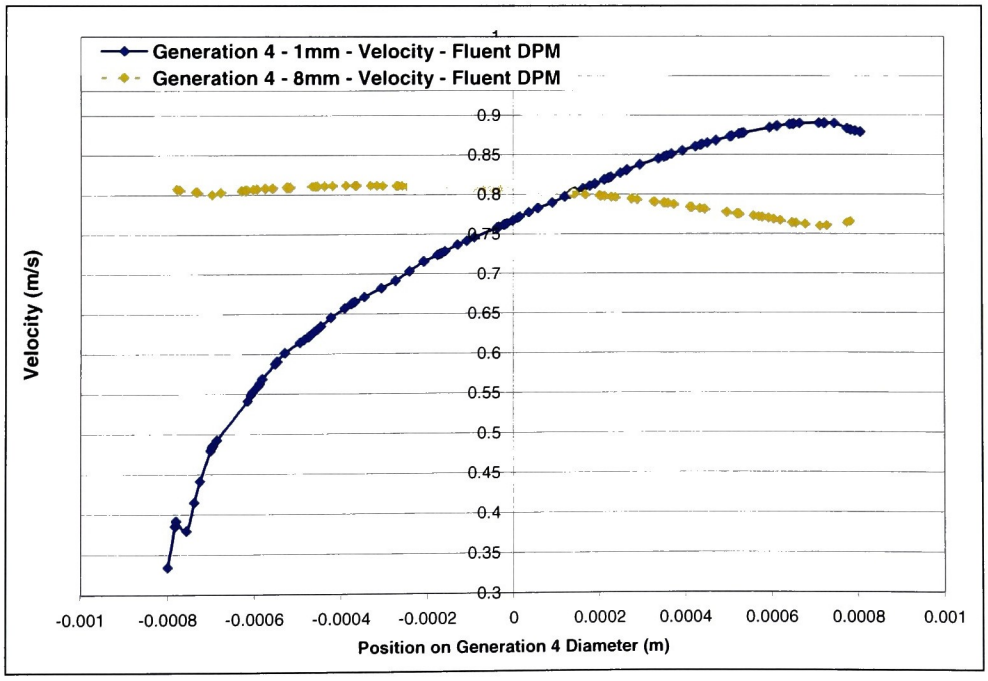


**Figure D.28 Uniform velocity profile at 1.5 lpm flow rate in generation four of the three generation lung geometry.**

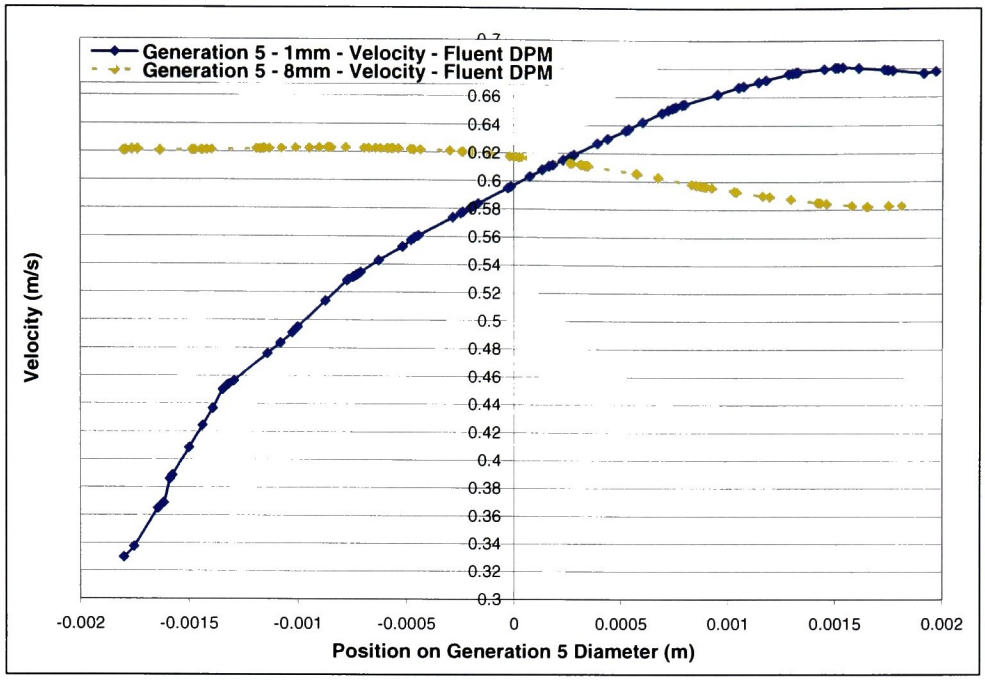


**Figure D.29 Uniform velocity profile at 1.5 lpm flow rate in generation five of the three generation lung geometry.**

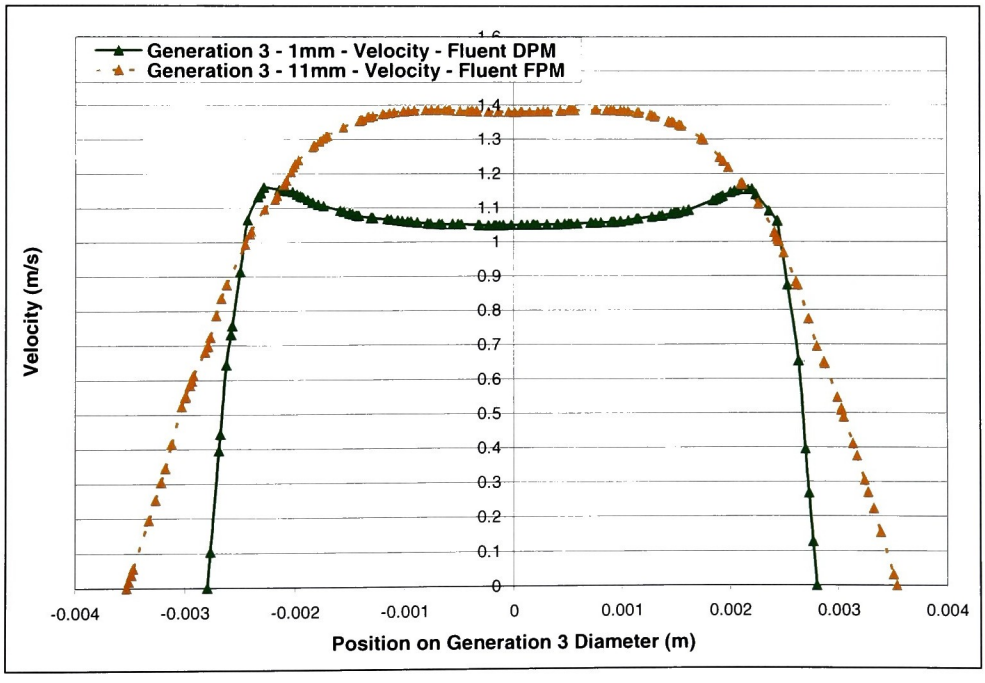


**Figure D.30 Developing velocity profile at 1.5 lpm flow rate in generation three of the three generation lung geometry.**

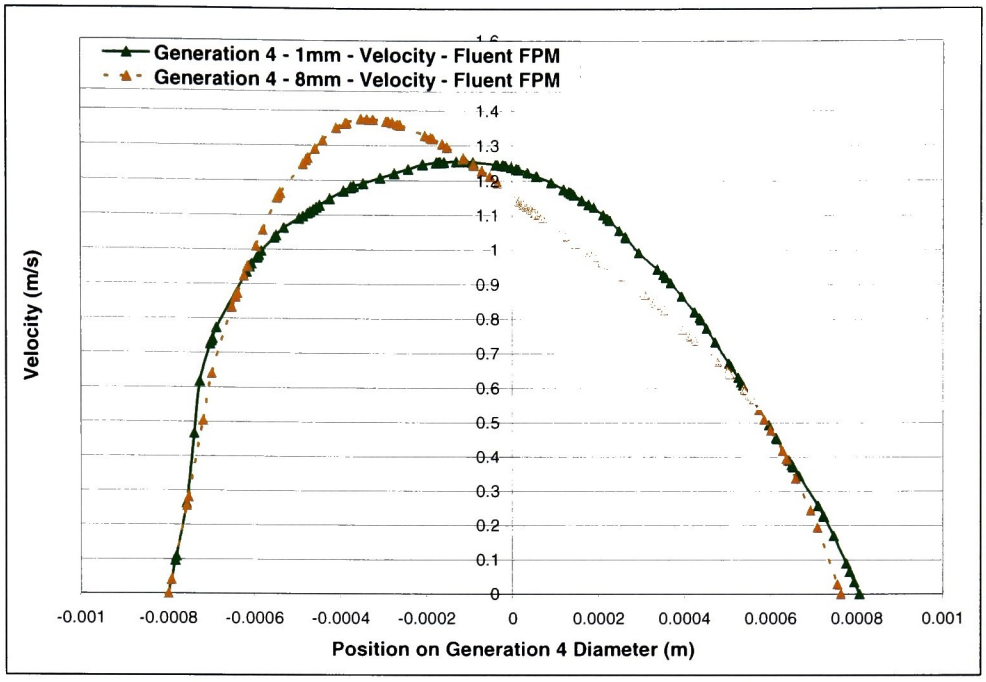


**Figure D.31 Developing velocity profile at 1.5 lpm flow rate in generation four of the three generation lung geometry.**

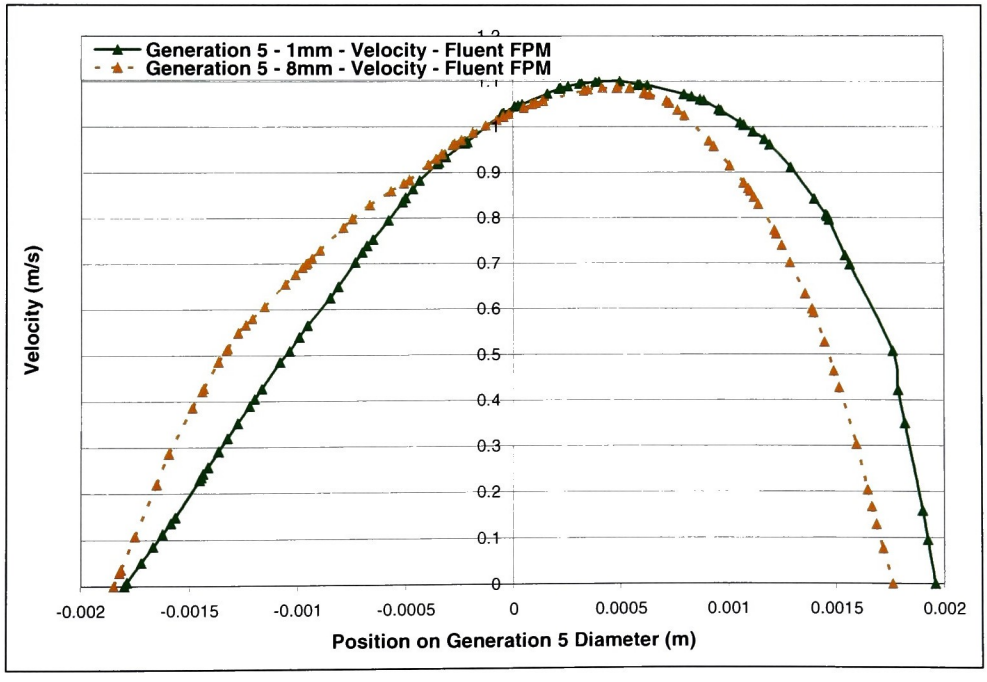


**Figure D.32 Developing velocity profile at 1.5 lpm flow rate in generation five of the three generation lung geometry.**

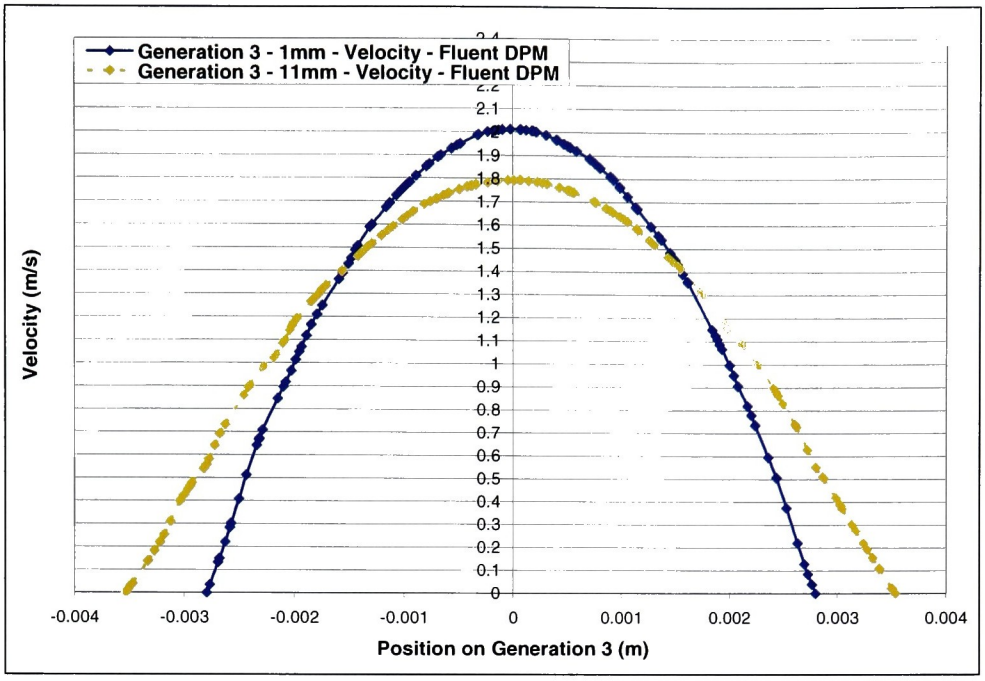


**Figure D.33 Parabolic velocity profile at 1.5 lpm flow rate in generation three of the three generation lung geometry.**

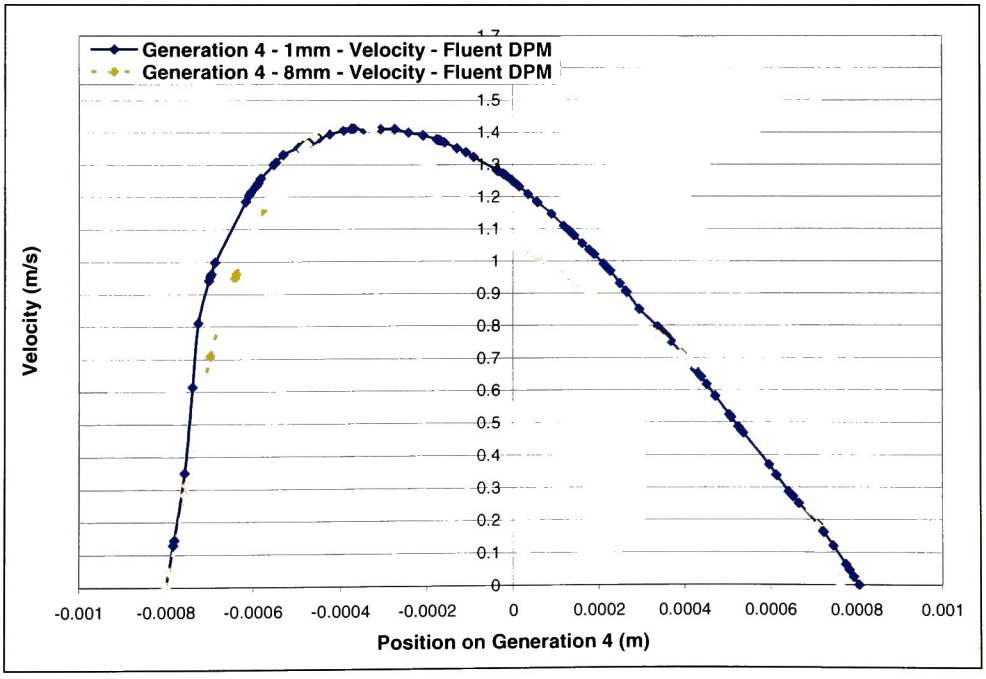


**Figure D.34 Parabolic velocity profile at 1.5 lpm flow rate in generation four of the three generation lung geometry.**

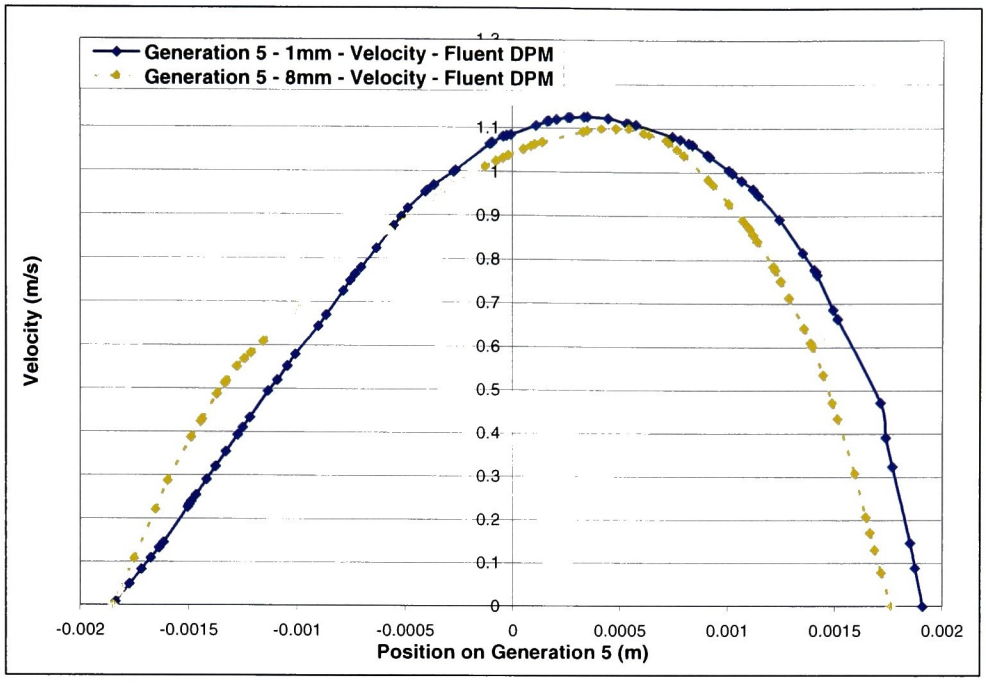


**Figure D.35 Parabolic velocity profile at 1.5 lpm flow rate in generation five of the three generation lung geometry.**

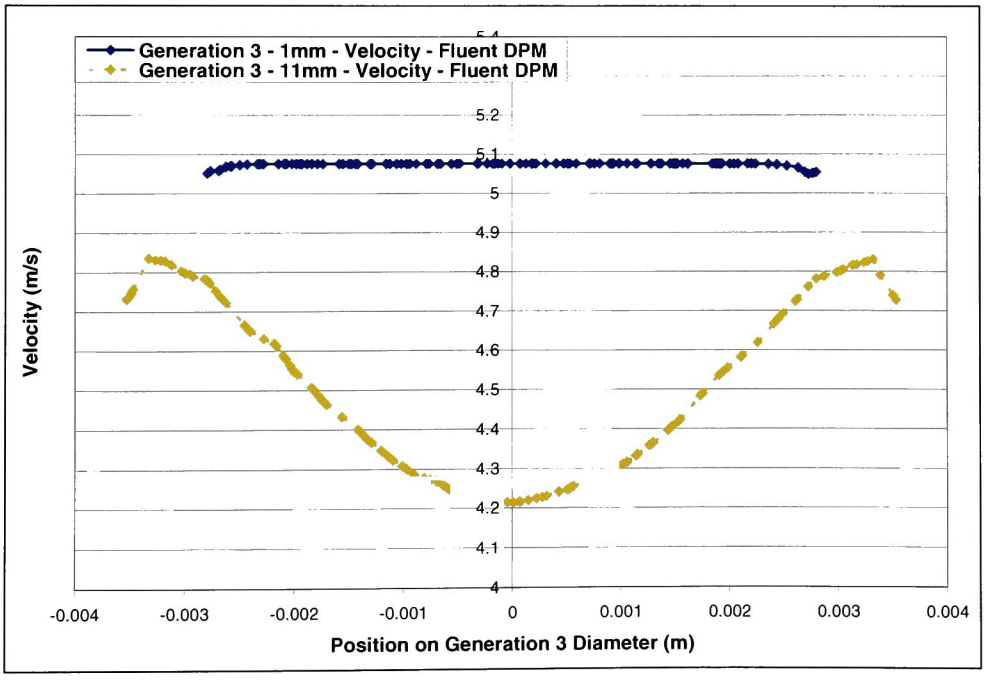


**Figure D.36 Uniform velocity profile at 7.5 lpm flow rate in generation three of the three generation lung geometry.**

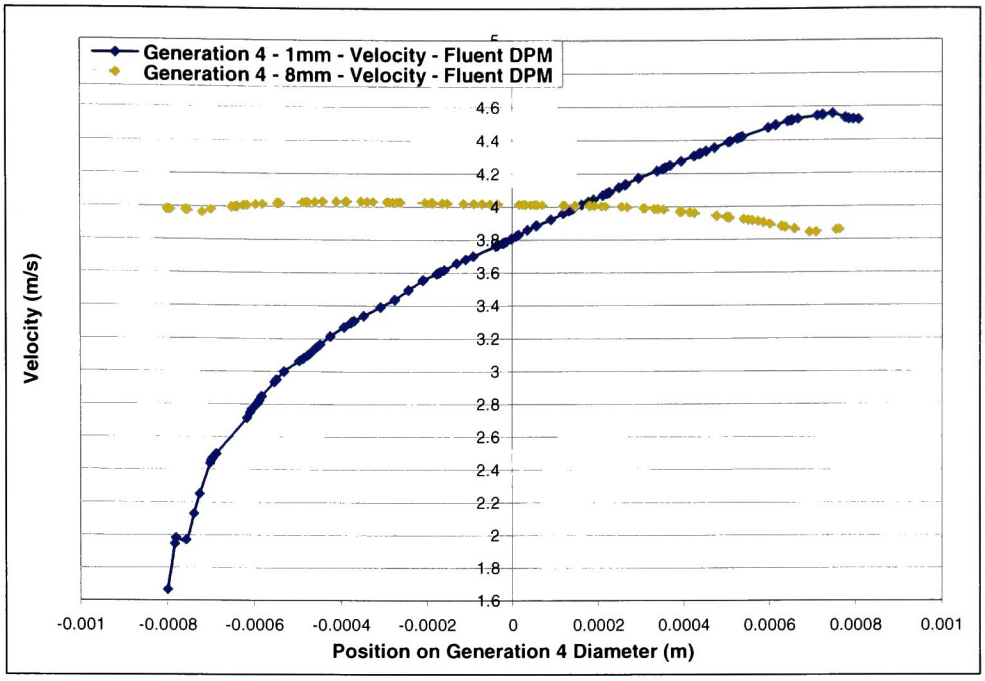


**Figure D.37 Uniform velocity profile at 7.5 lpm flow rate in generation four of the three generation lung geometry.**

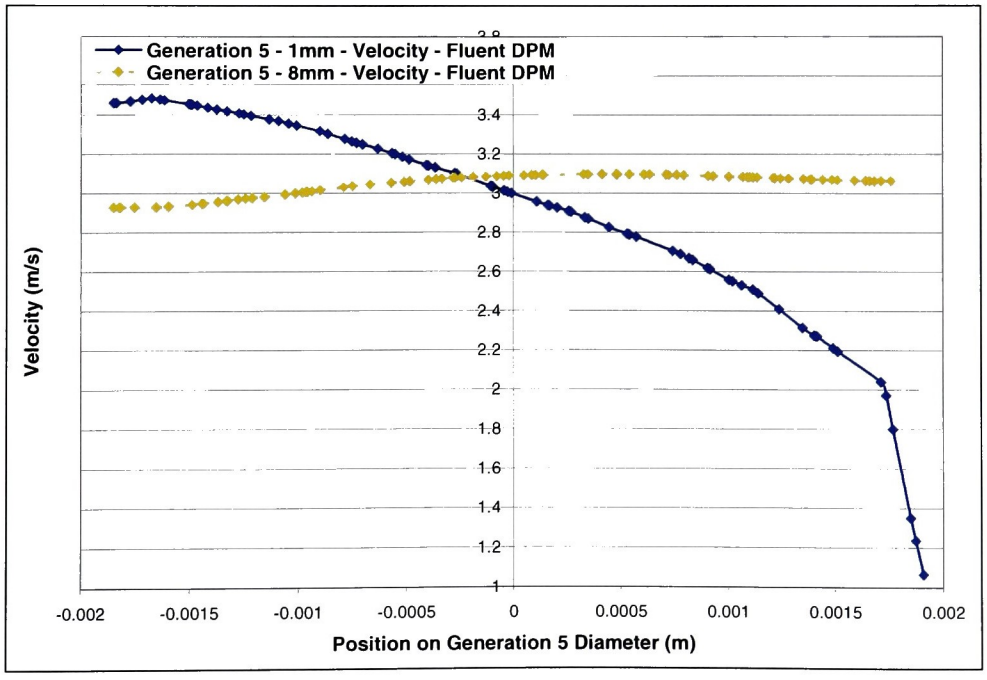


**Figure D.38 Uniform velocity profile at 7.5 lpm flow rate in generation five of the three generation lung geometry.**

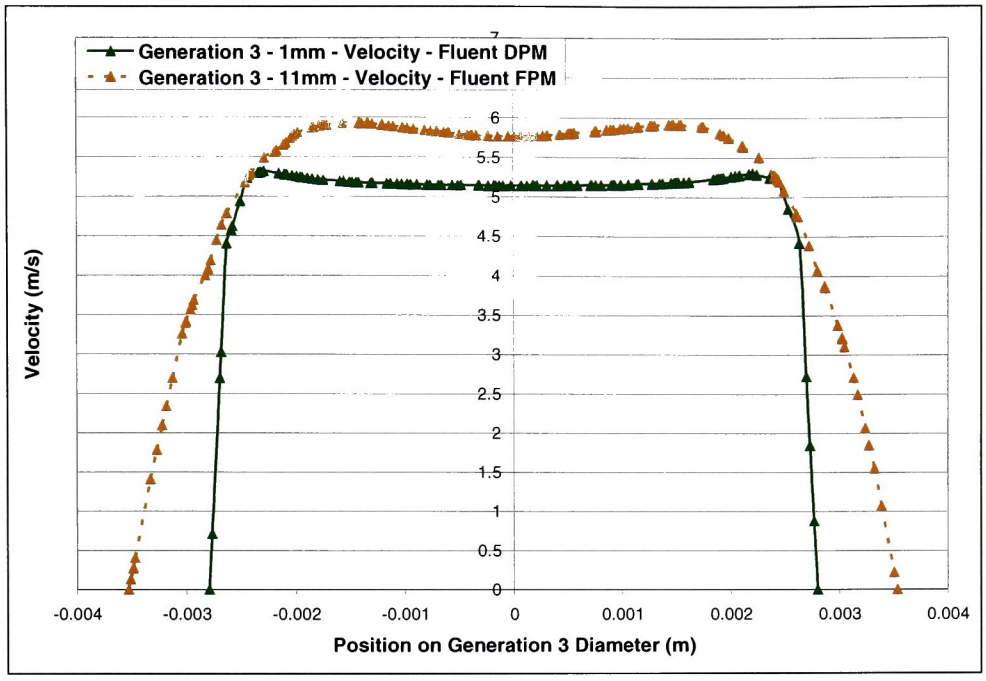


**Figure D.39 Developing velocity profile at 7.5 lpm flow rate in generation three of the three generation lung geometry.**

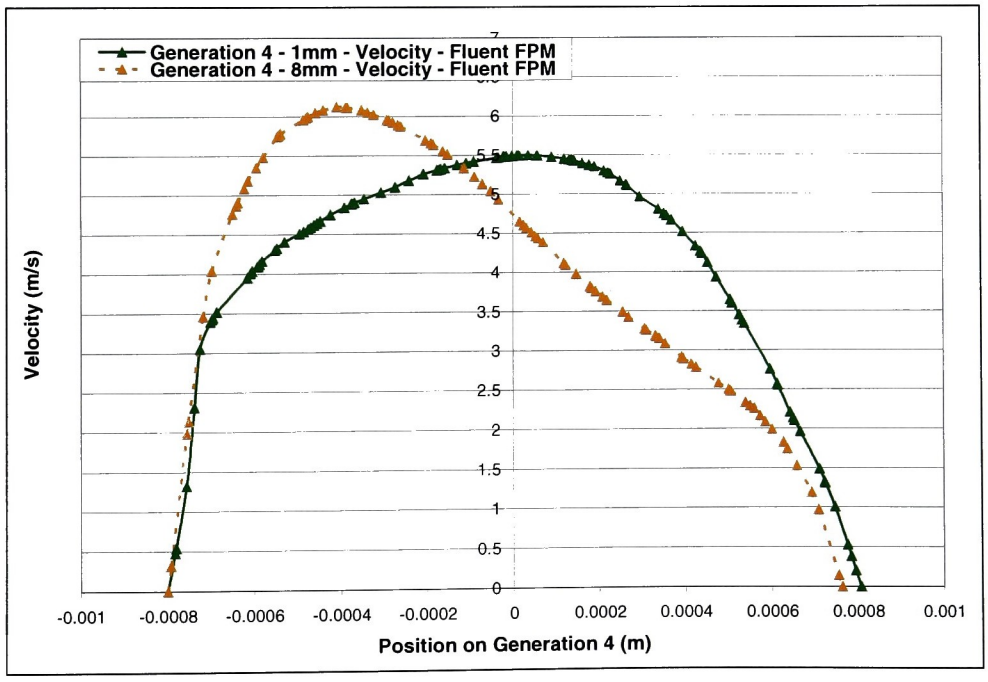


**Figure D.40 Developing velocity profile at 7.5 lpm flow rate in generation four of the three generation lung geometry.**

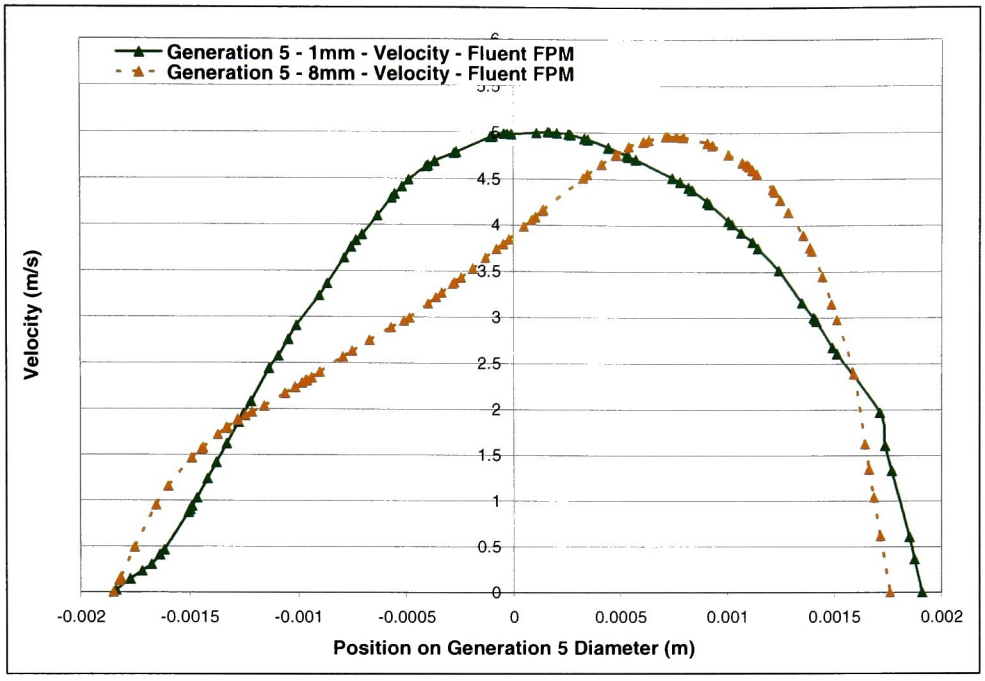


**Figure D.41 Developing velocity profile at 7.5 lpm flow rate in generation five of the three generation lung geometry.**

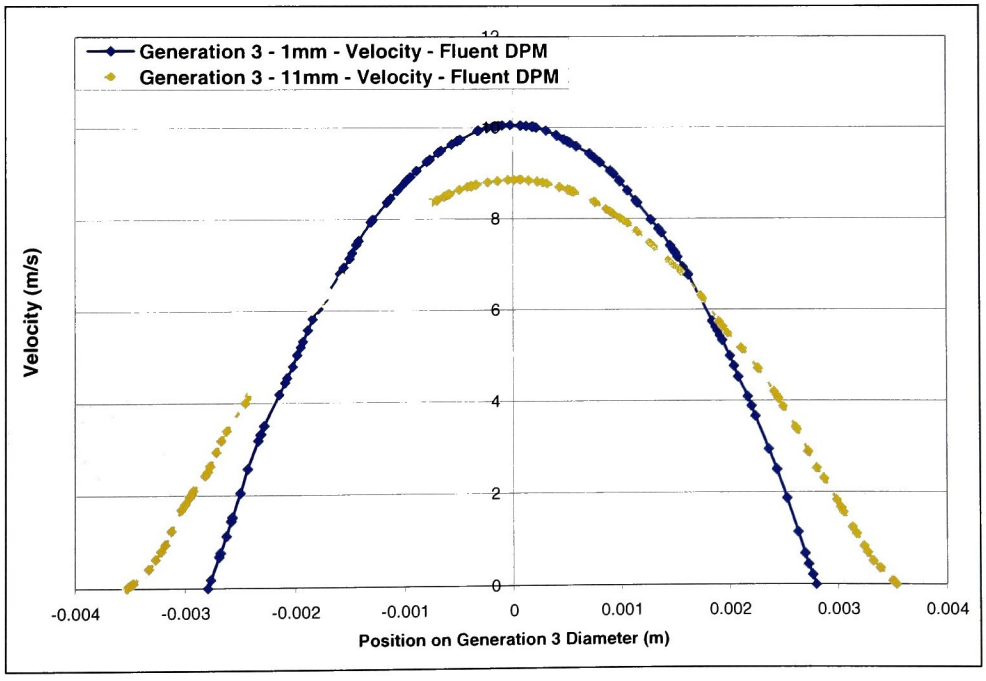


**Figure D.42 Parabolic velocity profile at 7.5 lpm flow rate in generation three of the three generation lung geometry.**

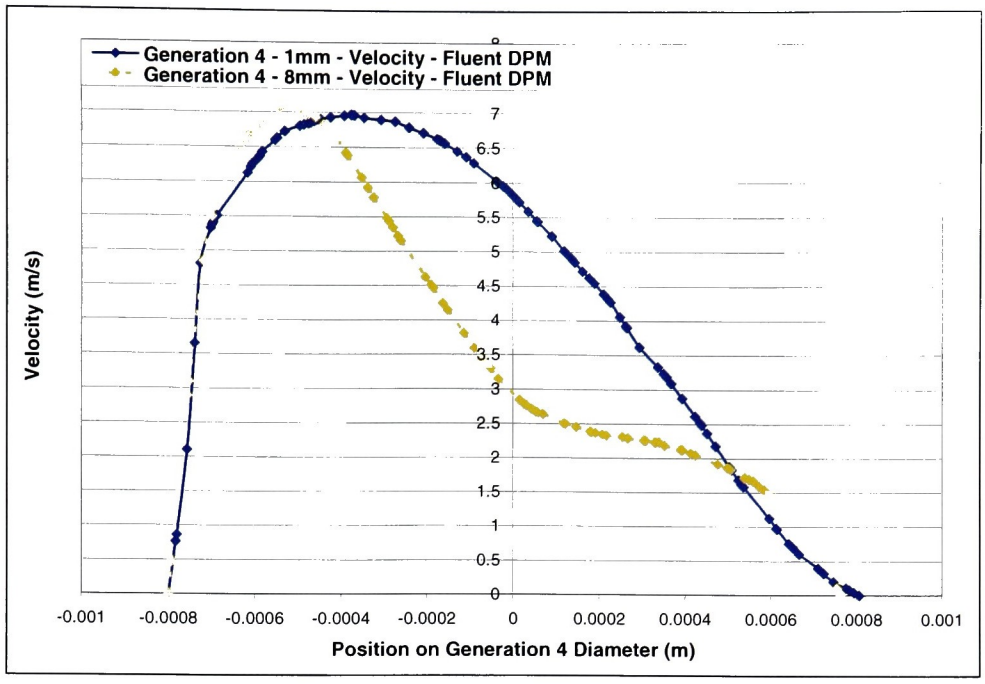


**Figure D.43 Parabolic velocity profile at 7.5 lpm flow rate in generation four of the three generation lung geometry.**

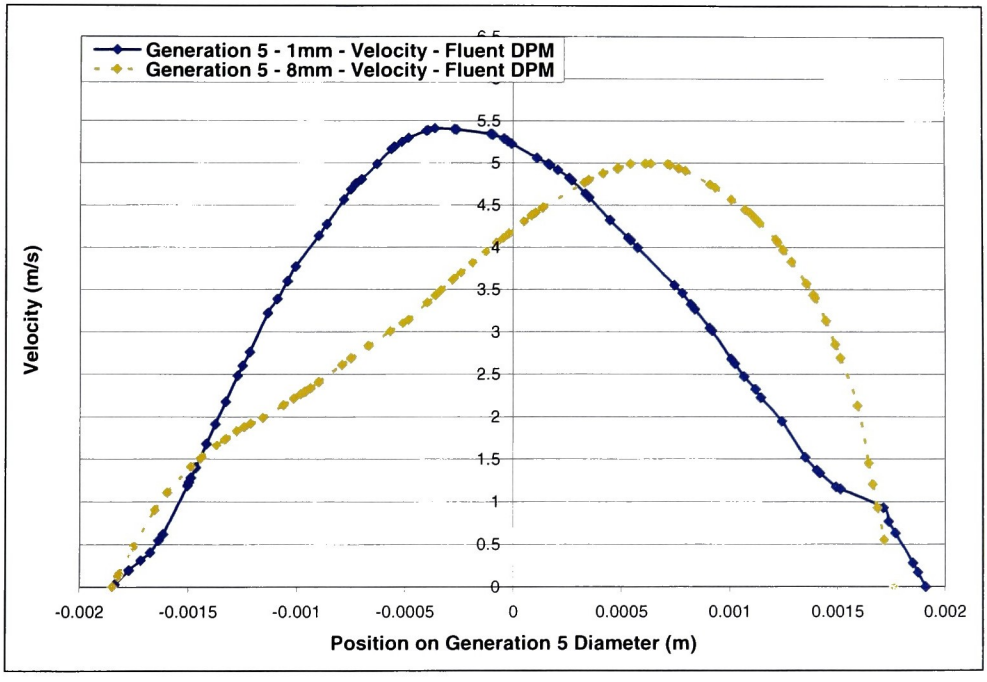


**Figure D.44 Parabolic velocity profile at 7.5 lpm flow rate in generation five of the three generation lung geometry.**

# Appendix E

# Fluent User Defined Function

```
#include "udf.h"  /* header file - necessary  */

DEFINE_PROFILE(inlet_x_velocity, thread , nv)
    /*  note the name of the function called inlet_x_velocity is defined here */
   /*  all UDF's begin with a define Macro  */
   /*  inlet_x_velocity  will be identified through the Fluent BC panel  */
   /*   thread, and nv are dynamic references and is used for internal book keeping */

{
  float x[3];   /* variable to hold position values*/
                /* in C  index starts at 0 - hence the three variables are x[0], x[1], x[2] */

 float a;      /* definition of a single precision real variable  y    */
 float z;              /* in C  all variables must be explicitly defined  */
 face_t f;     /*  a structure defined in "udf.h" by fluent */

 begin_f_loop(f,thread)  /* a looping MACRO used to access all cells or cell faces  */
 {
   F_CENTROID(x,f,thread);   /* a MACRO that assigns Cell positions to x  */
 a = x[0];
 z = x[2];
 F_PROFILE(f,thread,nv)= 10.1504-1285392*a*a-1285392*z*z;
     /*  the above MACRO assigns the profile to the face  f  */
 }

 end_f_loop(f,thread)
}
```

# Appendix F

# Dominate Deposition Mechanism in the Bifurcation Model

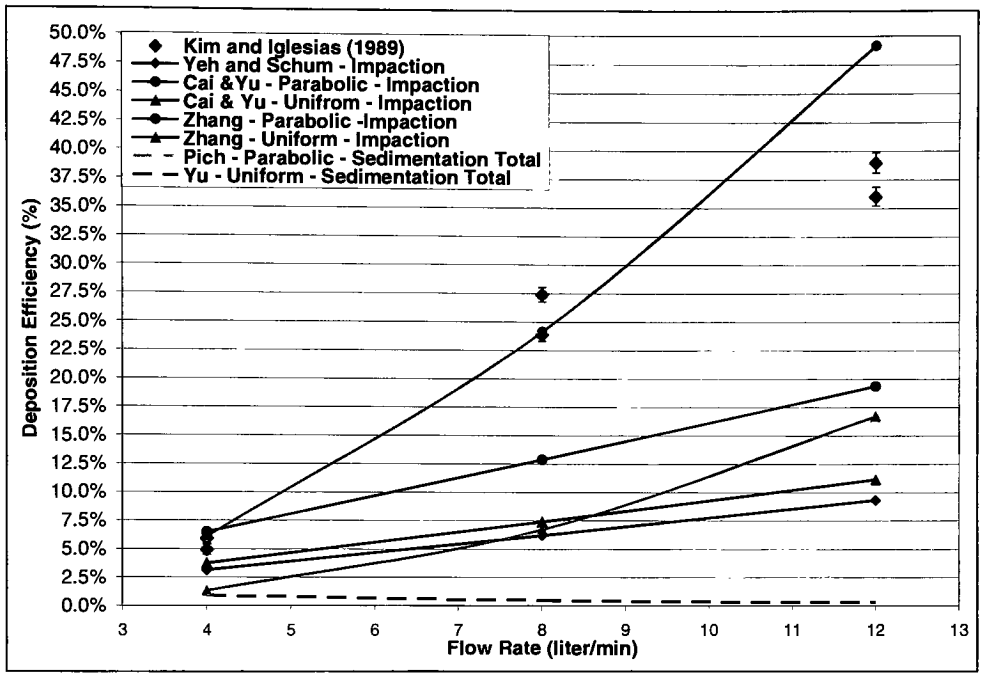


**Figure F.1 Analytical equations estimates of impaction and sedimentation in the bifurcating tube geometry for 5 μm particles at 4, 8, and 12 lpm flow rates.**

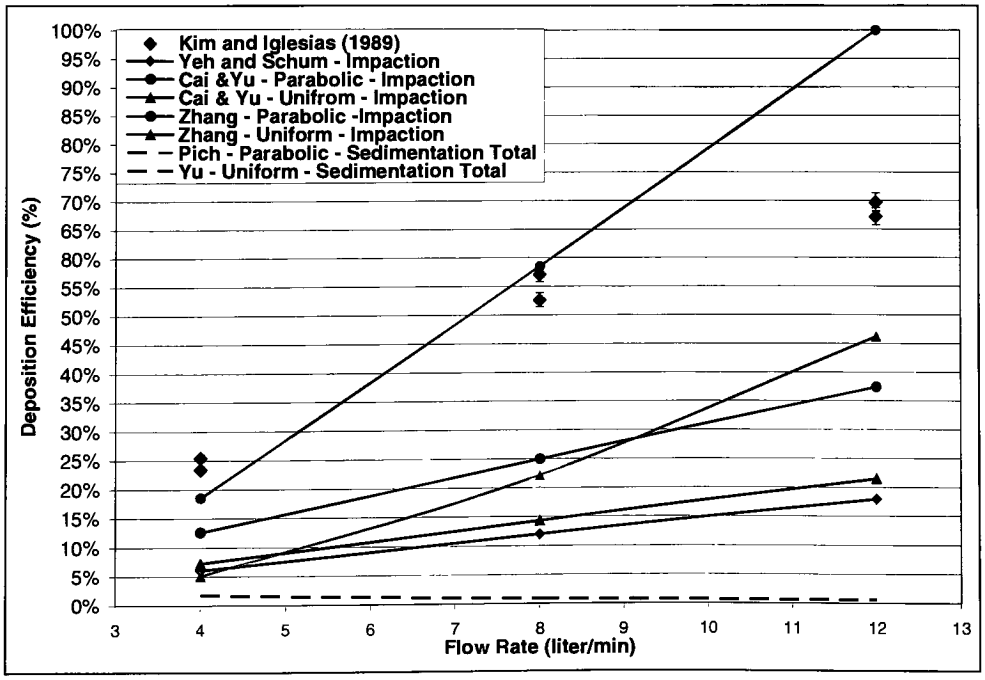


**Figure F.2 Analytical equations estimates of impaction and sedimentation in the bifurcating tube geometry for 7 μm particles at 4, 8, and 12 lpm flow rates.**

# Appendix G

# Affect of Varying Turbulence Intensity

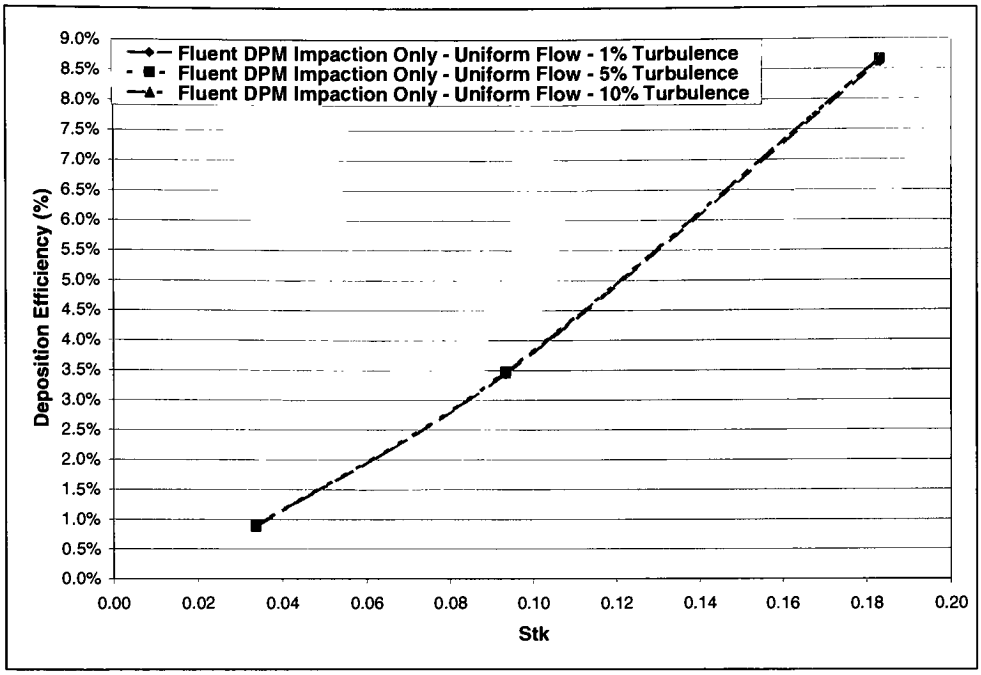


**Figure G.1 CFD predictions for Fluent DPM for 1%, 5%, and 10% turbulence intensities for uniform flow at the 8 lpm flow rate.**

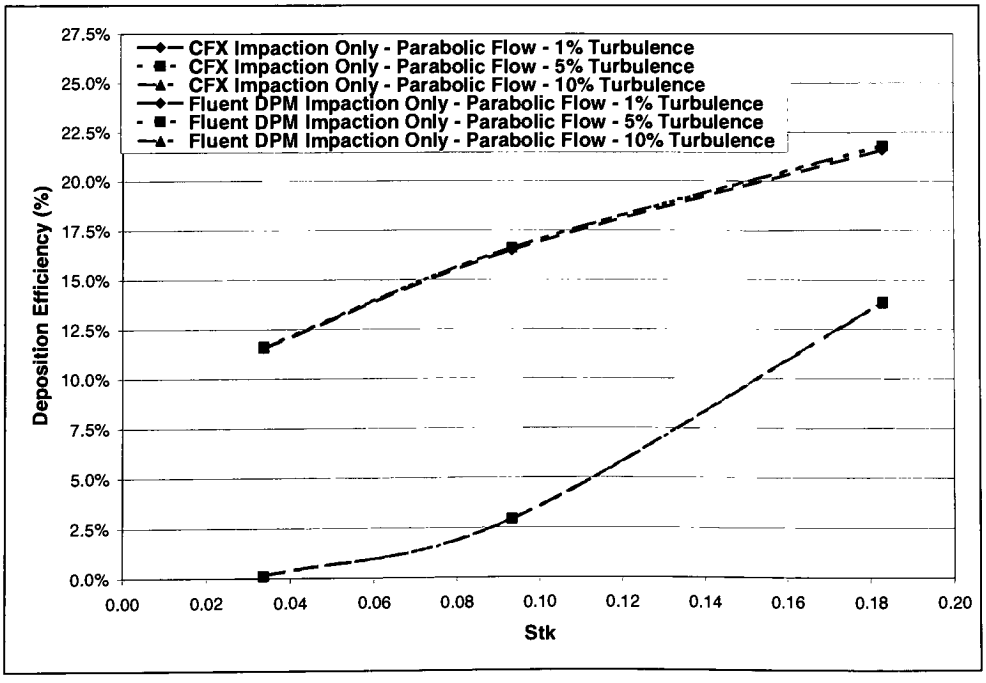


**Figure G.2 CFD predictions for CFX and Fluent DPM for 1%, 5%, and 10% turbulence intensities for parabolic flow at the 8 lpm flow rate.**

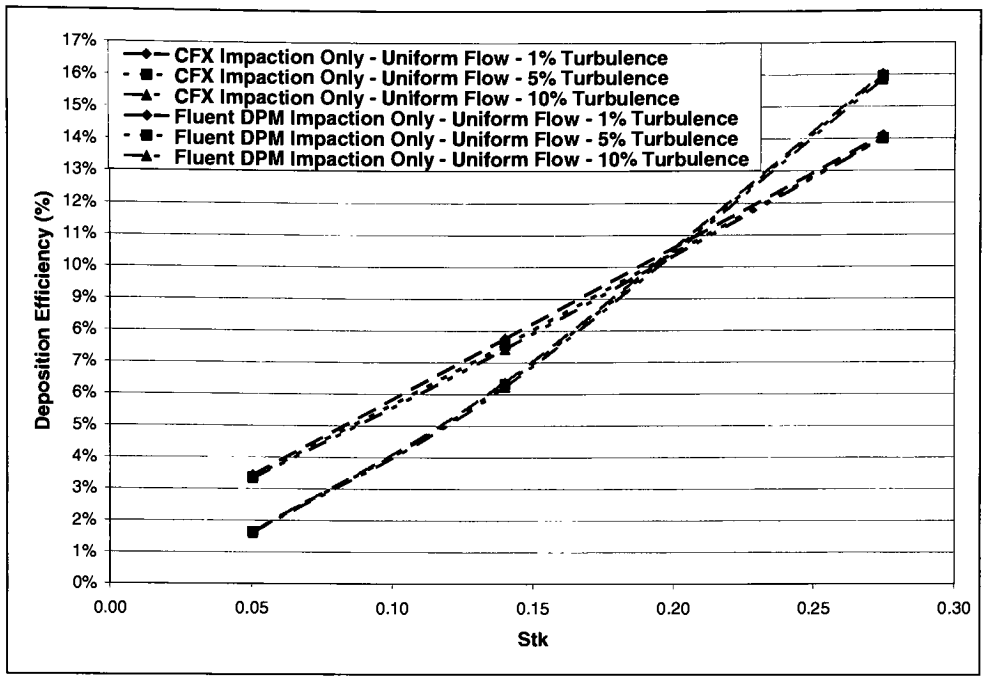


**Figure G.3 CFD predictions for CFX and Fluent DPM for 1%, 5%, and 10% turbulence intensities for uniform flow at the 12 lpm flow rate.**

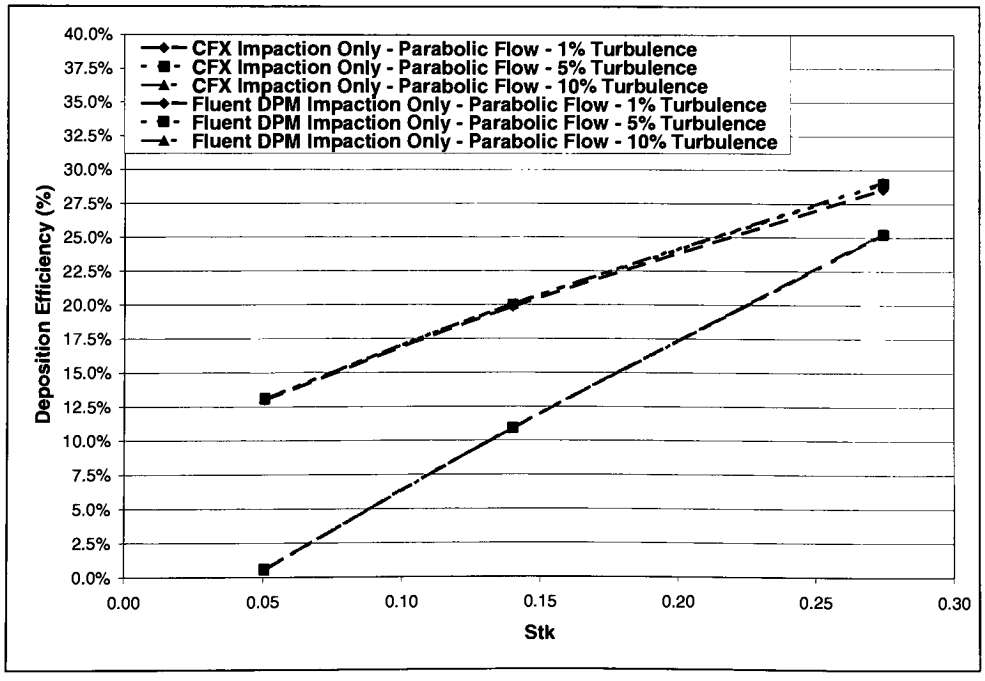


**Figure G.4 CFD predictions for CFX and Fluent DPM for 1%, 5%, and 10% turbulence intensities for parabolic flow at the 12 lpm flow rate.**